This is to certify that the

dissertation entitled

Numerical Solutions of Electromagnetic Problems by Integral Equation Methods and Finite-Difference Time-Domain Method

presented by

Xiaoyi Min

has been accepted towards fulfillment
of the requirements for

Ph.D degree in Electrical Engineering

Major professor

Date 8/1/89

NUMERICAL SOLUTIONS OF ELECTROMAGNETIC PROBLEMS BY INTEGRAL EQUATION METHODS AND FINITE-DIFFERENCE TIME-DOMAIN METHOD

By

Xiaoyi Min

A DISSERTATION

Submitted to
Michigan State University
in partial fulfillment of the requirements
for the degree of

DOCTOR OF PHILOSOPHY

Department of Electrical Engineering

1989

ABSTRACT

NUMERICAL SOLUTIONS OF ELECTROMAGNETIC PROBLEMS BY INTEGRAL EQUATION METHODS AND FINITE-DIFFERENCE TIME-DOMAIN METHOD

By

Xiaoyi Min

This thesis first presents the study of the interaction of electromagnetic waves with three-dimensional heterogeneous, dielectric, magnetic, and lossy bodies by surface integral equation modeling. Based on the equivalence principle, a set of coupled surface integral equations is formulated and then solved numerically by the method of moments. Triangular elements are used to model the interfaces of the heterogeneous body, and vector basis functions are defined to expand the unknown current in the formulation. The validity of this formualtion is verified by applying it to concentric spheres for which an exact solution exists. The potential applications of this formualtion to a partially coated sphere and a homogeneous human body are discussed.

Next, this thesis also introduces an efficient new set of integral equations for treating the scattering problem of a perfectly conducting body coated with a thin magnetically lossy layer. These electric field integral equations and magnetic field integral equations are numerically solved by the method of moments (MoM). To validate the derived integral equations, an alternative method to solve the scattering problem of an infinite circular cylinder coated with a thin magnetic lossy layer has also been developed, based on the eigenmode expansion. Results for the radar cross section and

current densities via the MoM and the eigenmode expansion method are compared. The agreement is excellent. The finite difference time domain method is subsequently implemented to solve a metallic object coated with a magnetic thin layer and numerical results are compared with that by the MoM.

Finally, this thesis presents an application of the finite-difference time-domain approach to the problem of electromagnetic receiving and scattering by a cavity-backed antenna situated on an infinite conducting plane. This application involves modifications of Yee's model, which applies the difference approximations of field derivatives to differential operators in the Maxwell's curl equations, and applies the radiation boundary condition on a truncated boundary surface. The modifications are based on the integral forms of the Maxwell equations and image theory. The effects of an infinitely thin impedance sheet on receiving and scattering characteristics of the antenna are investigated.

ACKNOWLEDGMENTS

The author wishes to express her heartfelt appreciation to her academic advisor, Dr. Kun-Mu Chen, for his sincere guidance and encouragement throughout the course of this work. She also wishes to appreciate Dr. D. P. Nyquist and Dr. E. J. Rothwell for their generous support and constructive suggestions during the period of this study.

A special note of thanks is due Dr. Byron C. Drachman for his special assistance and concern to the author.

In addition, the author thanks her parents, Mr. and Mrs. Longqiu Min, and her parents-in-law, Mr. and Mrs. Jiantang Sun for their continued love, sacrifice and encouragement in her research years.

The research reported in this thesis was supported by the National Science Foundation under Grant No. ECE 8509213.

Table of Contents

List of Figures

CHAPTER I

INTRODUCTION

In recent years, due to the increasing complexity of electromagnetic problems and advances in computer capability, much more attention of the research community is focused on seeking numerical solutions of various engineering problems in the field of electromagnetics. A number of numerical techniques have been introduced and applied to a variety of specific problems. However, there remains the demand for finding more efficient numerical methods to meet growing needs.

There are several numerical approaches available to study electromagnetic scattering by specific three-dimensional objects [1-7]. These approaches can be categorized into frequency-domain techniques, time-domain techniques and hybrid techniques. Frequency-domain techniques, including the method of moments (MoM), uni-moment method, finite-element method and iterative methods, treat electromagnetic scattering as a boundary value problem by deriving and then solving an integral equation for the electric field and/or magnetic field with specified boundary conditions. Time-domain techniques, including the finite-difference time-domain method (FD-TD), potential integral approach, and the Singularity Expansion Method, strive to examine the transient behavior of fields before the onset of a steady state and to model problems where non-sinusoidal excitations lead to scattering responses that may have no sinusoidal steady state. The hybrid techniques, including the method of moments/high frequency method, the FD-TD/method of moments and the FD-TD/high frequency method, are rooted in the combination of techniques in the other two categories.

In the past decade, most problems involving electromagnetic scattering have been handled by frequency-domain methods, especially by the method of moments. The basic steps of the moment method in solving integral equation formulations involve

converting the integral equation into a matrix equation and then solving the matrix equation by standard routines.

The method of moments is based on establishing an integral equation for a given geometry and composition. To solve a heterogeneous or inhomogeneous problem, a volume integral equation is normally used and discretized by tetrahedral modeling with a vector basis [8]. The surface integral equation approach is suited to analyzing homogeneous objects[12] or heterogeneous objects. The coupled surface integral equations are set up in terms of equivalent electric and magnetic currents on the interfaces of a heterogeneous body. In Chapter 2, this method is extended to analyze an arbitrarily shaped heterogenuous body. Based on the equivalence principle, a set of coupled surface integral equations is derived in section 2.2 and then solved numerically by the method of moments in section 2.3. Triangular elements are used to model the interfaces of the heterogeneous body, and vector basis functions are introduced to represent the unknown surface currents in the integral equations.

Because of its characteristics in matrix operation, the moment method becomes very inefficient and impractical when objects become electrically large. The finite difference time domain method provides a good alternative to the traditional moment method. The FD-TD method is a direct solution of Maxwell's time-dependent curl equations. The main algorithm of the FD-TD method includes Yee's model, which applies the simple second-order central-difference approximations of both spatial and temporal derivatives of the electric and magnetic fields directly to the differential operators of Maxwell's curl equations. It also applies the radiation boundary condition on the outer truncated boundary surfaces to simulate the outside extension when infinite space must be truncated. The system of equations developed by Yee [?] to update the field components is fully explicit such that the required computer storage and running time is proportional to the electrical size of the volume modeled. This

sets a remarkable difference from traditional moment-method which requires the inversion of a matrix.

The FD-TD method has been used to solve problems which include two and three dimensional electromagnetic wave scattering, electromagnetic wave penetration and coupling for both two and three dimensions, inverse scattering reconstructions in one and two dimensional cases, and microstrip and microwave circuit models. However, little effort has been made in the application of the FD-TD method to metallic objects coated with thin material and to transmitting and receiving antennas. Chapter 3 introduces the fundamental algorithm of the FD-TD method. It examines the derivation of Yee's model, the radiation boundary condition, and stability analysis, to provide a basis for extending the FD-TD method to important applications in Chapter 4 and Chapter 5.

It is known that a thin layer of electrically lossy material on a perfectly conducting body cannot efficiently reduce its radar cross section. The tangential component of electric field is very small near the surface of a perfect conductor and consequently the induced current and dissipated power in the coating layer are very small. On the other hand, if a thin magnetically lossy layer is used to coat the body, its radar cross section can be significantly reduced. The tangential component of magnetic field is very large on the surface of a conducting body, resulting in a large equivalent magnetic current and a high dissipated power in the coating layer.

In Chapter 4, a new set of coupled integral equations is derived for treating the scattering problem of a perfectly conducting body coated with a thin magnetically lossy layer. These electric field integral equations and magnetic field integral equations are numerically solved by the method of moments. To validate the derived integral equations, an alternative method to solve the scattering problem of an infinite circular cylinder coated with a thin magnetic lossy layer has also been developed,

based on the eigenmode expansion. Results for the radar cross section and current densities via the MoM and the eigenmode expansion method are compared. A special application of the FD-TD method to the thinly coated cylinder is also presented. A new algorithm for the FD-TD is developed based on the integral representation of Maxwell's equations.

In some applications, it is desirable to hide an airplane from the detection of radar systems. Since an antenna on the airplane is an efficient scatterer, it is necessary to cover the antenna with a lossy layer to reduce its radar cross section. In Chapter 5, the effects of an impedance sheet covering a cavity backed antenna, on the scattering and receiving characteristics, is studied. The integral equation technique is difficult to apply to this problem due to its complex geometry and the infinite conducing surface involved. Therefore, the finite difference time domain method is applied. Based on the fundamental theory described in Chapter III, Yee's model and the radiation boundary condition are modified for treating an infinitely thin impedance sheet and the infinite structure.

CHAPTER II

INTERACTION OF ELECTROMAGNETIC FIELDS WITH THREE-DIMENSIONAL, HETEROGENEOUS, DIELECTRIC, MAGNETIC AND LOSSY BODIES

2.1 Introduction

The interaction of electromagnetic waves with three-dimensional heterogeneous(or piecewise inhomogeneous), dielectric, magnetic, and lossy bodies has been extensively studied recently because of its relevance in the modification of the radar cross section of a metallic body by magnetic coating. Other motivations for the study are due to the need for quantifying the EM power deposition in human bodies and the application of EM fields in medical diagnostics. In the literature, a number of methods have been developed and applied to three-dimensional scattering problems [1-7]. Some of these methods have been demonstrated only for homogeneous bodies, while others are restricted to bodies of revolution. Even though the tetrahedral modeling, based on the volume integral equation [13], is applicable to arbitrarily shaped heterogeneous bodies, a more efficient and accurate numerical method is desirable.

More recently, the hybrid finite element method (HFEM) has received increasing attention and has been applied to two-dimensional electromagnetic scattering problems [16,18]. In this technique, the finite element method has been used for the near field region and the boundary-element method has been used for the exterior far field region. Objects to be modeled can simultaneously contain conductors, lossy dielectrics and lossy magnetic materials with complicated high aspect ratio geometries. This method can theoretically be applied to three-dimensional heterogeneous bodies, but so far only one such effort has been reported [16]. In that paper, the boundary conditions

across the interfaces of a heterogenuous body must be accounted for during the assembly of the matrix equations. Thus, the advantage of the HFEM for seeking a systematic solution to the complex geometries is lost, and this method becomes more difficult to apply.

With the rapid advance of supercomputers, the finite difference method in the time-domain (FD-TD) has become quite popular. The FD-TD method is a direct solution of Maxwell's time-dependent curl equations with boundary conditions and initial values. For an open-boundary problem, the infinite space is truncated into a finite space by introducing an artificial boundary condition or the radiation boundary condition. Space and time discretizations are selected to bound errors in the sampling process, and to insure numerical stability of the algorithm. The finite difference equations at each time step are fully explicit, so that the computer storage and running time are proportional to the electrical size of the volume to be modeled. This makes it promising when a very large body is involved, such as a man model with 50,000 volume cells [19,20]. However, for this method it is not easy to model complicated curved surfaces, and numerical artifacts such as instability and nonphysical wave reflections have to be discussed [17].

The surface integral equation approach is very well suited to analyzing homogeneous objects [12] or heterogeneous objects. The usual procedure in this method is to set up coupled surface integral equations in terms of equivalent electric and magnetic currents on the interfaces of a heterogeneous body. Instead of considering the whole domain, only boundaries have to be involved. We extend this method to analyze an arbitrarilly-shaped heterogeneous body by choosing an efficient and simple numerical scheme.

In this chapter, a method of solving this problem efficiently has been developed. Based on the equivalence principle, a set of coupled surface integral equations is

formulated in section 2.2, and then solved numerically by the method of moments in section 2.3. Triangular elements are used to model the interfaces of the heterogeneous body, and vector basis functions are defined within each triangular element to insure that the normal components of equivalent currents are continuous across triangular edges. The validity of this method will be established by applying it to a concentric sphere, with or without a perfectly conducting sphere inside which an exact solution exists. This method is applicable to a partially coated sphere and a homogeneous human model. This method will be compared with other existing methods in section 2.6.

2.2 Derivation of Coupled Surface Integral Equations for a Heterogeneous Body

The geometry of a heterogeneous body is shown in Figure 2.1. In this section, we will only consider two different cases: 1) A heterogeneous body without any perfect conductor inside and 2) A heterogeneous body which includes a perfect conductor. By methods similar to the formulations of these two problems, a set of coupled surface integral equations for a more complicated geometry can be easily derived.

2.2.1 The Preliminary Theorems

Before the coupled, surface integral equations are derived, we first review the general solutions of Maxwell's equations in terms of sources and surface fields.

Consider the geometry shown in Figure 2.2. An infinite region V is bounded by an infinite spherical surface S_∞, and within the region, there are volume EM sources, $\mathbf{J},\rho,\mathbf{J}_m,\rho_m$ and a closed surface S_1 which may enclose some other EM sources. $\hat{n}$ is the unit normal vector pointed outward from V. We can find **E** and **H** fields at an observation point $\mathbf{r}(x,y,z)$ maintained by all EM sources (including the sources inside S_1) and express them in terms of $\mathbf{J},\rho,\mathbf{J}_m,\rho_m$ and the surface fields (**E** and **H**) on S_1 as

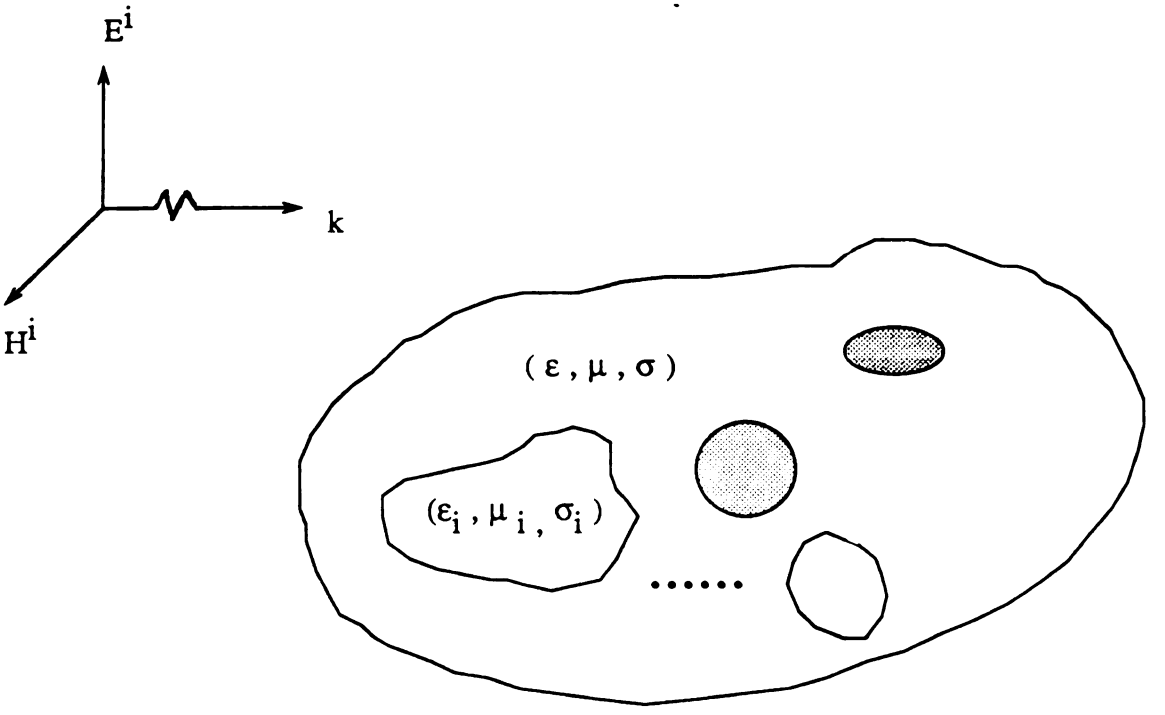

Fig. 2.1 Geometry of a heterogeneous body with a plane wave excitation

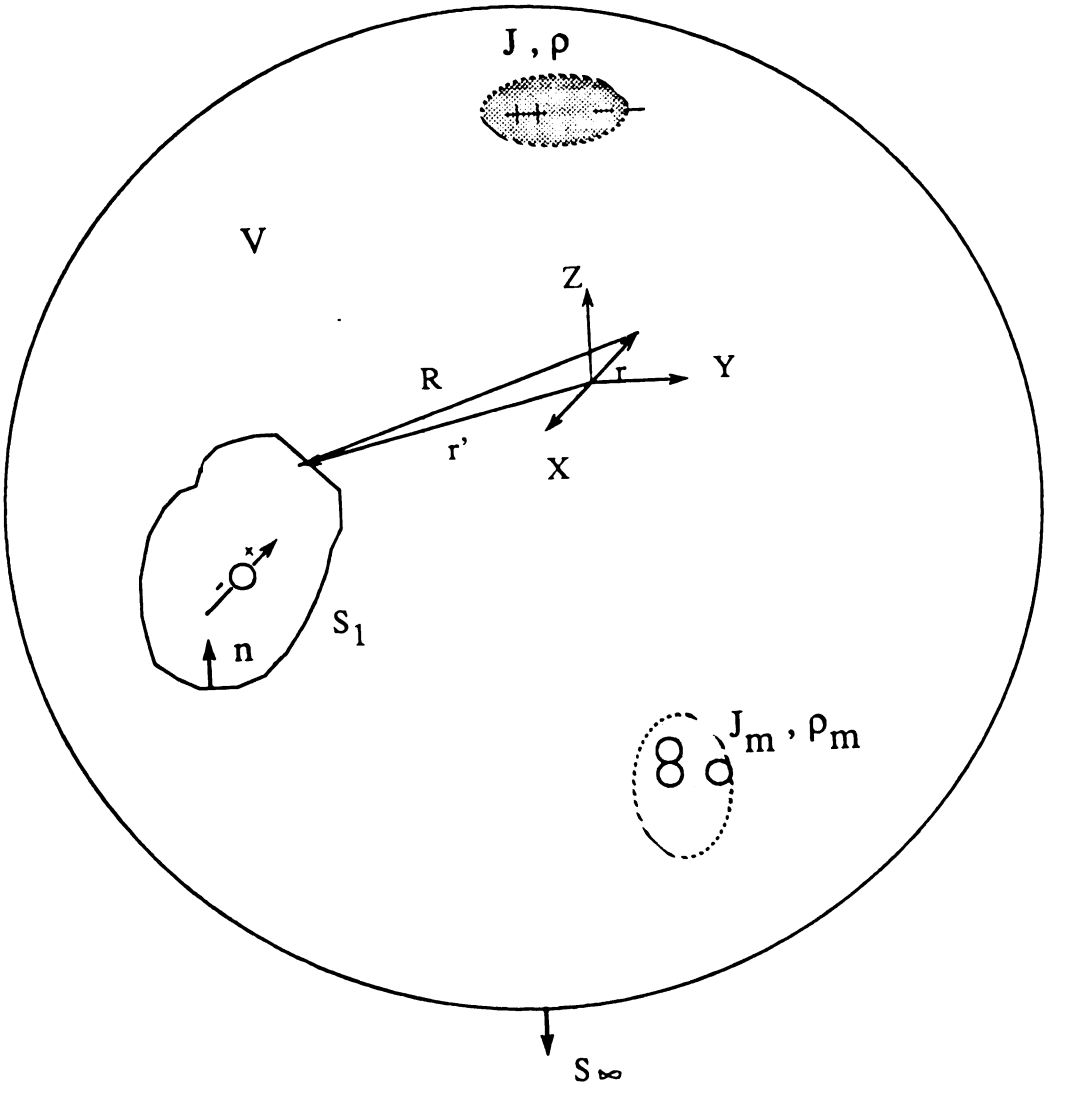

Figure 2.2 Geometry for illustration of the equivalence principles

follows:

$$\mathbf{E}(\mathbf{r}) = \frac{T}{4\pi}\int_V [-j\omega\mu\mathbf{J}\Phi - \mathbf{J}_m\times\nabla'\Phi + \frac{\rho}{\varepsilon}\nabla'\Phi]\, dV'$$
$$-\frac{T}{4\pi}\int_{S_1+S_-} [-j\omega\mu(\hat{n}\times\mathbf{H})\Phi + (\hat{n}\times\mathbf{E})\times\nabla'\Phi + (\hat{n}\cdot\mathbf{E})\,\nabla'\Phi]\, dS' \qquad (2.2.1a)$$

$$\mathbf{H}(\mathbf{r}) = \frac{T}{4\pi}\int_V [-j\omega\varepsilon\mathbf{J}_m\Phi + \mathbf{J}\times\nabla'\Phi + \frac{1}{\mu}\rho_m\nabla'\Phi]\, dV'$$
$$\frac{T}{4\pi}\int_{S_1+S_-} [j\omega\varepsilon(\hat{n}\times\mathbf{E})\Phi + (\hat{n}\times\mathbf{H})\times\nabla'\Phi + (\hat{n}\cdot\mathbf{H})\nabla'\Phi]\, dS' \qquad (2.2.1b)$$

The factor T comes from a singular integral surrounding the observation point :

$$T = \begin{cases} 1 & \mathbf{r} \text{ inside } V \\ 2 & \mathbf{r} \text{ on } S_1 \\ 0 & \text{otherwize} \end{cases}$$

with $\Phi = \frac{e^{-jkR}}{R}$ and $R = |\mathbf{r} - \mathbf{r}'|$, where $\mathbf{r}'$ is the position vector locating the source point and $\mathbf{r}$ represents an arbitrarily-located observation point. $k = \omega\sqrt{\mu\varepsilon}$ is the wavenumber. The complex permittivity ε is defined as $\varepsilon = \varepsilon_0(\varepsilon_r - j\frac{\sigma}{\omega\varepsilon_0})$ where ε_r is the dielectric constant, σ is the conductivity of the body and μ is its permeability. The integral over S_∞ vanishes by the radiation condition, and

$$\hat{n}\cdot\mathbf{E} = \frac{j}{\omega\varepsilon}\nabla'\cdot(\hat{n}\times\mathbf{H}) \qquad (2.2.2a)$$

$$\hat{n}\cdot\mathbf{H} = \frac{1}{j\omega\mu}\nabla'\cdot(\hat{n}\times\mathbf{E}) \qquad (2.2.2b)$$

The above relations between the normal components and tangential components of **E** and **H** fields are valid on a smooth surface and they are derived in appendix A.

2.2.2 A Heterogeneous Body Without Any Perfect Conductors Inside

We first consider the formulation of coupled surface integral equations for a heterogeneous body which does not enclose a perfect conductor. A heterogeneous

body as shown in Figure 2.3 consists of two different regions, V_1 and V_2. The surface S_2 encloses the inner region V_2 and $\hat{n}_2$ is the unit vector pointed outward from V_2. The surface S_1 encloses the whole body and $\hat{n}_1$ is the unit outward normal vector on S_1. An electric field $\mathbf{E}^i$ and a magnetic field $\mathbf{H}^i$, defined to be the fields due to the EM sources in the absence of the scatterer, are incident upon the body. The time dependence factor of $exp(j\omega t)$ is assumed and suppressed throughout the analysis. Based on the equivalence principle as discussd in section 2.1, the fields near the interfaces in the different regions can be determined in terms of equivalent surface currents.

In Region 1 V_0 (ε_0,μ_0) :

The medium in the region external to S_1 is assumed to be free space with permeability μ_0 and permittivity ε_0. According to the theory discussed in section 2.2.1, the total electric or total magnetic field just outside the surface S_1 can be expressed in terms of the incident $\mathbf{E}^i$ or the incident $\mathbf{H}^i$ field and tangential components of $\mathbf{E}$ and $\mathbf{H}$ fields on the surface S_1. Using Eq.(2.2.1a), we can write

$$\mathbf{E}(\mathbf{r}) = \frac{T}{4\pi}\int_V [-j\omega\mu\mathbf{J}\Phi - \mathbf{J}_m\times\nabla'\Phi + \frac{\rho}{\varepsilon}\nabla'\Phi]\, dV'$$
$$-\frac{T}{4\pi}\int_{S_1}[-j\omega\mu(\hat{n}\times\mathbf{H})\Phi + (\hat{n}\times\mathbf{E})\times\nabla'\Phi + (\hat{n}\cdot\mathbf{E})\,\nabla'\Phi]\, dS' \qquad (2.2.3a)$$

Where the volume integral in the expression is equal to $\mathbf{E}^i$. From Eq.(2.2.1a),

$$\mathbf{H}(\mathbf{r}) = \frac{T}{4\pi}\int_V [-j\omega\varepsilon\mathbf{J}_m\Phi + \mathbf{J}\times\nabla'\Phi + \frac{1}{\mu}\rho_m\nabla'\Phi]\, dV'$$
$$-\frac{T}{4\pi}\int_{S_1}[j\omega\varepsilon(\hat{n}\times\mathbf{E})\Phi + (\hat{n}\times\mathbf{H})\times\nabla'\Phi + (\hat{n}\cdot\mathbf{H})\nabla'\Phi]\, dS' \qquad (2.2.3b)$$

where the volume integral in the expression is equal to $\mathbf{H}^i$. When the observation point $\mathbf{r}$ approaches the surface S_1 from region 1, T equals to 2. The fields on S_1 in region 1 are denoted by $(\mathbf{E}^1, \mathbf{H}^1)$. $\hat{n}$ is directed as defined in section 2.2.1. Due to different definitions of $\hat{n},\hat{n}_1,\hat{n}_2$, there are sign changes of $\hat{n}$ when applying the above formula to our problems. Finally the expressions will have following forms:

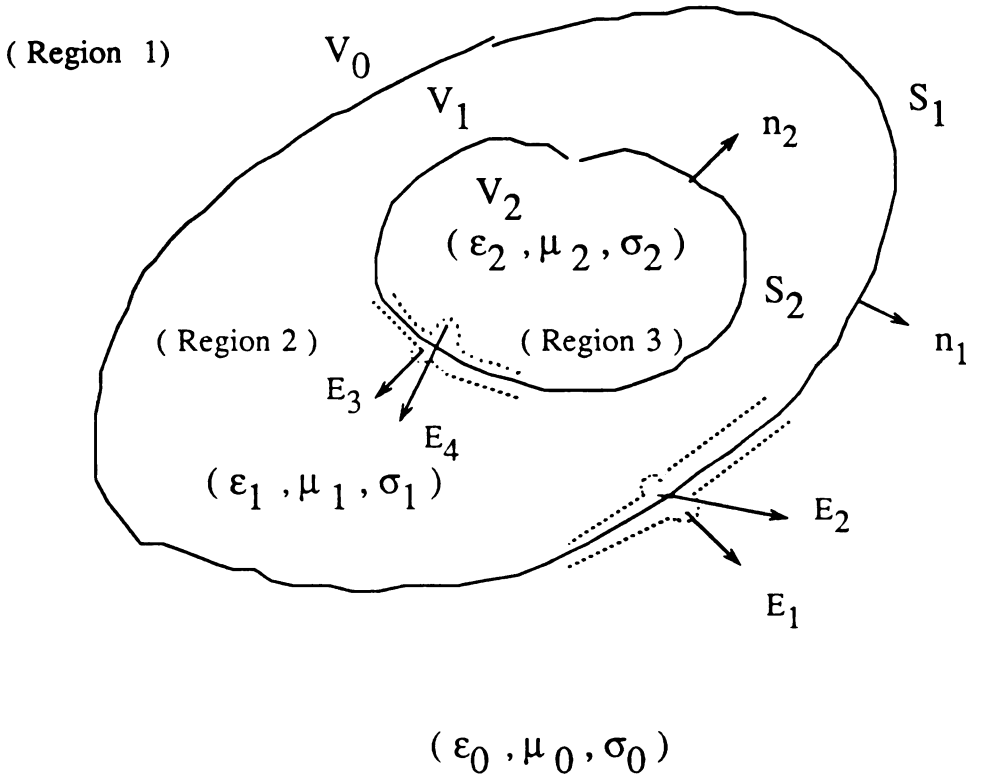

Fig. 2.3 A heterogeneous body without any perfect conductors

$$\mathbf{E}^1(\mathbf{r}) = 2\mathbf{E}^i + \frac{1}{2\pi}\int_{S_1}[-j\omega\mu_0(\hat{n}_1\times\mathbf{H}^1)\Phi_0 + (\hat{n}_1\times\mathbf{E}^1)\times\nabla'\Phi_0 + \frac{j}{\omega\varepsilon_0}\nabla'\cdot(\hat{n}_1\times\mathbf{H}^1)\,\nabla'\Phi_0]\,dS' \qquad (2.2.4a)$$

$$\mathbf{H}^1(\mathbf{r}) = 2\mathbf{H}^i + \frac{1}{2\pi}\int_{S_1}[j\omega\varepsilon_0(\hat{n}_1\times\mathbf{E}^1)\Phi_0 + (\hat{n}_1\times\mathbf{H}^1)\times\nabla'\Phi_0 + \frac{1}{j\omega\mu_0}\nabla'\cdot(\hat{n}_1\times\mathbf{E}^1)\,\nabla'\Phi_0]\,dS' \qquad (2.2.4b)$$

where $\Phi_0 = \dfrac{e^{-jk_0R}}{R}$ is the free space Green's function, and $k_0 = \omega\sqrt{\mu_0\varepsilon_0}$ is the free space wavenumber.

In Region 2 V_1 $(\varepsilon_1,\sigma_1,\mu_1)$:

In the region between surface S_1 and S_2, with permeability μ_1 and complex permittivity ε_1, the **E** and **H** fields just inside the surface S_1 or just outside the surface S_2 can be expressed by tangential components of **E** and **H** fields on the surfaces S_1 and S_2.

$$\mathbf{E}(\mathbf{r}) = \frac{T}{4\pi}\int_V [-j\omega\mu\mathbf{J}\Phi - \mathbf{J}_m\times\nabla'\Phi + \frac{\rho}{\varepsilon}\nabla'\Phi]\,dV'$$
$$-\frac{T}{4\pi}\int_{S_1+S_2}[-j\omega\mu(\hat{n}\times\mathbf{H})\Phi + (\hat{n}\times\mathbf{E})\times\nabla'\Phi + (\hat{n}\cdot\mathbf{E})\,\nabla'\Phi]\,dS' \qquad (2.2.5a)$$

The volume integral in the above expression is equal to zero because of no source within region 2. Similarly,

$$\theta\mathbf{H}(\mathbf{r}) = \frac{1}{4\pi}\int_V [-j\omega\varepsilon\mathbf{J}_m\Phi + \mathbf{J}\times\nabla'\Phi + \frac{1}{\mu}\rho_m\nabla'\Phi]\,dV'$$
$$-\frac{1}{4\pi}\int_{S_1+S_2}[j\omega\varepsilon(\hat{n}\times\mathbf{E})\Phi + (\hat{n}\times\mathbf{H})\times\nabla'\Phi + (\hat{n}\cdot\mathbf{H})\nabla'\Phi]\,dS' \qquad (2.2.5b)$$

where the volume integral is zero also. The factor T is equal to 2 when **r** is on S_1 in region 2 or on S_2 in region 2. Let ($\mathbf{E}^2$, $\mathbf{H}^2$) denote the electric and magnetic fields on S_1 in the region 2 side, and ($\mathbf{E}^3$, $\mathbf{H}^3$) denote the fields on S_2 in the region 2 side. Noting the sign changes in $\hat{n}$, and we can express fields in the forms:

When **r** is on S_1 ,

$$\mathbf{E}^2(\mathbf{r}) = \frac{-1}{2\pi}\int_{S_1}[-j\omega\mu_1(\hat{n}_1\times\mathbf{H}^2)\Phi_1 + (\hat{n}_1\times\mathbf{E}^2)\times\nabla'\Phi_1 + \frac{j}{\omega\varepsilon_1}\nabla'\cdot(\hat{n}_1\times\mathbf{H}^2)\,\nabla'\Phi_1]\,dS'$$
$$+\frac{1}{2\pi}\int_{S_2}[-j\omega\mu_1(\hat{n}_2\times\mathbf{H}^3)\Phi_1 + (\hat{n}_2\times\mathbf{E}^3)\times\nabla'\Phi_1 + \frac{j}{\omega\varepsilon_1}\nabla'\cdot(\hat{n}_2\times\mathbf{H}^3)\,\nabla'\Phi_1]\,dS' \qquad (2.2.6a)$$

$$\mathbf{H}^2(\mathbf{r}) = \frac{-1}{2\pi}\int_{S_1}[j\omega\varepsilon_1(\hat{n}_1\times\mathbf{E}^2)\Phi_1 + (\hat{n}_1\times\mathbf{H}^2)\times\nabla'\Phi_1 + \frac{1}{j\omega\mu_1}\nabla'\cdot(\hat{n}_1\times\mathbf{E}^2)\,\nabla'\Phi_1]\,dS'$$

$$+ \frac{1}{2\pi}\int_{S_2}[j\omega\varepsilon_1(\hat{n}_2\times\mathbf{E}^3)\Phi_1 + (\hat{n}_2\times\mathbf{H}^3)\times\nabla'\Phi_1 + \frac{1}{j\omega\mu_1}\nabla'\cdot(\hat{n}_2\times\mathbf{E}^3)\,\nabla'\Phi_1]\,dS' \qquad (2.2.6b)$$

When **r** is on S_2, the expressions for **E**,**H** essentially remain the same in form.

$$\mathbf{E}^3(\mathbf{r}) = \frac{-1}{2\pi}\int_{S_1}[-j\omega\mu_1(\hat{n}_1\times\mathbf{H}^2)\Phi_1 + (\hat{n}_1\times\mathbf{E}^2)\times\nabla'\Phi_1 + \frac{j}{\omega\varepsilon_1}\nabla'\cdot(\hat{n}_1\times\mathbf{H}^2)\,\nabla'\Phi_1]\,dS'$$

$$+ \frac{1}{2\pi}\int_{S_2}[-j\omega\mu_1(\hat{n}_2\times\mathbf{H}^3)\Phi_1 + (\hat{n}_2\times\mathbf{E}^3)\times\nabla'\Phi_1 + \frac{j}{\omega\varepsilon_1}\nabla'\cdot(\hat{n}_2\times\mathbf{H}^3)\,\nabla'\Phi_1]\,dS' \qquad (2.2.7a)$$

$$\mathbf{H}^3(\mathbf{r}) = \frac{-1}{2\pi}\int_{S_1}[j\omega\varepsilon_1(\hat{n}_1\times\mathbf{E}^2)\Phi_1 + (\hat{n}_1\times\mathbf{H}^2)\times\nabla'\Phi_1 + \frac{1}{j\omega\mu_1}\nabla'\cdot(\hat{n}_1\times\mathbf{E}^2)\,\nabla'\Phi_1]\,dS'$$

$$+ \frac{1}{2\pi}\int_{S_2}[j\omega\varepsilon_1(\hat{n}_2\times\mathbf{E}^3)\Phi_1 + (\hat{n}_2\times\mathbf{H}^3)\times\nabla'\Phi_1 + \frac{1}{j\omega\mu_1}\nabla'\cdot(\hat{n}_2\times\mathbf{E}^3)\,\nabla'\Phi_1]\,dS' \qquad (2.2.7b)$$

where $\Phi_1 = \dfrac{e^{-jk_1R}}{R}$ is the Green's function for region 2, and $k_1 = \omega\sqrt{\mu_1\varepsilon_1}$ is the complex wavenumber in this region.

In Region 3 $(\varepsilon_2,\sigma_2,\mu_2)$:

Similarly in region 3 where the permeability and permittivity are μ_2 and ε_2 respectively, the region is enclosed by S_2 with an outward unit normal $\hat{n}_2$. The **E** and **H** fields just inside the surface S_2 can be determined in terms of the tangential components of **E** and **H** on the surface S_2 as follows.

$$\mathbf{E}(\mathbf{r}) = \frac{T}{4\pi}\int_V[-j\omega\mu\mathbf{J}\Phi - \mathbf{J}_m\times\nabla'\Phi + \frac{\rho}{\varepsilon}\nabla'\Phi]\,dV'$$

$$-\frac{T}{4\pi}\int_{S_2}[-j\omega\mu(\hat{n}\times\mathbf{H})\Phi + (\hat{n}\times\mathbf{E})\times\nabla'\Phi + (\hat{n}\cdot\mathbf{E})\,\nabla'\Phi]\,dS' \qquad (2.2.8a)$$

$$\mathbf{H}(\mathbf{r}) = \frac{T}{4\pi}\int_V[-j\omega\varepsilon\mathbf{J}_m\Phi + \mathbf{J}\times\nabla'\Phi + \frac{1}{\mu}\rho_m\nabla'\Phi]\,dV'$$

$$-\frac{T}{4\pi}\int_{S_2}[j\omega\varepsilon(\hat{n}\times\mathbf{E})\Phi + (\hat{n}\times\mathbf{H})\times\nabla'\Phi + (\hat{n}\cdot\mathbf{H})\nabla'\Phi]\,dS' \qquad (2.2.8b)$$

The factor T equals to 2 when the fields on S_2 in region 3 are evaluated. The volume integral terms are equal to zero because of source free condition. Let ($\mathbf{E}^4$,$\mathbf{H}^4$) denote the electric and magnetic fields on S_2 in region 3. Then we can express these

fields in the forms:

$$\mathbf{E}^4(\mathbf{r}) = -\frac{1}{2\pi}\int_{S_2}[-j\omega\mu_2(\hat{n}_2\times\mathbf{H}^4)\Phi_2 + (\hat{n}_2\times\mathbf{E}^4)\times\nabla'\Phi_2 + \frac{j}{\omega\varepsilon_2}\nabla'\cdot(\hat{n}_2\times\mathbf{H}^4)\ \nabla'\Phi_2]\ dS' \tag{2.2.9a}$$

$$\mathbf{H}^4(\mathbf{r}) = -\frac{1}{2\pi}\int_{S_2}[j\omega\varepsilon_2(\hat{n}_2\times\mathbf{E}^4)\Phi_2 + (\hat{n}_2\times\mathbf{H}^4)\times\nabla'\Phi_2 + \frac{1}{j\omega\mu_2}\nabla'\cdot(\hat{n}_2\times\mathbf{E}^4)\ \nabla'\Phi_2]\ dS' \tag{2.2.9b}$$

where $\Phi_2 = \dfrac{e^{-jk_2R}}{R}$ is the Green's function for region 3, and $k_2 = \omega\sqrt{\mu_2\varepsilon_2}$ is complex wavenumber in this region.

Up to this point, we have the total induced fields (**E**,**H**) at the interfaces of the three different regions. Before going any further, we should introduce the boundary conditions which must be satisfied at the surfaces S_1 and S_2. The boundary conditions require the tangential components of the electric and magnetic field be continuous across S_1 and S_2.

Boundary Condition :

When the observation point **r** is on S_1, we may write

$$\mathbf{E}^1(\mathbf{r})|_{tan} = \mathbf{E}^2(\mathbf{r})|_{tan} \tag{2.2.10a}$$

$$\mathbf{H}^1(\mathbf{r})|_{tan} = \mathbf{H}^2(\mathbf{r})|_{tan} \tag{2.2.10b}$$

For **r** on S_2 :

$$\mathbf{E}^3(\mathbf{r})|tan = \mathbf{E}^4(\mathbf{r})|tan \tag{2.2.11a}$$

$$\mathbf{H}^3(\mathbf{r})|tan = \mathbf{H}^4(\mathbf{r})|tan \tag{2.2.11b}$$

Equivalently, we can write

$$\hat{n}_1\times\mathbf{E}^1(\mathbf{r}) = \hat{n}_1\times\mathbf{E}^2(\mathbf{r}) \tag{2.2.12a}$$

$$\hat{n}_1\times\mathbf{H}^1(\mathbf{r}) = \hat{n}_1\times\mathbf{H}^2(\mathbf{r}) \tag{2.2.12b}$$

$$\hat{n}_2\times\mathbf{E}^3(\mathbf{r}) = \hat{n}_2\times\mathbf{E}^4(\mathbf{r}) \tag{2.2.12c}$$

$$\hat{n}_2\times\mathbf{H}^3(\mathbf{r}) = \hat{n}_2\times\mathbf{H}^4(\mathbf{r}) \tag{2.2.12d}$$

By forcing the electric fields to satisfy the boundary conditions on the two interfaces, we have a set of so-called electric field integral equation(EFIE) as follows:

For $\mathbf{r}$ on S_1:

$$\mathbf{E}^1(\mathbf{r})|_{tan} = \mathbf{E}^2(\mathbf{r})|_{tan}$$

$$4\pi\mathbf{E}^i(\mathbf{r})|_{tan} = \int_{S_1}[j\omega(\hat{n}_1\times\mathbf{H}^1)(\mu_0\Phi_0 + \mu_1\Phi_1) - (\hat{n}_1\times\mathbf{E}^1)\times\nabla'(\Phi_0 + \Phi_1) -$$

$$\frac{j}{\omega}\nabla'\cdot(\hat{n}_1\times\mathbf{H}^1)\ \nabla'(\frac{\Phi_0}{\varepsilon_0} + \frac{\Phi_1}{\varepsilon_1})]\ dS' + \int_{S_2}[-j\omega\mu_1(\hat{n}_2\times\mathbf{H}^3)\Phi_1 +$$

$$(\hat{n}_2\times\mathbf{E}^3)\times\nabla'\Phi_1 + \frac{j}{\omega\varepsilon_1}\nabla'\cdot(\hat{n}_2\times\mathbf{H}^3)\ \nabla'\Phi_1]\ dS'|tan \qquad (2.2.13a)$$

For $\mathbf{r}$ on S_2 :

$$\mathbf{E}^3(\mathbf{r})|tan = \mathbf{E}^4(\mathbf{r})|tan$$

$$\int_{S_2}[j\omega(\hat{n}_2\times\mathbf{H}^3)(\mu_1\Phi_1 + \mu_2\Phi_2) - (\hat{n}_2\times\mathbf{E}^3)\times\nabla'(\Phi_1 + \Phi_2) - \frac{j}{\omega}\nabla'\cdot(\hat{n}_2\times\mathbf{H}^3)\ \nabla'(\frac{\Phi_1}{\varepsilon_1} + \frac{\Phi_2}{\varepsilon_2})]\ dS'|tan$$

$$= \int_{S_1}[j\omega\mu_1(\hat{n}_1\times\mathbf{H}^1)\Phi_1 - (\hat{n}_1\times\mathbf{E}^1)\times\nabla'\Phi_1 - \frac{j}{\omega\varepsilon_1}\nabla'\cdot(\hat{n}_1\times\mathbf{H}^1)\ \nabla'\Phi_1]\ dS'|tan \qquad (2.2.13b)$$

Similarly by forcing the magnetic fields to satisfy the boundary condition, a set of so-called magnetic field integral equation(MFIE) is formulated.

For $\mathbf{r}$ on S_1:

$$\mathbf{H}^1(\mathbf{r})]|_{tan} = \mathbf{H}^2(\mathbf{r})|_{tan}$$

$$4\pi\mathbf{H}^i(\mathbf{r})|_{tan} = \int_{S_1}[-j\omega(\hat{n}_1\times\mathbf{E}^1)(\varepsilon_0\Phi_0+\varepsilon_1\Phi_1) - (\hat{n}_1\times\mathbf{H}^1)\times\nabla'(\Phi_0 + \Phi_1) - \frac{1}{j\omega}\nabla'\cdot(\hat{n}_1\times\mathbf{E}^1)$$

$$\nabla'(\frac{\Phi_0}{\mu_0}+\frac{\Phi_1}{\mu_1})]dS' + \int_{S_2}[j\omega\varepsilon_1(\hat{n}_2\times\mathbf{E}^3)\Phi_1+(\hat{n}_2\times\mathbf{H}^3)\times\nabla'\Phi_1+\frac{1}{j\omega\mu_1}\nabla'\cdot(\hat{n}_2\times\mathbf{E}^3)\nabla'\Phi_1]dS'|tan \qquad (2.2.13c)$$

For $\mathbf{r}$ on S_2 :

$$\mathbf{H}^3(\mathbf{r})|tan = \mathbf{H}^4(\mathbf{r})|tan$$

$$\int_{S_2}[j\omega(\hat{n}_2\times\mathbf{E}^3)(\varepsilon_1\Phi_1 + \varepsilon_2\Phi_2) + (\hat{n}_2\times\mathbf{H}^3)\times\nabla'(\Phi_1 + \Phi_2) + \frac{1}{j\omega}\nabla'\cdot(\hat{n}_2\times\mathbf{E}^3)\ \nabla'(\frac{\Phi_1}{\mu_1} + \frac{\Phi_2}{\mu_2})]dS'|tan$$

$$= \int_{S_1}[j\omega\varepsilon_1(\hat{n}_1\times\mathbf{E}^1)\Phi_1 \pm (\hat{n}_1\times\mathbf{H}^1)\times\nabla'\Phi_1 + \frac{1}{j\omega\mu_1}\nabla'\cdot(\hat{n}_1\times\mathbf{E}^1)\ \nabla'\Phi_1]\ dS'|tan \qquad (2.2.13d)$$

To simplify the notations, let's define the equivalent surface current as follows:

$$\frac{-\hat{n}_1\times\mathbf{E}^1(\mathbf{r})}{\eta_0} = \mathbf{M}^1(\mathbf{r}) \qquad (2.2.14a)$$

$$\frac{-\hat{n}_2\times\mathbf{E}^3(\mathbf{r})}{\eta_0} = \mathbf{M}^2(\mathbf{r}) \tag{2.2.14b}$$

$$\hat{n}_1\times\mathbf{H}^1(\mathbf{r}) = \mathbf{K}^1(\mathbf{r}) \tag{2.2.14c}$$

$$\hat{n}_2\times\mathbf{H}^3(\mathbf{r}) = \mathbf{K}^2(\mathbf{r}) \tag{2.2.14d}$$

After matching boundary conditions and scaling the physical dimensions by k_0, we have a set of coupled surface integral equations:

$\mathbf{r}$ on S_1:

$$\frac{4\pi}{\eta_0}\mathbf{E}^i(\mathbf{r})|\tan = \int_{S_1}[j\mathbf{K}^1(\Phi_0 + \mu_{r1}\Phi_1) + \mathbf{M}^1\times\nabla'(\Phi_0 + \Phi_1) - j\nabla'\cdot\mathbf{K}^1\ \nabla'(\Phi_0 + \frac{\Phi_1}{\varepsilon_{r1}})]\ dS'$$

$$+ \int_{S_2}[-j\mu_{r1}\mathbf{K}^2\Phi_1 - \mathbf{M}^2\times\nabla'\Phi_1 + \frac{j}{\varepsilon_{r1}}\nabla'\cdot\mathbf{K}^2\nabla'\Phi_1]\ dS'|\tan \tag{2.2.15a}$$

$\mathbf{r}$ on S_2:

$$\int_{S_2}[j\mathbf{K}^2(\mu_{r1}\Phi_1 + \mu_{r2}\Phi_2) + \mathbf{M}^2\times\nabla'(\Phi_1 + \Phi_2) - j\nabla'\cdot\mathbf{K}^2\nabla'(\frac{\Phi_1}{\varepsilon_{r1}} + \frac{\Phi_2}{\varepsilon_{r2}})]\ dS'|\tan$$

$$= \int_{S_1}[j\mu_{r1}\mathbf{K}^1\Phi_1 + \mathbf{M}^1\times\nabla'\Phi_1 - \frac{j}{\varepsilon_{r1}}\nabla'\cdot\mathbf{K}^1\ \nabla'\Phi_1]\ dS'|\tan \tag{2.2.15b}$$

$\mathbf{r}$ on S_1:

$$4\pi\mathbf{H}^i(\mathbf{r})|_{\tan} = \int_{S_1}[j\mathbf{M}^1(\Phi_0 + \varepsilon_{r1}\Phi_1) - \mathbf{K}^1\times\nabla'(\Phi_0 + \Phi_1) + \frac{1}{j}\nabla'\cdot\mathbf{M}^1\ \nabla'(\Phi_0 + \frac{\Phi_1}{\mu_{r1}})]\ dS'$$

$$+ \int_{S_2}[-j\varepsilon_{r1}\mathbf{M}^2\Phi_1 + \mathbf{K}^2\times\nabla'\Phi_1 - \frac{1}{j\mu_{r1}}\nabla'\cdot\mathbf{M}^2\ \nabla'\Phi_1]\ dS'|\tan \tag{2.2.15c}$$

$\mathbf{r}$ on S_2:

$$\int_{S_2}[j\mathbf{M}^2(\varepsilon_{r1}\Phi_1 + \varepsilon_{r2}\Phi_2) - \mathbf{K}^2\times\nabla'(\Phi_1 + \Phi_2) + \frac{1}{j}\nabla'\cdot\mathbf{M}^2\ \nabla'(\frac{\Phi_1}{\mu_{r1}} + \frac{\Phi_2}{\mu_{r2}})]\ dS'|\tan$$

$$= \int_{S_1}[j\varepsilon_{r1}\mathbf{M}^1\Phi_1 - \mathbf{K}^1\times\nabla'\Phi_1 + \frac{1}{j\mu_{r1}}\nabla'\cdot\mathbf{M}^1\ \nabla'\Phi_1]\ dS'|\tan \tag{2.2.15d}$$

where $\mu_{ri} = \dfrac{\mu_i}{\mu_0}$ and $\varepsilon_{ri} = \dfrac{\varepsilon_i'}{\varepsilon_0} = \varepsilon_{ri}' - j\dfrac{\sigma}{\omega\varepsilon_0}$. Due to the normalization with respect to k_0, the Green's functions have the forms $\Phi_i = \dfrac{e^{-jk_{ri}R}}{R}$ and $k_{ri} = \dfrac{k_i}{k_0}$.

In the above four coupled surface integral equations, ($\mathbf{K}^1$,$\mathbf{M}^1$,$\mathbf{K}^2$,$\mathbf{M}^2$) are four unknowns which can be determined by solving by these four coupled surface integral equations.

2.2.3 A Heterogeneous Body Enclosing a Perfect Conductor

As shown in Figure 2.4, a perfect conductor covered by a dielectric, magnetic, and lossy medium is located in free space. The medium has the complex permittivity of $\varepsilon = \varepsilon_0(\varepsilon_r - j\frac{\sigma}{\omega\varepsilon_0})$, and permeability μ. A similar derivation to the previous case, with the exception of vanishing tangential components of electric field on the surface of the perfect conductor, will be presented.

In Region 1 (ε_0,μ_0) :

The expressions for $\mathbf{E}^1$,$\mathbf{H}^1$ remain the same as Eq.(2.2.4).

$$\mathbf{E}^1(\mathbf{r})=2\mathbf{E}^i\frac{+1}{2\pi}\int_{S_1}[-j\omega\mu_0(\hat{n}_1\times\mathbf{H}^1)\Phi_0+(\hat{n}_1\times\mathbf{E}^1)\times\nabla'\Phi_0+\frac{j}{\omega\varepsilon_0}\nabla'\cdot(\hat{n}_1\times\mathbf{H}^1)\nabla'\Phi_0]dS' \tag{2.2.16a}$$

$$\mathbf{H}^1(\mathbf{r})=2\mathbf{H}^i+\frac{1}{2\pi}\int_{S_1}[j\omega\varepsilon_0(\hat{n}_1\times\mathbf{E}^1)\Phi_0+(\hat{n}_1\times\mathbf{H}^1)\times\nabla'\Phi_0+\frac{1}{j\omega\mu_0}\nabla'\cdot(\hat{n}_1\times\mathbf{E}^1)\nabla'\Phi_0]dS' \tag{2.2.16b}$$

In Region 2 $(\varepsilon_1,\sigma_1,\mu_1)$:

Due to the zero tangential component of $\mathbf{E}$ field on the perfect conductor surface S_2, the integrands involving $\hat{n}_2\times\mathbf{E}^3$ over S_2 disappear. For the fields ($\mathbf{E}^2$,$\mathbf{H}^2$) on the surface S_1 in the region 2 side, we have the following simplified expressions:

$$\begin{aligned}\mathbf{E}^2(\mathbf{r}) = \frac{-1}{2\pi}\int_{S_1}[-j\omega\mu_1(\hat{n}_1\times\mathbf{H}^2)\Phi_1 + (\hat{n}_1\times\mathbf{E}^2)\times\nabla'\Phi_1 + \frac{j}{\omega\varepsilon_1}\nabla'\cdot(\hat{n}_1\times\mathbf{H}^2)\ \nabla'\Phi_1]\ dS' \\ + \frac{1}{2\pi}\int_{S_2}[-j\omega\mu_1(\hat{n}_2\times\mathbf{H}^3)\Phi_1 + \frac{j}{\omega\varepsilon_1}\nabla'\cdot(\hat{n}_2\times\mathbf{H}^3)\ \nabla'\Phi_1]\ dS'\end{aligned} \tag{2.2.17a}$$

$$\begin{aligned}\mathbf{H}^2(\mathbf{r}) = \frac{-1}{2\pi}\int_{S_1}[j\omega\varepsilon_1(\hat{n}_1\times\mathbf{E}^2)\Phi_1 + (\hat{n}_1\times\mathbf{H}^2)\times\nabla'\Phi_1 + \frac{1}{j\omega\mu_1}\nabla'\cdot(\hat{n}_1\times\mathbf{E}^2)\ \nabla'\Phi_1]\ dS' \\ + \frac{1}{2\pi}\int_{S_2}[\ + (\hat{n}_3\times\mathbf{H}^3)\times\nabla'\Phi_1]\ dS'\end{aligned} \tag{2.2.17b}$$

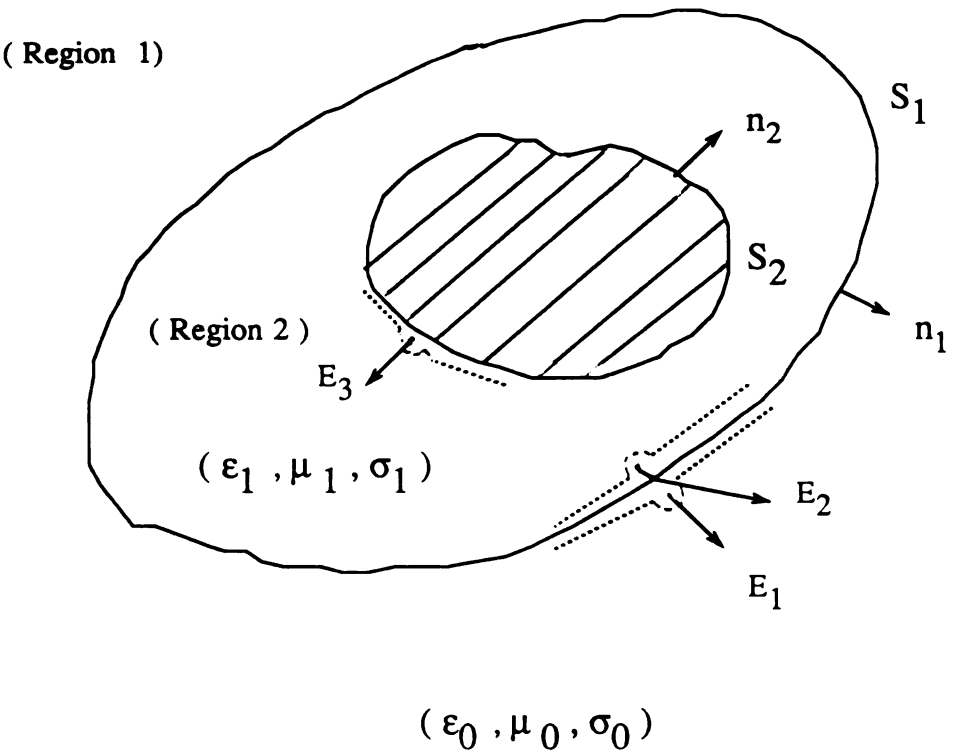

Fig. 2.4 A heterogeneous body with a perfect conductor inside

On the surface of the perfect conductor S_2, only the equation for $\mathbf{E}^3$ field in region 2 side is required.

$$\mathbf{E}^3(\mathbf{r}) = \frac{-1}{2\pi}\int_{S_1}[-j\omega\mu_1(\hat{n}_1\times\mathbf{H}^2)\Phi_1 + (\hat{n}_1\times\mathbf{E}^2)\times\nabla'\Phi_1 + \frac{j}{\omega\varepsilon_1}\nabla'\cdot(\hat{n}_1\times\mathbf{H}^2)\ \nabla'\Phi_1]\ dS'$$
$$+ \frac{1}{2\pi}\int_{S_2}[-j\omega\mu_1(\hat{n}_2\times\mathbf{H}^3)\Phi_1 + \frac{j}{\omega\varepsilon_1}\nabla'\cdot(\hat{n}_2\times\mathbf{H}^3)\ \nabla'\Phi_1]\ dS' \qquad (2.2.18)$$

Next we will apply the boundary condition to set up the coupled integral equations. On the surface S_1, tangential components of **E** and **H** should be continuous, while on the surface of the perfect conductor S_2, the tangential component of $\mathbf{E}^3$ is equal to zero.

r on S_1:

$$\mathbf{E}^1(\mathbf{r})|_{tan} = \mathbf{E}^2(\mathbf{r})|_{tan} \qquad (2.2.19a)$$
$$\mathbf{H}^1(\mathbf{r})|_{tan} = \mathbf{H}^2(\mathbf{r})|_{tan} \qquad (2.2.19b)$$

r on S_2 :

$$\mathbf{E}^3(\mathbf{r})|tan = 0 \qquad (2.2.19c)$$

Alternatively, we may write:

$$\hat{n}_1\times\mathbf{E}^1(\mathbf{r}) = \hat{n}_1\times\mathbf{E}^2(\mathbf{r}) \qquad (2.2.20a)$$
$$\hat{n}_1\times\mathbf{H}^1(\mathbf{r}) = \hat{n}_1\times\mathbf{H}^2(\mathbf{r}) \qquad (2.2.10b)$$
$$\hat{n}_2\times\mathbf{E}^3(\mathbf{r}) = 0 \qquad (2.2.20c)$$

with the equivalent surface currents defined as:

$$\frac{-\hat{n}_1\times\mathbf{E}^1(\mathbf{r})}{\eta_0} = \mathbf{M}^1(\mathbf{r}) \qquad (2.2.21a)$$
$$\hat{n}_1\times\mathbf{H}^1(\mathbf{r}) = \mathbf{K}^1(\mathbf{r}) \qquad (2.2.21b)$$
$$\hat{n}_2\times\mathbf{H}^3(\mathbf{r}) = \mathbf{K}^2(\mathbf{r}) \qquad (2.2.21c)$$

After matching boundary conditions and scaling by k_0 ,we have another set of coupled surface integral equations as follows:

For **r** on S_1:

$$\frac{4\pi}{\eta_0}\mathbf{E}^i(\mathbf{r})|_{tan} = \int_{S_1}[j\mathbf{K}^1(\Phi_0 + \mu_{r1}\Phi_1) + \mathbf{M}^1\times\nabla'(\Phi_0 + \Phi_1) - j\nabla'\cdot\mathbf{K}^1\ \nabla'(\Phi_0 + \frac{\Phi_1}{\varepsilon_{r1}})]\ dS'$$

$$+ \int_{S_2}[-j\mu_{r1}\mathbf{K}^2\Phi_1 + \frac{j}{\varepsilon_{r1}}\nabla'\cdot\mathbf{K}^2\nabla'\Phi_1]\ dS'|_{tan} \qquad (2.2.22a)$$

For $\mathbf{r}$ on S_2:

$$\int_{S_2}[j\mathbf{K}^2\mu_{r1}\Phi_1 - j\nabla'\cdot\mathbf{K}^2\nabla'\frac{\Phi_1}{\varepsilon_{r1}}]\ dS'|_{tan}$$

$$= \int_{S_1}[j\mu_{r1}\mathbf{K}^1\Phi_1 + \mathbf{M}^1\times\nabla'\Phi_1 - \frac{j}{\varepsilon_{r1}}\nabla'\cdot\mathbf{J}_e\ \nabla'\Phi_1]\ dS'|_{tan} \qquad (2.2.22b)$$

for $\mathbf{r}$ on S_1:

$$4\pi\mathbf{H}^i(\mathbf{r})|_{tan} = \int_{S_1}[j\mathbf{M}^1(\Phi_0 + \varepsilon_{r1}\Phi_1) - \mathbf{K}^1\times\nabla'(\Phi_0 + \Phi_1) + \frac{1}{j}\nabla'\cdot\mathbf{M}^1\ \nabla'(\Phi_0 + \frac{\Phi_1}{\mu_{r1}})]\ dS'$$

$$+ \int_{S_2}[\mathbf{K}^2\times\nabla'\Phi_1]\ dS'|_{tan} \qquad (2.2.22c)$$

where $\mu_{ri} = \frac{\mu_i}{\mu_0}$ and $\varepsilon_{ri} = \frac{\varepsilon_i'}{\varepsilon_0} = \varepsilon_{ri}' - j\frac{\sigma_i}{\omega\varepsilon_0}$. Due to the normalization with respect to k_0, the green's functions have the forms $\Phi_i = \frac{e^{-jk_{ri}R}}{R}$ and $k_{ri} = \frac{k_i}{k_0}$, the same forms as that of section 2.2.1.

On the surface S_2, only $\mathbf{K}^2$ is unknown because $\mathbf{M}^2$ equals zero. In this case, we have only three unknowns, $(\mathbf{K}^1,\mathbf{M}^1,\mathbf{K}^2)$. These three equations are sufficient to solve for the three unknowns.

2.2.4 Metallic Body with Partial Coating

A more general geometry than that of section 2.2.3 is a perfect conductor partially coated with a layer of dielectric, magnetic, and lossy material as shown in Fig. 2.5. $\mathbf{K}^1$ is the electric current on the uncoated area S_1 of the perfect conductor in region 1, and $\mathbf{K}^3$ denotes the electric current on the coated region S_3 of conducting body in region 2. $\mathbf{K}^2$ and $\mathbf{M}^2$ denotes the equivalent electric and magnetic currents on

the interface S_2 between free space and coated region in region 1. $\hat{n}$ denotes the unit outward vector of S_1 , S_2 and S_3 respectively as in Fig. 2.5. As S_1 shrinks to zero, we have a uniform coated conducting body which is the case of section 2.2.3. The study of the EM fields interacting with partially coated metallic body has its significance in the modification of the radar cross section of a radar target, and this topic has received considerable attentions recently.

We now consider the derivation of a set of coupled surface integral equations for the geometry of Fig. 2.5. Following the procedure previously, we will write the fields in the different regions and then use the boundary conditions to set up the coupled surface integral equations.

Define $\mathbf{K}_1^1 = \hat{n}\times\mathbf{H}_1$ on S_1 in region 1, $\mathbf{K}_1^2 = \hat{n}\times\mathbf{H}_2$ on S_2 in region 1 and $\mathbf{M}_1^2 = -\hat{n}\times\mathbf{E}_2$ on S_2 in region 1 as shown in Fig.2.6. We can then write the fields in region 1 $(\varepsilon_0,\sigma_0,\mu_0)$:

$$\mathbf{E}^1(\mathbf{r}) = T\,\mathbf{E}^i + \frac{T}{4\pi}\int_{S_1}[-j\omega\mu_0\mathbf{K}_1^1\Phi_0 + \frac{j}{\omega\varepsilon_0}\nabla'\cdot\mathbf{K}_1^1\,\nabla'\Phi_0]\,dS'$$
$$- \frac{T}{4\pi}\int_{S_2}[j\omega\mu_1\mathbf{K}_1^2\Phi_0 + \mathbf{M}_1^2\times\nabla'\Phi_1 - \frac{j}{\omega\varepsilon_1}\nabla'\cdot\mathbf{K}_1^2\,\nabla'\Phi_1]\,dS' \qquad (2.2.23a)$$

$$\mathbf{H}^1(\mathbf{r}) = T\,\mathbf{H}^i + \frac{T}{4\pi}\int_{S_2}[-j\omega\varepsilon_0\mathbf{M}_1^2\Phi_0 + \mathbf{K}_1^2\times\nabla'\Phi_0 + \frac{1}{j\omega\mu_0}\nabla'\cdot\mathbf{M}_1^2\,\nabla'\Phi_0]\,dS'$$
$$+ \frac{T}{4\pi}\int_{S_1}[\mathbf{K}_1^1\times\nabla'\Phi_0]\,dS' \qquad (2.2.23b)$$

Define $\mathbf{K}_2^2 = \hat{n}\times\mathbf{H}_2$ on S_2 in region 2, $\mathbf{M}_2^2 = -\hat{n}\times\mathbf{E}_2$ on S_2 in region 2 and $\mathbf{K}_2^3 = \hat{n}\times\mathbf{H}_3$ on S_3 in region 2 as Fig. 2.7. We can formulate the fields in region 2 $(\varepsilon_1,\sigma_1,\mu_1)$ as :

$$\mathbf{E}^2(\mathbf{r}) = -\frac{T}{4\pi}\int_{S_2}[-j\omega\mu_1\mathbf{K}_2^2\Phi_1 - \mathbf{M}_2^2\times\nabla'\Phi_1 + \frac{j}{\omega\varepsilon_1}\nabla'\cdot\mathbf{K}_2^2\,\nabla'\Phi_1]\,dS'$$
$$- \frac{T}{4\pi}\int_{S_3}[-j\omega\mu_1\mathbf{K}_2^3\Phi_1 + \frac{j}{\omega\varepsilon_1}\nabla'\cdot\mathbf{K}_2^3\,\nabla'\Phi_1]\,dS' \qquad (2.2.24a)$$

$$\mathbf{H}^2(\mathbf{r}) = \frac{T}{4\pi}\int_{S_2}[j\omega\varepsilon_1\mathbf{M}_2^2\Phi_1 - \mathbf{K}_2^2\times\nabla'\Phi_1 - \frac{1}{j\omega\mu_1}\nabla'\cdot\mathbf{M}_2^2\,\nabla'\Phi_1]\,dS'$$
$$+ \frac{T}{4\pi}\int_{S_3}[\,+\mathbf{K}_2^3\times\nabla'\Phi_1]\,dS' \qquad (2.2.24b)$$

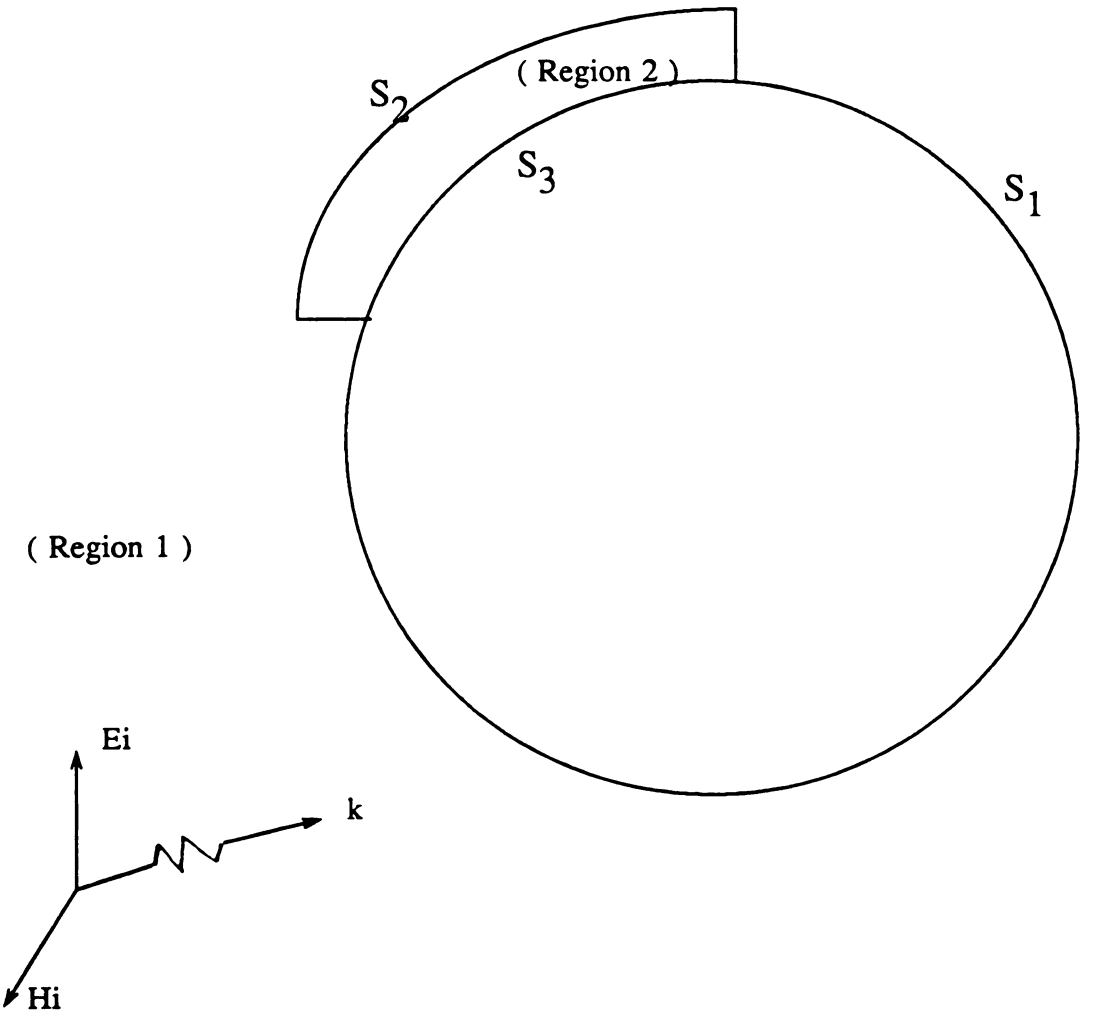

Fig. 2.5 A perfect conductor partially coated with lossy material

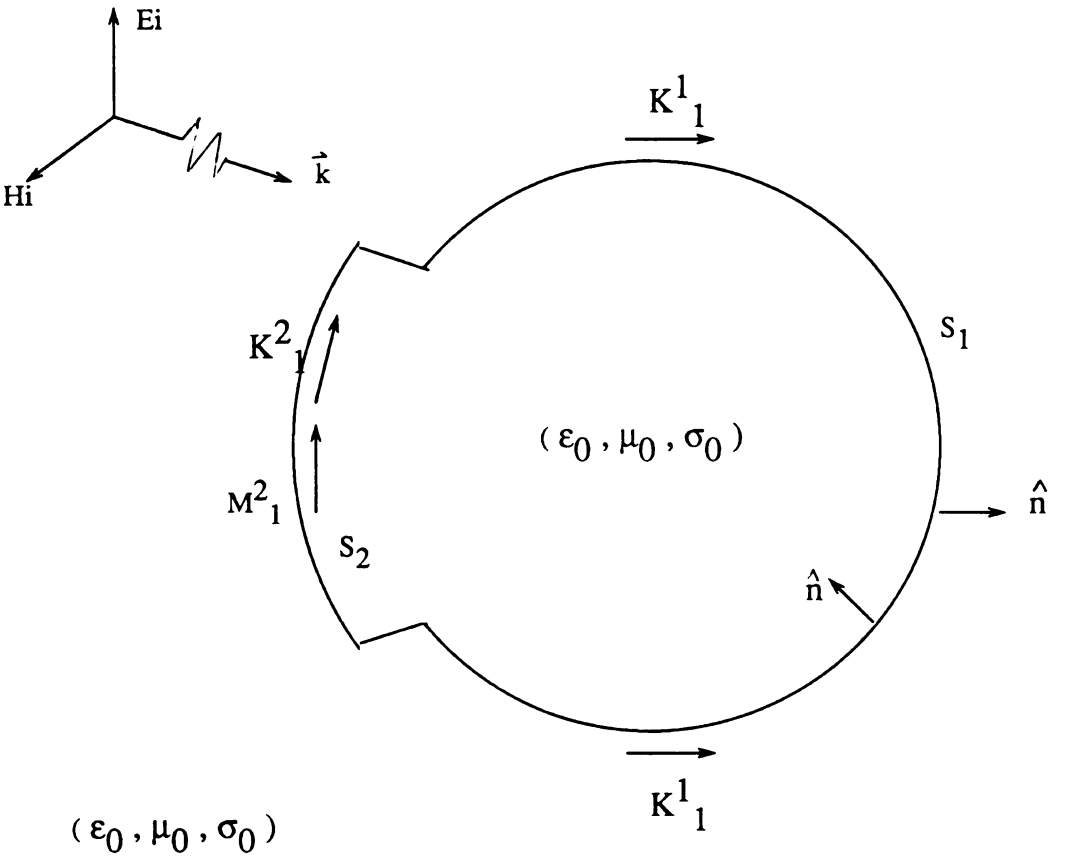

Fig. 2.6 Sources maintaining fields in region 1

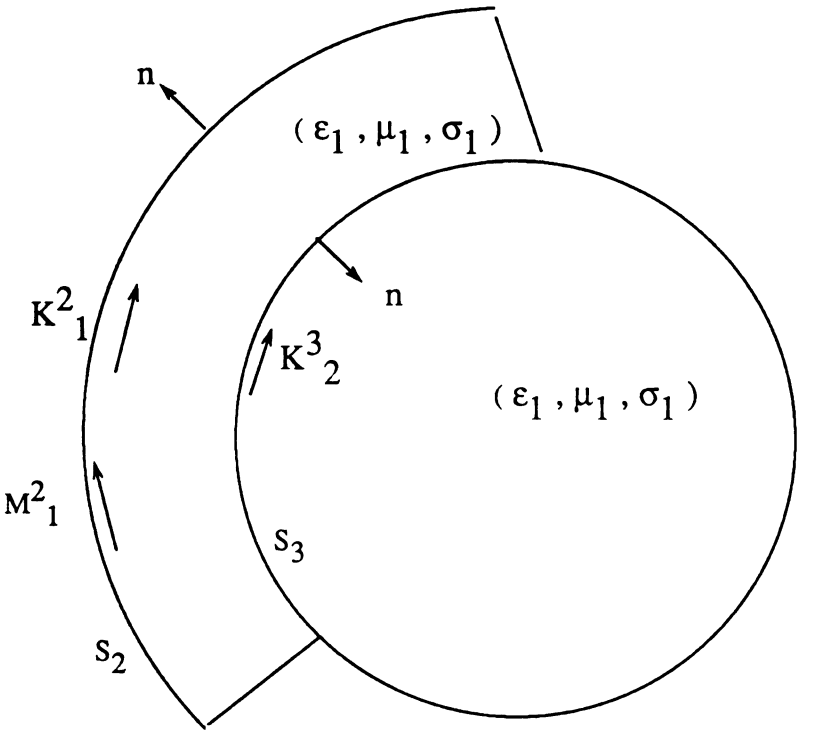

Fig. 2.7 Sources maintaining fields in region 2

where $\mathbf{K}_1^1$, $\mathbf{K}_1^2$ and $\mathbf{M}_1^2$ indicate equivalent currents on S_1 and S_2 in region 1, while $\mathbf{K}_2^2$, $\mathbf{M}_2^2$ and $\mathbf{K}_2^3$ indicate equivalent currents on S_2 and S_3 in region 2.

Since $\mathbf{K}_1^2 = \mathbf{K}_2^2$ and $\mathbf{M}_1^2 = \mathbf{M}_2^2$, we have only four unknowns, $\mathbf{K}_1^2$, $\mathbf{M}_1^2$, $\mathbf{K}_1^1$ and $\mathbf{K}_2^3$. For convenience, the subscripts of these four unknowns are omitted and they are referred to as $\mathbf{K}^2$, $\mathbf{M}^2$, $\mathbf{K}^1$ and $\mathbf{K}^3$. To determine these unknowns, four boundary conditions are required on the three interfaces, S_1, S_2, S_3 .

For $\mathbf{r}$ on S_2, tangential components of $\mathbf{E}$ and $\mathbf{H}$ are continuous across S_2 , i.e. $\mathbf{E}^1|_{tan} = \mathbf{E}^2|_{tan}$ and $\mathbf{H}^1|_{tan} = \mathbf{H}^2|_{tan}$ or alternatively $\mathbf{M}^1 = \mathbf{M}^2$ and $\mathbf{K}^1 = \mathbf{K}^2$. Applying these boundary conditions, we have:

$$
\begin{aligned}
4\pi\mathbf{E}^i(\mathbf{r})|\tan = \\
&\int_{S_2}[j\omega\mathbf{K}^2(\mu_0\Phi_0 + \mu_1\Phi_1) + \mathbf{M}^2\times\nabla'(\Phi_0 + \Phi_1) - \frac{j}{\omega}\nabla'\cdot\mathbf{K}^2\ \nabla'(\frac{\Phi_0}{\varepsilon_0} + \frac{\Phi_1}{\varepsilon_1})]\ dS' \\
&+ \int_{S_1}[j\omega\mu_0\mathbf{K}^1\Phi_0 + \frac{j}{\omega\varepsilon_0}\nabla'\cdot\mathbf{K}^1\nabla'\Phi_0]\ dS' \\
&+ \int_{S_3}[-j\omega\mu_1\mathbf{K}^3\Phi_1 + \frac{j}{\omega\varepsilon_1}\nabla'\cdot\mathbf{K}^3\nabla'\Phi_1]\ dS'|\tan
\end{aligned}
\qquad (2.2.25a)
$$

$$
\begin{aligned}
4\pi\mathbf{H}^i(\mathbf{r})|_{tan} = &\int_{S_2}[j\omega\mathbf{M}^2(\varepsilon_0\Phi_0+\varepsilon_1\Phi_1) - \mathbf{K}^2\times\nabla'(\Phi_0+\Phi_1) - \frac{j}{\omega}\nabla'\cdot\mathbf{M}^2\nabla'(\frac{\Phi_0}{\mu_0}+\frac{\Phi_1}{\mu_1})]\ dS' \\
&+ \int_{S_1}[-\mathbf{K}^1\times\nabla'\Phi_0]\ dS' \\
&+ \int_{S_3}[\mathbf{K}^3\times\nabla'\Phi_1]\ dS'|\tan
\end{aligned}
\qquad (2.2.25b)
$$

For $\mathbf{r}$ on S_3 , the tangential component of $\mathbf{E}$ is zero. Thus, we have :

$$
\begin{aligned}
0 = &\frac{1}{4\pi}\int_{S_2}[-j\omega\mu_1\mathbf{K}^2\Phi_1 - \mathbf{M}^2\times\nabla'\Phi_1 + \frac{j}{\omega\varepsilon_1}\nabla'\cdot\mathbf{K}^2\ \nabla'\Phi_1]\ dS' \\
&- \frac{1}{4\pi}\int_{S_3}[-j\omega\mu_1\mathbf{K}^3\Phi_1 + \frac{j}{\omega\varepsilon_1}\nabla'\cdot\mathbf{K}^3\ \nabla'\Phi_1]\ dS'|\tan
\end{aligned}
\qquad (2.2.26)
$$

For $\mathbf{r}$ on S_1 , again the tangential component of $\mathbf{E}$ is zero. From Eq.(2.2.23a) , it leads to:

$$4\pi \mathbf{E}^i(\mathbf{r})|_{\tan} = \int_{S_2} [j\omega\mu_0 \mathbf{K}^2 \Phi_0 + \mathbf{M}^2 \times \nabla' \Phi_0 - \frac{j}{\omega\varepsilon_0} \nabla' \cdot \mathbf{K}^2 \, \nabla' \Phi_0] \, dS'$$
$$+ \int_{S_1} [j\omega\mu_0 \mathbf{K}^1 \Phi_0 + \mathbf{M}^1 \times \nabla' \Phi_0 - \frac{j}{\omega\varepsilon_0} \nabla' \cdot \mathbf{K}^1 \, \nabla' \Phi_0] \, dS' \qquad (2.2.27)$$

We can scale these equations by the free space propagation constant k_0 and summarize them as follows:

For $\mathbf{r}$ on S_2 :

$$\frac{4\pi}{\eta_0} \mathbf{E}^i(\mathbf{r})|\tan = \int_{S_2} [j\mathbf{K}^2(\Phi_0 + \mu_{r1}\Phi_1) + \mathbf{M}^2 \times \nabla'(\Phi_0 + \Phi_1) - j\nabla' \cdot \mathbf{K}^2 \, \nabla'(\Phi_0 + \frac{\Phi_1}{\varepsilon_{r1}})] \, dS'$$
$$+ \int_{S_1} [j\mathbf{K}^0 \Phi_1 + j\nabla' \cdot \mathbf{K}^1 \nabla' \Phi_0] \, dS'$$
$$+ \int_{S_3} [-j\mu_{r1} \mathbf{K}^3 \Phi_1 + \frac{j}{\varepsilon_{r1}} \nabla' \cdot \mathbf{K}^3 \nabla' \Phi_1] \, dS'|\tan \qquad (2.2.28a)$$

$$4\pi \mathbf{H}^i(\mathbf{r})|\tan = \int_{S_2} [j\mathbf{M}^2(\Phi_0 + \varepsilon_{r1}\Phi_1) - \mathbf{K}^2 \times \nabla'(\Phi_0 + \Phi_1) + \frac{1}{j} \nabla' \cdot \mathbf{M}^2 \, \nabla'(\Phi_0 + \frac{\Phi_1}{\mu_{r1}})] \, dS'$$
$$+ \int_{S_1} [-\mathbf{K}^1 \times \nabla' \Phi_0] \, dS'$$
$$+ \int_{S_3} [\mathbf{K}^3 \times \nabla' \Phi_1] \, dS'|\tan \qquad (2.2.28b)$$

For $\mathbf{r}$ on S_3 :

$$0 = \frac{-1}{4\pi} \int_{S_2} [-j\mu_{r1} \mathbf{K}^2 \Phi_1 - \mathbf{M}^2 \times \nabla' \Phi_1 + \frac{j}{\varepsilon_{r1}} \nabla' \cdot \mathbf{K}^2 \, \nabla' \Phi_1] \, dS'$$
$$- \frac{1}{4\pi} \int_{S_3} [-j\mu_{r1} \mathbf{K}^3 \Phi_1 + \frac{j}{\varepsilon_{r1}} \nabla' \cdot \mathbf{K}^3 \, \nabla' \Phi_1] \, dS'|\tan \qquad (2.2.29)$$

For $\mathbf{r}$ on S_1 :

$$\frac{4\pi}{\eta_0} \mathbf{E}^i(\mathbf{r})|\tan = \int_{S_2} [j\mathbf{K}^2 \Phi_0 + \mathbf{M}^2 \times \nabla' \Phi_0 - j\nabla' \cdot \mathbf{K}^2 \, \nabla' \Phi_0] \, dS'$$
$$+ \int_{S_1} [j\mathbf{K}^1 \Phi_0 - j\nabla' \cdot \mathbf{K}^1 \, \nabla' \Phi_0] \, dS'|\tan \qquad (2.2.30)$$

The above equations can uniquely determine the four unknowns $\mathbf{K}^1$, $\mathbf{K}^2$, $\mathbf{K}^3$ and $\mathbf{M}^2$. As S_1 or S_3 shrinks to zero, two special cases are obtained as the cases of a perfect conductor with uniform coating or a perfect conductor without coating. Special

attention should be paid to the interface S_2 when a numerical scheme is applied, and this will be discussed later.

2.3 Numerical Algorithms

In the previous section, we have developed three sets of coupled surface integral equations. In this section, we will solve these coupled surface integral equations by the method of moments. Triangular elements are chosen to model arbitrarily-shaped surfaces. The advantages of triangular patch surface modeling have been elaboratly discussed in references[9,10]. Vector basis functions for the equivalent electric and magnetic currents are defined in each of the triangular surface patches, and a Galerkin method is implemented to solve for the unknown surface equivalent electric and magnetic current distributions.

2.3.1 Basis Function

Vector basis functions [8,10] are defined in this section both for electric current and magnetic current distributions. Detailed derivations of the basis functions are discussed in reference [10]. Figure 2.8 shows two triangles, T_n^+ and T_n^- with the n^{th} common edge. The electric and magnetic currents flow along radial direction, ρ_n^+, in triangle T_n^+, and similarly flows along radial direction, ρ_n^-, in triangle T_n^-. Referring to Figure 2.9, if l_n is the base lenth of common edge, then height lenths of triangles T_n^+ and T_n^- are respectively given by $2A_n^+/l_n$ and $2A_n^-/l_n$, where $A_n^\pm$ represents the areas of $T_n^\pm$. Any point in triangles $T_n^\pm$ can be conveniently defined either with respect to the global origin, 0, or with respect to vertices $0_n^\pm$. The plus or minus designation of the triangles is determined by the choice of a positive current reference direction [10] for the n^{th} edge, which is assumed to be from T_n^+ to T_n^-. We define a vector basis function associated with the n^{th} edge as

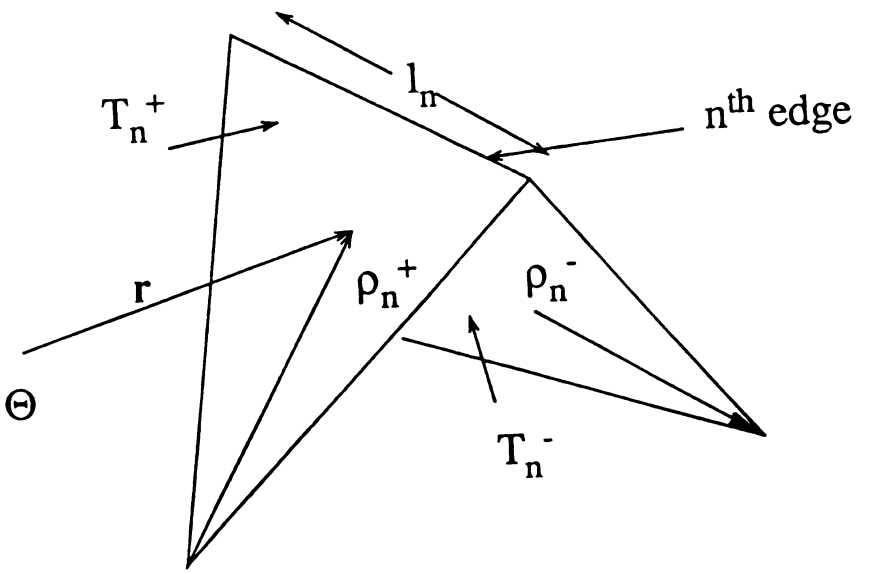

Figure 2.8 Local coordinates associated with an edge

$$\mathbf{f}_n(\mathbf{r}) = \begin{cases} \dfrac{l_n}{2A_n^+}\rho_n^+ & \mathbf{r} \quad in \quad T_n^+ \\ \dfrac{l_n}{2A_n^-}\rho_n^- & \mathbf{r} \quad in \quad T_n^- \\ 0 & otherwise \end{cases} \tag{2.3.1}$$

The vector basis function stated above is used to represent surface electric current, **K**, and surface magnetic current, **M**, on the triangulated surfaces of a given heterogeneous scatterer. Further mathematical properties of vector basis functions have been discussed in reference [10], and it gives some of the elegant properties in detail. In the following section, the main properties are summarized.

2.3.2 Properties of Vector Basis Function, $\mathbf{f}_n(\mathbf{r})$

(a) Along boundary edges, the currents flow basically parallel to the edges. Hence, they have no normal components to boundary, and no line charges exist along the boundary.

(b) The component of current normal to the n^{th} edge is constant and continuous across the edge as can be seen in Fig. 2.9, which shows that the normal components of $\rho_n^{\pm}$ along n^{th} is just the heights of triangles $T_n^{\pm}$ with edge n as the base and the height expressed as $(2A_n^{\pm})/l_n$. Using this term to normalize the vector basis, its normal component to the n^{th} edge, is unity. This result, together with a), implies that all edges of T_n^+ and T_n^- are free of line charges.

(c) The surface divergence of current basis function , which is, in fact, proportional to the corresponding surface charge density, is given by,

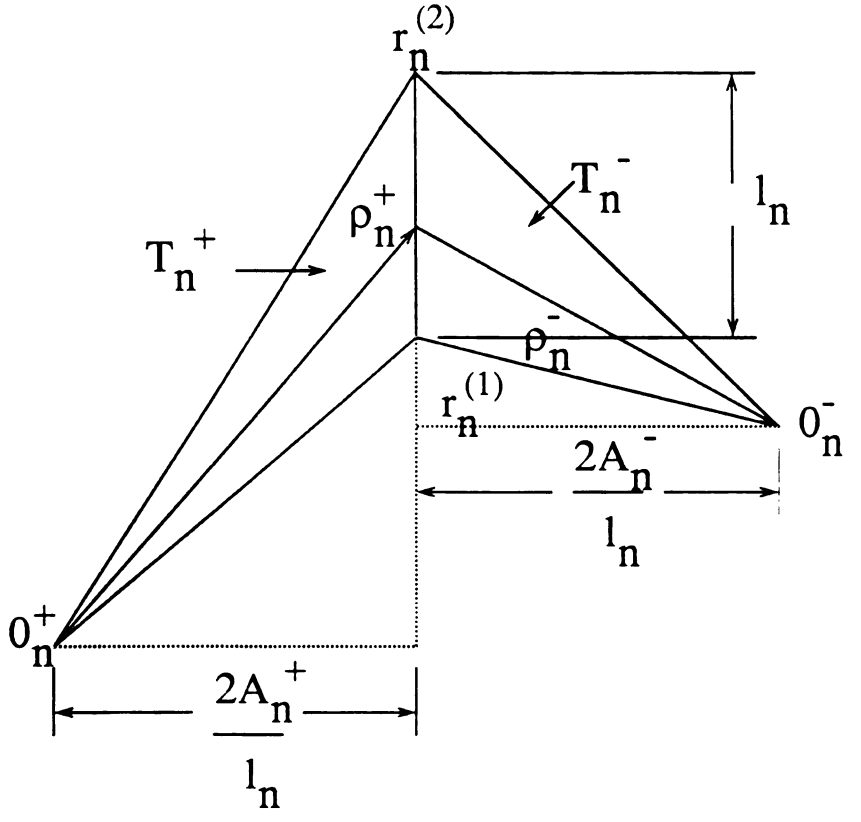

Fig. 2.9 Geometry for normal component of basis function at common edge

$$(\nabla_s \cdot \mathbf{f}_n(\mathbf{r})) = \begin{cases} \dfrac{l_n}{A_n^+} & \mathbf{r} \quad in \quad T_n^+ \\ \dfrac{l_n}{A_n^-} & \mathbf{r} \quad in \quad T_n^- \\ 0 & otherwise \end{cases} \tag{2.3.2}$$

The surface charge density is obviously constant in each triangle, total charge associated with the triangle pair T_n^+ and T_n^- is zero, and the basis functions for the charge evidently have the form of pulse doublets.

(d) The surface integral of basis function over adjacent triangles represents moment given by

$$\int_{T_n^+ + T_n^-} \int \mathbf{f}_n ds = \frac{l_n}{2}[\rho_n^{c+} + \rho_n^{c-}] \tag{2.3.3}$$
$$= l_n(\mathbf{r}_n^{c+} - \mathbf{r}_n^{-})$$

As shown in Fig 2.10, ρ_n^{c+} is the vector between the centroid of T_n^+ and 0_n^+ and ρ_n^{c-} is the vector between the centroid of T_n^- and 0_n^-. $\mathbf{r}_n^{c+}$ and $\mathbf{r}_n^{c-}$ are the distance vector to centroids of triangles T_n^+ and T_n^- from the global reference point, 0.

2.3.3 Testing Procedure and Matrix Equation

Either $(\mathbf{K}^1,\mathbf{M}^1,\mathbf{K}^2,\mathbf{M}^2)$ in section 2.2.2 or $(\mathbf{K}^1,\mathbf{M}^1,\mathbf{K}^2)$ in section 2.2.3, which need to be solved, are expanded in terms of vector basis functions defined in the previous section. If interfaces (S_1,S_2) are discretized into triangular patches with numbers of edges (N_1,N_2) respectively, then the equivalent currents can be represented by

$$\mathbf{K}^i(\mathbf{r}') = \sum_{n=1}^{N_i} I_n^i \mathbf{f}_n(\mathbf{r}') \tag{2.3.4}$$

and

$$\mathbf{M}^i(\mathbf{r}') = \sum_{n=1}^{N_i} M_n^i \mathbf{f}_n(\mathbf{r}') \tag{2.3.5}$$

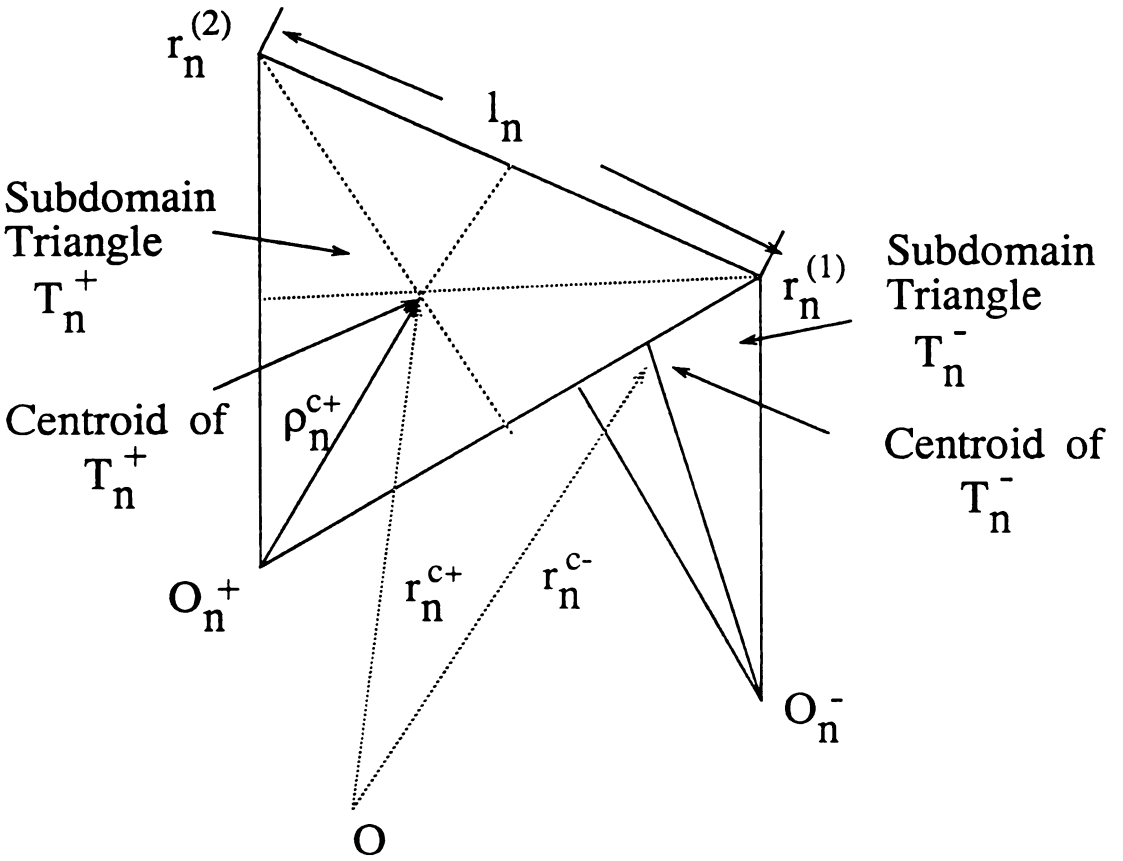

Fig. 2.10 Coordinate for calculating centroids and moment of basis vectors

where i = 1,2 for both **K** and **M** in section 2.2.2, and i = 1,2 for **K**, i = 1 for **M** in section 2.2.3. I_n^i and M_n^i are unknown coefficients to be determined. Since the normal component of $\mathbf{f}_n$ at the n^{th} common edge connecting T_n^+ and T_n^- is unity, each coefficient of I_n^i and M_n^i can be interpreted as the normal components of the electric and magnetic current densities flowing through the n^{th} edge. For a given triangular face, there exists three edges corresponding to three vector basis functions.

Substituting Eq.(2.3.4) and Eq.(2.3.5) into Eq.(2.2.15) and choosing the weighting function the same as the expansion function, Galerkin method, a matrix equation is formulated. Testing is enforced based on the following symmetric product to reduce the operator type integral equations to the corresponding functional type equations,

$$\langle \mathbf{f},\mathbf{g} \rangle = \iint_S \mathbf{f}\cdot\mathbf{g}\, ds \tag{2.3.6}$$

For the convenience to write the matrix equation into compact form, we define the electric and magnetic vector and scalar potentials as following:

$$\mathbf{A}_i = \int_S \mathbf{K}\, \Phi_i\, dS \tag{2.3.7a}$$

$$\mathbf{F}_i = \int_S \mathbf{M}\, \Phi_i\, dS \tag{2.3.7b}$$

$$V_i = \int_S \nabla'\cdot\mathbf{K}\, \nabla'\Phi_i\, dS \tag{2.3.7c}$$

$$U_i = \int_S \nabla'\cdot\mathbf{M}\, \nabla'\Phi_i\, dS \tag{2.3.7d}$$

and

$$\mathbf{P}_i = \int_S \mathbf{K}\times \nabla'\, \Phi_i\, dS \tag{2.3.7e}$$

$$\mathbf{Q}_i = \int_S \mathbf{M}\times \nabla'\, \Phi_i\, dS \tag{2.3.7f}$$

where i may vary from 0 to 2 in the case of section 2.2 or from 0 to 1 in the case of section 2.3.

The matrix equation for the coupled surface integral equations given in section

2.2.2 is:

$$\begin{bmatrix} Z_{11}^{EE} & Z_{12}^{EE} & C_{11}^{EM} & C_{12}^{EM} \\ Z_{21}^{EE} & Z_{22}^{EE} & C_{21}^{EM} & C_{22}^{EM} \\ D_{11}^{ME} & D_{12}^{EE} & Y_{11}^{MM} & Y_{12}^{MM} \\ D_{21}^{ME} & D_{22}^{EE} & Y_{21}^{MM} & Y_{22}^{MM} \end{bmatrix}_{2N\times 2N} \begin{bmatrix} I_1 \\ I_2 \\ M_1 \\ M_2 \end{bmatrix} = \begin{bmatrix} E \\ [0] \\ H \\ [0] \end{bmatrix} \tag{2.3.8}$$

where '1' indicates the outer surface or S_1 and '2' for the inner surface or S_2 , 'E' stands for EFIE and 'M' for MFIE. Z,Y,C and D are submatrices with size N_{1or2} by N_{1or2}. The system matrix size is 2N by 2N with $N = N_1 + N_2$. I, M, V and H are vectors with lengths of N_1 or N_2, and [0] is N_2 - zero vector . I, M are unknown vectors which will be solved for. The various matrix elements are given by the following expressions :

$$(Z_{11}^{EE})_{mn} = jl_m\left\{\frac{\rho_m^{c+}}{2}\cdot \sum_{i=0}^{1} \mu_{ri}A_{imn}^{+} + \frac{\rho_m^{c-}}{2}\cdot \sum_{i=0}^{1} \mu_{ri}A_{imn}^{-} + \sum_{i=0}^{1} \frac{1}{\varepsilon_{ri}}(V_{imn}^{+} - V_{imn}^{-})\right\} \tag{2.3.9a}$$

$$(Z_{12}^{EE})_{mn} = -jl_m\left\{\frac{\rho_m^{c+}}{2}\cdot \mu_{r1}A_{1mn}^{+} + \frac{\rho_m^{c-}}{2}\cdot \mu_{r1}A_{1mn}^{-} + \frac{1}{\varepsilon_{r1}}(V_{1mn}^{+} - V_{1mn}^{-})\right\} \tag{2.3.9b}$$

$$(Z_{21}^{EE})_{mn} = jl_m\left\{\frac{\rho_m^{c+}}{2}\cdot \mu_{r1}A_{1mn}^{+} + \frac{\rho_m^{c-}}{2}\cdot \mu_{r1}A_{1mn}^{-} + \frac{1}{\varepsilon_{r1}}(V_{1mn}^{+} - V_{1mn}^{-})\right\} \tag{2.3.9c}$$

$$(Z_{22}^{EE})_{mn} = -jl_m\left\{\frac{\rho_m^{c+}}{2}\cdot \sum_{i=1}^{2} \mu_{ri}A_{imn}^{+} + \frac{\rho_m^{c-}}{2}\cdot \sum_{i=1}^{2} \mu_{ri}A_{imn}^{-} + \sum_{i=1}^{2} \frac{1}{\varepsilon_{ri}}(V_{imn}^{+} - V_{imn}^{-})\right\} \tag{2.3.9d}$$

$$(Y_{11}^{MM})_{mn} = jl_m\left\{\frac{\rho_m^{c+}}{2}\cdot \sum_{i=0}^{1} \varepsilon_{ri}F_{imn}^{+} + \frac{\rho_m^{c-}}{2}\cdot \sum_{i=0}^{1} \varepsilon_{ri}F_{imn}^{-} + \sum_{i=0}^{1} \frac{1}{\mu_{ri}}(U_{imn}^{+} - U_{imn}^{-})\right\} \tag{2.3.9e}$$

$$(Y_{12}^{MM})_{mn} = -jl_m\left\{\frac{\rho_m^{c+}}{2}\cdot\ \varepsilon_{r1}\mathbf{F}_{1mn}^{+} + \frac{\rho_m^{c-}}{2}\cdot\ \varepsilon_{r1}\mathbf{F}_{1mn}^{-} + \frac{1}{\mu_{r1}}(U_{1mn}^{+} - U_{1mn}^{-})\right\} \tag{2.3.9f}$$

$$(Y_{21}^{MM})_{mn} = jl_m\left\{\frac{\rho_m^{c+}}{2}\cdot\ \varepsilon_{r1}\mathbf{F}_{1mn}^{+} + \frac{\rho_m^{c-}}{2}\cdot\ \varepsilon_{r1}\mathbf{F}_{1mn}^{-} + \frac{1}{\mu_{r1}}(U_{1mn}^{+} - U_{1mn}^{-})\right\} \tag{2.3.9g}$$

$$(Y_{22}^{MM})_{mn} = -jl_m\left\{\frac{\rho_m^{c+}}{2}\cdot\sum_{i=1}^{2}\varepsilon_{ri}\mathbf{F}_{imn}^{+} + \frac{\rho_m^{c-}}{2}\cdot\sum_{i=1}^{2}\varepsilon_{ri}\mathbf{F}_{imn}^{-} + \sum_{i=1}^{2}\frac{1}{\mu_{ri}}(U_{imn}^{+} - U_{imn}^{-})\right\} \tag{2.3.9h}$$

$$(C_{11}^{EM})_{mn} = \left\{\sum_{i=0}^{1}P_{imn}^{+} + \sum_{i=0}^{1}P_{imn}^{-}\right\}$$

$$= -(D_{11}^{MM})_{mn} \tag{2.3.9i}$$

$$(C_{12}^{EM})_{mn} = -\left\{P_{1mn}^{+} + P_{1mn}^{-}\right\}$$

$$= -(D_{12}^{MM})_{mn} \tag{2.3.9j}$$

$$(C_{21}^{EM})_{mn} = \left\{P_{1mn}^{+} + P_{1mn}^{-}\right\}$$

$$= -(D_{21}^{MM})_{mn} \tag{2.3.9k}$$

$$(C_{22}^{EM})_{mn} = -\left\{\sum_{i=1}^{2}P_{imn}^{+} + \sum_{i=1}^{2}P_{imn}^{-}\right\}$$

$$= -(D_{22}^{MM})_{mn} \tag{2.3.9l}$$

$$E_m = \frac{4\pi\, l_m}{\eta_0}\left[\frac{\rho_m^{c+}}{2}\cdot\mathbf{E}^{i+} + \frac{\rho_m^{c-}}{2}\cdot\mathbf{E}^{i-}\right] \tag{2.3.10a}$$

$$H_m = -4\pi\, l_m\left[\frac{\rho_m^{c+}}{2}\cdot\mathbf{H}^{i+} + \frac{\rho_m^{c-}}{2}\cdot\mathbf{H}^{i-}\right] \tag{2.3.10b}$$

For convenience, we write the matrix elements by testing at the centroids of the triangles, which is a special case of the general Galerkin method discussed.

Next, we consider the set of coupled surface integral equations in section 2.2.3 when a perfect conductor is inside the body. Similarly for the Eq.(2.2.22), the matrix equation can be formed as follows:

$$\begin{bmatrix} Z_{11}^{EE} & Z_{12}^{EE} & C_{11}^{EM} \\ Z_{21}^{EE} & Z_{22}^{EE} & C_{21}^{EM} \\ D_{11}^{ME} & D_{12}^{EE} & Y_{11}^{MM} \end{bmatrix} \begin{bmatrix} I_1 \\ I_2 \\ M_1 \end{bmatrix} = \begin{bmatrix} E \\ [0] \\ H \end{bmatrix} \tag{2.3.11}$$

Only a small modification of matrix elements in previous case will be needed to obtain the matrix elements for this problem.

$$(Z_{11}^{EE})_{mn} = jl_m \left\{ \frac{\rho_m^{c+}}{2} \cdot \sum_{i=0}^{1} \mu_{ri} A_{imn}^{+} + \frac{\rho_m^{c-}}{2} \cdot \sum_{i=0}^{1} \mu_{ri} A_{imn}^{-} + \sum_{i=0}^{1} \frac{1}{\epsilon_{ri}} (V_{imn}^{+} - V_{imn}^{-}) \right\} \tag{2.3.12a}$$

$$(Z_{12}^{EE})_{mn} = -jl_m \left\{ \frac{\rho_m^{c+}}{2} \cdot \mu_{r1} A_{1mn}^{+} + \frac{\rho_m^{c-}}{2} \cdot \mu_{r1} A_{1mn}^{-} + \frac{1}{\epsilon_{r1}} (V_{1mn}^{+} - V_{1mn}^{-}) \right\} \tag{2.3.12b}$$

$$(Z_{21}^{EE})_{mn} = jl_m \left\{ \frac{\rho_m^{c+}}{2} \cdot \mu_{r1} A_{1mn}^{+} + \frac{\rho_m^{c-}}{2} \cdot \mu_{r1} A_{1mn}^{-} + \frac{1}{\epsilon_{r1}} (V_{1mn}^{+} - V_{1mn}^{-}) \right\} \tag{2.3.12c}$$

$$(Z_{22}^{EE})_{mn} = -jl_m \left\{ \frac{\rho_m^{c+}}{2} \cdot \sum_{i=0}^{1} \mu_{ri} A_{imn}^{+} + \frac{\rho_m^{c-}}{2} \cdot \sum_{i=0}^{1} \mu_{ri} A_{imn}^{-} + \sum_{i=0}^{1} \frac{1}{\epsilon_{ri}} (V_{imn}^{+} - V_{imn}^{-}) \right\} \tag{2.3.12d}$$

$$(Y_{11}^{MM})_{mn} = jl_m \left\{ \frac{\rho_m^{c+}}{2} \cdot \sum_{i=0}^{1} \epsilon_{ri} F_{imn}^{+} + \frac{\rho_m^{c-}}{2} \cdot \sum_{i=0}^{1} \epsilon_{ri} F_{imn}^{-} + \sum_{i=0}^{1} \frac{1}{\mu_{ri}} (U_{imn}^{+} - U_{imn}^{-}) \right\} \tag{2.3.12e}$$

$$(C_{11}^{EM})_{mn} = \left\{ \sum_{i=0}^{1} P_{imn}^{+} + \sum_{i=0}^{1} P_{imn}^{-} \right\} = -(D_{11}^{MM})_{mn} \tag{2.3.12f}$$

$$(C_{21}^{EM})_{mn} = \left\{ P_{1mn}^{+} + P_{1mn}^{-} \right\}$$

$$= -(D_{21}^{MM})_{mn} \tag{2.3.12g}$$

$$E_m = \frac{4\pi\, l_m}{\eta_0} \left[\frac{\rho_m^{c+}}{2} \cdot \mathbf{E}^{i+} + \frac{\rho_m^{c-}}{2} \cdot \mathbf{E}^{i-} \right] \tag{2.3.13a}$$

$$H_m = -4\pi\, l_m \left[\frac{\rho_m^{c+}}{2} \cdot \mathbf{H}^{i+} + \frac{\rho_m^{c-}}{2} \cdot \mathbf{H}^{i-} \right] \tag{2.3.13b}$$

Now we move to partial coated perfect conductor as described in Eq.(2.2.28-2.2.30). The matrix structure can be written in a form as below:

$$\begin{bmatrix} Z_{33}^{EE} & [0] & Z_{32}^{EE} & C_{32}^{EM} \\ [0] & Zsub11^{EE} & Z_{12}^{EE} & C_{12}^{EM} \\ Z_{23}^{EE} & Z_{21}^{EE} & Z_{22}^{EE} & C_{22}^{EM} \\ D_{23}^{ME} & D_{21}^{ME} & D_{22}^{ME} & Y_{22}^{MM} \end{bmatrix} \begin{bmatrix} I_3 \\ I_1 \\ I_2 \\ M_2 \end{bmatrix} = \begin{bmatrix} [0] \\ E_1^i \\ E_2^i \\ H_2^i \end{bmatrix} \tag{2.3.14}$$

where the lower subscript indicates the numbering of the surfaces and upper subscript for distinguishing EFIE and MFIE, for example, Z_{33}^{EE} denotes source points and field points are both on S_3 by EFIE. Special attention should be paid for the fields on S_2 when a numerical scheme is applied. In our case, the boundary conditions for perfect conducting surface got to be applied to the triangle edges on S_2 which have connections with perfect conductor surface as illustrated in Fig.2.5.

The matrix elements have similar expressions as previous two cases, and will not exhibited here to avoid repetition.

The vector and the scalar potential integrals take the following forms:

$$\mathbf{A}_{imn}^{\pm} = \int\int_{(T_n^+ T_n^-)} \mathbf{f}_n(\mathbf{r}') \Phi_i(\mathbf{r}_m^{c\pm}, \mathbf{r}')\, dS' \tag{2.3.15a}$$

$$= \mathbf{F}_{imn}^{\pm}$$

$$V_{imn}^{\pm} = \int\int_{(T_n^+ T_n^-)} [\nabla' \cdot \mathbf{f}_n(\mathbf{r}')] \Phi_i(\mathbf{r}_m^{c\pm}, \mathbf{r}')\, dS' \tag{2.3.15b}$$

$$= U_{imn}^{\pm}$$

$$P_{imn}^{\pm} = \frac{l_m}{2A_m^{\pm}} \int\int_{T_m^{\pm}} \rho_m^{\pm} \cdot \left[\int\int_{(T_n^{+}T_n^{-})} \mathbf{f}_n(\mathbf{r}') \times \nabla' \Phi_i(\mathbf{r}_m^{c\pm}, \mathbf{r}') dS' \right] \tag{2.3.15c}$$

$$= Q_{imn}^{\pm}$$

and

$$\Phi_i(\mathbf{r}_m^{\pm}, \mathbf{r}') = \frac{e^{-jk_i R^{\pm}}}{R^{\pm}}$$

$$R^{\pm} = |\mathbf{r}_m^{\pm} - \mathbf{r}'|$$

$$\nabla' \Phi_i(\mathbf{r}_m^{c\pm}, \mathbf{r}') = (\mathbf{r}_m^{\pm} - \mathbf{r}')(1 + jk_i R^{\pm}) \frac{e^{-jk_i R^{\pm}}}{(R^{\pm})^3}$$

The above integrals are in a convenient form for numerical evaluation. However, each face has three edges associated with it. Identical integrals would be recomputed nine times if the elements were computed sequentially by edges. To avoid the costly and inefficient recomputation of integrals, we instead compute the various matrix elements by considering faces. This cuts down by approximately ninefold computer the time required to generate matrix elements. Morever, we note that elements of Z and Y only differ from each other by the appropriate coefficients which can be conveniently incorporated while filling matrix elements. Similarly for the elements of C and D, they are similar except by a multiplying constant such that elements of D can be directly obtained from the elements of C and vice versa.

We note also that the expressions of the submatrix elements contain terms belonging to different regions. These expressions of integrals are identical except for the characteristic parameters which appear in the propagation constants and in the multiplication constants. For numerical efficience, we use the same routine to generate the integrals in the different regions simultaneously which principally, make up various matrix elements.

In accordance with the above discussion, we now consider the evaluation of the various integrals. As illustrated in Fig.2.11, assume that an observation point in face p

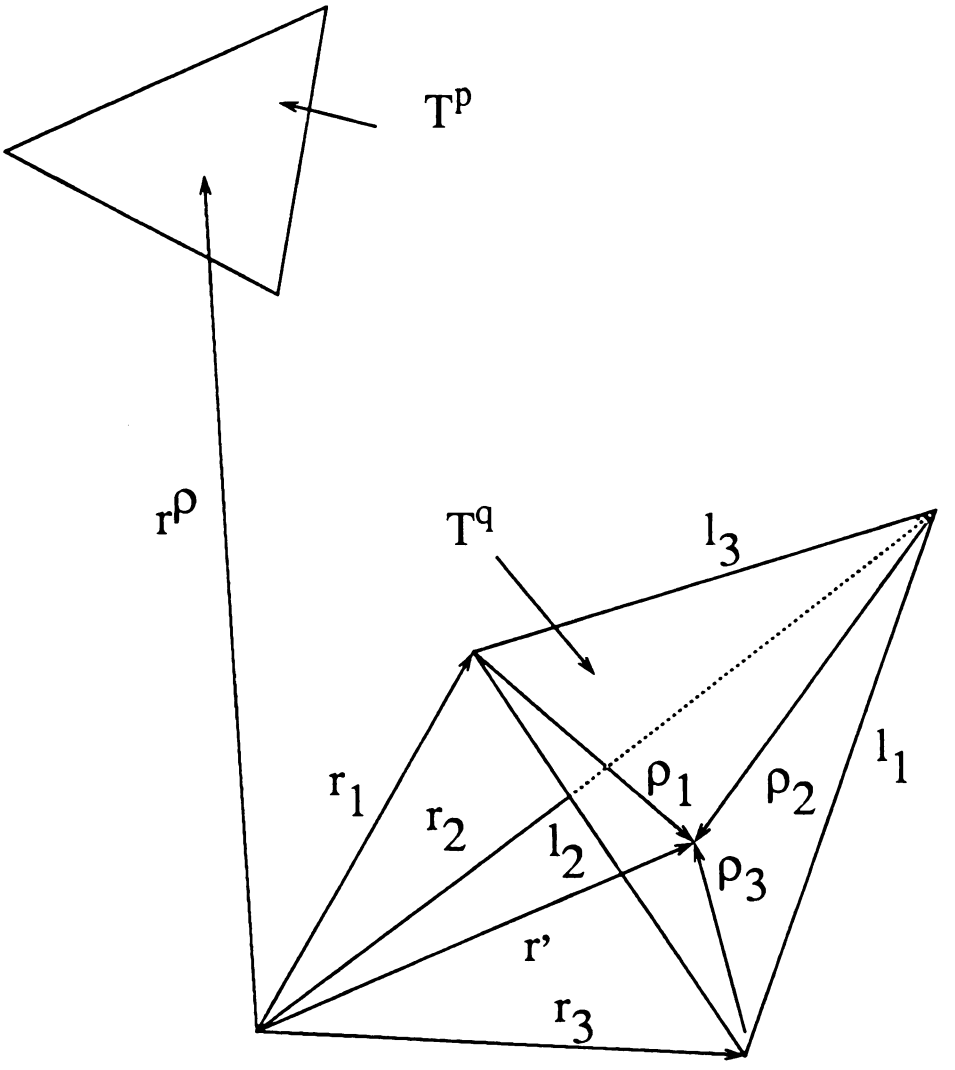

Fig. 2.11 Local coordinates and edges for source triangle T^q with observation point in triangle T^p.

and a source point residing in face q. Let's use a " local indexing scheme " for convenience. We number the edges of face q by 1, 2, 3 with edge length l_1,l_2, and l_3, and opposite vertices at $\mathbf{r}_1$,$\mathbf{r}_2$,$\mathbf{r}_3$, respectively. Face q will be denoted simply as triangle T^q with area A^q , and face p as T^p with area A^p. There are three integrals which essentially make up various matrix elements:

$$\int_{T^p} \mathbf{f}_j \cdot \mathbf{A}_i^q \, dS = \int_{T^p} \mathbf{f}_j \cdot \int_{T^q} \mathbf{f}_i(\mathbf{r}') \frac{e^{-jkR^p}}{R^p} \, dS' \tag{2.3.16a}$$

$$\int_{T^p} V_i^{pq} \, dS = \int_{T^p} (\frac{l_j}{A^p}) \int_{T^q} (\frac{l_i}{A^q}) \frac{e^{-jkR^p}}{R^p} \, dS' \tag{2.3.16b}$$

$$P_{imn}^{\pm} = \frac{l_m}{2A_m^{\pm}} \int\int_{T^p} \rho_m^{\pm} \cdot \left[\int\int_{T^q} \mathbf{f}_i(\mathbf{r}') \times \nabla' \Phi_i(\mathbf{r}^p, \mathbf{r}') dS' \right] \tag{2.3.16c}$$

and

$$R^p = |\mathbf{r}^p - \mathbf{r}'|$$

These three integrals are most conveniently evaluated by transforming to a local system of area coordinates [14]. As shown in Fig. 2.12, the vector ρ_i divide T^q into three regions of areas A_1, A_2, andA_3 which are constrained to satisfy $A_1+A_1+A_3 = A^q$. The normalized area coordinates are defined as

$$\xi = \frac{A_1}{A^q}, \eta = \frac{A_2}{A^q}, \zeta = \frac{A_3}{A^q}, \tag{2.3.17}$$

and

$$\xi + \eta + \zeta = 1. \tag{2.3.18}$$

(ξ, η, ζ) vary between zero and unit in T^q, and the triangle corners $\mathbf{r}_1$, $\mathbf{r}_2$ and $\mathbf{r}_3$, corresponding to the area coordinate (ξ,η,ζ) takes the values (1, 0, 0), (0, 1, 0), and (0, 0, 1) , respectively. The transformation from Cartesian to area coordinates may be written in vector form as

$$\mathbf{r}' = \xi \mathbf{r}_1 + \eta \mathbf{r}_2 + \zeta \mathbf{r}_3 \tag{2.3.19}$$

and surface integrals over T^q can be transformed as follows:

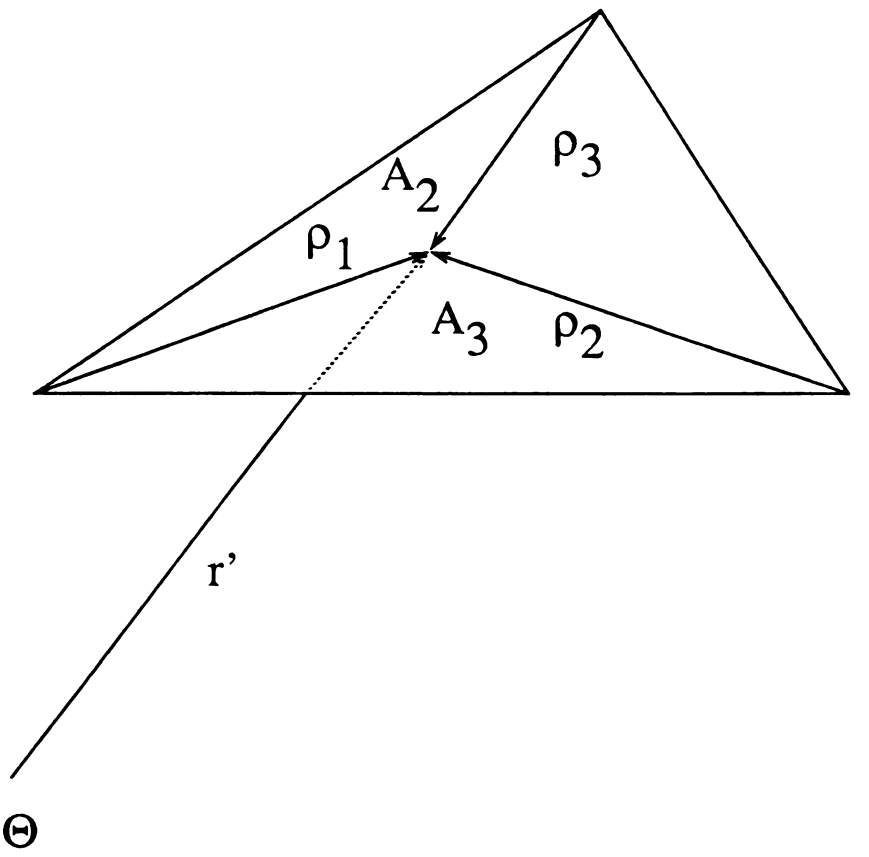

Fig. 2.12 Definitions of areas used in defining area coordinates

$$\int_{T^q} g(\mathbf{r})dS = 2A^q \int_0^1 \int_0^{1-\eta} g(\xi \mathbf{r}_1 + \eta \mathbf{r}_2 + (1-\xi-\eta)\mathbf{r}_3)d\xi d\eta. \qquad (2.3.20)$$

Numerical evaluation of the integrals in Eq.(2.3.16) may be accomplished by using numerical quadrature techniques specially developed for triangular domains [15] together with the procedures discussed in reference [10]. Appendix B carries out these three integrals (2.3.16) numerically in details.

2.4 Numerical Results

In this section, numerical results are presented for the equivalent electric and magnetic current distributions on some selected scatterers under plane wave illumination. The geometries considered are heterogeneous concentric spheres and a perfect conducting sphere with coating. To demonstrate applicability of the above formulation and to validate computer algorithms, numerical results for the concentric spheres are presented and compared with the exact solution of Mie series.

As the first example, an electrically-small two-layered sphere is investigated. The electric size of the inner sphere is $k_0 a_1 = 0.0595$ where $k_0 = \frac{2\pi}{\lambda}$ is free space propagation constant and a_1 is the radius of the inner sphere; For the outer surface, $k_0 a_2 = 0.13$ where a_2 is the radius of the outer sphere. The inner sphere has the relative dielectric constant of $\varepsilon_{r1} = 16$, lossy tangent $\tan(\delta) = 0.39$ and relative permeability $u_r = 4$. In the region between S_1 and S_2, the relative dielectric constant is $\varepsilon_{r2} = 9$. The inner and outer surfaces are modeled by 92 triangular patches respectively. There are in total 192 triangles consisting of 288 edges which result in a matrix size of 576 by 576. A plane wave is axially incident along the positive z direction. In Fig.2.13 to Fig. 2.20, equivalent electric and magnetic currents are shown along two circumferential priciple arcs that means that the θ component of **K** and the ϕ component of **M** are plotted

along the arc in $\phi = 0$ plane, and the ϕ component of **K** and the θ component of **M** are plotted along the arc in $\phi = \frac{\pi}{2}$ plane. In Fig. 2.13 to 2.16, ($\mathbf{K}_\theta^1$, $\mathbf{K}_\phi^1$, $\mathbf{M}_\theta^1$, $\mathbf{M}_\phi^1$) are the four components of equivalent currents on the outer surface S_1. In Fig. 2.17 to 2.20, ($\mathbf{K}_\theta^2$, $\mathbf{K}_\phi^2$, $\mathbf{M}_\theta^2$, $\mathbf{M}_\phi^2$) are the four components of equivalent currents on the inner surface S_2. The numerical solutions of all these eight components have very good agreement with the Mie series solutions.

Consider next a perfectly conducting sphere coated with a layer of dielectric, magnetic, and lossy material as the second example. The electric size of a perfectly conducting sphere is $k_0 a = 0.4\pi$ and the thickness of the layer is 0.1π . First, we consider a perfectly conducting sphere coated with a layer of air. Figs. 2.20 to 2.24 show the four equivalent current distributions ($\mathbf{K}_\theta^1$, $\mathbf{K}_\phi^1$, $\mathbf{M}_\theta^1$, $\mathbf{M}_\phi^1$) on the outer surface S_1, and two current distributions ($\mathbf{K}_\theta^1$, $\mathbf{K}_\phi^1$) on the perfectly conducting sphere are shown in Fig. 2.25 &2.26. This special case is used to check the coupled surface integral equations and the results are the same as that from electric field integral equation for a perfectly conducting sphere. All the results also agree very well with exact solutions. Next, a perfectly conducting sphere coated with a dielectric layer $\varepsilon_r = 4$ is considered. Again, all the six components on the outsuface and on the perfectly conducting sphere are plotted in Fig.2.27 to 2.32, and the results agree very well with exact solution. In the last case, the numerical results for a perfectly conducting sphere coated with a layer of magnetic material $\mu_r = 4$ are shown in Fig.2.33 to 2.38. Again all the six components have good correspondence to the exact solutions.

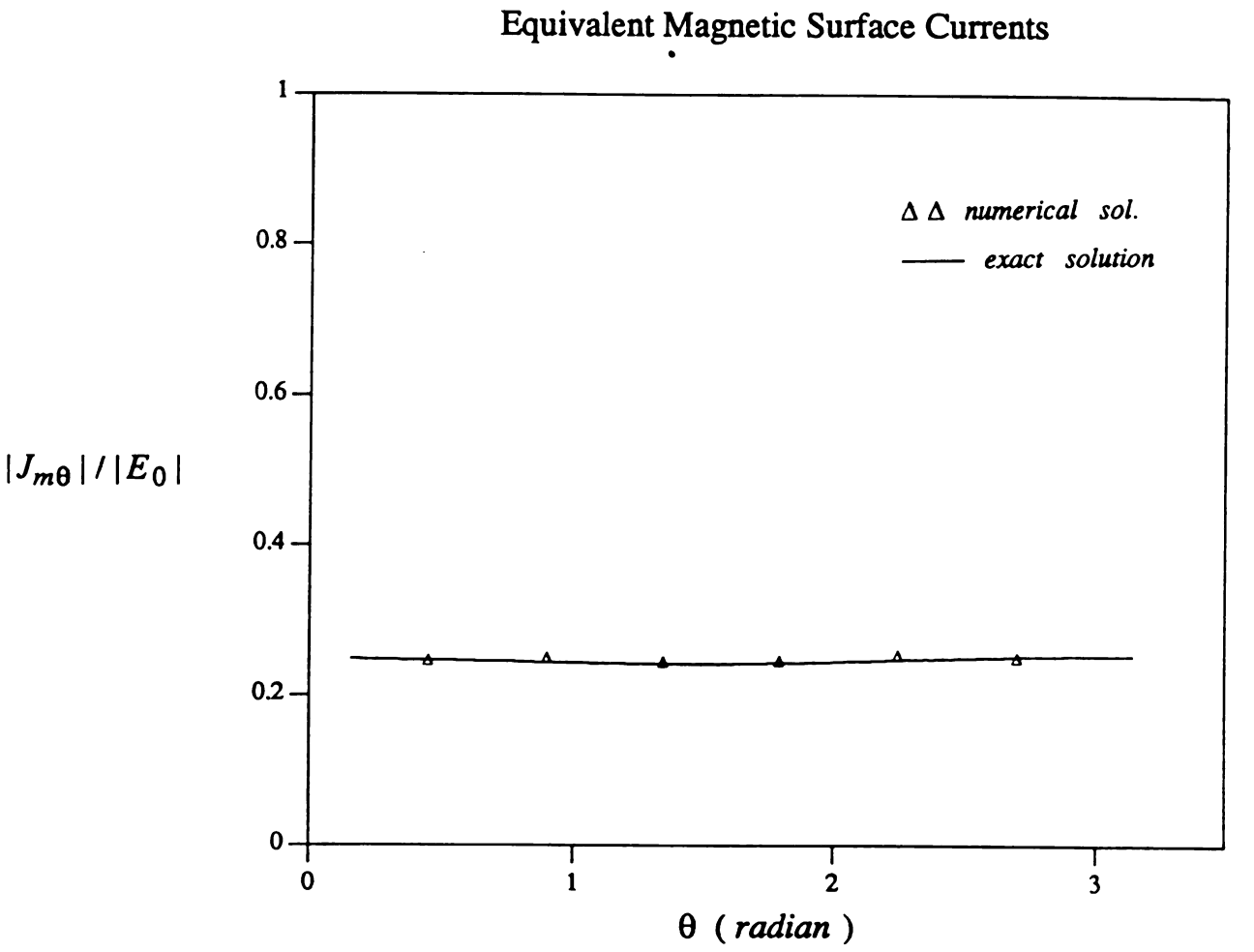

Figure 2.13 θ-component of equivalent magnetic current on the outer surface S_1 of a concentric sphere with:

($k_0a_2 = 0.0595$; $\varepsilon_{r2} = 16.0$; $\mu_{r2} = 4.0$; $\tan(\delta_2) = 0.39$)

($k_0a_1 = 0.13$; $\varepsilon_{r1} = 9.0$; $\mu_{r1} = 1.0$; $\tan(\delta_1) = 0.0$)

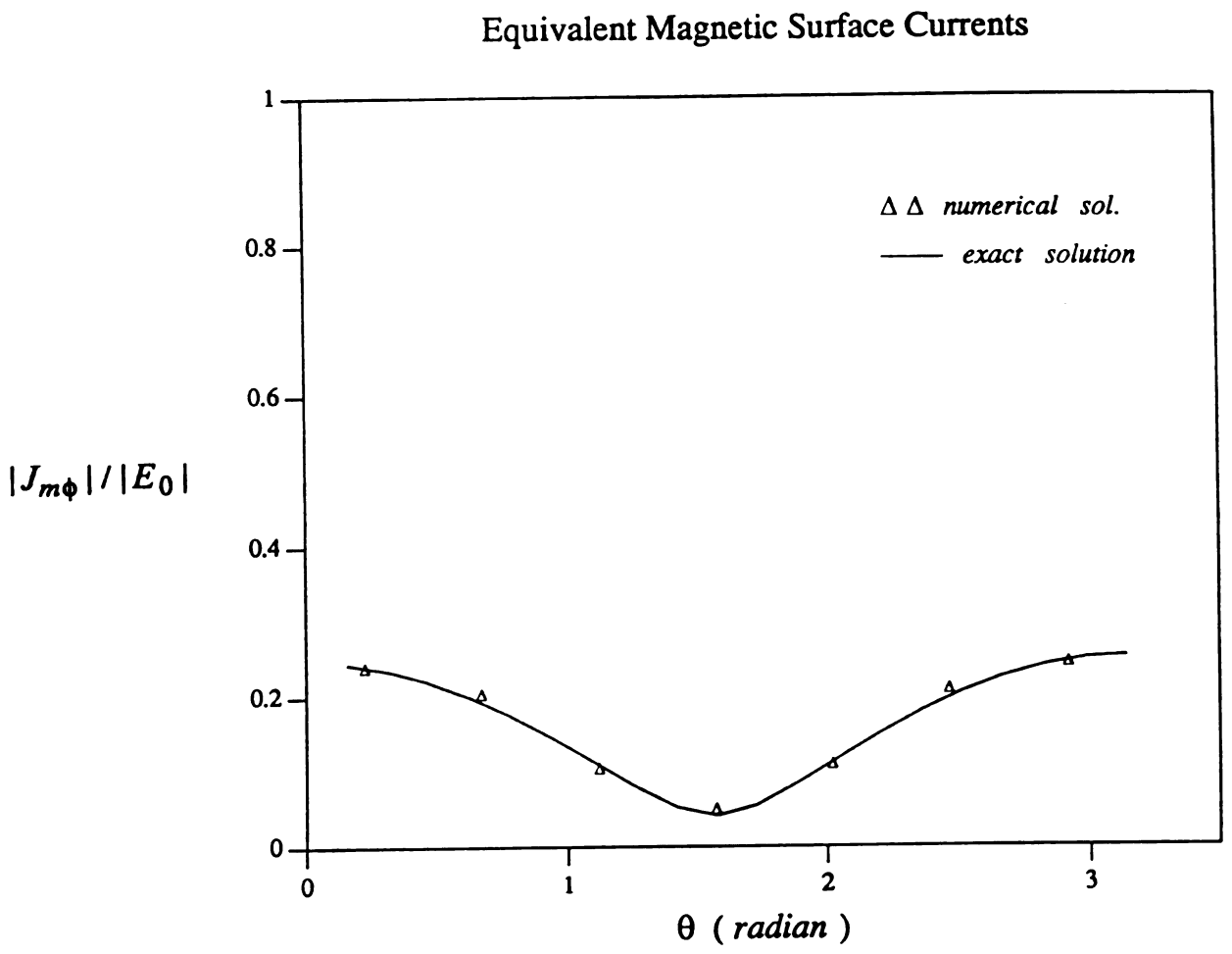

Figure 2.14 ϕ-component of equivalent magnetic current on the outer surface S_1 of a concentric sphere with:

($k_0 a_2 = 0.0595$; $\varepsilon_{r2} = 16.0$; $\mu_{r2} = 4.0$; $\tan(\delta_2) = 0.39$)

($k_0 a_1 = 0.13$; $\varepsilon_{r1} = 9.0$; $\mu_{r1} = 1.0$; $\tan(\delta_1) = 0.0$)

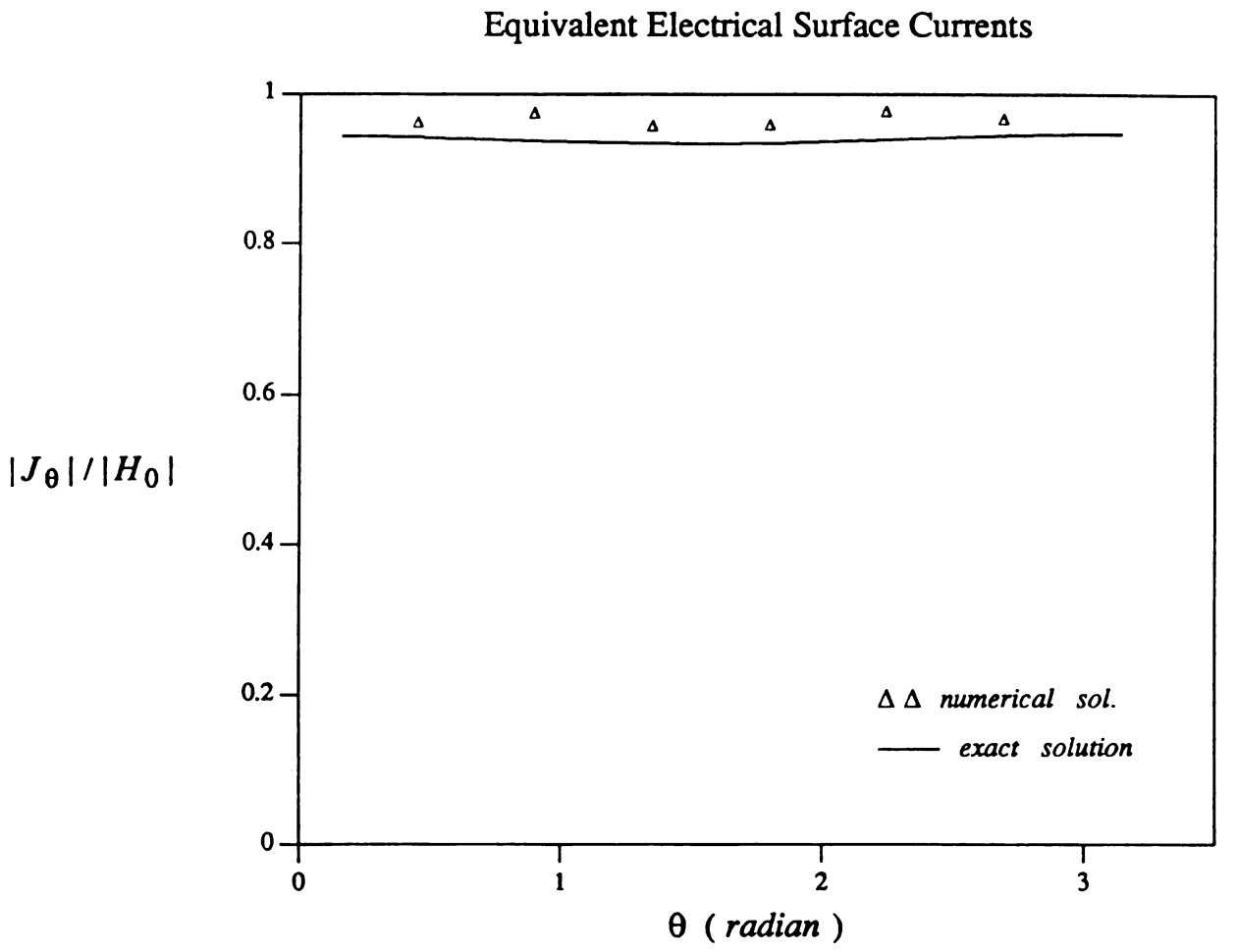

Figure 2.15 θ-component of equivalent electric current on the outer surface S_1 of a concentric sphere with:

($k_0a_2 = 0.0595$; $\varepsilon_{r2} = 16.0$; $\mu_{r2} = 4.0$; $\tan(\delta_2) = 0.39$)

($k_0a_1 = 0.13$; $\varepsilon_{r1} = 9.0$; $\mu_{r1} = 1.0$; $\tan(\delta_1) = 0.0$)

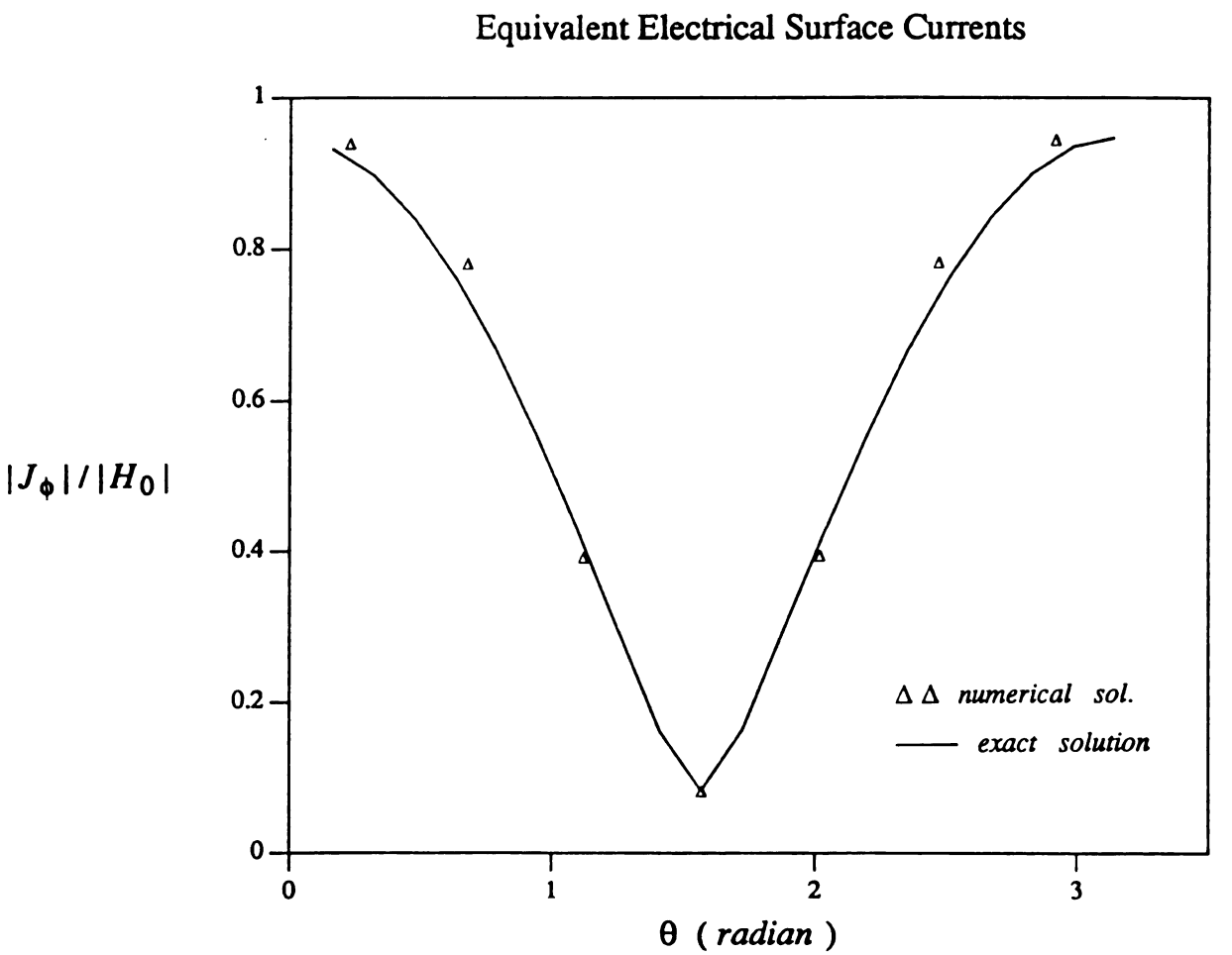

Figure 2.16 ϕ-component of equivalent electric current on the outer surface S_1 of a concentric sphere with:

($k_0 a_2 = 0.0595$; $\varepsilon_{r2} = 16.0$; $\mu_{r2} = 4.0$; $\tan(\delta_2) = 0.39$)

($k_0 a_1 = 0.13$; $\varepsilon_{r1} = 9.0$; $\mu_{r1} = 1.0$; $\tan(\delta_1) = 0.0$)

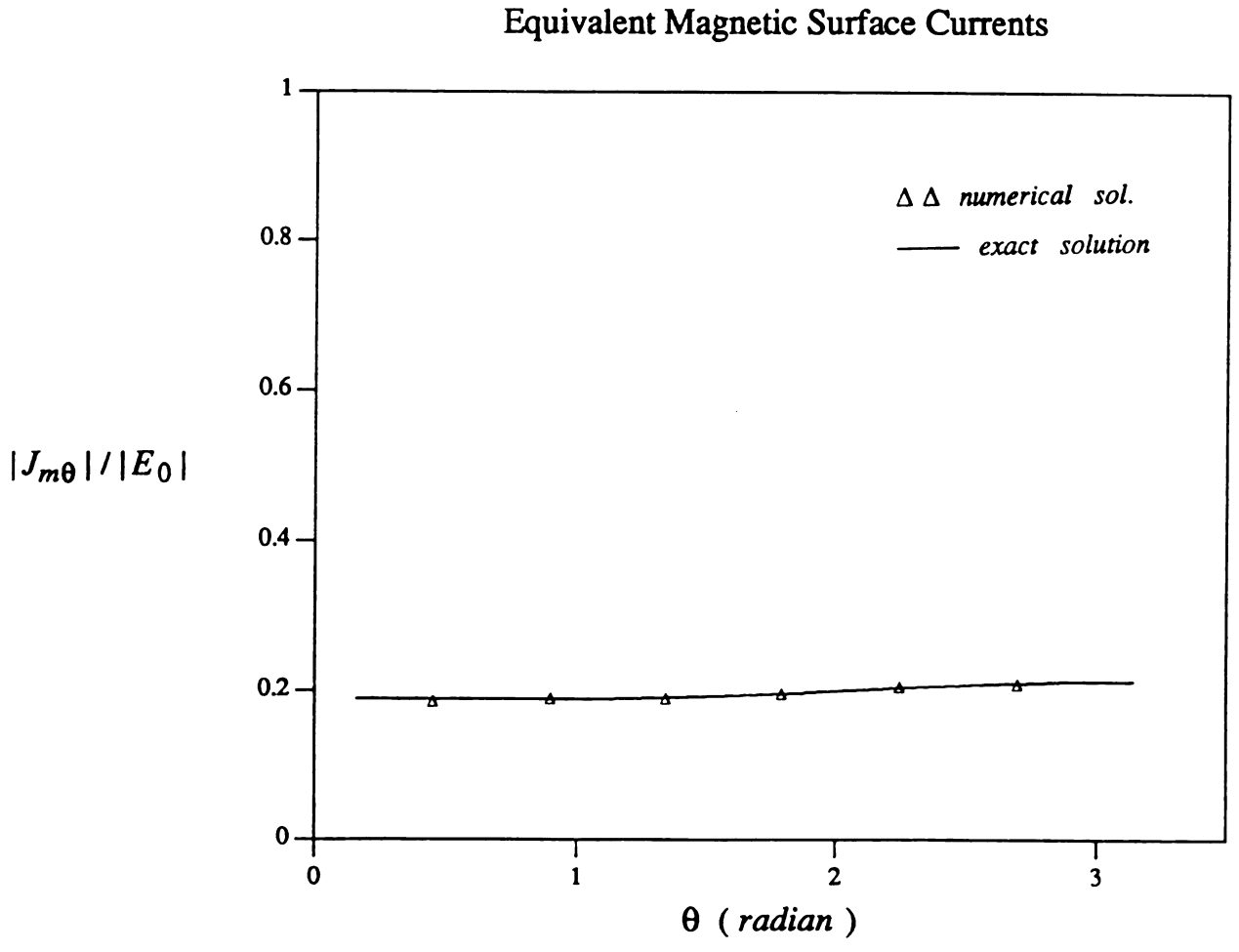

Figure 2.17 θ-component of equivalent magnetic current on the inner surface S_2 of a concentric sphere with:

($k_0 a_2 = 0.0595$; $\varepsilon_{r2} = 16.0$; $\mu_{r2} = 4.0$; $\tan(\delta_2) = 0.39$)

($k_0 a_1 = 0.13$; $\varepsilon_{r1} = 9.0$; $\mu_{r1} = 1.0$; $\tan(\delta_1) = 0.0$)

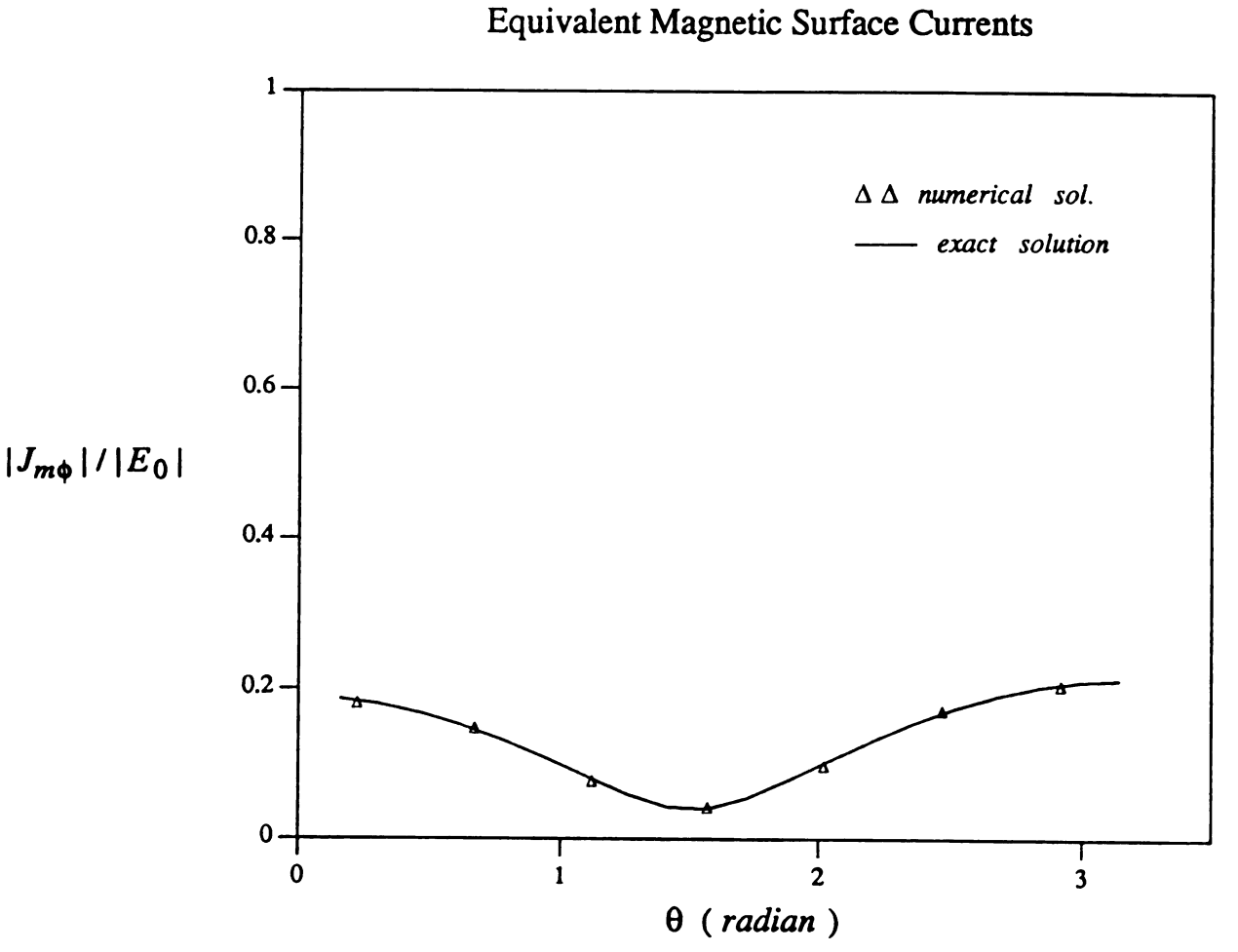

Figure 2.18 ϕ-component of equivalent magnetic current on the inner surface S_2 of a concentric sphere with:

($k_0 a_2 = 0.0595$; $\varepsilon_{r2} = 16.0$; $\mu_{r2} = 4.0$; $\tan(\delta_2) = 0.39$)

($k_0 a_1 = 0.13$; $\varepsilon_{r1} = 9.0$; $\mu_{r1} = 1.0$; $\tan(\delta_1) = 0.0$)

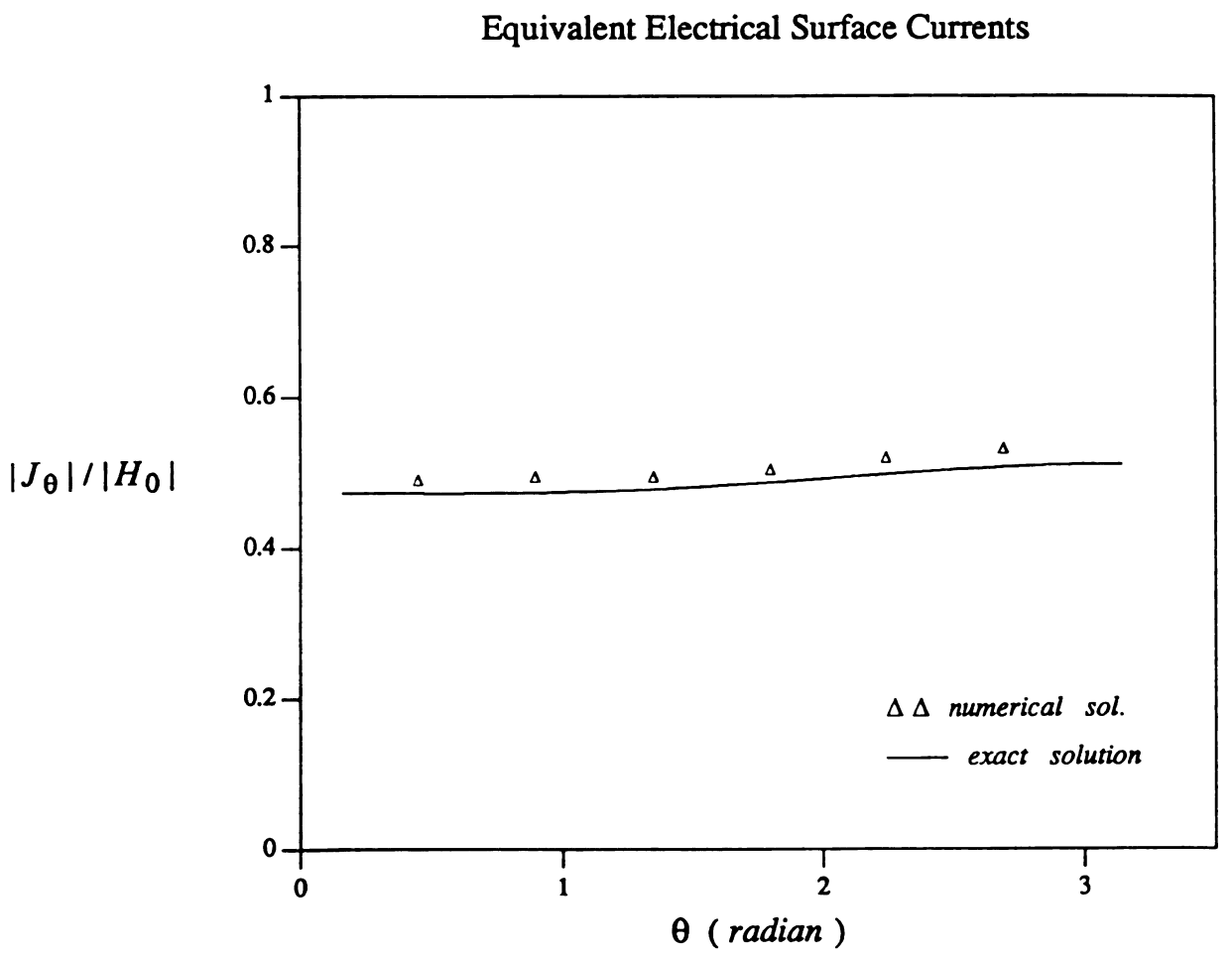

Figure 2.19 θ-component of equivalent electric current on the inner surface S_2 of a concentric sphere with:

($k_0 a_2 = 0.0595$; $\varepsilon_{r2} = 16.0$; $\mu_{r2} = 4.0$; $\tan(\delta_2) = 0.39$)

($k_0 a_1 = 0.13$; $\varepsilon_{r1} = 9.0$; $\mu_{r1} = 1.0$; $\tan(\delta_1) = 0.0$)

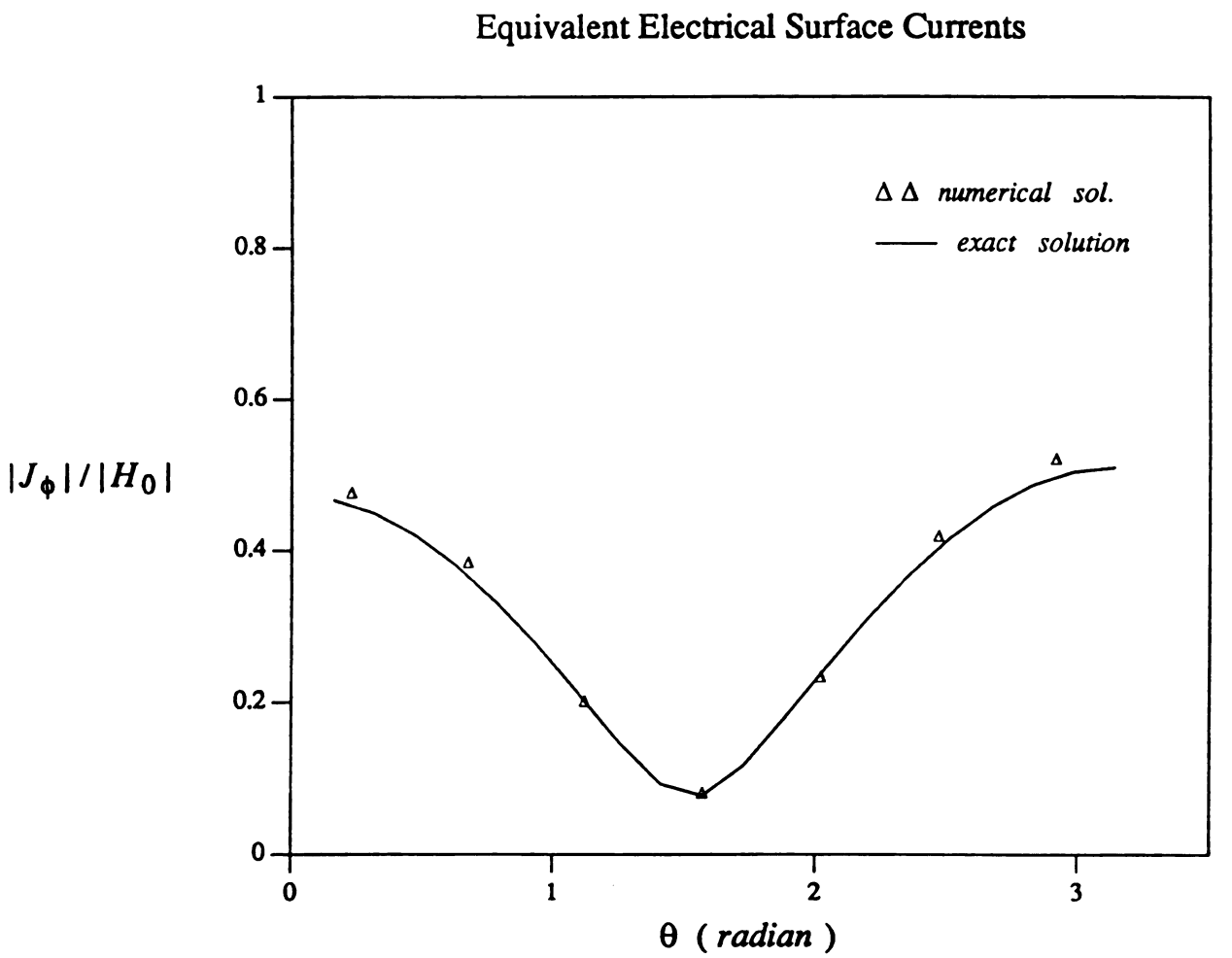

Figure 2.20 ϕ-component of equivalent electric current on the inner surface S_2 of a concentric sphere with:

($k_0 a_2 = 0.0595$; $\varepsilon_{r2} = 16.0$; $\mu_{r2} = 4.0$; $\tan(\delta_2) = 0.39$)

($k_0 a_1 = 0.13$; $\varepsilon_{r1} = 9.0$; $\mu_{r1} = 1.0$; $\tan(\delta_1) = 0.0$)

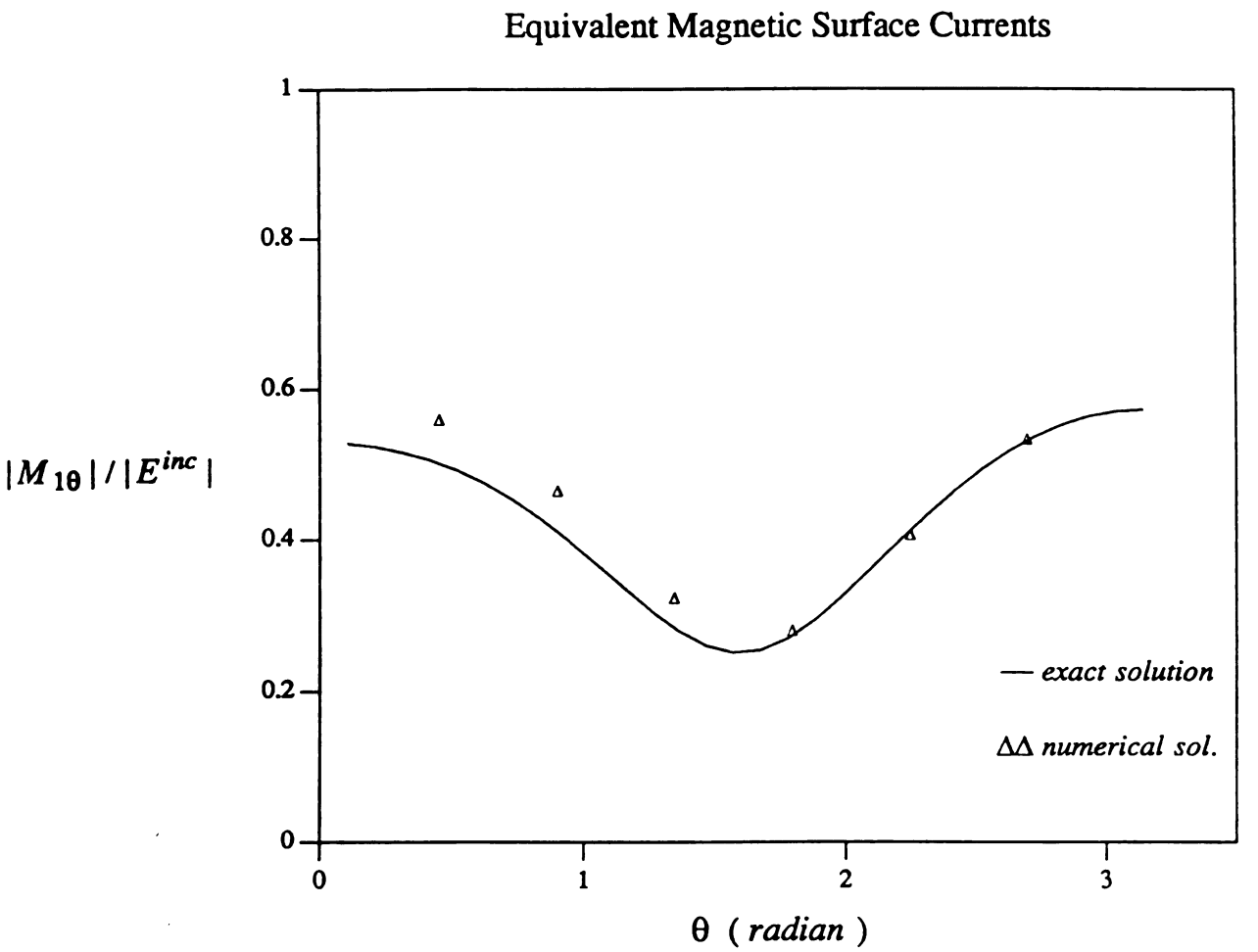

Figure 2.21 θ-component of equivalent magnetic current on the outer surface S_1 of a perfectly conducting sphere coated with a lossy layer.
($k_0a_2 = 0.4\pi$; $k_0a_1 = 0.5\pi$; $\varepsilon_r = 1.0$; $\mu_r = 1.0$; $\tan(\delta) = 0.0$)

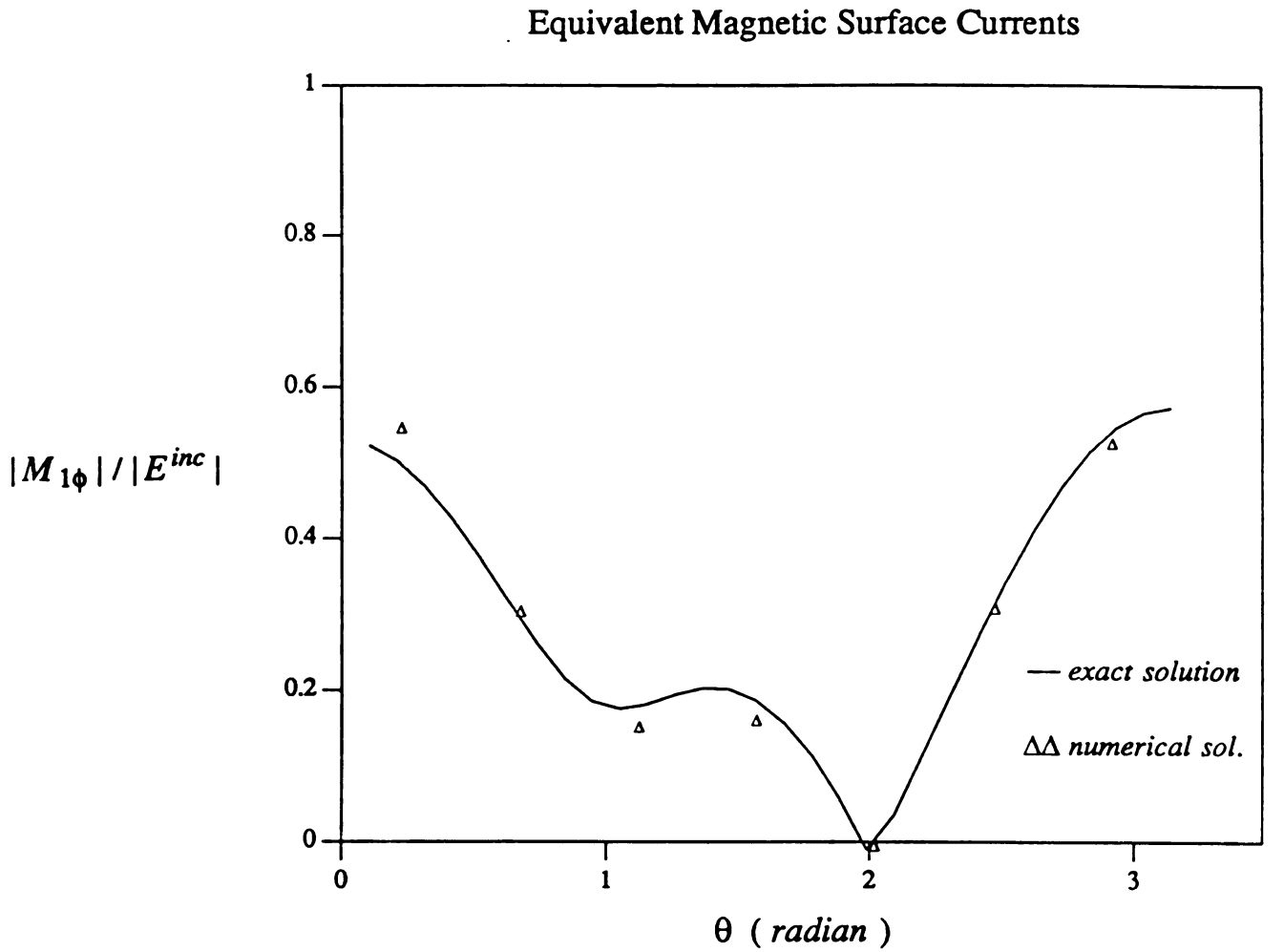

Figure 2.22 ϕ-component of equivalent magnetic current on the outer surface S_1 of a perfectly conducting sphere coated with a lossy layer.
($k_0 a_2 = 0.4\pi$; $k_0 a_1 = 0.5\pi$; $\varepsilon_r = 1.0$; $\mu_r = 1.0$; $\tan(\delta) = 0.0$)

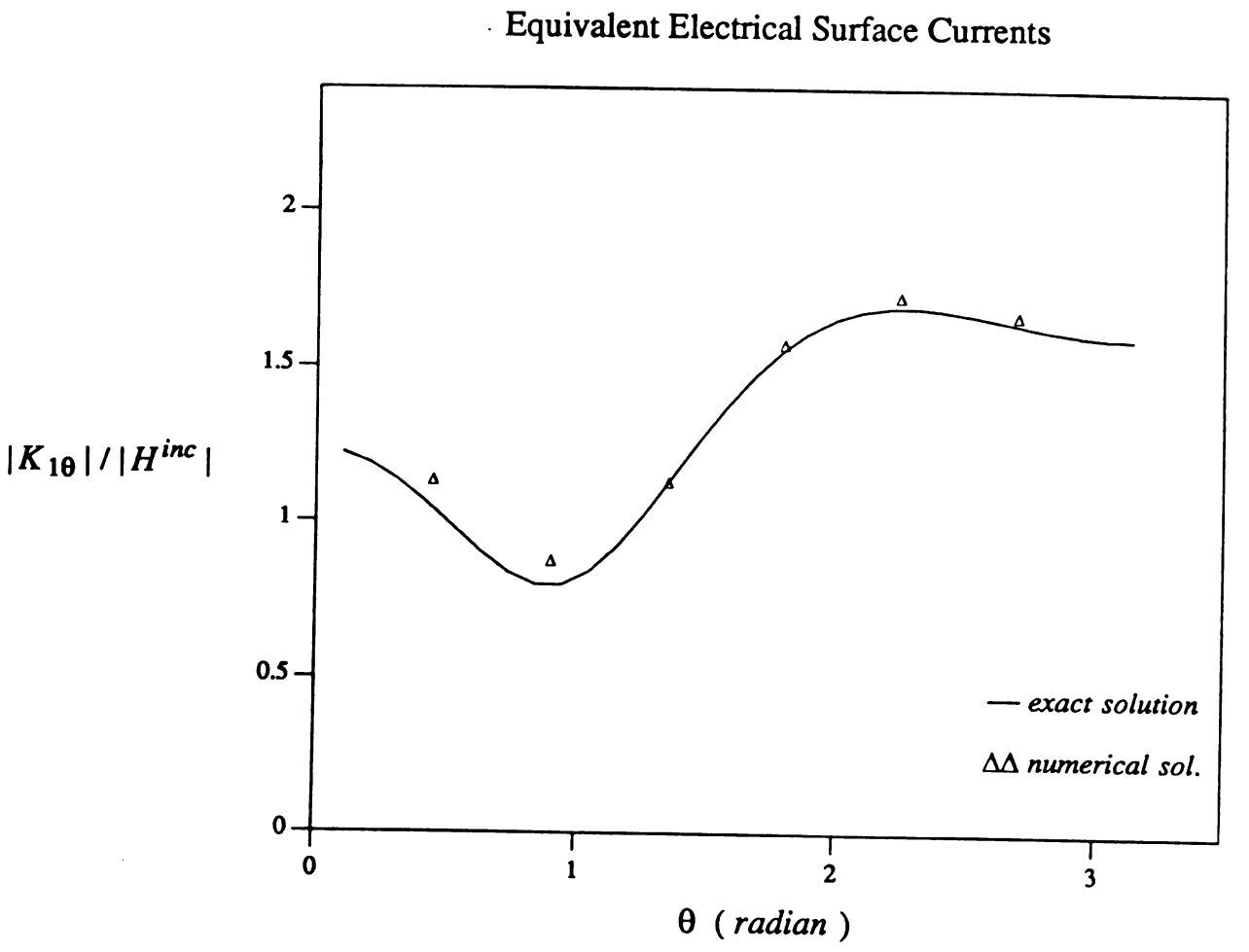

Figure 2.23 θ-component of equivalent electric current on the outer surface S_1 of a perfectly conducting sphere coated with a lossy layer.
($k_0a_2 = 0.4\pi$; $k_0a_1 = 0.5\pi$; $\varepsilon_r = 1.0$; $\mu_r = 1.0$; $\tan(\delta) = 0.0$)

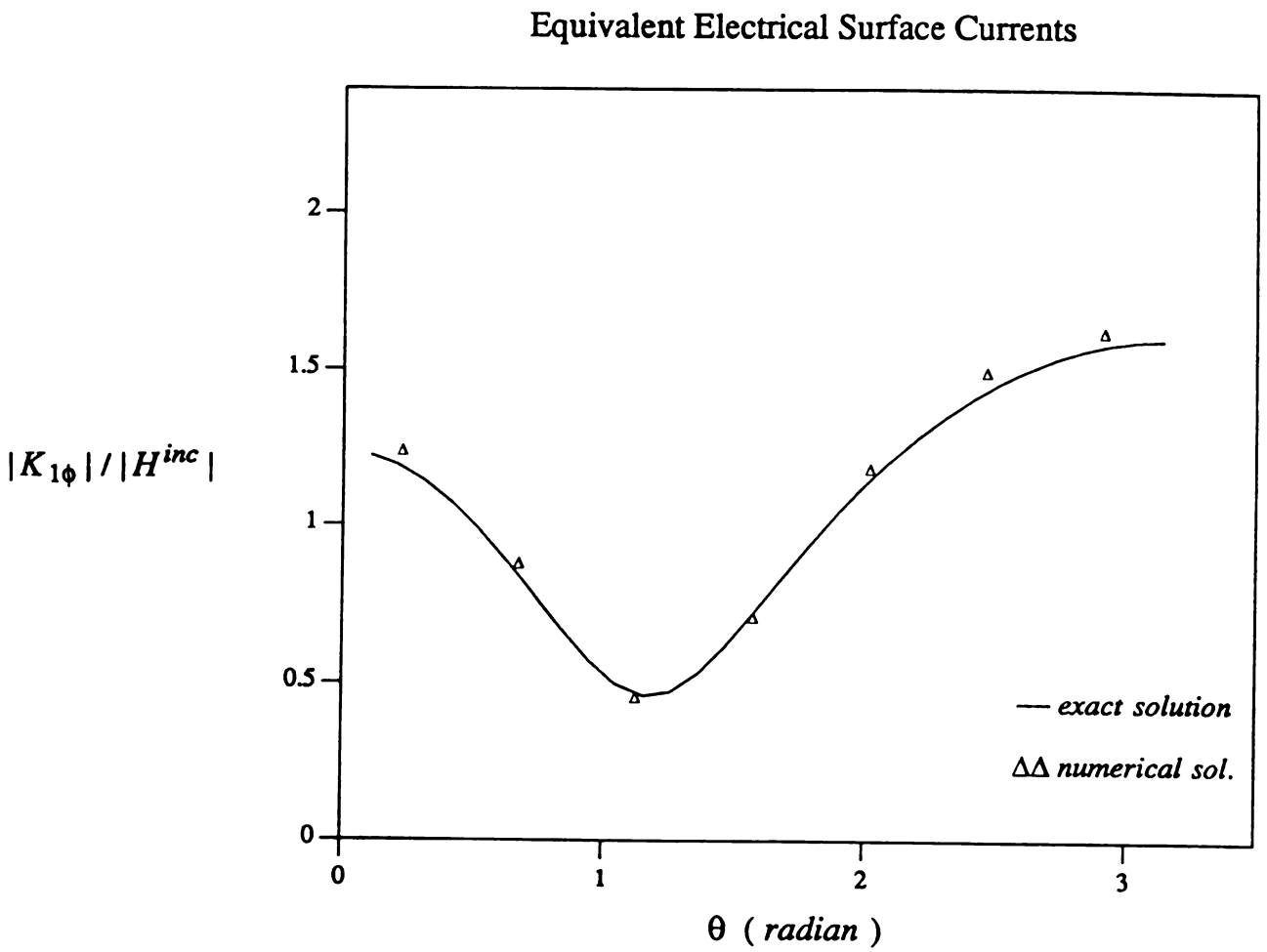

Figure 2.24 ϕ-component of equivalent electric current on the outer surface S_1 of a perfectly conducting sphere coated with a lossy layer.
($k_0 a_2 = 0.4\pi$; $k_0 a_1 = 0.5\pi$; $\varepsilon_r = 1.0$; $\mu_r = 1.0$; $\tan(\delta) = 0.0$)

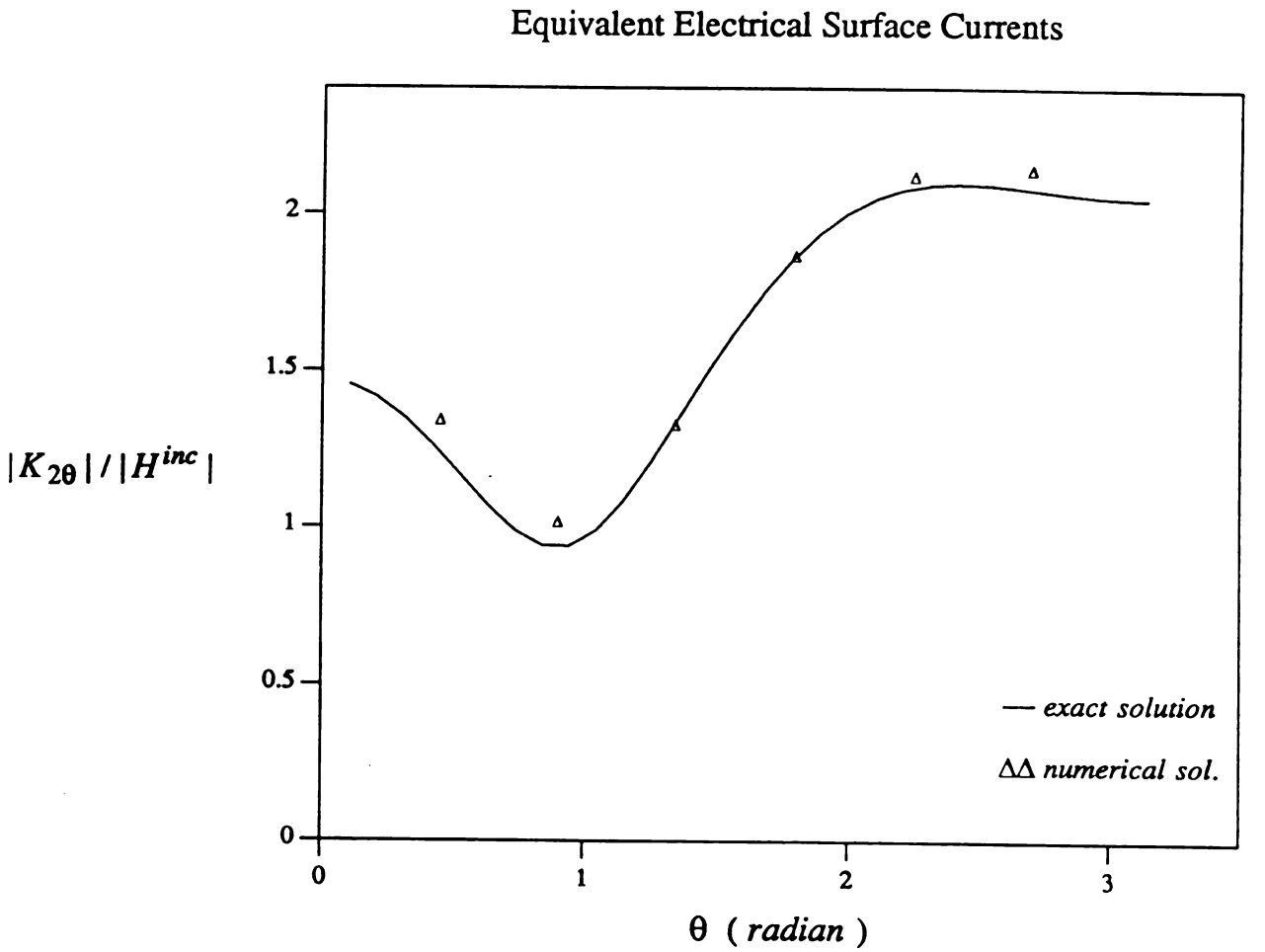

Figure 2.25 θ-component of electric current on the inner surface S_2 of a perfectly conducting sphere coated with a lossy layer.

($k_0a_2 = 0.4\pi$; $k_0a_1 = 0.5\pi$; $\varepsilon_r = 1.0$; $\mu_r = 1.0$; $\tan(\delta) = 0.0$)

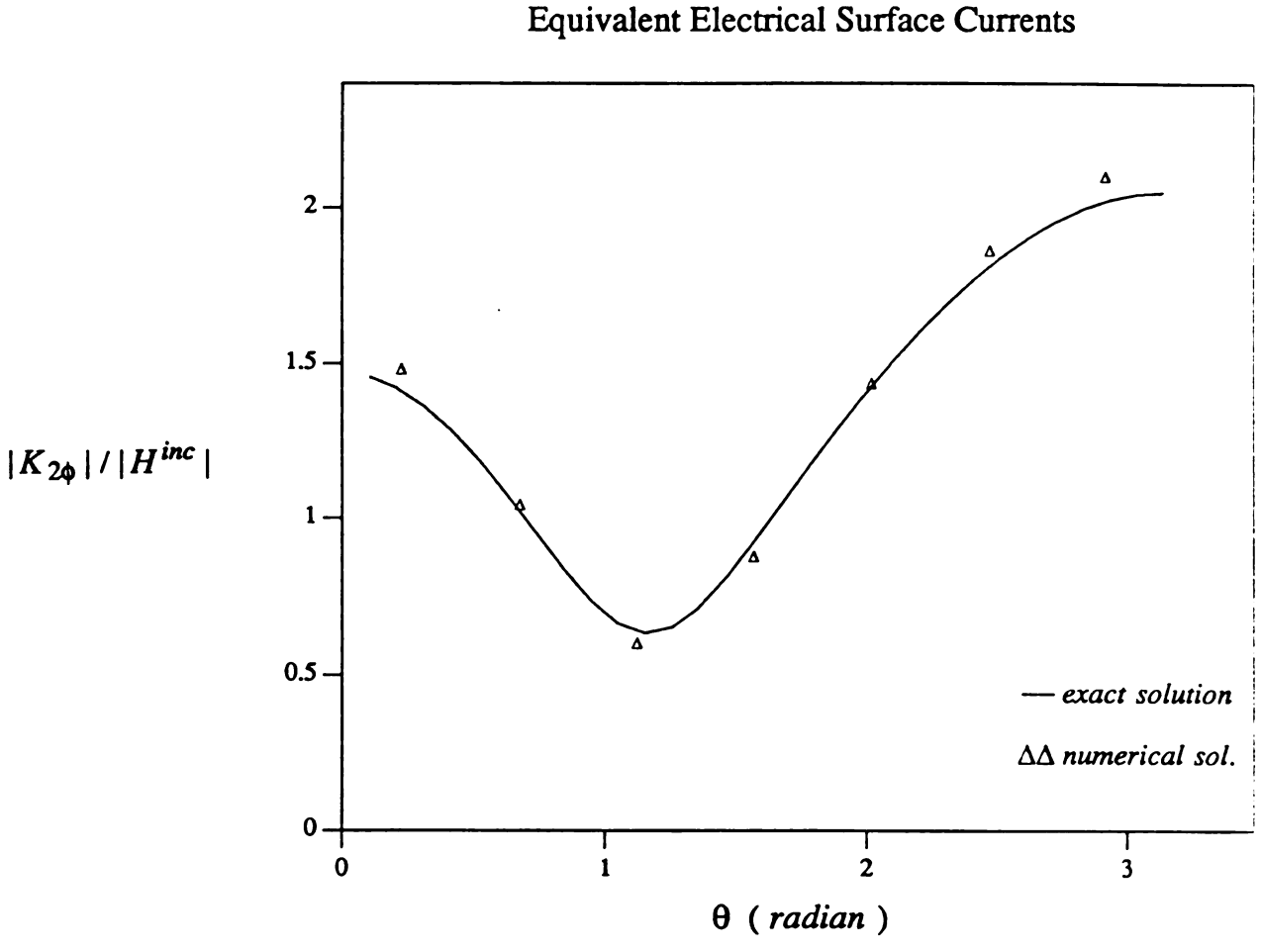

Figure 2.26 ϕ-component of electric current on the inner surface S_2 of a perfectly conducting sphere coated with a lossy layer.

($k_0 a_2 = 0.4\pi$; $k_0 a_1 = 0.5\pi$; $\varepsilon_r = 1.0$; $\mu_r = 1.0$; $\tan(\delta) = 0.0$)

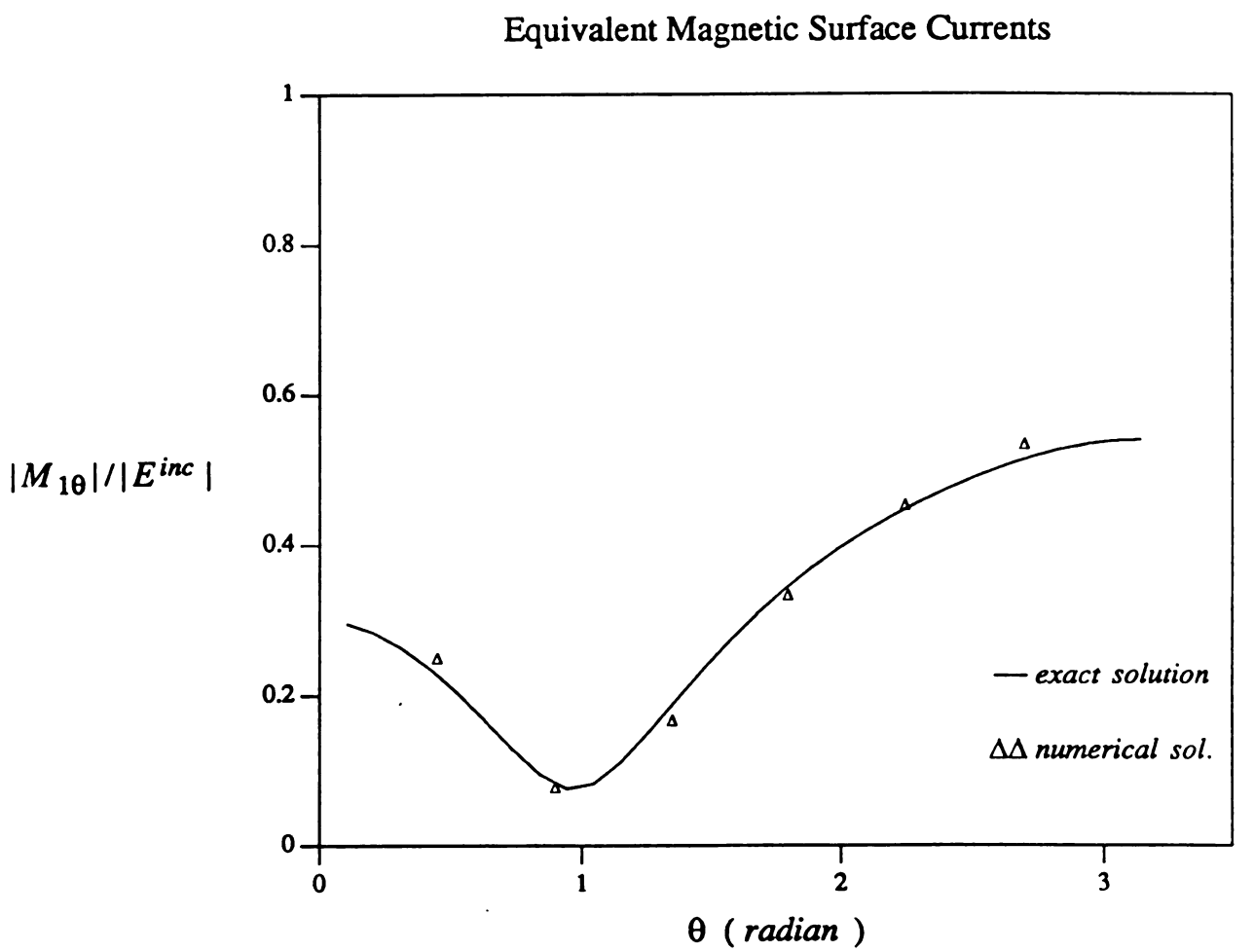

Figure 2.27 θ-component of equivalent magnetic current on the outer surface S_1 of a perfectly conducting sphere coated with a lossy layer.

($k_0a_2 = 0.4\pi$; $k_0a_1 = 0.5\pi$; $\varepsilon_r = 4.0$; $\mu_r = 1.0$; $\tan(\delta) = 0.0$)

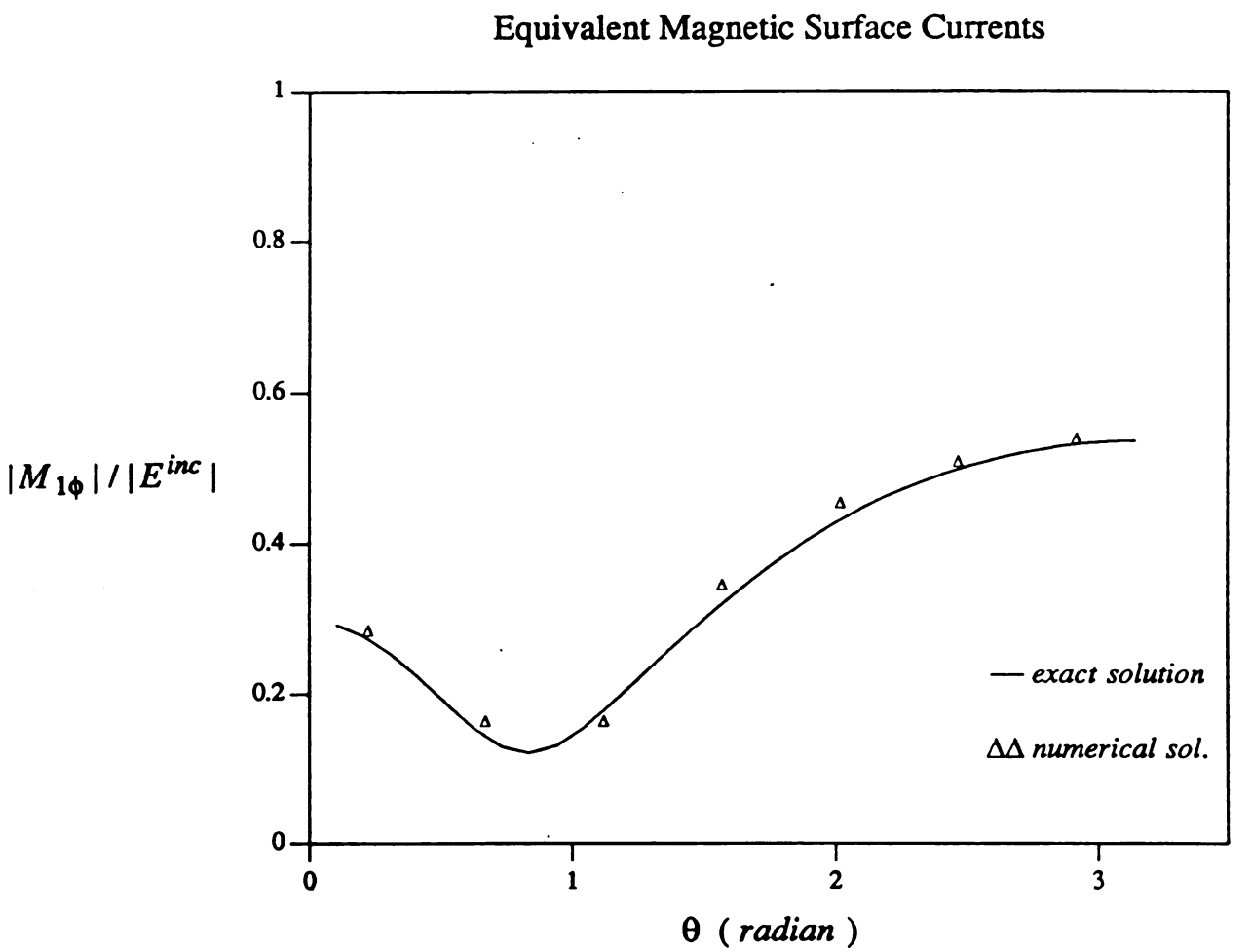

Figure 2.28 $-\phi$-component of equivalent magnetic current on the outer surface S_1 of a perfectly conducting sphere coated with a lossy layer.

($k_0 a_2 = 0.4\pi$; $k_0 a_1 = 0.5\pi$; $\varepsilon_r = 4.0$; $\mu_r = 1.0$; $\tan(\delta) = 0.0$)

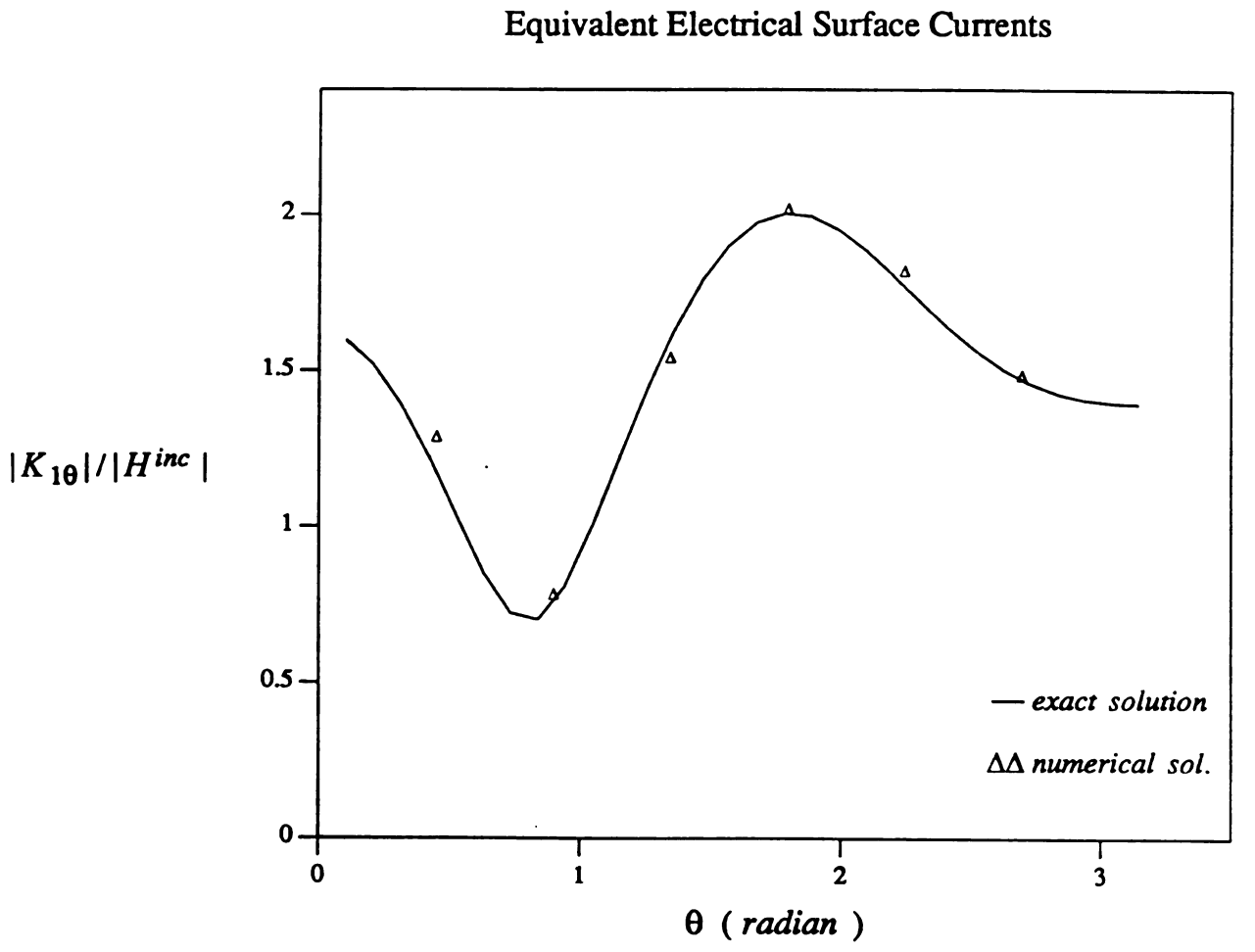

Figure 2.29 θ-component of equivalent electric current on the outer surface S_1 of a perfectly conducting sphere coated with a lossy layer.

($k_0a_2 = 0.4\pi$; $k_0a_1 = 0.5\pi$; $\varepsilon_r = 4.0$; $\mu_r = 1.0$; $\tan(\delta) = 0.0$)

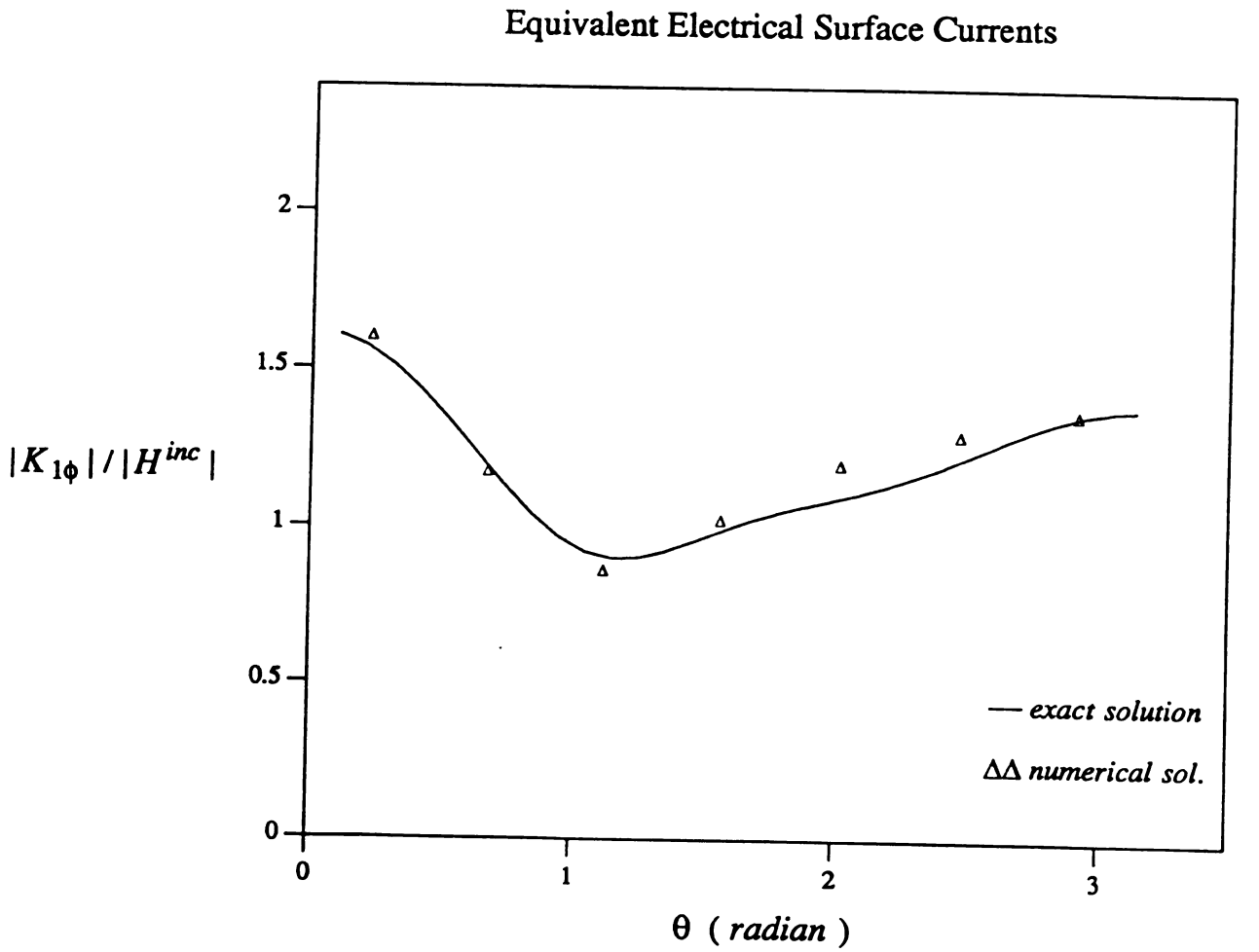

Figure 2.30 ϕ-component of equivalent electric current on the outer surface S_1 of a perfectly conducting sphere coated with a lossy layer.
($k_0a_2 = 0.4\pi$; $k_0a_1 = 0.5\pi$; $\varepsilon_r = 4.0$; $\mu_r = 1.0$; $\tan(\delta) = 0.0$)

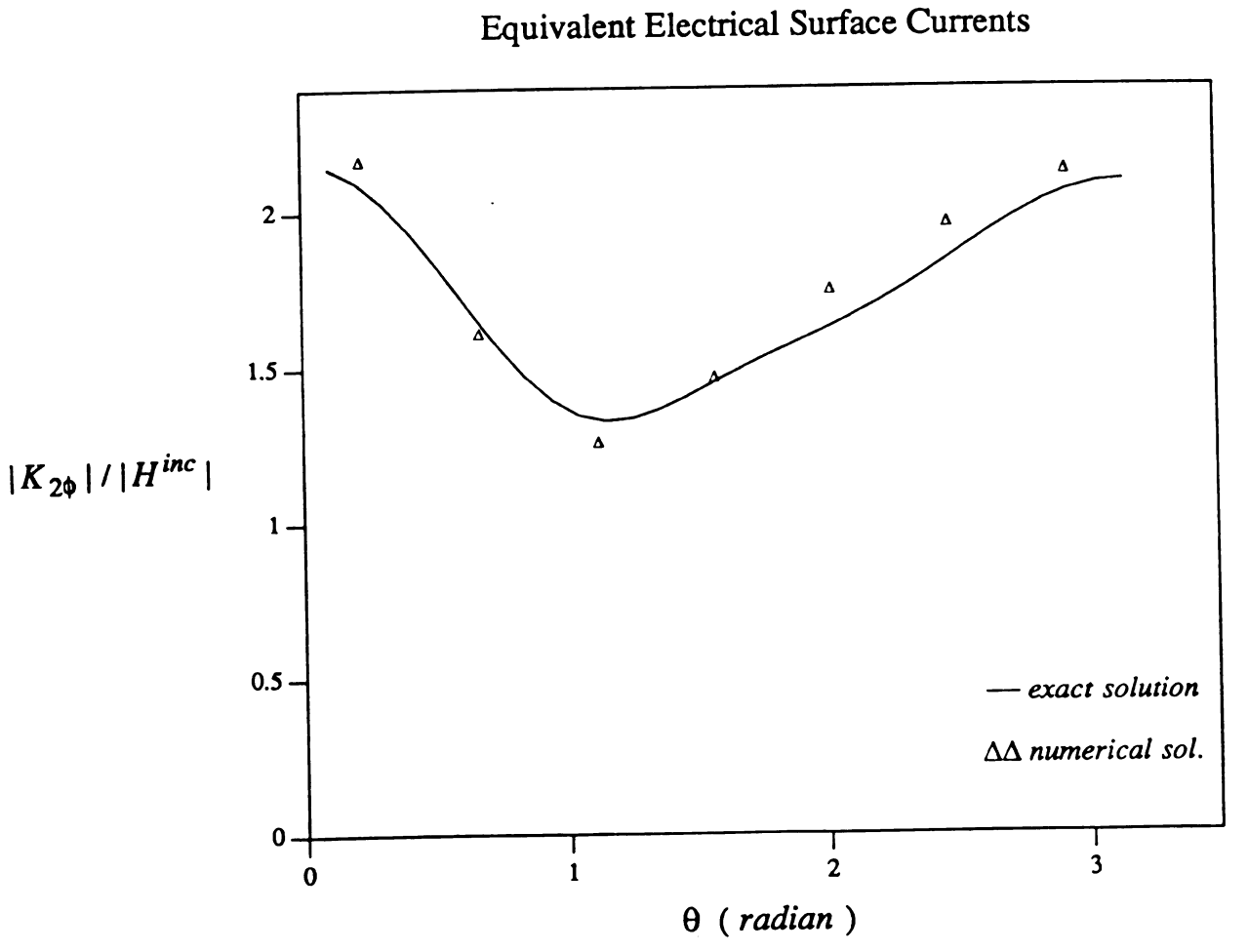

Figure 2.31 θ-component of electric current on the inner surface S_2 of a perfectly conducting sphere coated with a lossy layer.

($k_0 a_2 = 0.4\pi$; $k_0 a_1 = 0.5\pi$; $\varepsilon_r = 4.0$; $\mu_r = 1.0$; $\tan(\delta) = 0.0$)

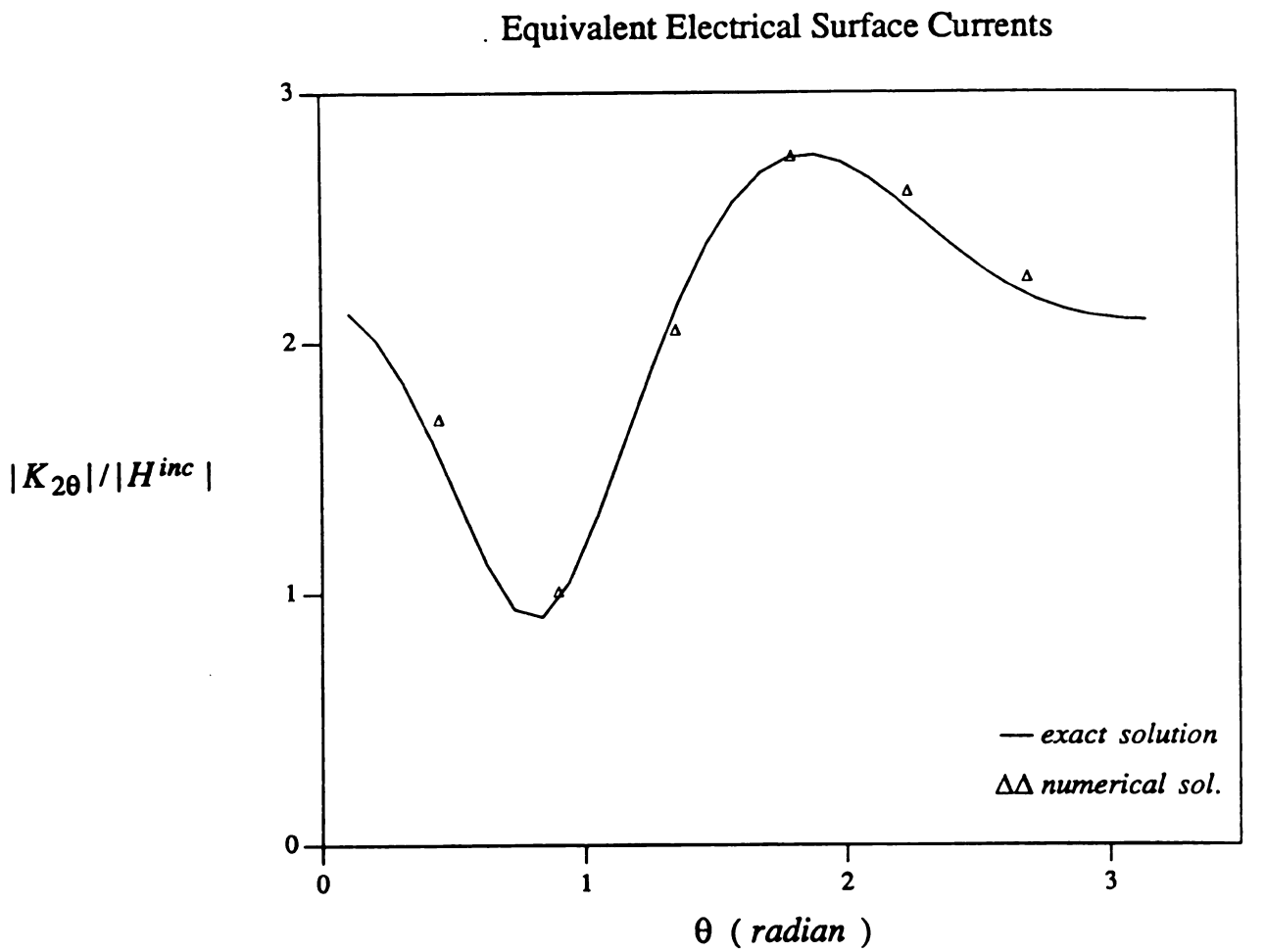

Figure 2.32 ϕ-component of electric current on the inner surface S_2 of a perfectly conducting sphere coated with a lossy layer.

($k_0a_2 = 0.4\pi$; $k_0a_1 = 0.5\pi$; $\varepsilon_r = 4.0$; $\mu_r = 1.0$; $\tan(\delta) = 0.0$)

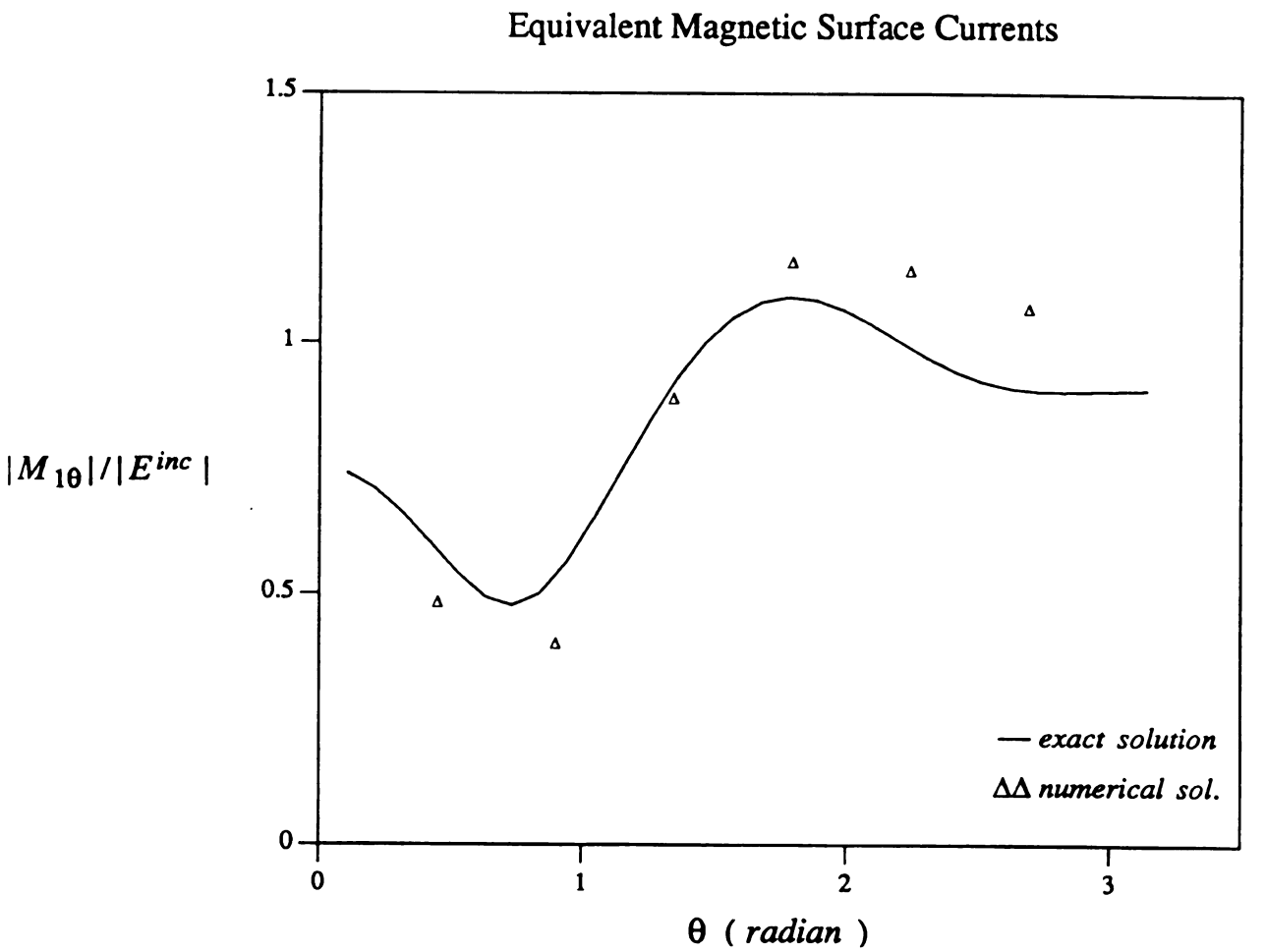

Figure 2.33 θ-component of equivalent magnetic current on the outer surface S_1 of a perfectly conducting sphere coated with a lossy layer.

($k_0a_2 = 0.4\pi$; $k_0a_1 = 0.5\pi$; $\varepsilon_r = 1.0$; $\mu_r = 4.0$; $\tan(\delta) = 0.0$)

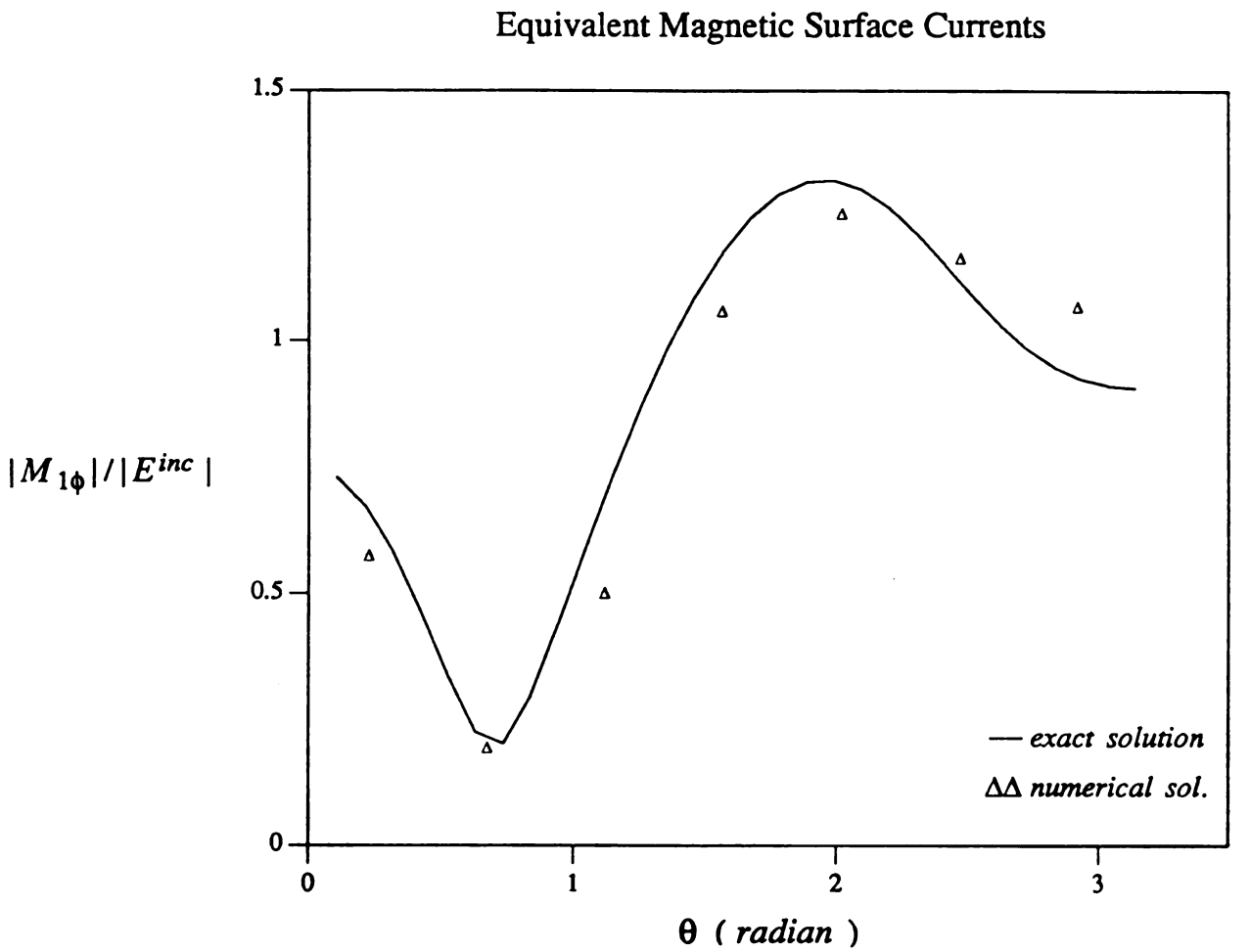

Figure 2.34 ϕ-component of equivalent magnetic current on the outer surface S_1 of a perfectly conducting sphere coated with a lossy layer.

($k_0 a_2 = 0.4\pi$; $k_0 a_1 = 0.5\pi$; $\varepsilon_r = 1.0$; $\mu_r = 4.0$; $\tan(\delta) = 0.0$)

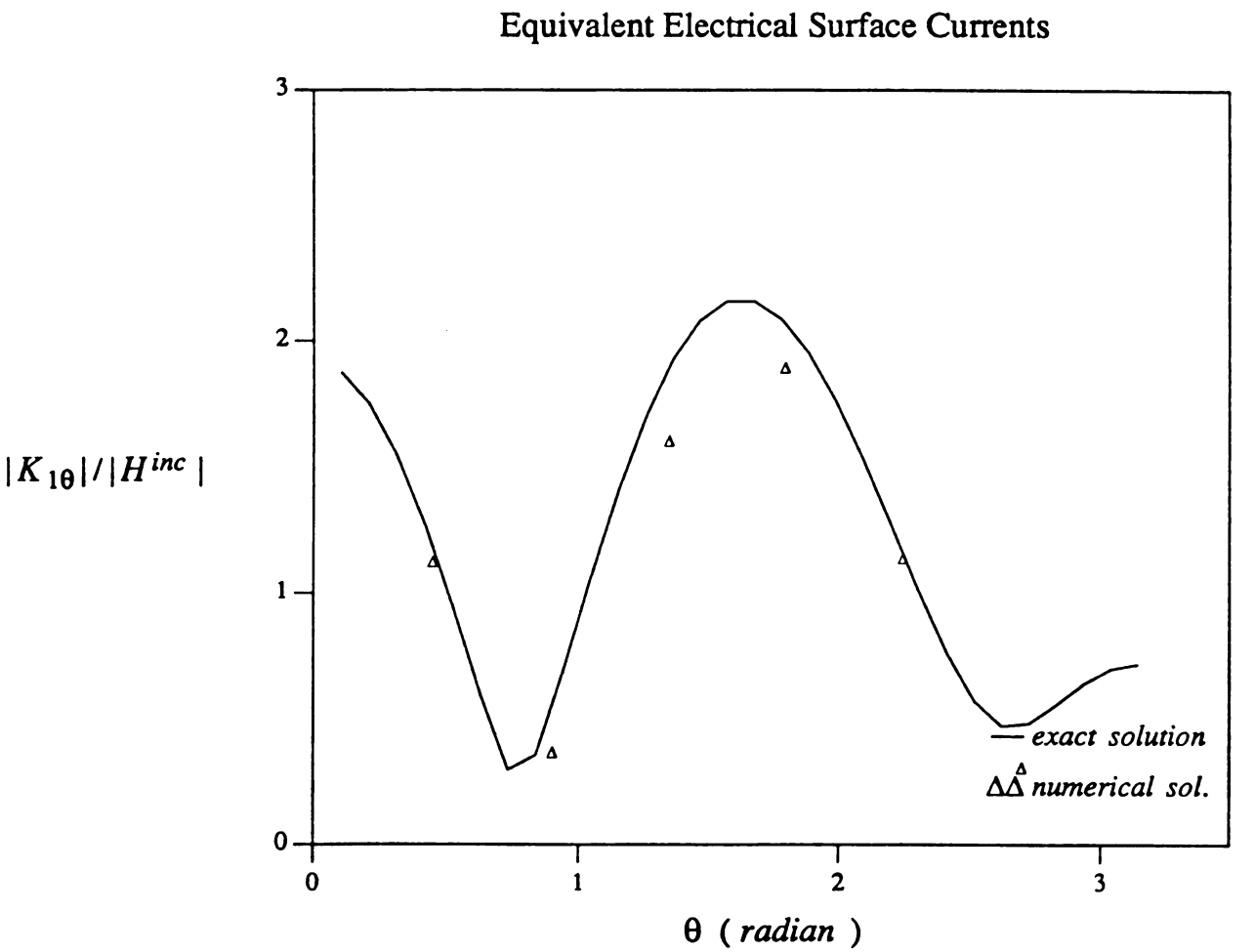

Figure 2.35 θ-component of equivalent electric current on the outer surface S_1 of a perfectly conducting sphere coated with a lossy layer.

($k_0a_2 = 0.4\pi$; $k_0a_1 = 0.5\pi$; $\varepsilon_r = 1.0$; $\mu_r = 4.0$; $\tan(\delta) = 0.0$)

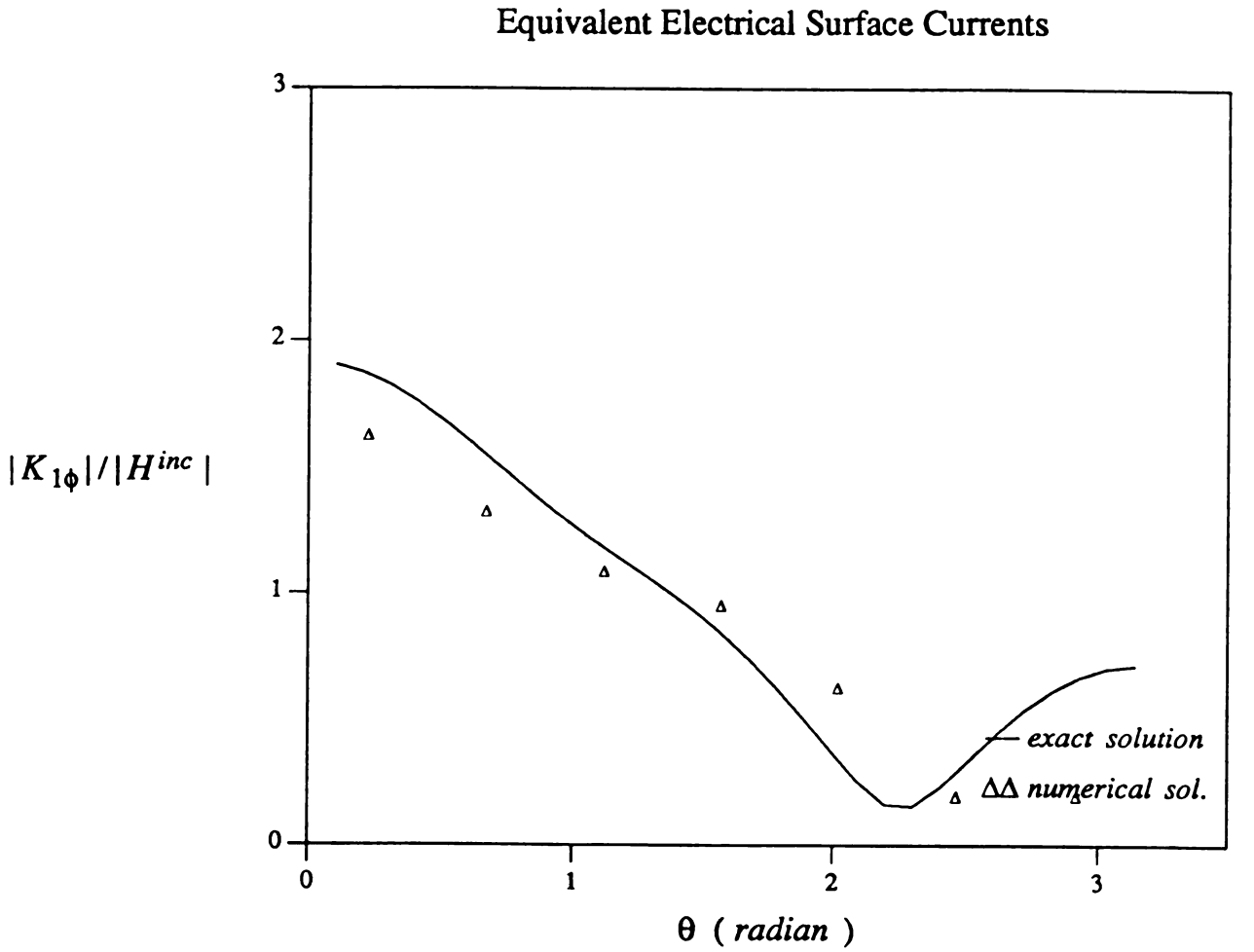

Figure 2.36 ϕ-component of equivalent electric current on the outer surface S_1 of a perfectly conducting sphere coated with a lossy layer.

($k_0a_2 = 0.4\pi$; $k_0a_1 = 0.5\pi$; $\varepsilon_r = 1.0$; $\mu_r = 4.0$; $\tan(\delta) = 0.0$)

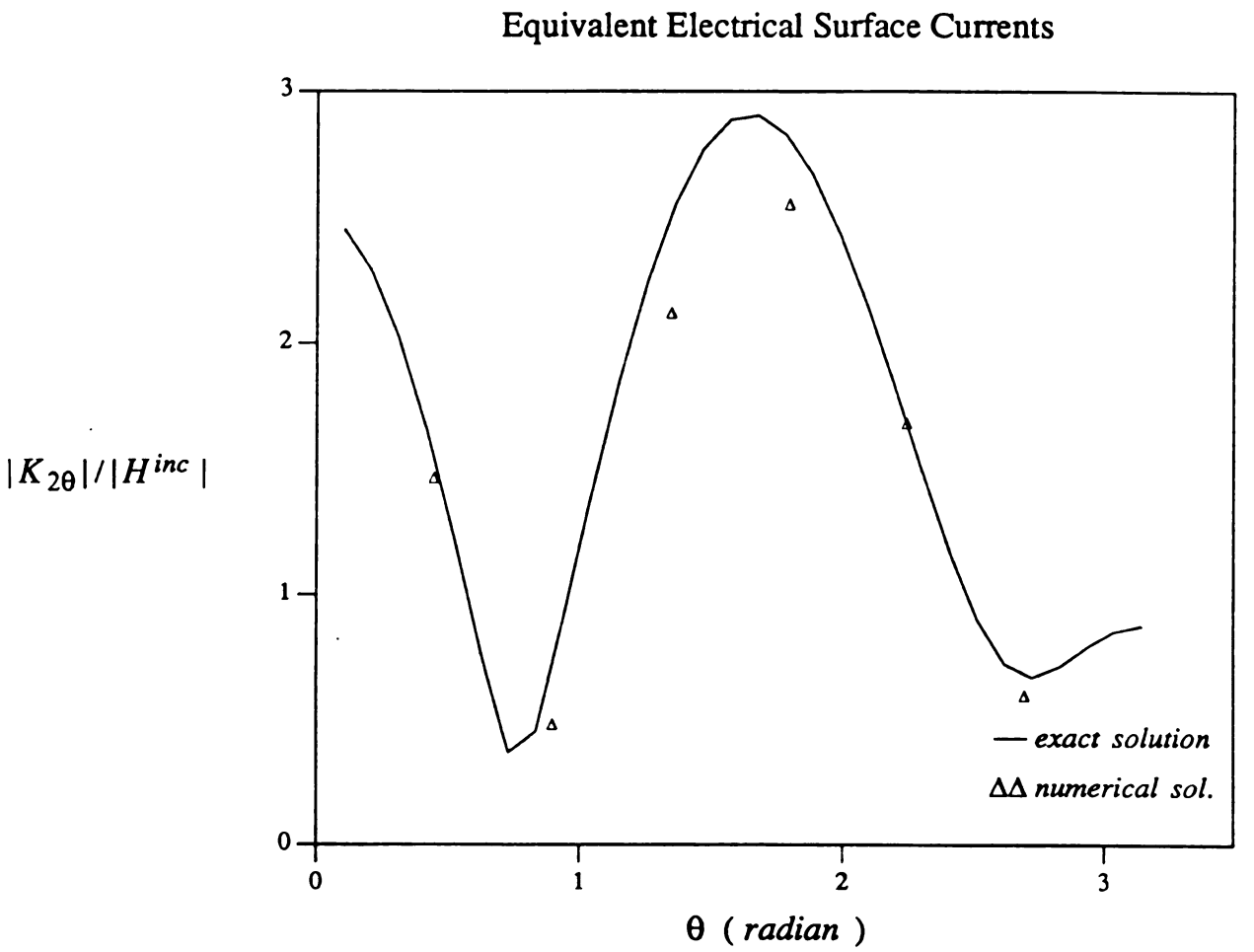

Figure 2.37 θ-component of electric current on the inner surface S_2 of a perfectly conducting sphere coated with a lossy layer.

($k_0a_2 = 0.4\pi$; $k_0a_1 = 0.5\pi$; $\varepsilon_r = 1.0$; $\mu_r = 4.0$; $\tan(\delta) = 0.0$)

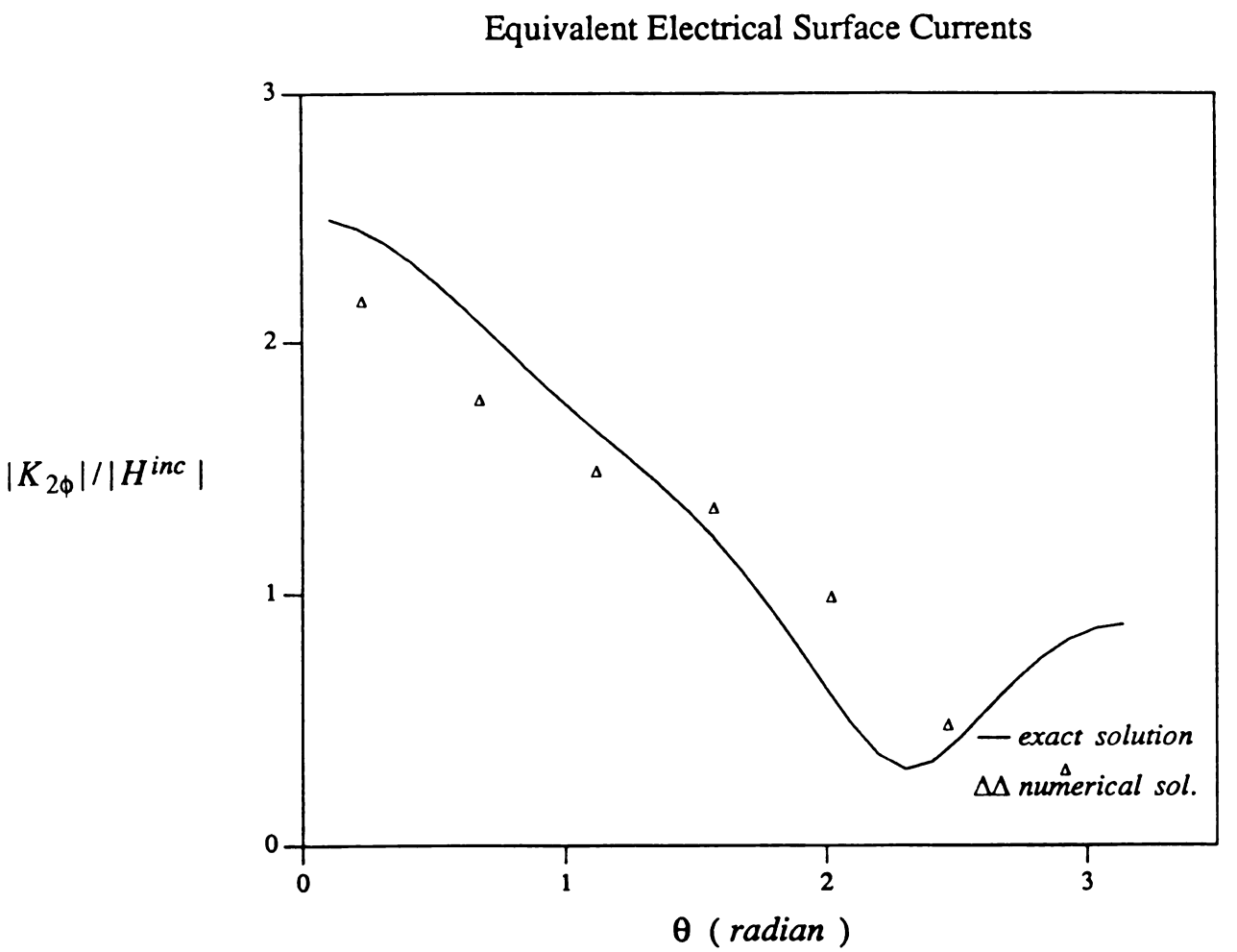

Figure 2.38 ϕ-component of electric current on the inner surface S_2 of a perfectly conducting sphere coated with a lossy layer.

($k_0a_2 = 0.4\pi$; $k_0a_1 = 0.5\pi$; $\varepsilon_r = 1.0$; $\mu_r = 4.0$; $\tan(\delta) = 0.0$)

2.5 Comparison with Other Methods

One of the existing methods to quantify the electromagnetic scattering by an arbitrarily shaped heterogeneous lossy body is to use the tetrahedral modeling method based on volume integral equations[13]. However, this method is not numerically efficient when the scatterer has a simple structure. The main advantage of the proposed method in this chapter is that instead of discretizing the whole domain as in the volume integral method, only the interfaces need to be discretized, thus, leading to much less unknowns. For example, let's take a concentric sphere with parameters of $\varepsilon_1 = 16, k_0 a_1 = 0.0595, \varepsilon_2 = 9, k_0 a_2 = 0.13$, the same as the first example in section 2.4., and compare the numerical results between these two method. For the tetrahedral modeling method, the sphere was modeled by 512 tetrahedral cells leading to 1088 unknowns which led to the results in reference [13]. While for the present triangular element method, only 576 unknowns associated with 192 triangular cells are used to obtain the results which agree very well with the exact solution. Furthermore, the accuracy of the latter method is superior to that of the former method. On the other hand, these two method provide the same modeling flexibility because the advantages of triangular elements for surface modeling are analogous to that of tetrahedral elements for volume modeling [8-9]. However, it is obvious that surface modeling is much simpler.

The proposed method may be used in many situations where the evaluation of the scattering by a composite object or the analysis of a coated structure is involved.

2.6 Some Comments

In section 2.2, a set of coupled surface integral equations for a heterogeneous body either with or without a perfect conductor inside has been developed. However,

the coupled surface integral equations are not suited for a heterogeneous body coated with a very thin layer on it. It can be seen that as the thickness of the layer approaches to zero, the equivalent electric and magnetic currents on the two interfaces of the layer become the same which leads to the resulted matrix become singular. The failure for this extreme case is due to the formulation of the integral equations. An alternative approach for this extreme case will be proposed and discussed in chapter 4.

Another thing we observed from the numerical results is that the convergence rate become pretty slow as the electric size of a body is increased. This is mainly resulted from the characteristics of moment method which needs to solve a matrix equation. For example, considering a perfectly conducting sphere coated with a layer of lossy material, we have six unknowns currents in the resulted coupled surface integral equations. Supposing each unknown current is expanded into vector basis functions and represented by N unknown coefficients, then we have $6N$ total unknowns which leads to $6N$ by $6N$ complex matrix. To get a good resolution of an electrically large body, the requirement of the storage easily exceeds the memory size of computer system.

For a more complex body, for example, a multilayer sphere or a heterogeneous body with more than one different media, a similar derivation of a set of coupled surface integral equation can be deduced. However, more equations or more terms in the set of integral equations may be resulted and the computer codes for solving the problem has to be changed. This prevents a systematic way to handle an arbitrary heterogeneous body.

2.7 Conclusion

To analyze electromagnetic scattering by arbitrarily shaped three dimensional heterogeneous objects, a set of coupled surface integral equations has been developed based on the equivalent principle. Using the method of moments, th coupled surface

integral equations are solved by an efficient and simple numerical algorithms. Concentric spheres are used as a test case to validate the theory and computer algorithms. Numerical results indicate that the proposed method is more efficient than the existing tetrahedral modeling method based on volume integral equations for simple composite structures.

CHAPTER III

FUNDAMENTALS OF FINITE DIFFERENCE TIME DOMAIN METHOD IN SOLUTIONS OF ELECTROMAGNETIC SCATTERING AND ANTENNA PROBLEMS

3.1 Introduction

The demand for solving electromagnetic problems involving electrically large bodies and complex structures is increasing in engineering designs. The problems may involve large composite bodies, cavities, anisotropic media and the bodies may have dimensions of a few wavelengths. To solve these large complex problems, the finite difference time domain method provides a good candidate over traditional moment method. The main idea of the finite difference time domain method(FD-TD) is quite straight forward. It is a direct solution of Maxwell's time-dependent curl equations. The main steps in this method will be discussed here.

The Yee's model [22] has been used almost universally. It applies simple, second-order central-difference approximations for both spatial and temporal derivatives of the electric and magnetic fields directly to the differential operators of the Maxwell's curl equations. Electric and magnetic field components are interleaved in space to permit a natural expression of Farady and Ampere's laws. Space and time discretizations are selected to bound errors and insure numerical stability of the algorithm. In addition, the system of equations developed by Yee[22] to update the field components is fully explicit such that the required computer storage and running time is proportional to the electrical size of the volume modeled. This sets a remarkable difference from traditional moment method which needs inversion of matrix.

When the fields must be computed is unbounded, as the case of scattering problems, the infinite space must be truncated into a finite region since it is impossible to store an unlimited amount of data into computers. A special technique, the radiation boundary condition, is proposed on the outer truncated boundary surfaces to simulate the outside extension. For example, the second order radiation boundary condition introduced by Mur[28] allows all outgoing scattered wave analogs ideally propagate through the lattice truncation planes with negligible reflection to exit the sample region.

Overall, the FD-TD method is a marching-in-time procedure which simulates the continuous actual waves by sampled-data numerical analogs propagating in a data space stored in a computer. Electromagnetic phenomena such as induction of surface currents, scattering and multiple scattering, penetration through apertures, and cavity excitation are modeled time-step by time-step by the action of the curl equations analog.

Recently, the FD-TD method has received more and more attentions because it has advantages over the moment method in solving problems involving electrically large bodies and complex structures. Most attentions can be addressed in two aspects: a) Improvement of the technique theoretically by investigating better radiation boundary condition. The most recent work proposed by Feng [27] is a new method to improve the radiation boundary condition by introducing a correcting factor. It seems that this method works more efficiently than others by raising the order of radiation boundary condition. However, it has been demonstrated only for two dimensional cases. b) Completing the algorithm for wider applications. By employing the integral interpretation of Yee's model, a new method [29,30] was developed for a simple but efficient modeling of thin-slot coupling, thin-wire coupling, and smoothly curved surfaces , thus, overcomes the main drawbacks of the FD-TD method.

The FD-TD method has been widely applied in electromagnetics area. It has been used to solve problems which include two and three dimensional electromagnetic wave scattering, electromagnetic wave penetration and coupling for both two and three dimensions, very complex three-dimensional structures like human bodies and anisotropic objects, inverse scattering reconstructions in one and two dimensional cases, and microstrip and microwave circuit models. However, little effort has been made in the application of the FD-TD method to metallic objects with thin material coating and to transmitting and receiving characteristics of antenna problems.

When solving the electromagnetic scattering problems of metallic objects with material coating by using moment method or the finite element method, these methods become very inefficient when the objects become electrically large or sharp curvature geometries are involved. For some antenna problems, such as cavity-backed antenna in a infinite ground plane, integral equation or modes matching techniques also become unpractical.

Main effort of this chapter is devoted towards providing a basis of expanding the FD-TD method to two important electromagnetic topics by using most advanced algorithms: two dimensional partial coating of metallic objects, and transmitting and receiving antennas.

In section 3.2, we start from Maxwell's curl equations to develop two dimensional basic FD-TD algorithm details. It includes Maxwell's equations, the Yee's algorithm. In section 3.3, radiation boundary conditions for two and three dimensional cases are studied intensively. Different approaches of deriving a radiation boundary condition are discussed and both first and second order radiation boundary conditions of two and three dimensional cases are derived. The radition boundary condition for corner points is also developed. In section 3.4, a systematic way of analyzing the stability is developed and this method is illustrated through a few examples of different

schemes. In section 3.5, dividing the truncated region into scattered field region and total field region is discussed. In section 3.6, the basic idear of implementing the integral intepretation of Maxwell's curl equations to conform the integration paths is introduced and the application of the idear will be expained in the chapter 4 and chapter 5 when a thin impedance sheet is taken into account.

As we mentioned above, the theories discussed in this chapter will provide a basis for the future applications. As a part of chapter 4, basic FD-TD algorithms will be modified to handle the two dimensional metallic objects coated with thin magnetic material. In chapter 5, the FD-TD method is employed and a few modifications are made to study the effects of an impedance sheet on the receiving and scattering characteristics of a cavity backed antenna.

3.2 BASIC FD-TD ALGORITHMS

3.2.1 Maxwell's Curl Equations

The FD-TD method is a direct implementation of the time-dependent Maxwell equations:

$$\frac{\partial \mathbf{D}}{\partial t} = \nabla \times \mathbf{H} - \mathbf{J} \qquad \frac{\partial \mathbf{B}}{\partial t} = -\nabla \times \mathbf{E} - \mathbf{J}_m \tag{3.2.1}$$

Consider a source-free region with constituent electrical parameters which are independent of time, Maxwell's curl equations can be rewritten into a form:

$$\frac{\partial \mathbf{E}}{\partial t} = \frac{1}{\varepsilon}\nabla \times \mathbf{H} - \frac{\sigma}{\varepsilon}\mathbf{E} \tag{3.2.2a}$$

$$\frac{\partial \mathbf{H}}{\partial t} = -\frac{1}{\mu}\nabla \times \mathbf{E} - \frac{\rho'}{\mu}\mathbf{H} \tag{3.2.2b}$$

Assuming ε, σ, ρ' and μ are isotropic, where ε is the electrical permittivity; σ is the electrical conductivity; ρ' is an equivalent magnetic resistivity and μ is the magnetic permeability; **E** is the electric field and **H** is the magnetic field .

If writing the above equations into scalar forms in the rectangular coordinate systems(x, y, z), we have a set of scalar equations for three dimensional cases:

$$\frac{\partial H_x}{\partial t} = \frac{1}{\mu}\left(\frac{\partial E_y}{\partial z} - \frac{\partial E_z}{\partial y} - \rho' H_x\right) \tag{3.2.3a}$$

$$\frac{\partial H_y}{\partial t} = \frac{1}{\mu}\left(\frac{\partial E_z}{\partial x} - \frac{\partial E_x}{\partial z} - \rho' H_y\right) \tag{3.2.3b}$$

$$\frac{\partial H_z}{\partial t} = \frac{1}{\mu}\left(\frac{\partial E_x}{\partial y} - \frac{\partial E_y}{\partial x} - \rho' H_z\right) \tag{3.2.3c}$$

$$\frac{\partial E_x}{\partial t} = \frac{1}{\varepsilon}\left(\frac{\partial H_z}{\partial y} - \frac{\partial H_y}{\partial z} - \sigma E_x\right) \tag{3.2.3d}$$

$$\frac{\partial E_y}{\partial t} = \frac{1}{\varepsilon}\left(\frac{\partial H_x}{\partial z} - \frac{\partial H_z}{\partial x} - \sigma E_y\right) \tag{3.2.3e}$$

$$\frac{\partial E_z}{\partial t} = \frac{1}{\varepsilon}\left(\frac{\partial H_y}{\partial x} - \frac{\partial H_x}{\partial y} - \sigma E_z\right) \tag{3.2.3f}$$

Now, consider two dimensional EM scattering problems. If we assume that neither the incident wave excitation nor the modeled geometry has any variation in the z direction, all the derivatives with respect to z are equal to zero ($\frac{\partial}{\partial z} = 0$) such that Maxwell equations are simplified. Due to the linearity of Maxwell equations, any polarization of incident wave excitation can be decomposed into a linear composition of a transverse magnetic (TM) mode and a transverse electric (TE) mode. Maxwell equations finally are simplified to two sets of scalar equations according to TM mode and TE mode to describe two-dimensional wave interaction with objects. The relevant equations for these two modes are as follows:

TM mode with $H_z = 0$, $E_x = 0$, and $E_y = 0$:

$$\frac{\partial H_x}{\partial t} = -\frac{1}{\mu}\left(\frac{\partial E_z}{\partial y} + \rho' H_x\right) \tag{3.2.4a}$$

$$\frac{\partial H_y}{\partial t} = \frac{1}{\mu}\left(\frac{\partial E_z}{\partial x} - \rho' H_y\right) \tag{3.2.4b}$$

$$\frac{\partial E_z}{\partial t} = \frac{1}{\varepsilon}\left(\frac{\partial H_y}{\partial x} - \frac{\partial H_x}{\partial y} - \sigma E_z\right) \tag{3.2.4c}$$

TE mode with $E_z = 0$, $H_x = 0$, and $H_y = 0$:

$$\frac{\partial E_x}{\partial t} = \frac{1}{\varepsilon}\left(\frac{\partial H_z}{\partial y} - \sigma E_x\right) \tag{3.2.5a}$$

$$\frac{\partial E_y}{\partial t} = \frac{-1}{\varepsilon}\left(\frac{\partial H_z}{\partial x} + \sigma E_y\right) \tag{3.2.5b}$$

$$\frac{\partial H_z}{\partial t} = \frac{1}{\mu}\left(\frac{\partial E_x}{\partial y} - \frac{\partial E_y}{\partial x} - \rho' H_z\right) \tag{3.2.5c}$$

3.2.2 Discretization of the scalar Maxwell equations by using Yee's model

The method of solving Maxwell equations directly is equivalent to the mathematical problem of solving a set of linear partial differential equations plus boundary conditions with initial values. The derivatives for both spatial variation and temporal variation will be approximated by using finite difference. The best numerical model available so far is the one proposed by Yee [22]. The reason is that from the mathematical point of view , it achieves the second order accuracy in the space and time increments respectively and also it is a natural geometrical interpolation of Maxwell equations. These facts will become very clear as we go through this chapter.

In 1966, Yee introduced a set of finite-difference equations for the systems of Eq.(3.2.3). Following Yee's notation, we denote a space point in a rectangular lattice as

$$(i, j, k) = (i\Delta x, j\Delta y, k\Delta z)$$
$$F^n(i, j, k) = F(i\Delta x, j\Delta y, k\Delta z, n\Delta t)$$

where Δx, Δy, and Δz are respectively, the lattice space increments in the x , y, and z coordinate directions; Δt is the time increment; and i, j, k, and n are integers.

To approximate the derivatives, central difference formula is used here.

$$\frac{\partial F^n(i, j, k)}{\partial x} = \frac{F^n(i+\frac{1}{2}, j, k) - F^n(i-\frac{1}{2}, j, k)}{\Delta x} + 0(\Delta x^2) \tag{3.2.6a}$$

$$\frac{\partial F^n(i, j, k)}{\partial t} = \frac{F^{n+\frac{1}{2}}(i, j, k) - F^{n-\frac{1}{2}}(i, j, k)}{\Delta t} + 0(\Delta t^2) \tag{3.2.6b}$$

Applying above central difference equations to the scalar forms of Maxwell equation (3.2.3), one may observe that in order to achieve the second order accuracy in spatial derivative, the components of **E** and **H** about a unit cell of the lattice are naturally positioned as shown in Fig. 3.1 , and also that in order to achieve the second order accuracy in temporal derivatives, **E** and **H** are evaluated at alternate half time steps. Using Eq(3.2.6) to approximate the derivatives of Eq.(3.2.3), we obtain a set of difference equations for three dimensional cases:

With the definitions of:

$$CA(i, j, k) = \frac{2Z_0\mu_r(i, j, k) - \rho'(i, j, k)c_0\Delta t}{2Z_0\mu_r(i, j, k) + \rho'(i, j, k)c_0\Delta t}$$

$$CB(i, j, k) = \frac{2Z_0\mu_r(i, j, k)}{2Z_0\mu_r(i, j, k) + \rho'(i, j, k)c_0\Delta t}$$

We have:

$$H_x^{n+\frac{1}{2}}(i, j+\frac{1}{2}, k+\frac{1}{2}) = CA(i, j+\frac{1}{2}, k+\frac{1}{2})H_x^{n-\frac{1}{2}}(i, j+\frac{1}{2}, k+\frac{1}{2}) \tag{3.2.7a}$$

$$- \frac{c_0\Delta t CB(i, j+\frac{1}{2}, k+\frac{1}{2})}{\mu_r(i, j+\frac{1}{2}, k+\frac{1}{2})\Delta y Z_0}[E_z^n(i, j+1, k+\frac{1}{2}) - E_z^n(i, j, k+\frac{1}{2})]$$

$$+ \frac{c_0\Delta t CB(i, j+\frac{1}{2}, k+\frac{1}{2})}{\mu_r(i, j+\frac{1}{2}, k+\frac{1}{2})\Delta z Z_0}[E_y^n(i, j+\frac{1}{2}, k+1) - E_y^n(i, j+\frac{1}{2}, k)]$$

$$H_y^{n+\frac{1}{2}}(i+\frac{1}{2}, j, k+\frac{1}{2}) = CA(i+\frac{1}{2}, j, k+\frac{1}{2})H_y^{n-\frac{1}{2}}(i+\frac{1}{2}, j, k+\frac{1}{2}) \tag{3.2.7b}$$

$$+ \frac{c_0\Delta t CB(i+\frac{1}{2}, j, k+\frac{1}{2})}{\mu_r(i+\frac{1}{2}, j, k+\frac{1}{2})\Delta x Z_0}[E_z^n(i+1, j, k+\frac{1}{2}) - E_z^n(i, j, k+\frac{1}{2})]$$

$$- \frac{c_0\Delta t CB(i+\frac{1}{2}, j, k+\frac{1}{2})}{\mu_r(i+\frac{1}{2}, j, k+\frac{1}{2})\Delta z Z_0}[E_x^n(i+\frac{1}{2}, j, k+1) - E_x^n(i+\frac{1}{2}, j, k)]$$

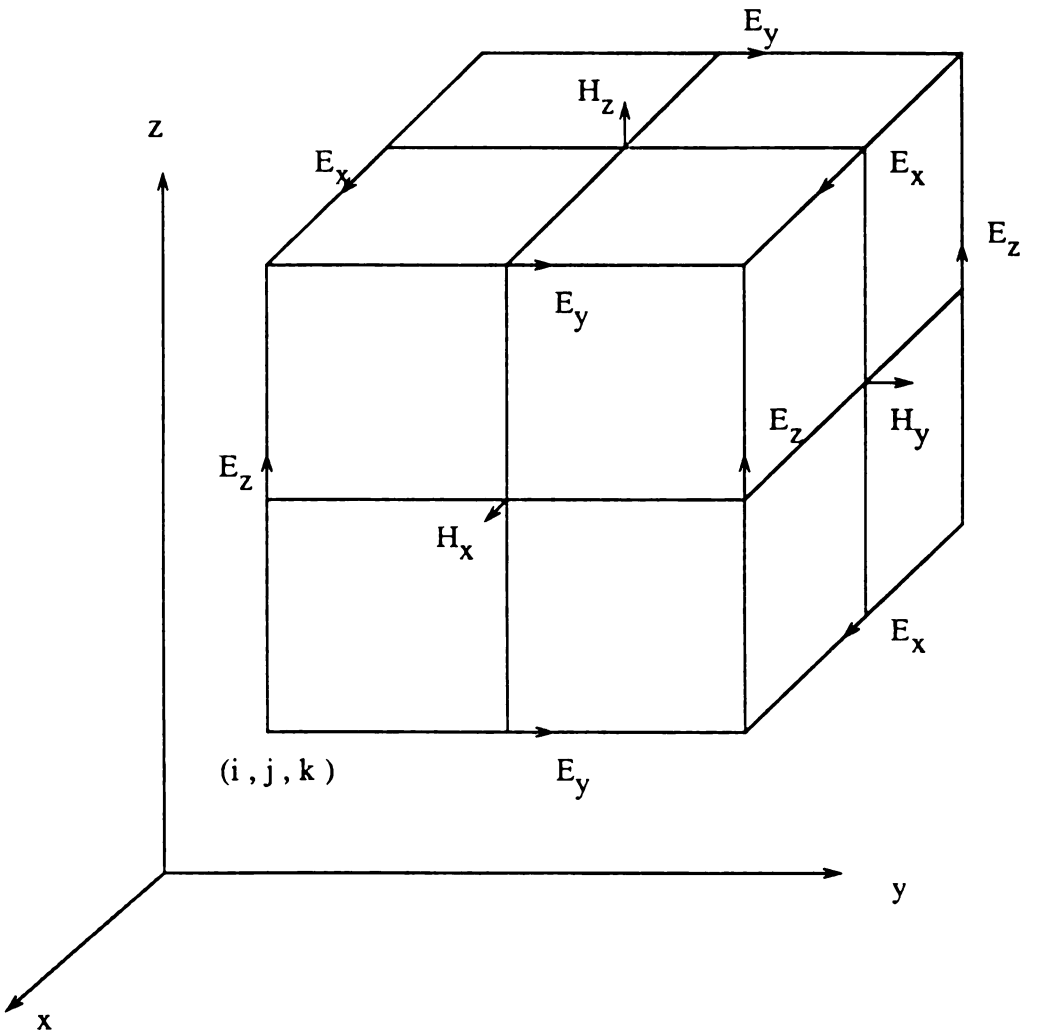

Fig. 3.1 Lattice Unit Cell ----Yee's Model

$$H_z^{n+\frac{1}{2}}(i+\frac{1}{2}, j+\frac{1}{2}, k)= CA(i+\frac{1}{2}, j+\frac{1}{2}, k)H_z^{n-\frac{1}{2}}(i+\frac{1}{2}, j+\frac{1}{2}, k) \tag{3.2.7c}$$

$$+ \frac{c_0\Delta t CB(i+\frac{1}{2}, j+\frac{1}{2}, k)}{\mu_r(i+\frac{1}{2}, j+\frac{1}{2}, k)\Delta y Z_0}[E_x^n(i+\frac{1}{2}, j+1, k) - E_x^n(i+\frac{1}{2}, j, k)]$$

$$- \frac{c_0\Delta t CB(i+\frac{1}{2}, j+\frac{1}{2}, k)}{\mu_r(i+\frac{1}{2}, j+\frac{1}{2}, k)\Delta x Z_0}[E_y^n(i+1, j+\frac{1}{2}, k) - E_y^n(i, j+\frac{1}{2}, k)]$$

$$E_x^{n+1}(i+\frac{1}{2}, j, k) = \frac{2\varepsilon(i+\frac{1}{2}, j, k)-\Delta t\sigma(i+\frac{1}{2}, j, k)}{2\varepsilon(i+\frac{1}{2}, j, k)+\Delta t\sigma(i+\frac{1}{2}, j, k)}E_x^n(i+\frac{1}{2}, j, k) \tag{3.2.7d}$$

$$+ \frac{2\Delta t}{\Delta y(2\varepsilon(i+\frac{1}{2}, j, k)+\Delta t\sigma(i+\frac{1}{2}, j, k))}[H_z^{n+\frac{1}{2}}(i+\frac{1}{2}, j+\frac{1}{2}, k) - H_z^{n+\frac{1}{2}}(i+\frac{1}{2}, j-\frac{1}{2}, k)]$$

$$- \frac{2\Delta t}{\Delta z(2\varepsilon(i+\frac{1}{2}, j, k)+\Delta t\sigma(i+\frac{1}{2}, j, k))}[H_y^{n+\frac{1}{2}}(i+\frac{1}{2}, j, k+\frac{1}{2}) - H_y^{n+\frac{1}{2}}(i+\frac{1}{2}, j, k-\frac{1}{2})]$$

$$E_y^{n+1}(i, j+\frac{1}{2}, k) = \frac{2\varepsilon(i, j+\frac{1}{2}, k)-\Delta t\sigma(i, j+\frac{1}{2}, k)}{2\varepsilon(i, j+\frac{1}{2}, k)+\Delta t\sigma(i, j+\frac{1}{2}, k)}E_y^n(i, j+\frac{1}{2}, k) - \tag{3.2.7e}$$

$$\frac{2\Delta t}{\Delta x(2\varepsilon(i, j+\frac{1}{2}, k)+\Delta t\sigma(i, j+\frac{1}{2}, k))}[H_z^{n+\frac{1}{2}}(i+\frac{1}{2}, j+\frac{1}{2}, k) - H_z^{n+\frac{1}{2}}(i-\frac{1}{2}, j+\frac{1}{2}, k)]$$

$$\frac{2\Delta t}{\Delta z(2\varepsilon(i, j+\frac{1}{2}, k)+\Delta t\sigma(i, j+\frac{1}{2}, k))}[H_x^{n+\frac{1}{2}}(i, j+\frac{1}{2}, k+\frac{1}{2}) - H_x^{n+\frac{1}{2}}(i, j+\frac{1}{2}, k-\frac{1}{2})]$$

$$E_z^{n+1}(i, j, k+\frac{1}{2}) = \frac{2\varepsilon(ij, k+\frac{1}{2})-\Delta t\sigma(i, j, k+\frac{1}{2})}{2\varepsilon(ij, k+\frac{1}{2})+\Delta t\sigma(i, j, k+\frac{1}{2})}E_z^n(i, j, k+\frac{1}{2}) \tag{3.2.7f}$$

$$+ \frac{2\Delta t}{\Delta x(2\varepsilon(i, j, k+\frac{1}{2})+\Delta t\sigma(i, j, k+\frac{1}{2}))}[H_y^{n+\frac{1}{2}}(i+\frac{1}{2}, j, k+\frac{1}{2}) - H_y^{n+\frac{1}{2}}(i-\frac{1}{2}, j, k+\frac{1}{2})]$$

$$- \frac{2\Delta t}{\Delta y(2\varepsilon(i, j, k+\frac{1}{2})+\Delta t\sigma(i, j, k+\frac{1}{2}))}[H_x^{n+\frac{1}{2}}(i, j+\frac{1}{2}, k+\frac{1}{2}) - H_x^{n+\frac{1}{2}}(i, j-\frac{1}{2}, k+\frac{1}{2})]$$

In a similar way, two dimensional models for the TM or TE mode can be described in the Fig. 3.2 a or Fig. 3.2 b. Following Fig.3.2 , Eq(3.2.4) and Eq(3.2.5), finite difference equations for both TM and TE cases result in:

Define:

$$CA(i.\ j) = 2\mu(i,\ j) + \rho'(i,\ j)\Delta t$$
$$CB(i.\ j) = 2\mu(i,\ j) - \rho'(i,\ j)\Delta t$$

For the TM case:

$$E_z^{n+1}(i,\ j) = \frac{2\varepsilon(i,j)-\Delta t\sigma(i,\ j)}{2\varepsilon(i,\ j)+\Delta t\sigma(i,\ j)} E_z^n(i,\ j) + \frac{2\Delta t}{\Delta x(2\varepsilon(i,\ j)+\Delta t\sigma(i,\ j))}[H_y^{n+\frac{1}{2}}(i+\frac{1}{2},\ j) - H_y^{n+\frac{1}{2}}(i-\frac{1}{2},\ j)] - \frac{2\Delta t}{\Delta y(2\varepsilon(i,j)+\Delta t\sigma(i,\ j))}[H_x^{n+\frac{1}{2}}(i,\ j+\frac{1}{2}) - H_x^{n+\frac{1}{2}}(i,\ j-\frac{1}{2})] \tag{3.2.8a}$$

$$H_x^{n+\frac{1}{2}}(i,\ j+\frac{1}{2}) = \frac{CB(i,\ j+\frac{1}{2})}{CA(i,\ j+\frac{1}{2})}(H_x^{n-\frac{1}{2}}(i,\ j+\frac{1}{2}) - \frac{2\Delta t}{CA(i,\ j+\frac{1}{2})\Delta y}[E_z^n(i,\ j+1) - E_z^n(i,\ j)] \tag{3.2.8b}$$

$$H_y^{n+\frac{1}{2}}(i+\frac{1}{2},\ j) = \frac{CB(i+\frac{1}{2},\ j)}{CA(i+\frac{1}{2},\ j)} H_y^{n-\frac{1}{2}}(i+\frac{1}{2},\ j) + \frac{2\Delta t}{CA(i+\frac{1}{2},\ j)\Delta x}[E_z^n(i+1,\ j) - E_z^n(i,\ j)] \tag{3.2.8c}$$

For the TE case:

$$E_x^{n+1}(i+\frac{1}{2},\ j) = \frac{2\varepsilon(i+\frac{1}{2},\ j)-\Delta t\sigma(i+\frac{1}{2},\ j)}{2\varepsilon(i+\frac{1}{2},\ j)+\Delta t\sigma(i+\frac{1}{2},\ j)} E_x^n(i+\frac{1}{2},\ j) + \frac{2\Delta t}{\Delta y(2\varepsilon(i+\frac{1}{2},\ j)+\Delta t\sigma(i+\frac{1}{2},\ j))}[H_z^{n+\frac{1}{2}}(i+\frac{1}{2},\ j+\frac{1}{2}) - H_z^{n+\frac{1}{2}}(i+\frac{1}{2},\ j-\frac{1}{2})] \tag{3.2.9a}$$

$$E_y^{n+1}(i,\ j+\frac{1}{2}) = \frac{2\varepsilon(i,\ j+\frac{1}{2})-\Delta t\sigma(i,\ j+\frac{1}{2})}{2\varepsilon(i,\ j+\frac{1}{2})+\Delta t\sigma(i,\ j+\frac{1}{2})} E_x^n(i,\ j+\frac{1}{2}) - \tag{3.2.9b}$$

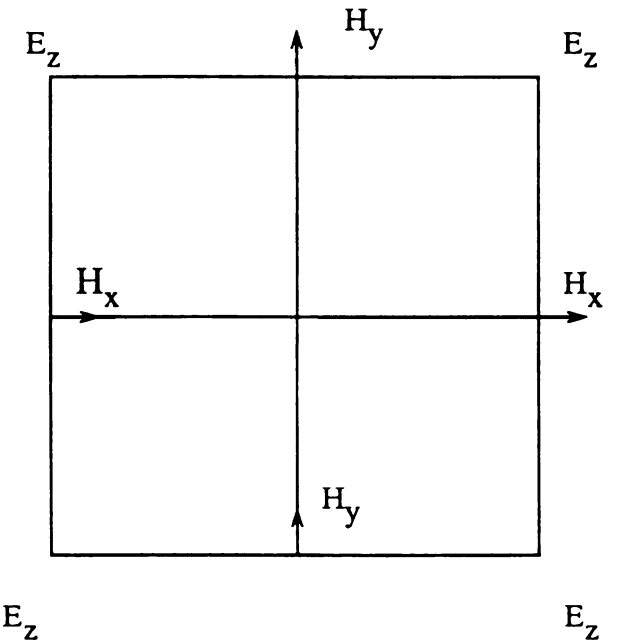

(a) For TM Mode

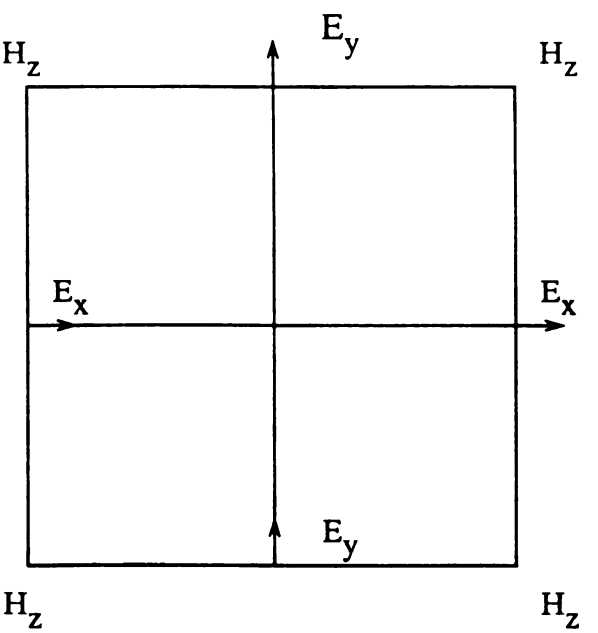

(b) For TE Mode

Fig. 3.2 Two Dimensional Lattice Unit Cells

$$\frac{2\Delta t}{\Delta x(2\varepsilon(i, j+\frac{1}{2})+\Delta t\sigma(i, j+\frac{1}{2}))}[H_z^{n+\frac{1}{2}}(i+\frac{1}{2}, j+\frac{1}{2}) - H_z^{n+\frac{1}{2}}(i-\frac{1}{2}, j+\frac{1}{2})]$$

$$H_z^{n+\frac{1}{2}}(i+\frac{1}{2}, j+\frac{1}{2}) = \frac{CB(i+\frac{1}{2}, j+\frac{1}{2})}{CA(i+\frac{1}{2}, j+\frac{1}{2})} H_z^{n-\frac{1}{2}}(i+\frac{1}{2}, j+\frac{1}{2}) \qquad (3.2.9c)$$

$$+ \frac{2\Delta t}{CA(i+\frac{1}{2}, j+\frac{1}{2})\Delta y}[E_x^n(i+\frac{1}{2}, j) - E_x^n(i-\frac{1}{2}, j)]$$

$$- \frac{2\Delta t}{CA(i+\frac{1}{2}, j+\frac{1}{2})\Delta x}[E_y^n(i, j+\frac{1}{2}) - E_y^n(i, j-\frac{1}{2})]$$

The increments should satisfy $\Delta t \le \frac{1}{c_{max}[\frac{1}{\Delta x^2} + \frac{1}{\Delta y^2}]^{\frac{1}{2}}}$ for two dimensional case and $\Delta t \le \frac{1}{c_{max}[\frac{1}{\Delta x^2} + \frac{1}{\Delta y^2} + \frac{1}{\Delta z^2}]^{\frac{1}{2}}}$ for three dimensional cases to insure the stability for above equations. This will be discussed in details in section 3.4.

3.3 Radiation Boundary Conditions

Considering the " open " problems where the domain of the computed field is ideally unbounded, that is the whole space, it is obvious that the infinite space needs to be truncated into a finite space to fit in the finite storage of a computer. The computation zone must be large enough to enclose the structure of interest, and an artificial boundary condition must be posed on the outmost truncated surfaces to simulate the outside extension of the infinite space. Based on the physical meaning, this boundary condition should be transparent to outgoing wave from the computation zone theoretically and numerical implementation of the boundary condition should limit the

reflections of outward propagating waves to some acceptable level. This boundary condition has been called either the radiation boundary condition or the artificial boundary condition.

From a mathematical point of view, boundary conditions are necessary for solving a set of partial differential equations. For the " open " problem, Sommerfeld radiation boundary condition at infinity plays a role as the boundary condition. For a finite computation zone, the radiation boundary condition at outer lattice truncation interfaces is needed instead of Sommerfeld condition. We can see that the radiation boundary condition must be used through the detailed finite difference schemes. From the Yee's model and the numerical algorithm of Maxwell curl equations as described in section 3.2.2, the radiation boundary condition can not be directly obtained. As illustrated in Fig. 3.2, a central difference scheme requires knowledge of the field one-half space cell to each side of an observation point. We can not use the same scheme on the outmost lattice plane as interior point because no information for the field one-half space cell outside the outmost lattice plane is available which is illustrated in Fig.3.3.

In 1966 when Yee first employed the FD-TD method to solve an EM problem, he used perfect conductor condition, tangential components of E field being equal to zero, on the outmost surface which definitely caused a lot of reflection. Perhaps that was the reason that the FD-TD method didn't become popular because of limited applications. Later on, a number of better methods were developed to compute the fields at boundary nodes: Taylar et al. [31] used simple space extrapolation ; Taflove & Brodwin [23] used averaged process in an attempt to account for all possible angles of propagation of outgoing waves; Merewether [32] and Kunz and Lee [33] used far field approxmation at large distances from the center of the scatteres to obtain an absorbing boundary condition. All these methods mentioned above are equivalent to the first order approximation of the radiation boundary condition. They have disadvantages of

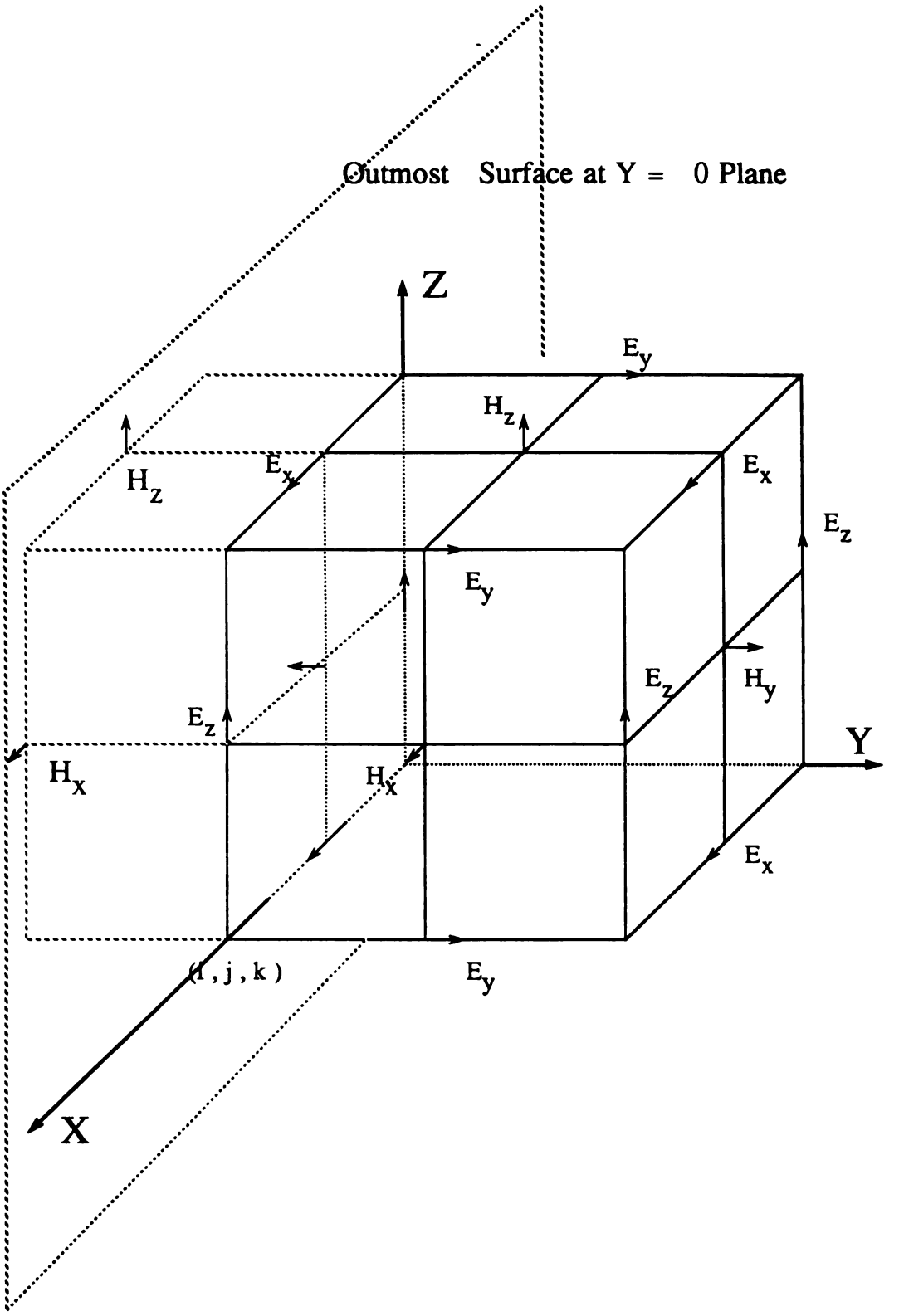

Fig. 3.3 Lattice Unit Cells Near Outmost Surface (Y=0 Plane)

causing considerable reflections when the fields near the boundary of mesh do not propagate in a specific direction (either the direction normal to the boundary or radial direction from the center of the scatter).

Only after Mur [28] in 1981 employed the Engquist and Majda's first and second order absorbing boundary conditions [24], which are first one and two terms of Pade expansion of the exact absorbing boundary condition for electromagnetic field problems, it was made possible for the FD-TD method to be employed to much wider applications of solving EM problems. So far the second order Engquist and Majda's absorbing boundary condition is the best among the methods mentioned above. This section will develop the theory and numerical implementation of the radiation boundary condition through different view points based on Engquist and Majda's theory.

3.3.1. Derivation of Radiation Boundary Condition by Wave Equation

Through Eq.(3.2.3) of section 3.2 and Yee's model as shown in Fig.3.1, radiation boundary conditions for the Maxwell's equations on the outmost mesh are only required for the three components of electric fields if the outmost surface is placed as shown in Fig.3.3. The reason is that to evaluate the magnetic fields in the computational zone, the electric fields needed in Eq.(3.2.3) are also inside computational region which are available and that to calculate electric fields on the truncated lattice mesh, we need the magnetic fields outside of the computational region for which we have no information about them. For the same reason, if the outmost surface is placed half cell away from that in Fig.3.3, the radiation boundary condition is only needed for the magnetic field components.

a. The First method

Maxwell equations permit wave propagation in all directions, and after eliminat-

ing H field from Maxwell's equations, we obtain

$$(\partial_x^2 + \partial_y^2 + \partial_z^2 - c_0^{-2}\partial_t^2)\mathbf{E} = 0 \tag{3.3.1}$$

That means each component of electric fields independently satisfies the three-dimensional wave equation. If we denote the each component of electric fields as W, then

$$(\partial_x^2 + \partial_y^2 + \partial_z^2 - c_0^{-2}\partial_t^2)W = 0 \tag{3.3.2}$$

As stated in the previous discussion, we need radiation boundary condition at outmost lattice. This means that a partial differential equation which permits wave propagation only in certain directions, which is called a "one-way wave equation", is needed.

Consider a function W(x, y, z, t) and the Fourier transform over the space domain of it as $w(k_x, k_y, k_z, t)$. Taking the Fourier transform of Eq.(3.3.2), which yields:

$$-(k_x^2 + k_y^2 + k_z^2)w(k_x, k_y, k_z, t) - c_0^{-2}\partial_t^2 w(k_x, k_y, k_z, t) = 0 \tag{3.3.3}$$

Solving Eq. (3.3.3) $w(k_x, k_y, k_z, t)$, we have:

$$w(k_x, k_y, k_z, t) = A(k_x, k_y, k_z)e^{jc_0kt} + B(k_x, k_y, k_z)e^{-jc_0kt} \tag{3.3.4}$$

where $k^2 = k_x^2 + k_y^2 + k_z^2$, A and B are coefficients with parameters (k_x, k_y, k_z) . We can see that the general spectral solution of wave equation (3.3.2) are two waves traveling along opposite directions. This can be seen more clearly if we write $W(x, y, z,t)$ in terms of its spectra:

$$W(x, y, z,t) = \frac{1}{2\pi^3}\int_{-\infty}^{+\infty} w(k_x, k_y, k_z, t)e^{-j\vec{k}\cdot\vec{r}}\, dk_x\, dk_y\, dk_z \tag{3.3.5}$$

Denoting $\vec{k} = (k_x, k_y, k_z)$ and $\vec{r} = (x, y,z)$, Substituting Eq.(3.3.4) into Eq. (3.3.5), we have

$$W(x, y, z,t) = \frac{1}{2\pi^3}\int_{-\infty}^{+\infty} [A(k_x, k_y, k_z)e^{jc_0kt-j\vec{k}\cdot\vec{r}} + B(k_x, k_y, k_z)e^{-jc_0kt-j\vec{k}\cdot\vec{r}}]\, dk_x\, dk_y\, dk_z \tag{3.3.6}$$

From Eq.(3.3.6), an arbitrary $W(x, y, z, t)$ is a superposition of two waves propagating in opposite direction , $\vec{k}$ and $-\vec{k}$, over the whole spectral domain. Now let's consider only the wave in one direction along $\vec{k}$, Eq.(3.3.6) becomes:

$$W(x, y, z,t) = \frac{1}{2\pi^3}\int_{-\infty}^{+\infty} A(k_x, k_y, k_z)e^{jc_0kt-j\vec{k}\cdot\vec{r}}\, dk_x\, dk_y\, dk_z \tag{3.3.7}$$

Denoting $A(k_x, k_y, k_z)e^{jc_0kt-j\vec{k}\cdot\vec{r}}$ by $wa(k_x, k_y, k_z, t)$, if represents a wave propagating along $\vec{k}$, let's consider $\frac{\partial wa}{\partial t}$ and the derivative of wa along the direction $\vec{n}$, $\frac{\partial wa}{\partial n}$:

$$\frac{\partial wa}{\partial t} = jc_0kwa \tag{3.3.8a}$$

$$\begin{aligned}\frac{\partial wa}{\partial n} &= \frac{\partial wa}{\partial x}\frac{\partial x}{\partial n} + \frac{\partial wa}{\partial y}\frac{\partial y}{\partial n} + \frac{\partial wa}{\partial z}\frac{\partial z}{\partial n} \\ &= -jwa[k_x\frac{\partial x}{\partial n} + k_y\frac{\partial y}{\partial n} + k_z\frac{\partial z}{\partial n}] \\ &= -jwa\vec{k}\cdot[\hat{x}\frac{\partial x}{\partial n} + \hat{y}\frac{\partial y}{\partial n} + \hat{z}\frac{\partial z}{\partial n}]\end{aligned} \tag{3.3.8b}$$

Comparing these two equations, we observe that by multiplying proper coefficients, one equation can be related to another:

$$\frac{\partial wa}{\partial t}\frac{\vec{k}}{k}\cdot[\hat{x}\frac{\partial x}{\partial n} + \hat{y}\frac{\partial y}{\partial n} + \hat{z}\frac{\partial z}{\partial n}] + c_0\frac{\partial wa}{\partial n} = 0 \tag{3.3.9a}$$

If we denote $c_0^{-1}\frac{\vec{k}}{k} = \vec{x}s_x + \vec{y}s_y + \vec{z}s_z$, then $s_x^2 + s_y^2 + s_z^2 = c_0^{-2}$. Equation(3.3.7) becomes:

$$\frac{\partial wa}{\partial t}[s_x\frac{\partial x}{\partial n} + s_y\frac{\partial y}{\partial n} + s_z\frac{\partial z}{\partial n}] + \frac{\partial wa}{\partial n} = 0 \tag{3.3.9b}$$

This can be interpreted physically as shown in Fig.3.4. For any wa which satisfies above partial differential equation, waves will exit ideally the plane with its normal $\hat{n}$ propagating along direction $\vec{k}$. If $\vec{k}$ is parallel to $\hat{n}$, Eq.(3.3.9) is reduced to :

$$\frac{\partial wa}{\partial n} + c_0^{-1}\frac{\partial wa}{\partial t} = 0 \tag{3.3.10}$$

This is called the first order approximation of the radiation boundary condition which describes a wave propagating along $\hat{n}$. In other words, by using Eq.(3.3.10), it

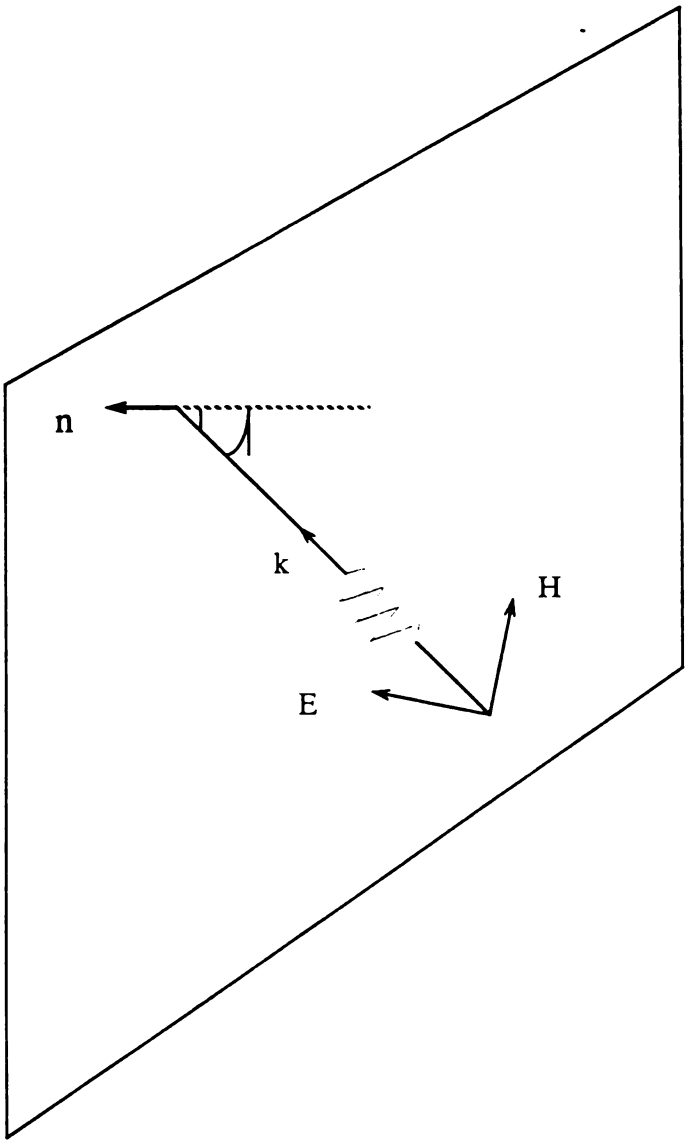

Fig. 3.4 Graphic Interpretation Of Eq. (3.3.9b)

causes no reflection for waves propagating along $\hat{n}$.

If , in particular but without loss of generality, taking $\hat{n}$ as $-\hat{x}$ direction and assuming the mesh is located in the region 0<x, we give the boundary condition for the plane x=0. Eq.(3.3.9) is changed to a form:

$$(-\frac{\partial}{\partial t}s_x - \frac{\partial}{\partial x})wa|_{x=0} = 0 \tag{3.3.11}$$

By using relation $s_x^2 + s_y^2 + s_z^2 = c_0^{-2}$ and noting $s_x<0$, we have an equation which is consistent with Eq.(8) of Mur's[28]:

$$(\frac{\partial}{\partial x} - (c_0^{-2} - s_y^2 - s_z^2)^{\frac{1}{2}}\frac{\partial}{\partial t})wa|_{x=0} = 0 \tag{3.3.12}$$

For given values of s_y, s_z , the solution of above equation will determine a *wa* on the outer surface which is consistent with an outgoing wave. Since the angles of incidence of the wave approaching the surface is unknown, an approximation of Eq (3.3.12) must be made. By approximating $(c_0^{-2} - s_y^2 - s_z^2)$ with Taylor expansion, it will result in different order approximation of the radiation boundary condition.

By taking first term of Taylor expansion:

$$(1 - (c_0 s_y)^2 - (c_0 s_z)^2)^{\frac{1}{2}} = 1 + 0((c_0 s_y)^2 + (c_0 s_z)^2) \tag{3.3.13}$$

We obtain as a first order approximation:

$$(\frac{\partial}{\partial x} - c_0^{-1}\frac{\partial}{\partial t})wa|_{x=0} = 0 \tag{3.3.14}$$

It is also a special case of Eq.(3.3.11) when $\vec{n}$ is $-\vec{x}$.

If we keep the first two terms of Taylor expansion, then:

$$(1 - (c_0 s_y)^2 - (c_0 s_z)^2)^{\frac{1}{2}} = 1 - 0.5[(c_0 s_y)^2 + (c_0 s_z)^2] + 0(((c_0 s_y)^2 + (c_0 s_z)^2)^2) \tag{3.3.15}$$

After substituting Eq(3.3.15) into Eq.(3.3.12), the second order approximation is yielded:

$$(c_0^{-1}\partial_{xt}^2 - c_0^{-2}\partial_t^2 + \frac{1}{2}(\partial_y^2 + \partial_z^2))W|_{x=0} = 0 \qquad (3.3.16)$$

The second order approximation of radiation boundary condition for waves towards other planes ($x = 0, h, y = 0, h, z = 0, h$) can be derived through a similar process. They are summarized as follows:

$$(c_0^{-1}\partial_{xt}^2 - c_0^{-2}\partial_t^2 + \frac{1}{2}(\partial_y^2 + \partial_z^2))W|_{x=0} = 0 \qquad (3.3.17a)$$

$$(c_0^{-1}\partial_{xt}^2 + c_0^{-2}\partial_t^2 - \frac{1}{2}(\partial_y^2 + \partial_z^2))W|_{x=h} = 0 \qquad (3.3.17b)$$

$$(c_0^{-1}\partial_{yt}^2 - c_0^{-2}\partial_t^2 + \frac{1}{2}(\partial_x^2 + \partial_z^2))W|_{y=0} = 0 \qquad (3.3.17c)$$

$$(c_0^{-1}\partial_{yt}^2 + c_0^{-2}\partial_t^2 - \frac{1}{2}(\partial_x^2 + \partial_z^2))W|_{y=h} = 0 \qquad (3.3.17d)$$

$$(c_0^{-1}\partial_{zt}^2 - c_0^{-2}\partial_t^2 + \frac{1}{2}(\partial_x^2 + \partial_y^2))W|_{z=0} = 0 \qquad (3.3.17e)$$

$$(c_0^{-1}\partial_{zt}^2 + c_0^{-2}\partial_t^2 - \frac{1}{2}(\partial_x^2 + \partial_y^2))W|_{z=h} = 0 \qquad (3.3.17f)$$

For a two dimensional problem, we can simplify the Eq.(3.3.17) by taking $\partial_z^2 W = 0$ or it can be further simplified in such a way : For TM mode , we only have E_z, H_x, H_y and Eq.(3.2.4a) becomes :

$$\mu_0 \partial_t H_x = -\partial_y E_z \qquad (3.3.18)$$

substituting (3.3.18) into (3.3.16) with $W = E_z$ and noting $\frac{\partial}{\partial z} = 0$, after integrating with respect to t with $E_z = 0$ for $t < 0$ we obtain:

$$(\partial_x E_z - c_0^{-1}\partial_t E_z - (c_0\mu_0/2)\partial_y H_x)_{x=0} = 0 \qquad (3.3.19)$$

For the TE mode, we only have H_z, E_x, E_y . In this case, we can go through a similar derivation as the TM case or directly use the equation for the TM mode by changing E_z to H_z and E_x to $-H_x$ based on the complementary properties of Maxwell curl equations. We then obtain:

$$(\partial_x H_z - c_0^{-1}\partial_t H_z + (c_0\mu_0/2)\partial_y E_x)_{x=0} = 0 \qquad (3.3.20)$$

b. The Second Method

Another approach to derive the radiation boundary condition is to use operator factoring . Rewritting wave Eq.(3.3.2) as:

$$(\partial_x^2 + \partial_y^2 + \partial_z^2 - c_0^{-2}\partial_t^2)W = 0 \tag{3.3.21}$$

Define partial differential operator L as follows:

$$L = D_x^2 + D_y^2 + D_z^2 - \frac{1}{c_0^2}D_t^2 \tag{3.3.22}$$

Where

$$D_x^2 = \frac{\partial^2}{\partial x^2};\ D_y^2 = \frac{\partial^2}{\partial y^2};\ D_z^2 = \frac{\partial^2}{\partial z^2};\ D_t^2 = \frac{\partial^2}{\partial t^2} \tag{3.3.23}$$

Now Eq (3.3.21) can be written as:

$$LW = 0 \tag{3.3.24}$$

Observe that L can be factored into L^+ and L^-:

$$L = L^+L^- = ((D_x^2 + D_y^2 + D_z^2)^{\frac{1}{2}} + \frac{1}{c_0}D_t)((D_x^2 + D_y^2 + D_z^2)^{\frac{1}{2}} - \frac{1}{c_0}D_t) \tag{3.3.25}$$

where L^+ and L^- are :

$$L^+ = ((D_x^2 + D_y^2 + D_z^2)^{\frac{1}{2}} + \frac{1}{c_0}D_t) \tag{3.3.26a}$$

$$L^- = ((D_x^2 + D_y^2 + D_z^2)^{\frac{1}{2}} - \frac{1}{c_0}D_t) \tag{3.3.26b}$$

Applying L^- to the wave function W will result in an analytical radiation boundary condition which will absorb a plane wave propagating towards the boundary , for example, towards x=0 plane from the right at any angles. On the other hand, operator L^+ will perform on the same function as L^- does except for the wave propagating towards opposite direction, for example, towards x=0 plane from the left .

If, as shown in Fig.3.4, we consider the waves out of x=0 plane from the right half space where the meshes are located, the approximations are made by expanding L^-

into Taylor series:

$$D_x(1 + (\frac{D_y}{D_x})^2 + (\frac{D_z}{D_x})^2)^{\frac{1}{2}} = D_x(1 + 0.5(\frac{D_y}{D_x})^2 + 0.5(\frac{D_z}{D_x})^2) \tag{3.3.27}$$

For $\frac{D_y}{D_x} \ll 1$ and $\frac{D_z}{D_x} \ll 1$, Substituting it back into $L^- = 0$:

$$[D_x(1 + (\frac{D_y}{D_x})^2 + (\frac{D_z}{D_x})^2)^{\frac{1}{2}} - \frac{1}{c_0}D_t]W = [D_x(1 + 0.5(\frac{D_y}{D_x})^2 + 0.5(\frac{D_z}{D_x})^2) - \frac{1}{c_0}D_t]W = 0 \tag{3.3.28}$$

Multiplying both sides of the equation by D_x , we then have:

$$((D_x^2 + 0.5D_y^2 + 0.5D_z^2) - \frac{1}{c_0}D_xD_t))W = 0 \tag{3.3.29}$$

Replacing D_x^2 by using wave equation (3.3.21), it leads to:

$$((c_0^{-2}D_t^2 - 0.5D_y^2 - 0.5D_z^2) - \frac{1}{c_0}D_xD_t))W = 0 \tag{3.3.30}$$

After rearranging above equation, we have the same second order equation as Eq.(12) of Mur's [28] :

$$(\frac{1}{c_0}\partial_{xt}^2 - c_0^{-2}\partial_t^2 + 0.5(\partial_y^2 + \partial_z^2))W|_{x=0} = 0 \tag{3.3.31}$$

3.3.2 Finite-difference Approximation of Radiation Boundary Conditions

In this subsection, we will do the numerical implementation for both second and first approximations of the radiation boundary condition and we will discuss this for two and three dimensional cases separately.

a. Three Dimensional case

First, the numerical scheme of the second order approximation introduced by Mur will be illustrated here. According to Mur's formula, this scheme can be explained graphically as shown in Fig.3.5 for the three-dimensional grid case at the x=0 grid

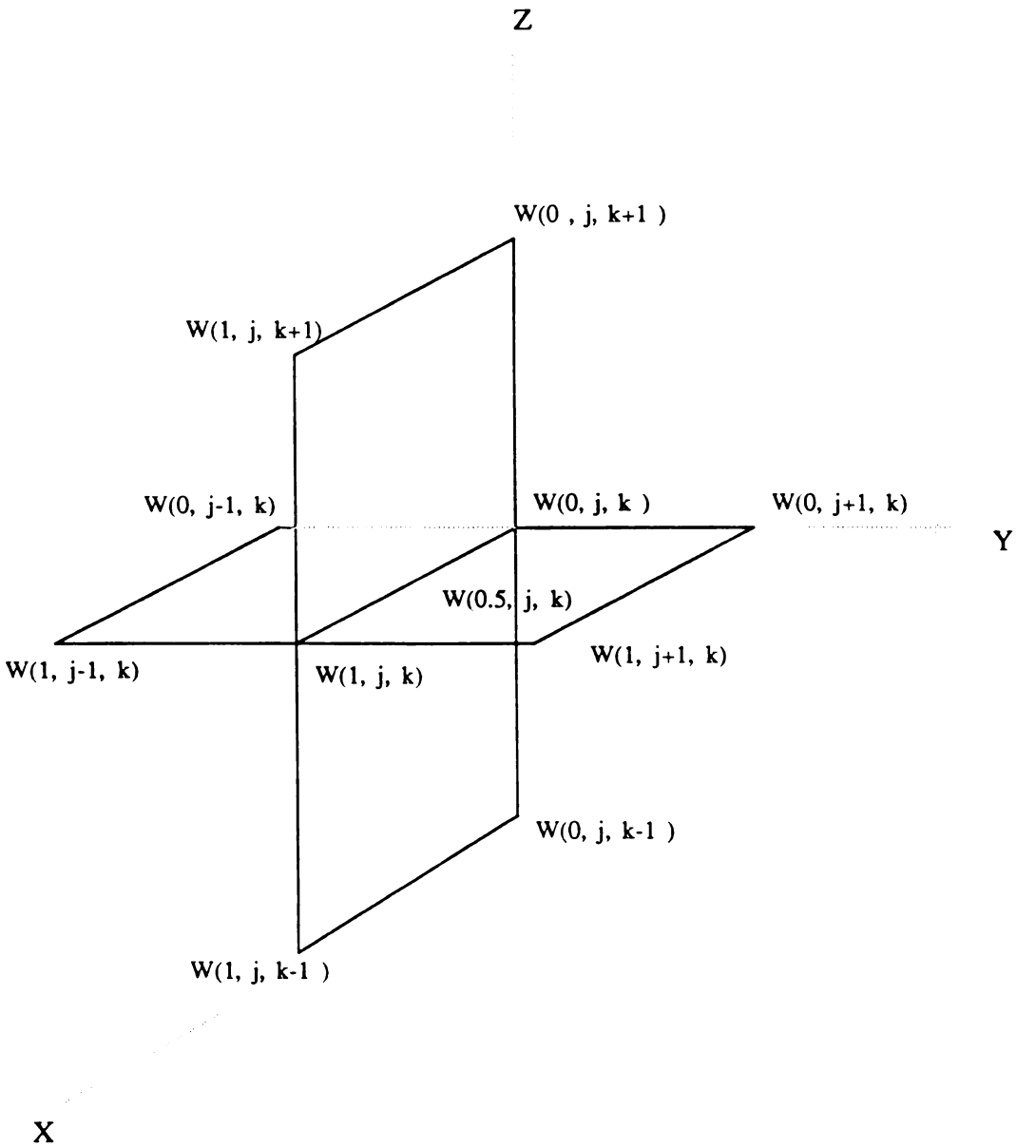

Fig. 3.5 Points Used in the Mur's Second Order Approximation

boundary. Referring to Fig. 3.5, $W^n(i, j, k)$ represents the component of **E** or **H** field which is located at the x=0 grid plane and is tangential to it. For example, $W^n(0, j, k)$ can be determined by the previous values of points surrounding it as illustrated in Fig 3.5. In the following, the Mur's scheme will be derived step by step:

Rewritting Eq.(3.3.16):

$$(c_0^{-1}\partial_{xt}^2 - c_0^{-2}\partial_t^2 + \frac{1}{2}(\partial_y^2 + \partial_z^2))W|_{x=0} = 0 \tag{3.3.32}$$

In the above equation, $\partial_{xt}^2 W$, $\partial_y^2 W$, $\partial_z^2 W$ and $\partial_t^2 W$ must be approximated. Mur employed a finite difference scheme to write Eq.(3.3.32) as:

$$D_o^t D_o^x W^n_{\frac{1}{2},j,k} - \frac{1}{2}D_+^t D_-^t (W^n_{0,j,k} + W^n_{1,j,k}) + \frac{1}{4}D_+^y D_-^y (W^{n-1}_{0,j,k} + W^{n+1}_{1,j,k}) + \frac{1}{4}D_+^z D_-^z (W^{n-1}_{0,j,k} + W^{n+1}_{1,j,k}) = 0 \tag{3.3.33}$$

where the subscript of D indicates different scheme to approximate derivatives, o means central difference, + means forward difference, and - means backward difference. The superscript of D indicates which variable the differential operator is operating on. For example, D_o^t means using central difference formula to approximate the temporal derivative. We will look at the terms of the Eq.(3.3.33) one by one.

The first term $\partial_{xt}^2 W$ is approximated by using central difference for temporal derivative at $t=n\Delta t$ and by central difference for spatial derivative of x at $x = \frac{1}{2}$.

$$W^n_{xt}(\frac{1}{2}, j, k) = \frac{\frac{\partial W}{\partial x}^{n+1}(\frac{1}{2}, j, k) - \frac{\partial W}{\partial x}^{n-1}(\frac{1}{2}, j, k)}{2\Delta t} \tag{3.3.34a}$$

$$= \frac{[\frac{W^{n+1}(1, j, k) - W^{n+1}(0, j, k)}{\Delta x}] - [\frac{W^{n-1}(1, j, k) - W^{n-1}(0, j, k)}{\Delta x}]}{2\Delta t}$$

Second term $\partial_{tt}^2 W$ can be approximated by averaging $\partial_{tt}^2 W$ at x=1 and x=0 and then using formula for second derivative to t :

$$W^n_{tt}(\frac{1}{2}, j, k) = \frac{[\frac{\partial^2 W^n}{\partial t^2}(0, j, k) + \frac{\partial^2 W^n}{\partial t^2}(1, j, k)]}{2} \tag{3.3.34b}$$

$$= \left[\frac{W^{n+1}(0, j, k) - 2W^{n}(0, j, k) + W^{n-1}(0, j, k)}{\Delta t^2} \right.$$

$$\left. + \frac{W^{n+1}(1, j, k) - 2W^{n}(1, j, k) + W^{n-1}(1, j, k)}{\Delta t^2} \right] /2$$

Similarly for the third term $\partial^2_{yy}W$, first take the average of $\partial^2_{yy}W$ at x=0 and x=1 and then approximate $\partial^2_{yy}W$ at x=0 and x=1:

$$W^{n}_{yy}(\frac{1}{2}, j, k) = \frac{[\frac{\partial^2 W^n}{\partial y^2}(0, j, k) + \frac{\partial^2 W^n}{\partial y^2}(1, j, k)]}{2} \tag{3.3.34c}$$

$$= \left[\frac{W^{n}(0, j+1, k) - 2W^{n}(0, j, k) + W^{n}(0, j-1, k)}{\Delta y^2} + \right.$$

$$\left. \frac{W^{n}(1, j+1, k) - 2W^{n}(1, j, k) + W^{n}(1, j-1, k)}{\Delta y^2} \right] /2$$

The same procedure for $\partial^2_{zz}W$.

$$W^{n}_{zz}(\frac{1}{2}, j, k) = \frac{[\frac{\partial^2 W^n}{\partial z^2}(0, j, k) + \frac{\partial^2 W^n}{\partial z^2}(1, j, k)]}{2} \tag{3.3.34d}$$

$$= \left[\frac{W^{n}(0, j, k+1) - 2W^{n}(0, j, k) + W^{n}(0, j, k-1)}{\Delta z^2} + \right.$$

$$\left. \frac{W^{n}(1, j, k+1) - 2W^{n}(1, j, k) + W^{n}(1, j, k-1)}{\Delta z^2} \right] /2$$

Substituting Eq.(3.3.34) into Eq.(3.3.32) and solve for $W^{n+1}(0, j, k)$, we obtain the following time stepping difference scheme at the x=0 grid plane:

$$W^{n+1}(0, j, k) = -W^{n-1}(1, j, k) + \frac{c_0\Delta t - \Delta x}{c_0\Delta t + \Delta x}[W^{n+1}(1, j, k) + W^{n-1}(0, j, k)] \tag{3.3.35a}$$

$$+ \frac{2\Delta x}{c_0\Delta t + \Delta x}[W^{n}(1, j, k) + W^{n}(0, j, k)]$$

$$+ \frac{(c_0\Delta t)^2\Delta x}{2\Delta y^2(c_0\Delta t + \Delta x)}[W^{n}(0, j+1, k) - 2W^{n}(0, j, k) + W^{n}(0, j-1, k)$$

$$+ W^{n}(1, j+1, k) - 2W^{n}(1, j, k) + W^{n}(1, j-1, k)]$$

$$\frac{(c_0\Delta t)^2\Delta x}{2\Delta z^2(c_0\Delta t+\Delta x)}[W^n(0, j, k+1) - 2W^n(0, j, k) + W^n(0, j, k-1) +$$

$$W^n(1, j, k+1) - 2W^n(1, j, k) + W^n(1, j, k-1)]$$

For a cubic cell, $\Delta x = \Delta y = \Delta z = \delta$. The above formula can be reduced to that is given in Mur's paper.

The second order finite difference equations for waves propagating along the other planes can be derived in a similar way by using the same numerical scheme as described in Eq.(3.3.33) and Eq.(3.3.17). Those equations are summarized as follows:

For the wave traveling in the direction of increasing x towards the x=1 plane (only for E_y, E_z) :

$$W^{n+1}(1, j, k) = -W^{n-1}(0, j, k) + \frac{c_0\Delta t-\Delta x}{c_0\Delta t+\Delta x}[W^{n+1}(0, j, k) + W^{n-1}(1, j, k)] + \tag{3.3.35b}$$

$$\frac{2\Delta x}{c_0\Delta t+\Delta x}[W^n(1, j, k) + W^n(0, j, k)]$$

$$+ \frac{(c_0\Delta t)^2\Delta x}{2\Delta y^2(c_0\Delta t+\Delta x)}[W^n(0, j+1, k) - 2W^n(0, j, k) + W^n(0, j-1, k)$$

$$+ W^n(1, j+1, k) - 2W^n(1, j, k) + W^n(1, j-1, k)]$$

$$+ \frac{(c_0\Delta t)^2\Delta x}{2\Delta z^2(c_0\Delta t+\Delta x)}[W^n(0, j, k+1) - 2W^n(0, j, k) + W^n(0, j, k-1) +$$

$$W^n(1, j, k+1) - 2W^n(1, j, k) + W^n(1, j, k-1)]$$

For the wave traveling in the direction of decreasing y towards the y=0 plane (for E_x, E_z):

$$W^{n+1}(i, 0, k) = -W^{n-1}(i, 1, k) + \frac{c_0\Delta t-\Delta y}{c_0\Delta t+\Delta y}[W^{n+1}(i, 1, k) + W^{n-1}(i, 0, k)] + \tag{3.3.35c}$$

$$\frac{2\Delta y}{c_0\Delta t+\Delta y}[W^n(i, 1, k) + W^n(i, 0, k)]$$

$$+ \frac{(c_0\Delta t)^2\Delta y}{2\Delta x^2(c_0\Delta t+\Delta y)}[W^n(i+1, 0, k) - 2W^n(i, 0, k) + W^n(i-1, 0, k)$$

$$+ W^n(i+1, 1, k) - 2W^n(i, 1, k) + W^n(i-1, 1, k)]$$

$$+ \frac{(c_0\Delta t)^2\Delta y}{2\Delta z^2(c_0\Delta t+\Delta y)}[W^n(i, 0, k+1) - 2W^n(i, 0, k) + W^n(i, 0, k-1) +$$

$$W^n(i, 1, k+1) - 2W^n(i, 1, k) + W^n(i, 1, k-1)]$$

For the wave traveling in the direction of increasing y towards the y=1 plane (only for E_x, E_z):

$$W^{n+1}(i, 1, k) = -W^{n-1}(i, 0, k) + \frac{c_0\Delta t-\Delta y}{c_0\Delta t+\Delta y}[W^{n+1}(i, 0, k) + W^{n-1}(i, 1, k)] \qquad (3.3.35d)$$

$$+ \frac{2\Delta y}{c_0\Delta t+\Delta y}[W^n(i, 1, k) + W^n(i, 0, k)]$$

$$+ \frac{(c_0\Delta t)^2\Delta y}{2\Delta x^2(c_0\Delta t+\Delta y)}[W^n(i+1, 0, k) - 2W^n(i, 0, k) + W^n(i-1, 0, k)$$

$$+ W^n(i+1, 1, k) - 2W^n(i, 1, k) + W^n(i-1, 1, k)]$$

$$+ \frac{(c_0\Delta t)^2\Delta y}{2\Delta z^2(c_0\Delta t+\Delta y)}[W^n(i, 0, k+1) - 2W^n(i, 0, k) + W^n(i, 0, k-1) +$$

$$W^n(i, 1, k+1) - 2W^n(i, 1, k) + W^n(i, 1, k-1)]$$

For the wave traveling in the direction of decreasing z towards the z=0 plane (only for E_x, E_y):

$$W^{n+1}(i, j, 0) = -W^{n-1}(i, j, 1) + \frac{c_0\Delta t-\Delta z}{c_0\Delta t+\Delta z}[W^{n+1}(i, j, 1) + W^{n-1}(i, j, 0)] \qquad (3.3.35e)$$

$$+ \frac{2\Delta z}{c_0\Delta t+\Delta z}[W^n(i, j, 1) + W^n(i, j, 0)]$$

$$+ \frac{(c_0\Delta t)^2\Delta z}{2\Delta x^2(c_0\Delta t+\Delta z)}[W^n(i+1, j, 0) - 2W^n(i, j, 0) + W^n(i-1, j, 0)$$

$$+ W^n(i+1, j, 1) - 2W^n(i, j, 1) + W^n(i-1, j, 1)]$$

$$+ \frac{(c_0\Delta t)^2\Delta z}{2\Delta y^2(c_0\Delta t+\Delta z)}[W^n(i, j+1, 0) - 2W^n(i, j, 0) + W^n(i, j-1, 0) +$$

$$W^n(i, j+1, 1) - 2W^n(i, j, 1) + W^n(i, j-1, 1)]$$

For the wave traveling in the direction of increasing z towards the z=1 plane (only for E_x, E_y):

$$W^{n+1}(i, j, 1) = -W^{n-1}(i, j, 0) + \frac{c_0\Delta t-\Delta z}{c_0\Delta t+\Delta z}[W^{n+1}(i, j, 0) + W^{n-1}(i, j, 1)] + \tag{3.3.35f}$$

$$\frac{2\Delta z}{c_0\Delta t+\Delta z}[W^n(i, j, 1) + W^n(i, j, 0)]$$

$$+ \frac{(c_0\Delta t)^2\Delta z}{2\Delta x^2(c_0\Delta t+\Delta z)}[W^n(i+1, j, 0) - 2W^n(i, j, 0) + W^n(i-1, j, 0)$$

$$+ W^n(i+1, j, 1) - 2W^n(i, j, 1) + W^n(i-1, j, 1)]$$

$$+ \frac{(c_0\Delta t)^2\Delta z}{2\Delta y^2(c_0\Delta t+\Delta z)}[W^n(i, j+1, 0) - 2W^n(i, j, 0) + W^n(i, k-1, 0) +$$

$$W^n(i, j+1, 1) - 2W^n(i, j, 1) + W^n(i, j-1, 1)]$$

It seems that with Eq (3.3.35) we can now handle the grid points on the outer surfaces. However, we observe that at corner points of the outer boundary as illustrated in Fig. 3.5, the formulae for the second approximation just derived also use the points outside computational region. Unfortunately, we can not apply the second approximation to corner grid points . Instead of the second approximation, a formula of first order approximation will be derived for the points at grid corners of the outmost boundary and this will be discussed in section 3.3.3.

b. Two Dimensional case

Derivation of finite difference equation for the two dimensional second order approximation is straight forward from Eq.(3.3.35) by just setting terms related to $\frac{\partial^2 W}{\partial z^2} = 0$:

As shown in Fig.3.6, for the wave traveling in the direction of decreasing x towards the x=0 plane:

$$W^{n+1}(0, j) = -W^{n-1}(1, j) + \frac{c_0\Delta t-\Delta x}{c_0\Delta t+\Delta x}[W^{n+1}(1, j) + W^{n-1}(0, j)] + \tag{3.3.36a}$$

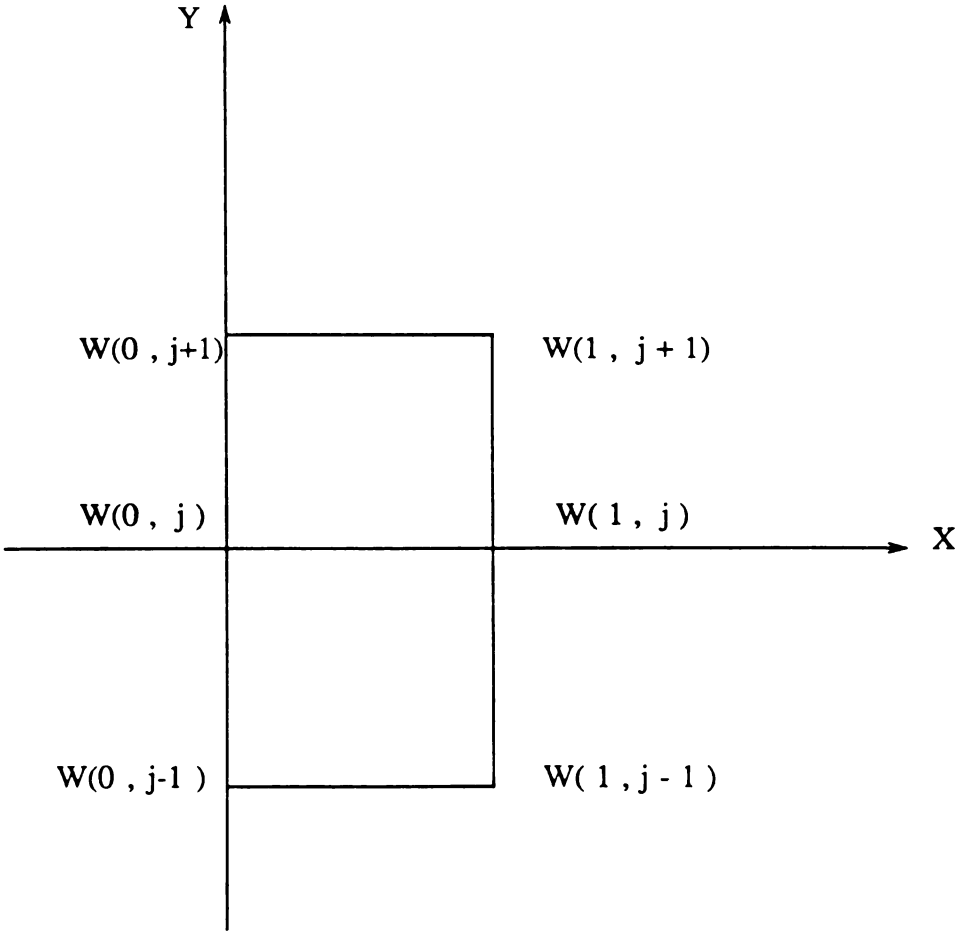

Fig. 3.6 Two Dimensional Mur's Second Order Approx.

$$\frac{2\Delta x}{c_0\Delta t+\Delta x}[W^n(1, j) + W^n(0, j)]$$

$$\frac{(c_0\Delta t)^2\Delta x}{2\Delta y^2(c_0\Delta t+\Delta x)}[W^n(0, j+1) - 2W^n(0, j) + W^n(0, j-1) +$$

$$W^n(1, j+1) - 2W^n(1, j) + W^n(1, j-1)]$$

For the wave traveling in the direction of increasing x towards the x=1 plane:

$$W^{n+1}(1, j) = -W^{n+1}(0, j) + \frac{c_0\Delta t-\Delta x}{c_0\Delta t+\Delta x}[W^{n+1}(0, j) + W^{n-1}(1, j)] + \tag{3.3.36b}$$

$$\frac{2\Delta x}{c_0\Delta t+\Delta x}[W^n(1, j) + W^n(0, j)]$$

$$\frac{(c_0\Delta t)^2\Delta x}{2\Delta y^2(c_0\Delta t+\Delta x)}[W^n(0, j+1) - 2W^n(0, j) + W^n(0, j-1) +$$

$$W^n(1, j+1) - 2W^n(1, j) + W^n(1, j-1)]$$

For the wave traveling in the direction of decreasing y towards the y=0 plane:

$$W^{n+1}(i, 0) = -W^{n-1}(i, 1) + \frac{c_0\Delta t-\Delta y}{c_0\Delta t+\Delta y}[W^{n+1}(i, 1) + W^{n-1}(i, 0)] + \tag{3.3.36c}$$

$$\frac{2\Delta y}{c_0\Delta t+\Delta y}[W^n(i, 1) + W^n(i, 0)]$$

$$\frac{(c_0\Delta t)^2\Delta y}{2\Delta x^2(c_0\Delta t+\Delta y)}[W^n(i+1, 0) - 2W^n(i, 0) + W^n(i-1, 0) +$$

$$W^n(i+1, 1) - 2W^n(i, 1) + W^n(i-1, 1)]$$

For the wave traveling in the direction of increasing y towards the y=1 plane:

$$W^{n+1}(i, 1) = -W^{n+1}(i, 0) + \frac{c_0\Delta t-\Delta y}{c_0\Delta t+\Delta y}[W^{n+1}(i, 0) + W^{n-1}(i, 1)] + \tag{3.3.36d}$$

$$\frac{2\Delta y}{c_0\Delta t+\Delta y}[W^n(i, 1) + W^n(i, 0)]$$

$$\frac{(c_0\Delta t)^2\Delta y}{2\Delta x^2(c_0\Delta t+\Delta y)}[W^n(i+1, 0) - 2W^n(i, 0) + W^n(i-1, 0) +$$

$$W^n(i+1, 1) - 2W^n(i, 1) + W^n(i-1, 1)]$$

For the two dimensional case, W represents E_z or H_z for TM mode or TE mode, respectively.

If we use the further simplified equations(3.2.4) of the second order approximation, the algorithm is developed for TM mode as follows:

Rewriting Eq(3.2.4)

$$(\partial_x E_z - c_0^{-1}\partial_t E_z - (c_o\mu_0/2)\partial_y H_x)_{x=0} = 0$$

The central difference is used to approximate the derivatives of Eq.(3.3.19) and the derivatives are averaged. For example, $\frac{\partial E_z}{\partial t}$ and $\frac{\partial E_z}{\partial x}$ are approximated as follows:

$$\frac{\partial E_z}{\partial x} = \frac{[E_z^{n+1}(1, j) - E_z^{n+1}(0, j) + E_z^n(1, j) - E_z^n(0, j)]}{2\Delta x} \tag{3.3.37}$$

$$\frac{\partial E_z}{\partial t} = \frac{[E_z^{n+1}(1, j) - E_z^n(1, j) + E_z^{n+1}(0, j) - E_z^n(0, j)]}{2\Delta t} \tag{3.3.38}$$

In the same way, the other derivatives of Eq(3.3.19) are approximated such that a set of difference equations are obtained:

For wave propagating in the direction of decreasing x towards x=0 plane:

$$\begin{aligned} E_z^{n+1}(0, j) = E_z^n(1, j) &+ \frac{c_0\Delta t - \Delta x}{c_0\Delta t + \Delta x}(E_z^{n+1}(1, j) - E_z^n(0, j)) \\ &- \frac{c_0^2\mu_0\Delta t\Delta x}{2(c_0\Delta t + \Delta x)\Delta y}[H_x^{n+\frac{1}{2}}(0, j+\frac{1}{2}) - H_x^{n+\frac{1}{2}}(0, j-\frac{1}{2}) \\ &+ H_x^{n+\frac{1}{2}}(1, j+\frac{1}{2}) - H_x^{n+\frac{1}{2}}(1, j-\frac{1}{2})] \end{aligned} \tag{3.3.39a}$$

For the wave propagating in the direction of increasing x towards x=1 plane:

$$\begin{aligned} E_z^{n+1}(1, j) = E_z^n(0, j) &+ \frac{c_0\Delta t - \Delta x}{c_0\Delta t + \Delta x}(E_z^{n+1}(0, j) - E_z^n(1, j)) \\ &- \frac{c_0^2\mu_0\Delta t\Delta x}{2(c_0\Delta t + \Delta x)\Delta y}[H_x^{n+\frac{1}{2}}(0, j+\frac{1}{2}) - H_x^{n+\frac{1}{2}}(0, j-\frac{1}{2}) \\ &+ H_x^{n+\frac{1}{2}}(1, j+\frac{1}{2}) - H_x^{n+\frac{1}{2}}(1, j-\frac{1}{2})] \end{aligned} \tag{3.3.39b}$$

For wave propagating in the direction of decreasing y towards y=0 plane:

$$E_z^{n+1}(i,0) = E_z^n(i,1) + \frac{c_0\Delta t - \Delta y}{c_0\Delta t + \Delta y}(E_z^{n+1}(i,1) - E_z^n(i,0)) \tag{3.3.39c}$$
$$- \frac{c_0^2\mu_0\Delta t\Delta y}{2(c_0\Delta t + \Delta y)\Delta x}[H_y^{n+\frac{1}{2}}(i+\frac{1}{2},0) - H_y^{n+\frac{1}{2}}(i-\frac{1}{2},0)$$
$$+ H_y^{n+\frac{1}{2}}(i+\frac{1}{2},1) - H_y^{n+\frac{1}{2}}(i-\frac{1}{2},1)]$$

For wave propagating in the direction of increasing y towards y=1 plane:

$$E_z^{n+1}(i,1) = E_z^n(i,0) + \frac{c_0\Delta t - \Delta y}{c_0\Delta t + \Delta y}(E_z^{n+1}(i,0) - E_z^n(i,1)) \tag{3.3.39d}$$
$$- \frac{c_0^2\mu_0\Delta t\Delta y}{2(c_0\Delta t + \Delta y)\Delta x}[H_y^{n+\frac{1}{2}}(i+\frac{1}{2},0) - H_y^{n+\frac{1}{2}}(i-\frac{1}{2},0)$$
$$+ H_y^{n+\frac{1}{2}}(i+\frac{1}{2},1) - H_y^{n+\frac{1}{2}}(i-\frac{1}{2},1)]$$

Equations (3.3.39), two dimensional second order approximation, are used as radiation boundary conditions in solving two-dimensional problems in this chapter. For the three dimensional case, this two dimensional second order approximation can not be applied to the corner points on the outer boundary as shown in Fig. 3.6 so that the first approximation has to be used. This point will be discussed in section 3.3.3.

3.3.3 Radiation Boundary Condition for the 2D and 3D Corner Points

As discussed before, the second order approximation can not be applied to the corner points of two and three dimensional outmost boundaries. This can be easily seen from Figs 3.5&3.6 since the formula also uses points outside the boundary which are not available. For the corner points, we have to use other schemes which are equivalent to the first order approximation. This prevents further improvement of the radiation boundary condition by raising the order of it, thus, searching for a better radiation boundary condition remains an interesting topic.

Back to section 3.3.1, the general form of the first order approximation can be written into a form:

$$\frac{\partial wa}{\partial n} + c_0^{-1}\frac{\partial wa}{\partial t} = 0 \tag{3.3.40}$$

If we assume scattered waves propagating spherically from the origin, then the $\hat{n}$ in the above equation would be taken in the outgoing radial direction for the corner points. The derivative along the radial direction becomes:

$$\frac{\partial wa}{\partial r} = \frac{\partial wa}{\partial x}\frac{\partial x}{\partial r} + \frac{\partial wa}{\partial y}\frac{\partial y}{\partial r} + \frac{\partial wa}{\partial z}\frac{\partial z}{\partial r} \tag{3.3.41}$$

Where

$$\frac{\partial x}{\partial r} = \frac{x}{\sqrt{(x^2+y^2+z^2)}}; \tag{3.3.42a}$$

$$\frac{\partial y}{\partial r} = \frac{y}{\sqrt{(x^2+y^2+z^2)}}; \tag{3.3.42b}$$

$$\frac{\partial z}{\partial r} = \frac{z}{\sqrt{(x^2+y^2+z^2)}}; \tag{3.3.42c}$$

$$r = \sqrt{(x^2+y^2+z^2)} \tag{3.3.42d}$$

Substituting Eq.(3.3.41) & (3.3.42) back to Eq.(3.3.40), we have:

$$\frac{\partial wa}{\partial x}\frac{x}{\sqrt{(x^2+y^2+z^2)}} + \frac{\partial wa}{\partial y}\frac{y}{\sqrt{(x^2+y^2+z^2)}} + \frac{\partial wa}{\partial z}\frac{z}{\sqrt{(x^2+y^2+z^2)}} + c_0^{-1}\frac{\partial wa}{\partial t} = 0 \tag{3.3.43}$$

To discretize above equation to difference equation, special attention should be paid to the partial derivatives of wa to ensure the stability of the schemes which will be discussed in details in the next section. Concerning the stability, the first order approximation for the corner points in different regions have the following forms:

In the region (x>0, y>0, z>0):

$$wa^{n+1}(i, j, k) = wa^n(i, j, k) \tag{3.3.44a}$$

$$- c_0\Delta t/r\left\{\frac{x}{\Delta x}[wa^n(i, j, k) - wa^n(i-1, j, k)] + \frac{y}{\Delta y}[wa^n(i, j, k) - wa^n(i, j-1, k)]\right.$$

$$\left. + \frac{z}{\Delta z}[wa^n(i, j, k) - wa^n(i, j, k-1)]\right\}$$

In the region (x<0, y>0, z>0):

$$wa^{n+1}(i,j,k) = wa^{n}(i,j,k) - c_0\Delta t/r\left\{-\frac{x}{\Delta x}[wa^{n}(i+1,j,k) - wa^{n}(i,j,k)]\right. \tag{3.3.44b}$$
$$\left. + \frac{y}{\Delta y}[wa^{n}(i,j,k) - wa^{n}(i,j-1,k)] + \frac{z}{\Delta z}[wa^{n}(i,j,k) - wa^{n}(i,j,k-1)]\right\}$$

In the region (x>0, y<0, z>0):

$$wa^{n+1}(i,j,k) = wa^{n}(i,j,k) - c_0\Delta t/r\left\{\frac{x}{\Delta x}[wa^{n}(i,j,k) - wa^{n}(i-1,j,k)]\right. \tag{3.3.44c}$$
$$\left. - \frac{y}{\Delta y}[wa^{n}(i,j+1,k) - wa^{n}(i,j,k)] + \frac{z}{\Delta z}[wa^{n}(i,j,k) - wa^{n}(i,j,k-1)]\right\}$$

In the region (x<0, y<0, z>0):

$$wa^{n+1}(i,j,k) = wa^{n}(i,j,k) - c_0\Delta t/r\left\{-\frac{x}{\Delta x}[wa^{n}(i+1,j,k) - wa^{n}(i,j,k)]\right. \tag{3.3.44d}$$
$$\left. - \frac{y}{\Delta y}[wa^{n}(i+1,j,k) - wa^{n}(i,j,k)] + \frac{z}{\Delta z}[wa^{n}(i,j,k) - wa^{n}(i,j,k-1)]\right\}$$

In the region (x>0, y>0, z<0):

$$wa^{n+1}(i,j,k) = wa^{n}(i,j,k) - c_0\Delta t/r\left\{\frac{x}{\Delta x}[wa^{n}(i,j,k) - wa^{n}(i-1,j,k)]\right. \tag{3.3.44e}$$
$$\left. + \frac{y}{\Delta y}[wa^{n}(i,j,k) - wa^{n}(i,j-1,k)] - \frac{z}{\Delta x}[wa^{n}(i,j,k+1) - wa^{n}(i,j,k)]\right\}$$

In the region (x<0, y>0, z<0):

$$wa^{n+1}(i,j,k) = wa^{n}(i,j,k) - c_0\Delta t/r\left\{-\frac{x}{\Delta x}[wa^{n}(i+1,j,k) - wa^{n}(i,j,k)]\right. \tag{3.3.44f}$$
$$\left. + \frac{y}{\Delta y}[wa^{n}(i,j,k) - wa^{n}(i,j-1,k)] - \frac{z}{\Delta z}[wa^{n}(i,j,k+1) - wa^{n}(i,j,k)]\right\}$$

In the region (x>0, y<0, z<0):

$$wa^{n+1}(i,j,k) = wa^{n}(i,j,k) - c_0\Delta t/r\left\{\frac{x}{\Delta x}[wa^{n}(i,j,k) - wa^{n}(i-1,j,k)]\right. \tag{3.3.44g}$$
$$\left. - \frac{y}{\Delta y}[wa^{n}(i,j+1,k) - wa^{n}(i,j,k)] - \frac{z}{\Delta z}[wa^{n}(i,j,k+1) - wa^{n}(i,j,k)]\right\}$$

In the region (x<0, y<0, z<0):

$$wa^{n+1}(i,j,k) = wa^{n}(i,j,k) - c_0\Delta t/r\left\{-\frac{x}{\Delta x}[wa^{n}(i+1,j,k) - wa^{n}(i,j,k)]\right. \tag{3.3.44h}$$

$$\left. -\frac{y}{\Delta y}[wa^{n}(i+1,j,k) - wa^{n}(i,j,k)] - \frac{z}{\Delta z}[wa^{n}(i,j,k+1) - wa^{n}(i,j,k)]\right\}$$

We have used the above scheme to handle corner points in our numerical applications. The results show that this scheme is stable as it is analyzed theoretically in section 3.4.

The first approximation for two-dimensional cases can be developed in a similar way by letting $\frac{\partial wa}{\partial z} = 0$

There are other ways to handle corner points, one way we want to mention here is that used by Taflove et.al.[30]. They simulated the outgoing radial waves in a different way and a stable scheme who also proposed.

3.4 THE STABILITY ANALYSIS OF THE FD-TD METHOD SCHEMES

The finite difference time domain method (FD-TD) has been increasingly used to solve a variety of open bounded electromagnetic problems. Its stability criterion has also been established based on the iterative behavior of fields discretized in an interior space. In fact, the stability of a scheme is attributed to the behavior of fields discretized both in the interior space and on the boundary of the truncated space. This section introduces a systematic way to analyze the stability of a FD-TD scheme when an artificial boundary is introduced. As examples, a few well known schemes used in electromagnetic problems are analyzed. It is shown that the conclusion by the theory is consistent with the empirical rule in numerical practice. But the application of the introduced method is applicable to general schemes.

In the early years of applying the FD-TD method to electromagnetic problems, Yee [22] proposed a finite difference scheme and established a stability criterion which was based on the behavior of fields at the points inside a closed region. Later Taflove [23] conducted a mathematical derivation and modified this criterion. Nowadays, engineering designs are involved in many complex models which may include lossy, inhomogeneous, and anisotropic systems and of which the structure may involve apertures, cavities, and antennas [21]. In most realistic cases, the basic algorithms of the FD-TD method have to be modified and the study of stability becomes very important for a successful difference scheme.

As an example, when an open bounded electromagnetic scattering problem is considered, the infinite space has to be truncated and the truncation is implemented by enforcing a radiation boundary condition on the outer surface of a truncated finite space as discussed in section 3.3. Thus the open bounded problem is changed into a bounded one, which is comprised of Maxwell's curl equations satisfied at the interior points and the radiation boundary condition matched on the outer surface. The variant boundary conditions enforced on the truncated space and different approximations of derivatives yield various finite difference schemes. The established criterion is no longer suitable to all numerical schemes.

The stability is a vital factor to determine the applicability of a new modification of the FD-TD method scheme, when a modification of well known difference schemes has to be made for a specific problem. Different approximations on the boundary conditions may result in different numerical schemes, thus result in different stability requirements. It is necessary to introduce a systematic way to study the stability of a FD-TD scheme before its numerical solution is attempted.

In fact, the stability of a scheme is attributed not only to the property of fields discretized at the interior points of a truncated space but also to that of fields

discretized at the points on the boundary. This section introduces a theoretical approach to analyze the stability of a whole system. One of the popular FD-TD numerical model is taken as an example which is constructed by applying the Yee's model to the interior points, the Mur's second order radiation boundary condition to the boundary points except for the corner points, and the first order radiation boundary condition to the corner points. But the analysis is applicable to any specific schemes.

3.4.1 The Methods of Stability Analysis

Without the loss of generality, the stability is discussed for the model which is constructed by applying the Yee's model to the interior points, the Mur's second order radiation boundary condition to the boundary points, and the first order radiation boundary condition to the corner points. In the interior region, the set of difference equations derived by using Yee's model is stable in iteration if

$$\Delta t \geq \frac{1}{c[1/\Delta x^2 + 1/\Delta y^2 + 1/\Delta z^2]^{1/2}} \tag{3.4.1}$$

holds. Eq. (3.4.1) has been mathematically verified by Taflove. However, Eq. (3.4.1) is not generally true for the stability of the finite difference equations discretized from a radiation boundary condition. An alternative approach can be introduced here to reach the same stability restriction for the interior finite difference equations, and to find the new criterion for the finite difference equations from a radiation boundary condition.

Based on the Yee's model, a set of explicit finite difference equations was developed [22]. These equations can be written into a matrix form as

$$X^{n+1} = A\,X^n + B^n \tag{3.4.2}$$

Assume an error E^0 is somehow introduced at the initial step. After n steps the error is accumulated up to

$$E^n = A^n E^0 \tag{3.4.3}$$

where A is the matrix of the detailed finite difference equations, which are finite difference approximations on the Maxwell equations and the radiation boundary conditions. The sufficient and necessary condition for the stability of Eq.(3.4.2) can be stated as [25]

$$\rho(A) = \max_i |\lambda_i| \leq 1 \tag{3.4.4}$$

if A has a full set of eigenvectors with $\rho(A)$ being the spectral radius of A. If A does not possess a full set of eigenvectors (such as A has a repeated eigenvalue), the sufficient condition for the stability of Eq.(3.4.2) is then

$$\rho(A) = \max_i |\lambda_i| < 1 \tag{3.4.5}$$

If the eigenvalues of the matrix A can be found, the stability criterion of Eq.(3.4.2) is consequently obtained. The stability study by a matrix method [25] is based on seeking the eigenvalues of the matrix A.

Hereafter the Fourier method (Von Neumann) [25] is introduced for the general analysis. The Fourier method can be applied to both the interior finite difference equations and the finite difference equations on the radiation boundary. It is based on the separation of time variable and space variable in the Fourier transform domain. The applicability of the method is justified by considering a function $f(t, x,y,z)$, which is a general function of time and space, it can be represented by its Fourier spectrum as

$$f(t, x,y,z) = (\frac{1}{2\pi})^3 \int_{-\infty}^{\infty} F(t, \theta, \phi, \gamma) e^{c_j \theta x} e^{c_j \phi y} e^{c_j \gamma z} \, d\theta d\phi d\gamma \tag{3.4.6}$$

where $c_j = \sqrt{-1}$, $F(t, \theta,\phi,\gamma)$ is the Fourier spectrum of $f(t, x,y,z)$ in spatial domain, θ, ϕ, γ are the space frequencies. If the function $f(t, x,y,z)$ is stable as time is stepped, the functions of $F(t, \theta,\phi,\gamma)e^{c_j \theta x} e^{c_j \phi y} e^{c_j \gamma z}$ should be stable at any time and space frequencies. Thus, the stability analysis of $f(t, x,y,z)$ is resorted to the stability analysis of $F(t, \theta,\phi,\gamma)e^{c_j \theta x} e^{c_j \phi y} e^{c_j \gamma z}$ at all frequency values.

Instead of working on the whole set of the finite difference equations grouped from both the interior region and the radiation boundary, the Fourier method can be applied respectively to finite difference equations of interior region and those of the radiation boundary. Since the criterion of Eq.(3.4.1) has been established and validated true for the finite difference equations based on Yee's model in an interior region, the emphasis here is put on the analysis of the first order radiation boundary conditions. The Mur's second order radiation boundary condition can also be analyzed via the same method.

The first order radiation boundary condition is often used at the corner points on the radiation boundary [24,26]. It is mathematically represented by:

$$\frac{\partial w}{\partial n} + c_0^{-1}\frac{\partial w}{\partial t} = 0 \tag{3.4.7}$$

where w is a scalar wave function, c_0 is the light speed in free space, and $\hat{n}$ is the normal direction of the outgoing wave-front. If the scattered wave is approximated as a spheric wave radiated from the origin, the normal derivative in Eq.(3.4.7) is given by

$$\frac{\partial w}{\partial R} = \frac{\partial w}{\partial x}\frac{\partial x}{\partial R} + \frac{\partial w}{\partial y}\frac{\partial y}{\partial R} + \frac{\partial w}{\partial z}\frac{\partial z}{\partial R} \tag{3.4.8}$$

and it can be shown that Eq.(3.4.7) leads to

$$\frac{\partial w}{\partial x}\frac{x}{\sqrt{(x^2+y^2+z^2)}} + \frac{\partial w}{\partial y}\frac{y}{\sqrt{(x^2+y^2+z^2)}} + \frac{\partial w}{\partial z}\frac{z}{\sqrt{(x^2+y^2+z^2)}} + c_0^{-1}\frac{\partial w}{\partial t} = 0 \tag{3.4.9}$$

A discrete form of Eq.(3.4.9) can be created by substituting finite differences for the derivatives in Eq.(3.4.9). A proper forward, or backward finite difference is used to avoid the possible occurrence of the instability. For example, in $x > 0$ and $y > 0$ and $z > 0$ region the discrete form of Eq.(3.4.9) is written as:

$$w^{n+1}(i, j, k) = w^n(i, j, k) - c_0\Delta t/R\left\{\frac{x}{\Delta x}[w^n(i, j, k) - w^n(i-1, j, k)]\right. \tag{3.4.10}$$

$$\left. + \frac{y}{\Delta y}[w^n(i, j, k) - w^n(i, j-1, k)] + \frac{z}{\Delta z}[w^n(i, j, k) - w^n(i, j, k-1)]\right\}$$

where the superscript n indicates the n^{th} step of time, and $R = \sqrt{x^2 + y^2 + z^2}$. As discussed previously the stability analysis by a Fourier method is alternated to analyze the wave functions of $F(t, \theta, \phi, \gamma)\, e^{c_j\theta x} e^{c_j\phi y} e^{c_j\gamma z}$. Therefore, the separation of variables of w can be assumed as

$$w^n(i, j, k) = T^n W(i, j, k) \tag{3.4.11}$$

where T^n is the function of time at the n^{th} step, and W is the function of space. Substituting Eq.(3.4.11) into Eq.(3.4.10) yields:

$$\frac{T^{n+1}}{T^n} = \eta \tag{3.4.12a}$$

$$\eta\, W(i, j, k) = W(i, j, k) - \tau/\delta[(W(i, j, k) - W(i-1, j, k))\frac{i\delta}{R} \tag{3.4.12b}$$

$$+ (W(i, j, k) - W(i, j-1, k))\frac{j\delta}{R} + (W(i, j, k) - W(i, j, k-1))\frac{k\delta}{R}$$

where $\Delta x = \Delta y = \Delta z = \delta$ is taken, η is a constant to be determined from (12.b), and τ equals $c_0\Delta t$. It can be deducted from the linearity of Eq.(3.4.12) that if an error e is introduced at the initial step, the error function obeys the same equation as w, thus the error function may be represented in the same form of Eq.(3.4.11)

$$e^n_{i, j, k} = T^n W(i, j, k) \tag{3.4.13}$$

from (3.4.12a) the function T^n is related to the initial T^0 by

$$T^n = \eta^n T^0 \tag{3.4.14}$$

T^0 can be assigned to unity without the loss of generality. The boundness of the error function Eq.(3.4.13) is thus turned to the establishment of $|\eta| \leq 1$, which is determined by Eq.(3.4.12b).

Consider all the possible solutions of η in Eq.(3.4.12b) which are represented in a Von Neumann's form

$$W(i, j, k) = e^{c_j i\theta}\, e^{c_j j\phi}\, e^{c_j k\gamma} \tag{3.4.15}$$

where θ, ϕ, γ are real space frequencies in the Fourier frequency domain, and $c_j = \sqrt{-1}$.

Now η in Eq.(3.4.12b) is dependent on θ, ϕ, γ and $\frac{\tau}{\delta}$ since different values of η will be resulted from Eq.(3.4.12b) at different frequencies.

It is seen that the numerical scheme Eq. (3.4.9) is stable for a given $\frac{\tau}{\delta}$ if

$$|\eta(\theta, \phi, \gamma, \frac{\tau}{\delta})| \leq 1 \tag{3.4.16}$$

holds for all real θ, ϕ, γ .

At the initial step of the iteration, the error function is

$$e^0_{i,j,k} = W(i, j, k)T^0 = W(i, j, k) \tag{3.4.17}$$

Using the Von Neumann's form Eq. (3.4.15) for $W(i, j, k)$ in Eq. (3.4.12b) results in:

$$\begin{aligned}\eta &= 1 - r\delta/R\ [(i + j + k) - (ie^{c_j\theta} + je^{c_j\phi} + ke^{c_j\gamma})] \\ &= (1 - \frac{r(i + j + k)}{\sqrt{(i^2 + j^2 + k^2)}}) + \frac{r}{\sqrt{(i^2 + j^2 + k^2)}}[i\cos\theta + j\cos\phi + k\cos\gamma] \\ &- c_j\frac{r}{\sqrt{(i^2 + j^2 + k^2)}}[i\sin\theta + j\sin\phi + k\sin\gamma]\end{aligned} \tag{3.4.18}$$

where r is defined as $c_0\Delta t/\delta$. The amplitude of η should be bounded by:

$$\begin{aligned}|\eta|^2 = &\left[(1 - \frac{r(i + j + k)}{\sqrt{(i^2 + j^2 + k^2)}}) + \frac{r}{\sqrt{(i^2 + j^2 + k^2)}}(i\cos\theta + j\cos\phi + k\cos\gamma)\right]^2 \\ &+ \left[\frac{r}{\sqrt{(i^2 + j^2 + k^2)}}(i\sin\theta + j\sin\phi + k\sin\gamma)\right]^2 \leq 1\end{aligned} \tag{3.4.19}$$

or

$$\begin{aligned}&\left[(\sqrt{(i^2 + j^2 + k^2)} - r(i + j + k)) + r(i\cos\theta + j\cos\phi + k\cos\gamma)\right]^2 \\ &\quad + \left[r(i\sin\theta + j\sin\phi + k\sin\gamma)\right]^2 \leq (i^2 + j^2 + k^2)\end{aligned} \tag{3.4.20}$$

should hold for any combination of θ, ϕ, γ. After a few steps of algebraic manipulation, an equivalent form of Eq.(3.4.20) can be obtained:

$$\begin{aligned}&r(i + j + k)^2 + i^2 + j^2 + k^2 + 2r(ij\cos(\theta - \phi) + ik\cos(\theta - \gamma) + jk\cos(\phi - \gamma)) \\ &\quad + 2(i\cos\theta + j\cos\phi + k\cos\gamma)[\sqrt{(i^2 + j^2 + k^2)} - r(i + j + k)] \\ &\quad \leq 2\sqrt{(i^2 + j^2 + k^2)}(i + j + k)\end{aligned} \tag{3.4.21}$$

It can be shown that Eq.(3.4.21) holds if

$$\sqrt{(i^2 + j^2 + k^2)} - r(i + j + k) \geq 0 \tag{3.4.22}$$

To find the solution of Eq.(3.4.22) for r, it is helpful to introduce the relation

$$(\frac{1}{m}\sum_{i=1}^{m} a_i^2)^{\frac{1}{2}} \geq \frac{a_1 + a_2 + .. + a_m}{m} \tag{3.4.23}$$

It is deduced:

$$\sqrt{i^2 + j^2 + k^2} \geq \frac{1}{\sqrt{3}}(i + j + k) \tag{3.4.24}$$

The possible range of r for Eq.(3.4.22) to be valid is restricted to

$$r \leq \frac{1}{\sqrt{3}} \tag{3.4.25}$$

then the satisfaction of Eq.(3.4.21) is provided by Eq.(3.4.25). Finally it can be stated that if $r \leq \frac{1}{\sqrt{3}}$, the $|\eta(\theta, \phi, \gamma, r)| \leq 1$ holds, then the equations created from Eq.(3.4.10) are stable.

It is informative to see that the criterion (3.4.1) established from the interior finite difference equations by the Yee's model is reduced to (3.4.25) when $\Delta x = \Delta y = \Delta z$ is forced. This criterion also holds for the Mur's second order approximation on the radiation boundary condition. At this point, it can be concluded that (3.4.25) is the stability criterion for the system specified in the introduction section. As a matter of fact, the conclusion has already been verified by the numerical practice of applying the FD-TD to three dimensional scattering problems in transient or steady state.

Next two different approximations on the first order radiation boundary condition for two dimensional corner points are presented to investigate the stability. The first scheme to be presented is the analysis on the scheme we used in the research. The first order radiation boundary condition was proposed in the region $x<0$ and $y<0$ as

$$c_0^{-1}\frac{\partial w}{\partial t} - \frac{1}{\sqrt{2}}(\frac{\partial w}{\partial x} + \frac{\partial w}{\partial y}) = 0 \tag{3.4.26}$$

If the forward finite differences are used to replace the derivatives in Eq.(3.4.26), Eq.(3.4.26) will lead to a stable scheme. But a different approach may result in an instable scheme.

First, Eq.(3.4.26) is discretized by forward finite differences into the form

$$\sqrt{2}c_0^{-1}[w^{n+1}(i, j) - w^n(i, j)]/\Delta t = [w^n(i+1, j) - w^n(i, j)]/\Delta x + [w^n(i, j+1) - w^n(i, j)]/\Delta y \quad (3.4.27)$$

Using Eq.(3.4.11) in Eq.(3.4.27) yields

$$r\,\eta W(i, j) = [(r - 2)W(i, j) + W(i+1, j) + W(i, j+1)] \quad (3.4.28)$$

where W is a two dimensional function, and r is defined as $r = \sqrt{2}\Delta x/(c_0\Delta t)$. Subsequently the W is replaced by its Von Neumann's form, The equation

$$0 = [(r - 2 - r\eta) + e^{c_j\theta} + e^{c_j\phi}] \quad (3.4.29)$$

is obtained. The stability Eq.(3.4.26) requires $|\eta| \le 1$. It is equivalent to require

$$|\eta|^2 = \frac{[r - 2 + \cos\theta + \cos\phi]^2 + [(\sin\theta + \sin\phi)]^2}{r^2} \le 1 \quad (3.4.29)$$

The solution for r is shown to be

$$r\,(2 - (\cos\theta + \cos\phi)) \ge 3 - 2(\cos\theta + \cos\phi) + \cos\theta\cos\phi + \sin\theta\sin\phi \quad (3.4.30)$$

When $\cos\theta = 1$ and $\cos\phi = 1$, both sides become zeros and equality holds. Otherwise

$$r \ge \frac{3 - 2(\cos\theta + \cos\phi) + \cos\theta\cos\phi + \sin\theta\sin\phi}{2 - (\cos\theta + \cos\phi)} \quad (3.4.31)$$

It can be proven that the right hand side of Eq.(3.4.31) is bounded by 2, thus $r \ge 2$ guarantees the satisfaction of Eq.(3.4.29). Note that $r \ge 2$ implies $c_0\Delta \le \delta/\sqrt{2}$ which is the same criterion for the finite difference equations of the interior region points.

However, if Eq.(3.4.26) is discretized by the finite differences suggested in [24], an unconditionally instable scheme results. This can be demonstrated as follows. Assume the finite differences are taken in Eq.(3.4.26) as denoted in [24]

$$(D_+^x + D_+^y)(u_{ij}^n + u_{ij}^{n+1}) - \frac{2}{3}\sqrt{2}c_0 D_+^t(u_{i,j+1}^n + u_{i+1,j}^n + u_{ij}^n) = 0 \tag{3.4.32}$$

The operator D_+^x denotes forward finite difference on x variable, and the similar notations are used for D_+^y , D_+^t . This algorithm seems better because derivatives w.r.t. the space coordinates are averaged on the two time instants $t = n\Delta t$ and $t = (n+1)\Delta t$, and the derivative respect to space is averaged over three locations (i, j), $(i+1, j)$, and $(i, j+1)$. But it creates an instable scheme.

The explicit form of Eq.(3.4.32) is written as

$$\begin{aligned} w^{n+1}(i, j) = {} & \frac{(r-2)}{(r+2)} w^n(i, j) + \frac{(1-r)}{(r+2)}(w^{n+1}(i+1, j) + w^{n+1}(i, j+1)) \\ & + \frac{(1+r)}{(r+2)}(w^n(i+1, j) + w^n(i, j+1)) \end{aligned} \tag{3.4.33}$$

Using of Eq.(3.4.11) gives rise to the equations

$$\eta = \frac{T^{n+1}}{T^n} \tag{3.4.34a}$$

$$\eta = \frac{\frac{(r-2)}{(r+2)} W(i, j) + \frac{(1+r)}{(r+2)}(W(i+1, j) + W(i, j+1))}{W(i, j, k) - \frac{(1-r)}{(r+2)}(W(i+1, j) + W(i, j+1))} \tag{3.4.34b}$$

If the W is substituted by its Von Neumann's form, then η is given by

$$\eta = \frac{(r-2) + (1+r)(e^{c_j\theta} + e^{c_j\phi})}{(r+2) - (1-r)(e^{c_j\theta} + e^{c_j\phi})} \tag{3.4.35}$$

For the scheme to be stable, η should be bounded by

$$|\eta|^2 = \frac{[(r-2) + (1+r)(\cos\theta + \cos\phi)]^2 + (\sin\theta + \sin\phi)^2(1+r)^2}{[(r+2) - (1-r)(\cos\theta + \cos\phi)]^2 + (\sin\theta + \sin\phi)^2(1-r)^2} \le 1 \tag{3.4.36}$$

Unfortunately the further expansion of Eq.(3.4.36) yields

$$-(\cos\theta + \cos\phi) + 2(\sin\phi\sin\theta + \cos\theta\cos\phi) \le 0 \tag{3.4.37}$$

which is independent of r, and the inequality is apparently faulty at many values of θ and ϕ. The criterion of Eq.(3.4.36) is no longer satisfied for any θ and ϕ. Thus the scheme constructed by Eq.(3.4.32) is not a stable one. This conclusion agrees with the

numerical practice in which the practical numerical application of Eq.(3.4.32) experienced the instability.

Several other modifications used by Taflove et al.[26] have also been verified by the proposed method, the analysis results are consistent with their empirical conclusions.

3.4.2 Summary

The Fourier method has been introduced to analyze the stability of a FD-TD scheme. Instead of investigating the stability of a whole numerical scheme, the introduced method can be applied respectively to the interior region, the radiation boundary and the corner points. It is useful when a modification on the boundary condition, or on the finite difference formula for the interior points is required. The stability analysis becomes extremely important when a FD-TD method is used to solve steady EM problems since a steady state takes long time to be reached, and the knowledge of the iterative behavior of the FD-TD scheme helps save numerical computation efforts.

Several popular schemes used in the application of the FD-TD to electromagnetic problems have been analyzed via the method. The deducted conclusions for stability are consistent with the numerical practice.

3.5 Total Field Region and Scattered Field Region

Due to the linearity of Maxwell's equations, the numerical algorithms derived from the Maxwell's equations can be applied to incident EM fields, scattered fields or the total fields. On the outmost surface, radiation boundary condition has to be applied to the outgoing waves where in most cases they are scattered fields. While on the interfaces of different mediums, tangential components of total E and H fields must be continuous across the interfaces. One technique to treat these two cases is to zone the numerical space lattice into two distinct regions, as shown in Fig.3.7, separated by a

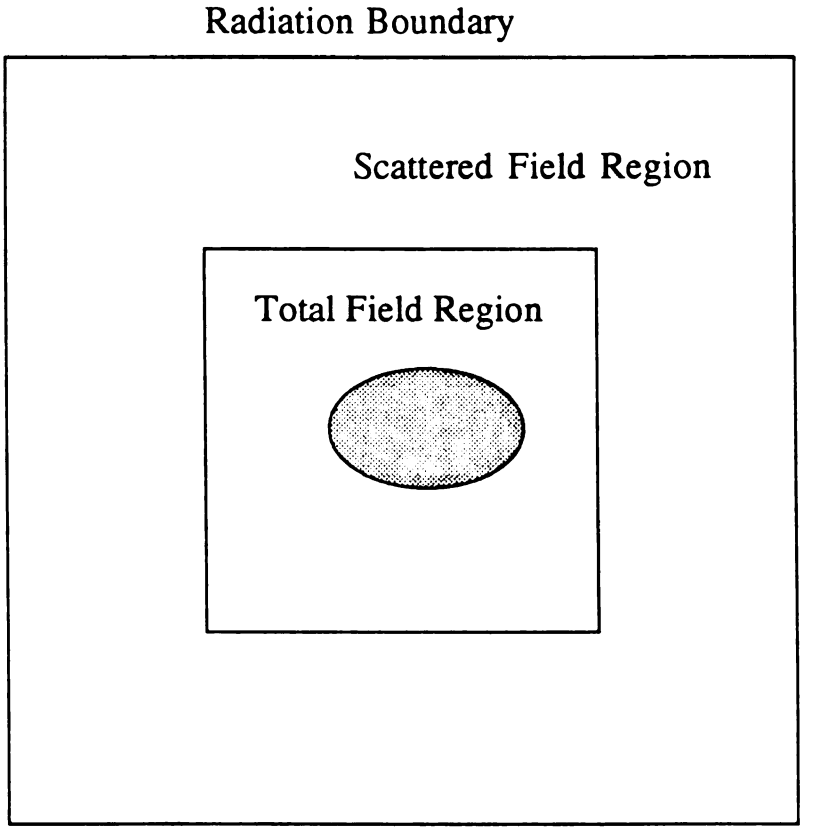

Fig. 3.7 Total Field And Scattered Field Region

rectangular surface which serves to connect the fields in two regions[34].

Total field region is the inner region of the FD-TD lattice. It includes all interacting structure of interest. The finite difference system for the Maxwell's equations operates on the total field vector components.

The outer region of the FD-TD lattice is denoted as the scattered field region. In this region, the finite different system for the curl equations operates only on the scattered field vector components. Radiation boundary condition can be applied directly to the points on the outmost truncated surface.

Dividing the FD-TD space lattice into two regions, it provides some convenience. In addition to the advantages of applying radiation boundary conditions and boundary conditions across the interfaces, the incident plane waves can be generated on the connection surface of two regions to insure the consistence of the fields in using the finite difference systems.

3.6 Integral Interpretation of the FD-TD Algorithms

In most realistic cases, many problems involve thin wires, slots and curved surfaces. However, the Yee's algorithm for the FD-TD method was originally interpreted as a direct approximation of the pointwise derivatives of Maxwell's time dependent curl equations. This resulted in a staircase approximation of the curved surfaces which might limit the predictive powers of the FD-TD method.

A few work has been done in this area to come up with new FD-TD algorithms for curved surfaces. Recently, a simple but efficient technique has been used successfully based on the integral interpolation of Maxwell's curl equations. Maxwell's curl equations can be written in integral forms which are called Ampere's law and Farady's law.

$$\int_l \mathbf{H}\cdot\vec{dl} = \int_S \rho\mathbf{E}\cdot\vec{dS} + \frac{\partial}{\partial t}\int_S \mathbf{D}\cdot\vec{dS} \qquad (3.6.1a)$$

$$\int_l \mathbf{E}\cdot d\vec{l} = \int_S \mathbf{J}_m \cdot d\vec{S} - \frac{\partial}{\partial t}\int_S \mathbf{B}\cdot d\vec{S} \tag{3.6.1b}$$

As shown in Fig.3.8, the above integral equation can be implemented in a geometrical interpretation. These contours intersect in the manner of links in a chain. With this geometrical interpolation, surface curvature can be conformed by deforming contour paths. Specifically, if we take the contours as shown in Fig.3.8, we find out that it yields the identical Yee's scheme. Here we take the Ampere's law as an example. The equivalence of Yee's formula and contour integral can be seen as follows:

$$\frac{\partial}{\partial t}\int_{S_1} \mathbf{D}\cdot dS = \int_{C_1} \mathbf{H}\cdot dl$$

As shown in Fig.3.8, we apply the Ampere's law along contour C_1 . Assuming that the field value at a midpoint of one side of the contour equals the average value of that field component along that side, the right side of the equation becomes:

$$\int_{C_1} \mathbf{H}\cdot d\vec{l} = H_x^{n+\frac{1}{2}}(i, j-\frac{1}{2}, k)\Delta x + H_y^{n+\frac{1}{2}}(i+\frac{1}{2}, j\ k)\Delta y - H_x^{n+\frac{1}{2}}(i, j+\frac{1}{2}, k)\Delta x \tag{3.6.2}$$

$$- H_y^{n+\frac{1}{2}}(i-\frac{1}{2}, j, k)\Delta y$$

If we further assume that $E_z(i, j\ k)$ equals the average value of E_z over the surface S_1 , and $\Delta x = \Delta y = \Delta z = \delta$. The time derivative can be numerically realized using a central-difference expression, and left side of the equation also can be simplified:

$$\frac{\partial}{\partial t}\int_{S_1} \mathbf{D}\cdot dS = \varepsilon_0\delta^2\left[\frac{E_z^{n+1}(i, j, k) - E_z^n(i, j, k)}{\Delta t}\right] \tag{3.6.3}$$

After equating (3.6.2) and (3.6.3), the equation becomes:

$$\varepsilon_0\delta^2\left[\frac{E_z^{n+1}(i, j, k) - E_z^n(i, j, k)}{\Delta t}\right] = \left[H_x^{n+\frac{1}{2}}(i, j-\frac{1}{2}, k) + H_y^{n+\frac{1}{2}}(i+\frac{1}{2}, j\ k)\right.$$

$$\left. - H_x^{n+\frac{1}{2}}(i, j+\frac{1}{2}, k) - H_y^{n+\frac{1}{2}}(i-\frac{1}{2}, j, k)\right]\delta \tag{3.6.4}$$

where the superscript indicate field values at time steps n, $n+\frac{1}{2}$ and $n+1$. Rearranging

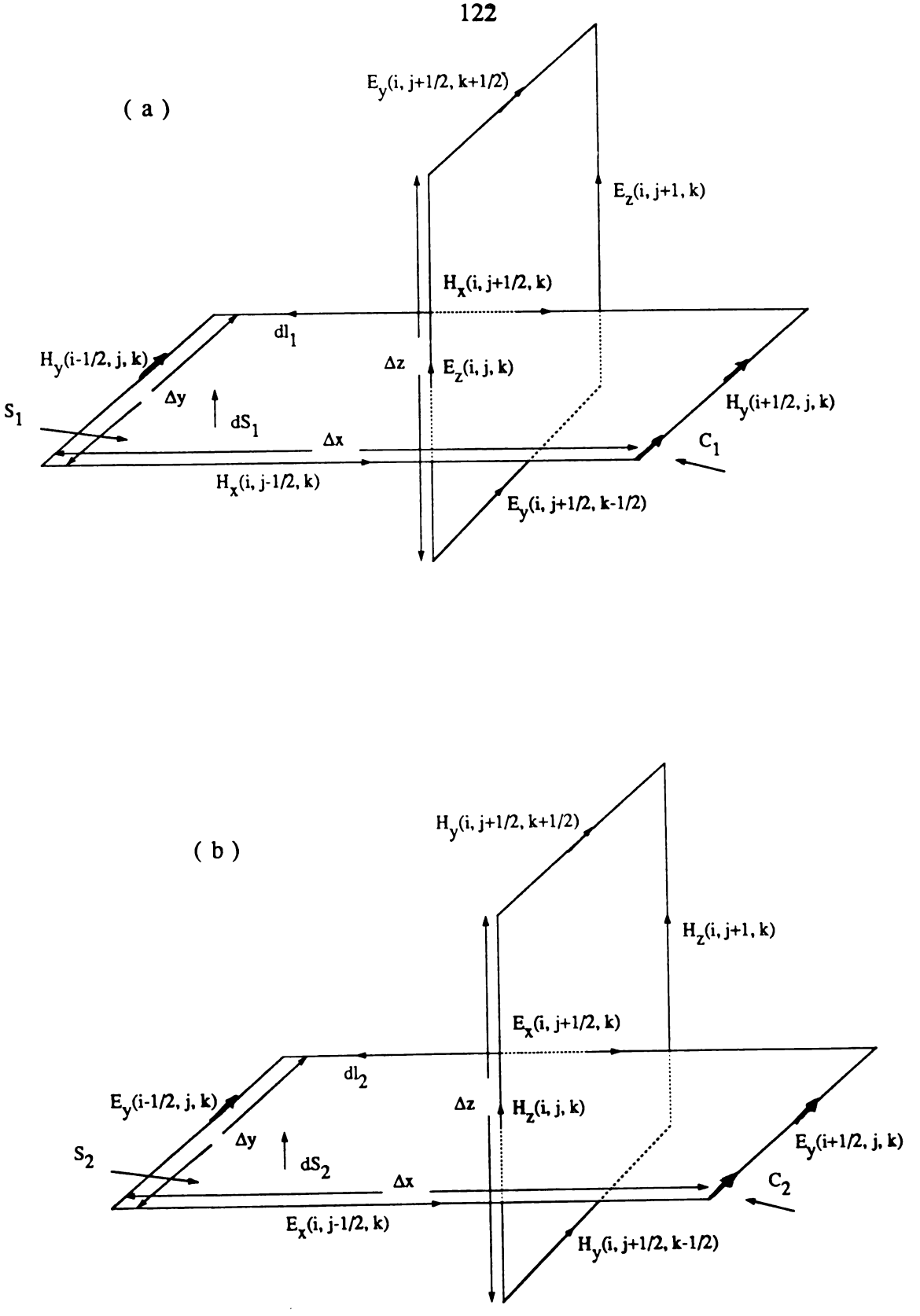

Figure 3.8 Examples of spatially orthogonal contours in free space. (a) Ampere's Law for E_z ; (b) Farady's Law for H_z .

the above equation:

$$E_z^{n+1}(i,j,k) = E_z^n(i,j,k) + \frac{\Delta t}{\varepsilon_0 \delta^2}\left[H_x^{n+\frac{1}{2}}(i,j-\frac{1}{2},k) + H_y^{n+\frac{1}{2}}(i+\frac{1}{2},j\,k)\right.$$
$$\left. - H_x^{n+\frac{1}{2}}(i,j+\frac{1}{2},k) - H_y^{n+\frac{1}{2}}(i-\frac{1}{2},j,k)\right]\delta \qquad (3.6.5)$$

We get exactly the Yee's expression for E_z , for the free space case, which was derived directly from the Maxwell's curl H equation.

Similarly, we can apply the Faraday's law along contour C_2 in Fig.3.8b. which yields the same expression as Yee's from the Maxwell's curl E equation.

By using integral interpretation of the curl equations, the Yee's model can be modified to handle the surface curvature, infinite thin sheets. In next Chapter, we are going to use integral interpretation to develop algorithms for two dimensional scattering problems.

3.7 Numerical Implementation and Validation of FD-TD Modeling

The main applications of the FD-TD method we concern can be stated as: a) Two dimensional metallic objects coated with magnetic material; b) Three dimensional cavity backed antenna with an impedance sheet over it. Based on the theory and algorithms discussed in this chapter, a few modifications will be made to solve above problems. Since a lot of details are involved, these two topics will be investigated separately in chapter 4 and chapter 5.

In this section, only a few well known examples have been chosen to validate the computer program and the standard FD-TD algorithms. As the first example, a infinite long perfectly conducting square cylinder is tested to verify the program and algorithm. As shown in Fig.3.9. , each side of the square cylinder equals to $k_0 a = 2\pi$. EM wave is propagating along y direction with TM polarization and both solutions of FD-TD and MoM are plotted in Fig.3.9. Another simple example is a perfectly

conducting strip as shown in Fig.3.10 and a strip of thin film with variable conductivity $\eta = 1/(\sigma t Z_0) = 2(x/a)^2$ as shown in Fig.3.11, where a is the half length of a strip. It can be seen that the results of both FD-TD and MoM agree with each other very well.

The capability of FD-TD in solving the electrically large bodies can be seen in the following example of a two dimensional electrically large airplane wing. The airplane wing is approximated as shown in Fig.3.12 and field distribution is plotted in Fig.3.13-3.15. The length of the airplane wing is about six wavelength and one end of it is very sharp. We can see the field singular behaviors around sharp corners and some small discontinuity of fields resulted from the staircase approximation of the surface of an airplane wing.

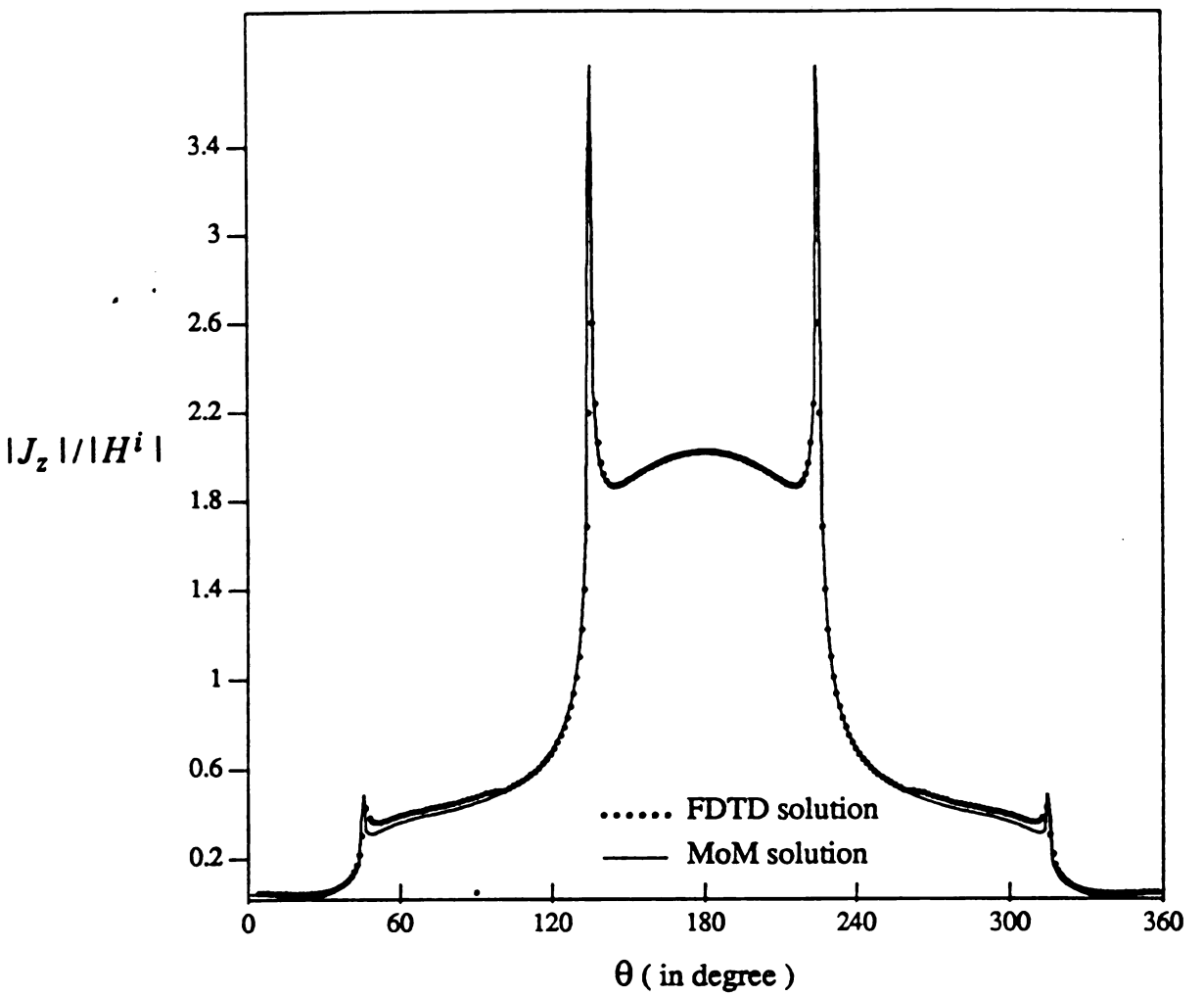

Figure 3.9 Current distribution on an infinite long, perfectly conducting rectangular cylinder without coating in the case of the TM excitation ($k_0 a = 2\pi$)

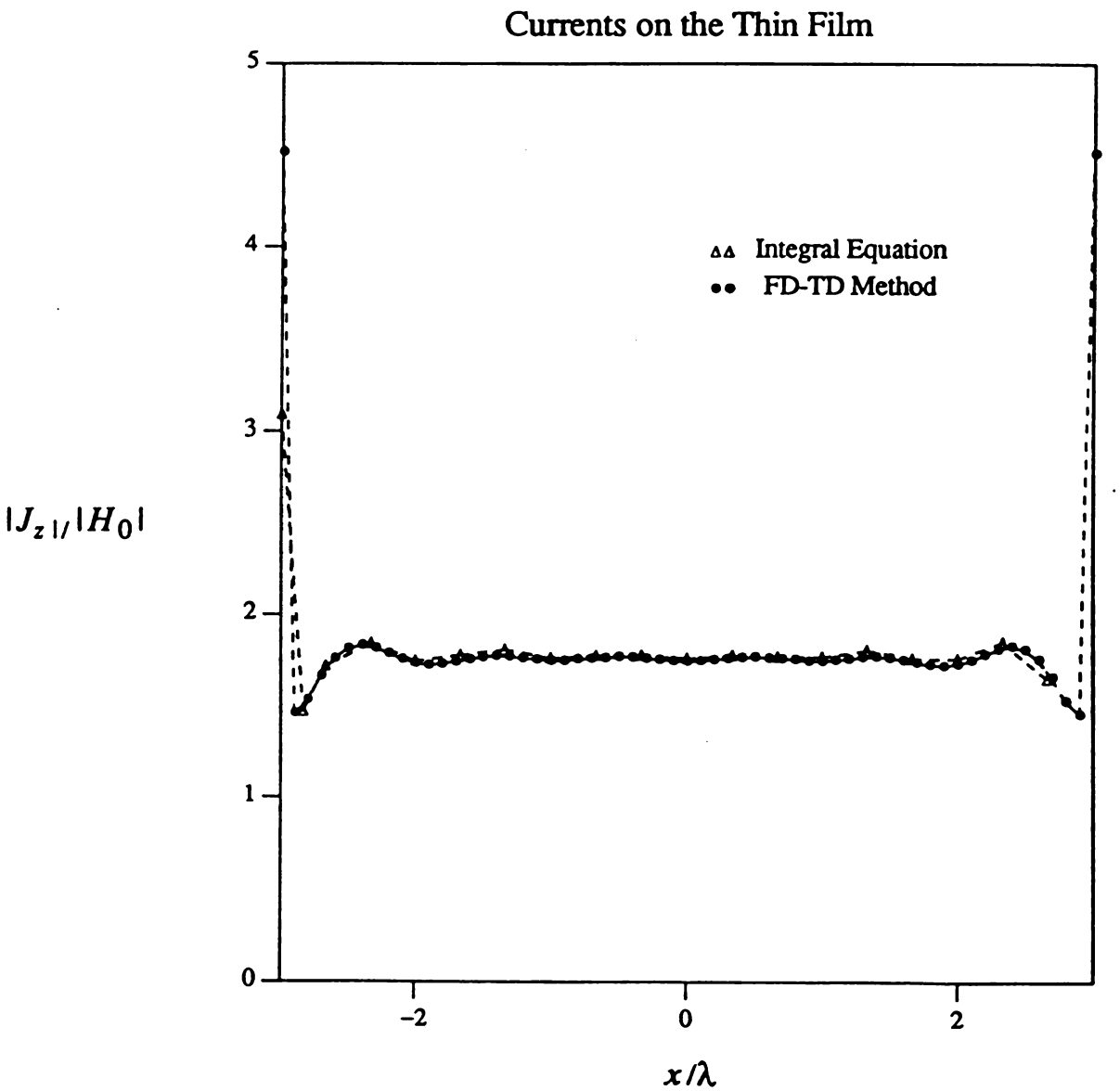

Figure 3.10 Comparison of results on the induced current on a perfectly conducting strip using integral equations and the FD-TD method

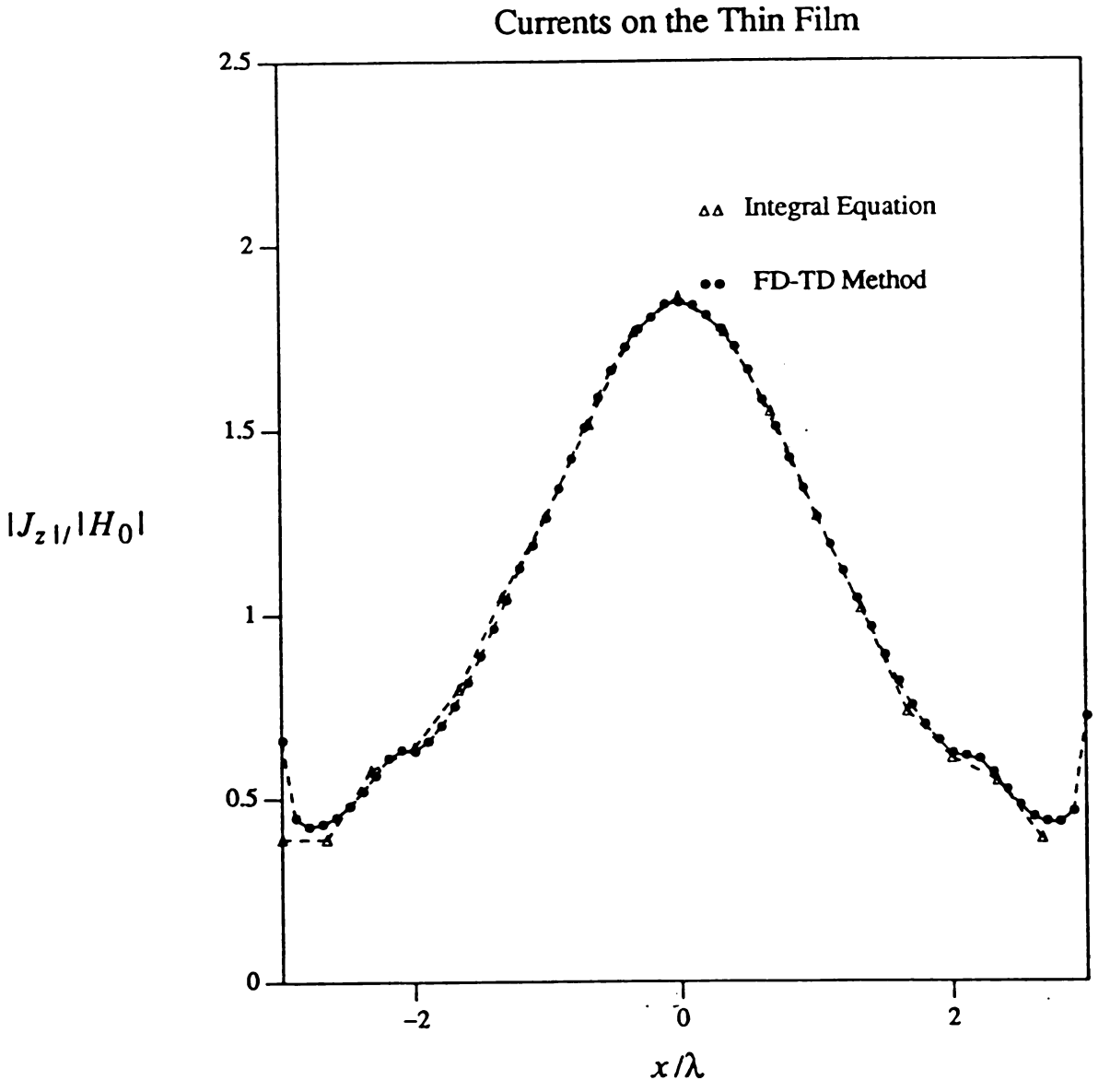

Figure 3.11 Induced current on a strip of thin film with variable conductivity: $\eta = 1/(\sigma t Z_0) = 2(x/a)^2$

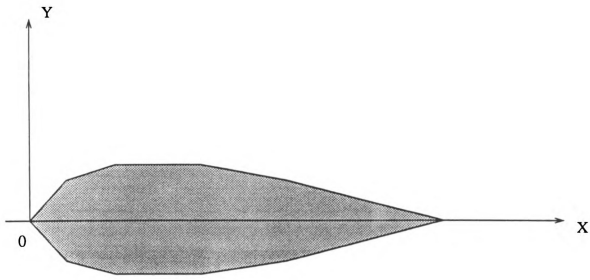

Figure 3.12 A perfectly conducting wing-shaped cylinder

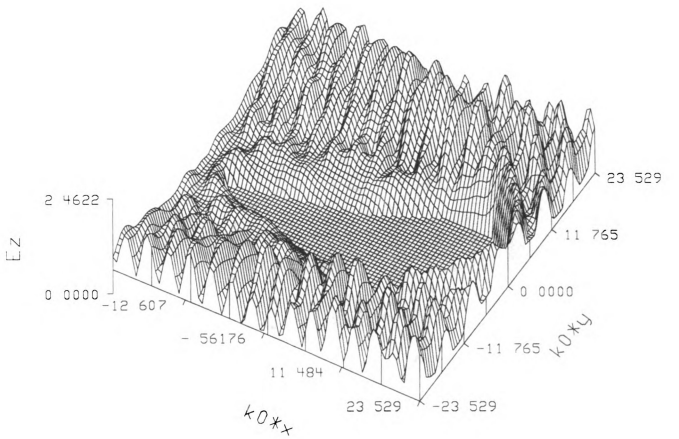

Figure 3.13 Amplitude distribution of the z-component electric field in the total field region with $k_0a = 20$

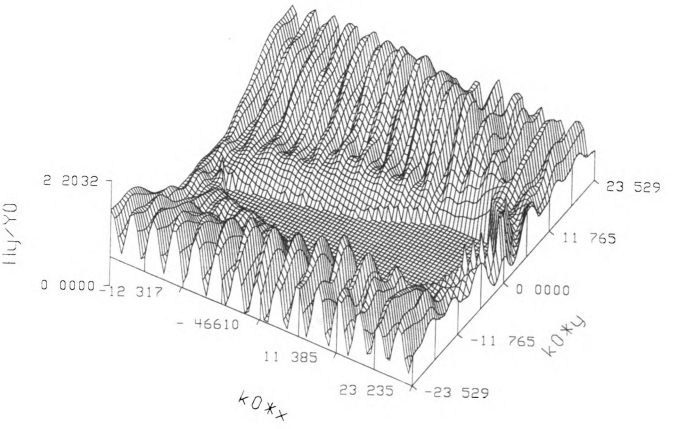

Figure 3.14 Amplitude distribution of the y-component magnetic field in the total field region with $k_0a = 20$

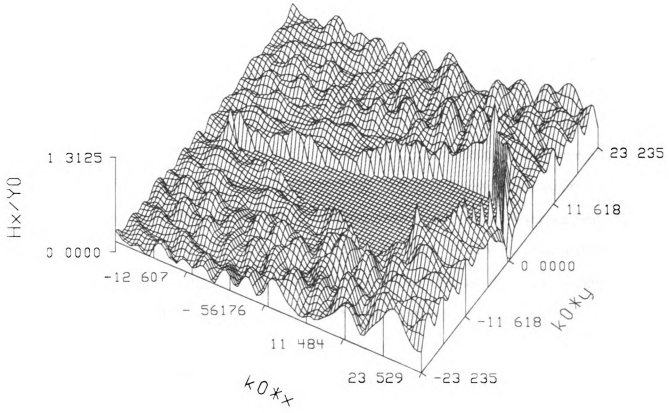

Figure 3.15 Amplitude distribution of the x-component magnetic field in the total field region with $k_0a = 20$

CHAPTER IV

APPLICATION OF FINITE DIFFERENCE TIME DOMAIN METHOD AND MOMENT TO TWO DIMENSIONAL ELECTROMAGNETIC SCATTERING PROBLEMS

4.1 Introduction

It is known that radar cross section of a conducting body can be reduced if it is coated by an electrically or magnetically lossy layer. In practice, it is desirable to make the coating layer thin. A thin layer of electrically lossy material on a perfectly conducting body can not reduce its radar cross section because the tangential component of electric field is very small near the surface of a perfect conductor and consequently the induced current and dissipated power in the coating layer are very small. On the other hand, if a thin magnetically lossy layer is used to coate the body, its radar cross section can be significantly reduced because the tangential component of magnetic field is very large on the surface of a conducting body, resulting in a large equivalent magnetic current and a high dissipated power in the coating layer.

In this chapter, a new set of coupled integral equations is derived for treating the scattering problem of a perfectly conducting body coated with a thin magnetically lossy layer. These electric field integral equation and the magnetic field integral equation are deduced and numerically solved by the method of moments (MoM). To validate the derived integral equations, an alternative method to solve the scattering problem of an infinite circular cylinder coated with a thin magnetic lossy layer has also been developed based on the eigenmode expansion. The results of the radar cross section and currents via the MoM and the eigenmode expansion method are compared. The agreement is excellent. The finite difference time domain method is then implen-

mented to solve a metallic object coated with a magnetic thin layer and numerical results are compared with that by the MoM.

4.2 Integral Equations for Perfectly Conducting Cylinders Coated with Thin Magnetic Materials

4.2.1 Derivation of Integral Equations for three-dimensional structures

A new set of integral equations is derived based on the equivalent principle, focusing on the extreme case of a perfect conductor with a thin magnetic coating. Let's start from Maxwell's Equations:

$$\nabla\times\mathbf{H} = \frac{\partial \mathbf{D}}{\partial t} + \mathbf{J}_e \tag{4.1a}$$

$$\nabla\times\mathbf{E} = -\frac{\partial \mathbf{B}}{\partial t} - \mathbf{J}_m \tag{4.1b}$$

$$\nabla\cdot\mathbf{D} = \rho_e \tag{4.1c}$$

$$\nabla\cdot\mathbf{B} = \rho_m \tag{4.1d}$$

and continuity equations of

$$\nabla\cdot\mathbf{J}_e + \frac{\partial}{\partial t}\rho_e = 0 \tag{4.1e}$$

$$\nabla\cdot\mathbf{J}_m + \frac{\partial}{\partial t}\rho_m = 0 \tag{4.1f}$$

In the frequency domain, the fields are preassumed to be harmonic dependence of $e^{j\omega t}$. Thus the Maxwell's equations become:

$$\nabla\times\mathbf{H} = j\omega\varepsilon\mathbf{E} + \mathbf{J}_e \tag{4.2a}$$

$$\nabla\times\mathbf{E} = -j\omega\mu\mathbf{H} - \mathbf{J}_m \tag{4.2b}$$

$$\nabla\cdot(\varepsilon\mathbf{E}) = \rho_e \tag{4.2c}$$

$$\nabla\cdot(\mu\mathbf{H}) = \rho_m \tag{4.2d}$$

where **E** and **H** are the electric field and the magnetic field, ε and μ are permittivity and permeability of the media, $\mathbf{J}_e$ and $\mathbf{J}_m$ are the electric current and magnetic

current, and ρ_e and ρ_m are the electric and magnetic charges. The above equations can also be rewritten as:

$$\nabla\times\mathbf{H} = j\omega\varepsilon_0\mathbf{E} + j\omega(\varepsilon - \varepsilon_0)\mathbf{E} + \mathbf{J}_e \tag{4.3a}$$

$$\nabla\times\mathbf{E} = -j\omega\mu_0\mathbf{H} - j\omega(\mu - \mu_0)\mathbf{H} - \mathbf{J}_m \tag{4.3b}$$

$$\nabla\cdot(\varepsilon_0\mathbf{E}) = -\nabla\cdot((\varepsilon - \varepsilon_0)\mathbf{E}) + \rho_e \tag{4.3c}$$

$$\nabla\cdot(\mu_0\mathbf{H}) = -\nabla\cdot((\mu - \mu_0)\mathbf{H}) + \rho_m \tag{4.3d}$$

When the permittivity and permeability of a medium are different from that of free space, equivalent sources can be defined:

$$\mathbf{J}_m^{eq} = \mathbf{J}_m + j\omega(\mu - \mu_0)\mathbf{H} \tag{4.4a}$$

$$\mathbf{J}_e^{eq} = \mathbf{J}_e + j\omega(\varepsilon - \varepsilon_0)\mathbf{E} \tag{4.4b}$$

$$\rho_e^{eq} = -\nabla\cdot((\varepsilon - \varepsilon_0)\mathbf{E}) + \rho_e \tag{4.4c}$$

$$\rho_m^{eq} = -\nabla\cdot((\mu - \mu_0)\mathbf{H}) + \rho_m \tag{4.4d}$$

In the real-source free region where $\mathbf{J}_m$, $\mathbf{J}_e$, ρ_e, ρ_m are zeros, the equivalent sources become:

$$\mathbf{J}_m^{eq} = j\omega(\mu - \mu_0)\mathbf{H} = \sigma_m\mathbf{H} \tag{4.5a}$$

$$\mathbf{J}_e^{eq} = j\omega(\varepsilon - \varepsilon_0)\mathbf{E} = \sigma\mathbf{E} \tag{4.5b}$$

$$\rho_e^{eq} = -\nabla\cdot((\varepsilon - \varepsilon_0)\mathbf{E}) \tag{4.5c}$$

$$\rho_m^{eq} = -\nabla\cdot((\mu - \mu_0)\mathbf{H}) \tag{4.5d}$$

The equivalent sources are depicted in Fig. 4.1, and they obey the continuity equations of

$$\nabla\cdot\mathbf{J}_e^{eq} = -j\omega\rho_e^{eq} \tag{4.6a}$$

$$\nabla\cdot\mathbf{J}_m^{eq} = -j\omega\rho_m^{eq} \tag{4.6b}$$

However, It can be shown that the total equivalent charges per unit surface area are zero in the thin film in the limiting case. As shown in Fig. 4.2, the equivalent charges on two surfaces of the coated film are:

$$\rho_1 = \hat{n}\cdot(\varepsilon - \varepsilon_0)\mathbf{E}_2 \tag{4.7a}$$

$$\rho_2 = -\hat{n}\cdot(\varepsilon - \varepsilon_0)\mathbf{E}_2 \tag{4.7b}$$

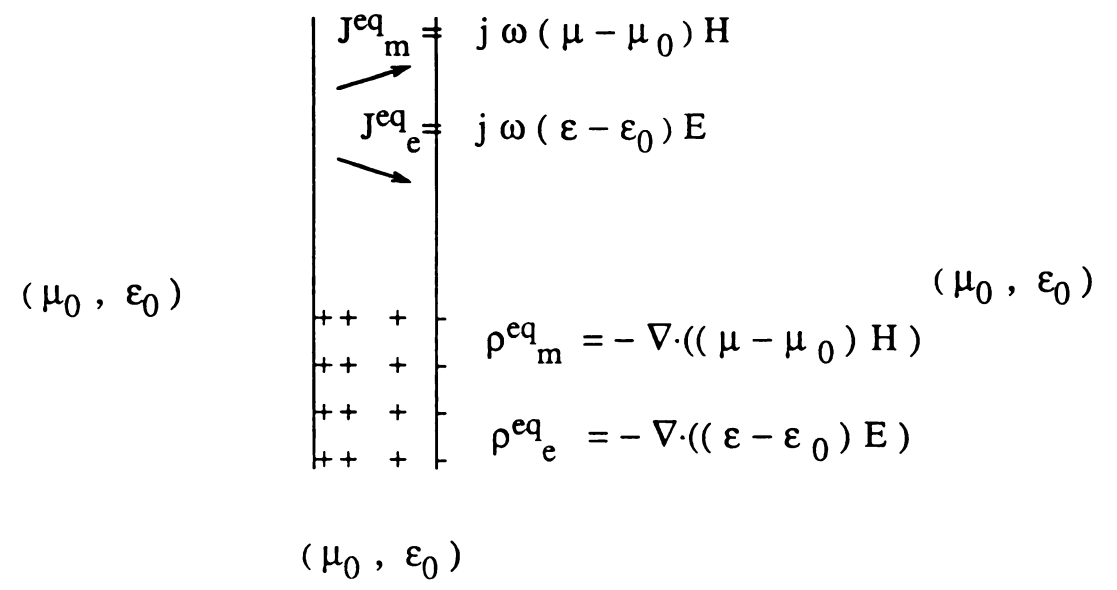

Fig. 4.1 The illustration of equivalent currents and equivalent charges

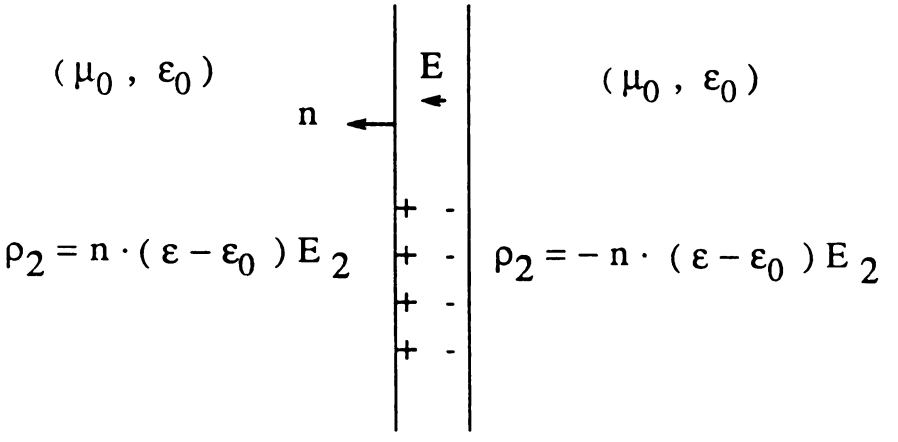

Fig. 4.2 Total equivalent charges on a thin layer

When the film thickness approaches zero, the total equivalent charge per surface area diminishes to zero since $\mathbf{E}_2$ is the same on two surfaces of the film.

$$\rho^{total} = \rho_1 + \rho_2 = 0 \tag{4.7c}$$

Following the same argument, it can be shown that the total equivalent magnetic charge per surface area diminishes too.

$$\rho_m^{total} = 0 \tag{4.7d}$$

As shown in Fig. 4.3 the total fields inside region 1 can be considered to be summation of the incident fields and the scattered fields maintained by the equivalent sources in the thin layer and the electric current on the surface of the perfect conductor. Based on the equivalence principles, the general integral equations for **E**, **H** fields can be established:

$$\begin{aligned}\mathbf{E}^{total}(\mathbf{r}) = T\iiint_V [&- j\omega\mu_0 \mathbf{J}_e^i \Phi - \mathbf{J}_m^i \times \nabla'\Phi + \frac{\rho_e^i}{\varepsilon_0}\nabla'\Phi]dV' \\ &+ T\iiint_V [- j\omega\mu_0 \mathbf{J}_e^{eq} \Phi - \mathbf{J}_m^{eq} \times \nabla'\Phi + \frac{\rho_e^{eq}}{\varepsilon_0}\nabla'\Phi]dV' \\ &+ T\iint_S [- j\omega\mu_0 (\hat{n}\times\mathbf{H})\Phi + (\hat{n}\times\mathbf{E})\times\nabla'\Phi + (\hat{n}\cdot\mathbf{E})\nabla'\Phi]\, dS'\end{aligned} \tag{4.8a}$$

$$\begin{aligned}\mathbf{H}^{total}(\mathbf{r}) = T\iiint_V [&- j\omega\varepsilon_0 \mathbf{J}_m^i \Phi + \mathbf{J}_e^i \times \nabla'\Phi + \frac{\rho_m^i}{\mu_0}\nabla'\Phi]dV' \\ &+ T\iiint_V [- j\omega\varepsilon_0 \mathbf{J}_m^{eq} \Phi + \mathbf{J}_e^{eq} \times \nabla'\Phi + \frac{\rho_m^{eq}}{\mu_0}\nabla'\Phi]dV' \\ &+ T\iint_S [j\omega\varepsilon_0 (\hat{n}\times\mathbf{E})\Phi + (\hat{n}\times\mathbf{H})\times\nabla'\Phi + (\hat{n}\cdot\mathbf{H})\nabla'\Phi]\, dS'\end{aligned} \tag{4.8b}$$

where $\Phi(\mathbf{r}, \mathbf{r}') = \dfrac{e^{-jkR}}{4\pi R}$, $R = |\mathbf{r} - \mathbf{r}'|$, and T is 2 when $\mathbf{r}$ is on the surface of the perfect conductor and is 1 when $\mathbf{r}$ is in the space outside the perfect conductor.

The second volume integrals are contributed by the equivalent sources in the coated magnetic layer, and the third surface integrals are contributed by the equivalent sources on the surface of the conductor.

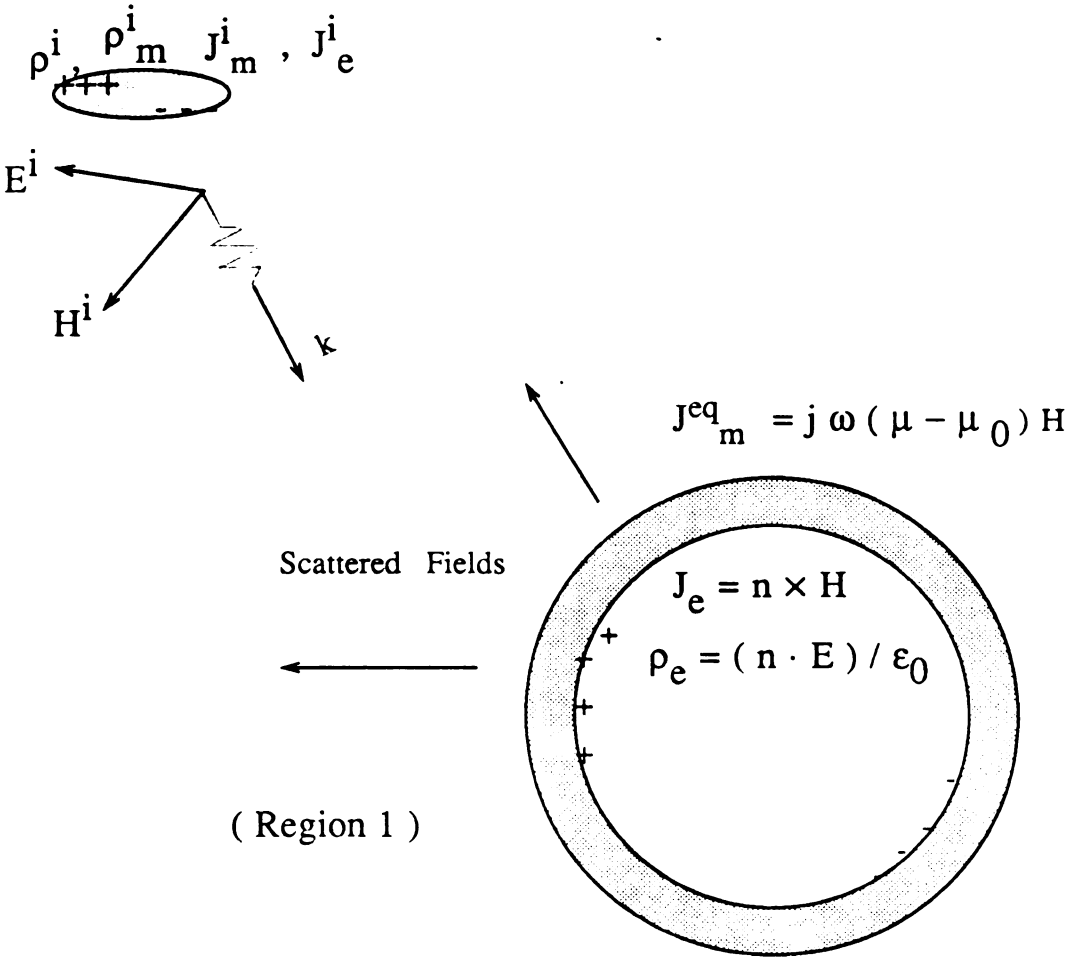

Fig. 4.3 Seperation of the total fields into incident fields and scattered fields maintained by equivalent sources

The first volume integrals, which are contributed by real sources to maintain the incident fields, is denoted respectively by $T\mathbf{E}^i$ in the electric field integral equation and $T\mathbf{H}^i$ in the magnetic field integral equation.

$$\mathbf{E}^{total}(\mathbf{r}) = T\mathbf{E}^i + T\int_V [- j\omega\mu_0 \mathbf{J}_e^{eq}\Phi - \mathbf{J}_m^{eq}\times\nabla'\Phi + \frac{\rho_e^{eq}}{\varepsilon_0}\nabla'\Phi]dV'$$
$$+ T\int_S [- j\omega\mu_0(\hat{n}\times\mathbf{H})\Phi + (\hat{n}\times\mathbf{E})\times\nabla'\Phi + (\hat{n}\cdot\mathbf{E})\nabla'\Phi]\, dS' \qquad (4.9a)$$

$$\mathbf{H}^{total}(\mathbf{r}) = T\mathbf{H}^i + T\int_V [- j\omega\varepsilon_0 \mathbf{J}_m^{eq}\Phi + \mathbf{J}_e^{eq}\times\nabla'\Phi + \frac{\rho_m^{eq}}{\mu_0}\nabla'\Phi]dV'$$
$$+ T\int_S [j\omega\varepsilon_0(\hat{n}\times\mathbf{E})\Phi + (\hat{n}\times\mathbf{H})\times\nabla'\Phi + (\hat{n}\cdot\mathbf{H})\nabla'\Phi]\, dS' \qquad (4.9b)$$

On the surface of a perfectly conducting body

$$\hat{n}\times\mathbf{E} = 0 \qquad (4.10a)$$
$$\hat{n}\cdot\mathbf{H} = 0 \qquad (4.10b)$$

and

$$\mathbf{J}_e^{eq} = \sigma\mathbf{E} = 0 \qquad (4.11)$$

By assuming the null electric conductivity, $\sigma = 0$. Note that the tangential component of electric field is not continuous across the magnetic current sheet due to $\hat{n}\times(\mathbf{E}_1 - \mathbf{E}_2) = -\mathbf{J}_m^{eq}t$. Consequently $\mathbf{J}_e^{eq} = 0$ is not deduced from $\hat{n}\times\mathbf{E} = 0$ on the surface of the perfect conductor. In fact, $\hat{n}\times\mathbf{E}$ is not zero in the thin layer when a magnetic current sheet exists . It is also interesting to note that the nullity of the currents in an electrically lossy layer is provided by the null tangential component of electric field on the surface of the perfect conductor and its continuation across the lossy layer. However, when a magnetic sheet exists electric current $\mathbf{J}_e^{eq} = \sigma\mathbf{E}$ in the thin layer may contribute to the scattered fields and then radar cross section if σ is not equal to zero. For the time being, only the case of $\sigma = 0$ is considered. It is also easy to justify that

$$\rho_e^{eq} = 0, \qquad t \to 0 \qquad (4.12a)$$
$$\rho_m^{eq} = 0, \qquad t \to 0 \qquad (4.12b)$$

where t is the thickness of the coated layer. Using above conditions, equations 4.9 are simplified to:

$$\mathbf{E}^{total}(\mathbf{r}) = T\mathbf{E}^{i} + T\int_{V}[-\mathbf{J}_{m}^{eq}\times\nabla'\Phi]dV' \tag{4.13a}$$
$$+ T\int_{S}[-j\omega\mu_0(\hat{n}\times\mathbf{H})\Phi + (\hat{n}\cdot\mathbf{E})\nabla'\Phi]\,dS'$$
$$\mathbf{H}^{total}(\mathbf{r}) = T\mathbf{H}^{i} + T\int_{V}[-j\omega\varepsilon_0\mathbf{J}_{m}^{eq}\Phi]dV' \tag{4.13b}$$
$$+ T\int_{S}[(\hat{n}\times\mathbf{H})\times\nabla'\Phi]\,dS'$$

Using $\hat{n}\cdot\mathbf{H} = 0$ on the surface of a perfect conductor , and shrinking the volume integrals into surface integrals, when t is very thin, leads to:

$$\mathbf{E}^{total}(\mathbf{r}) = T\mathbf{E}^{i} + T\int_{S}[-(\sigma_m t)\mathbf{H}\times\nabla'\Phi - j\omega\mu_0(\hat{n}\times\mathbf{H})\Phi + (\hat{n}\cdot\mathbf{E})\nabla'\Phi]\,dS' \tag{4.14a}$$
$$\mathbf{H}^{total}(\mathbf{r}) = T\mathbf{H}^{i} + T\int_{S}[-j\omega\varepsilon_0\sigma_m t\mathbf{H}\Phi + (\hat{n}\times\mathbf{H})\times\nabla'\Phi]\,dS' \tag{4.14b}$$

where (4.5.a) is used and

$$\mathbf{E}^{total} = \mathbf{E}^{s} + \mathbf{E}^{i} \tag{4.15a}$$
$$\mathbf{H}^{total} = \mathbf{H}^{s} + \mathbf{H}^{i} \tag{4.15b}$$

If the currents are related to the tangential components of the fields and proper boundary conditions are applied, both the electric field integral equation and the magnetic field integral equation can be established.

The tangential component of total **E** field is zero on the surface of perfect conductor, that is $\hat{n}\times\mathbf{E}^{total} = 0$. However, matching the boundary condition on the surface of perfect conductor will result in an incorrect integral equation. $\mathbf{E}^{total}(\mathbf{r})$ on the left side of (4.14a) should be understood as the total field on the outer surface of the magnetic thin layer, which will be illustrated in Appendix C. If the observing point is on the outer surface of the thin layer, boundary condition is $\hat{n}\times\mathbf{E}^{total} = -\mathbf{J}_{m}^{eq}\,t$. Matching the boundary condition on the outer surface of the thin layer and setting $T = 2$ result in:

$$\frac{1}{2}\hat{n}\times\mathbf{J}_m^{eq}\,t|_{\tan} = \mathbf{E}^i(\mathbf{r})|_{\tan} + \left\{\int_S [\,-(\sigma_m t)\mathbf{H}\times\nabla'\Phi - j\omega\mu_0(\hat{n}\times\mathbf{H})\Phi + (\hat{n}\cdot\mathbf{E})\nabla'\Phi]\,dS'\right\}_{\tan}$$

or

$$-\mathbf{E}^i(\mathbf{r})|_{\tan} = -\frac{1}{2}\hat{n}\times\sigma_m t\mathbf{H}|_{\tan} + \left\{\int_S [-(\sigma_m t)\mathbf{H}\times\nabla'\Phi - j\omega\mu_0(\hat{n}\times\mathbf{H})\Phi + (\hat{n}\cdot\mathbf{E})\nabla'\Phi]dS'\right\}_{\tan} \tag{4.16}$$

By using $\hat{n}\cdot\mathbf{E} = \frac{j}{\varepsilon\omega}\nabla\cdot\mathbf{J}$, an integral equation in terms of the unknown of $\hat{n}\times\mathbf{H}$ is obtained.

$$-\mathbf{E}^i(\mathbf{r})|_{\tan} = -\frac{1}{2}\hat{n}\times\sigma_m t\mathbf{H}|_{\tan} + \left\{\int_S [-(\sigma_m t)\mathbf{H}\times\nabla'\Phi - j\omega\mu_0(\hat{n}\times\mathbf{H})\Phi + \frac{j}{\varepsilon_0\omega}\nabla'\cdot(\hat{n}\times\mathbf{H})\nabla'\Phi]dS'\right\}_{\tan} \tag{4.17}$$

This integral equation is the electric field integral equation (EFIE) for arbitrarily shaped three-dimensional bodies coated with thin magnetic layers, and it is the second kind of Fredhelm integral equation.

Similarly, the magnetic field integral equation can be derived. The tangential component of the magnetic field, which is continuous across the magnetic sheet when σ is zero, is related to the electric current on the surface of a perfect conductor as $\hat{n}\times\mathbf{H} = \mathbf{J}_e$.

Using the boundary condition:

$$\hat{n}\times\mathbf{H} = \mathbf{J}_e \tag{4.18a}$$

and

$$\hat{n}\cdot\mathbf{H} = 0 \tag{4.18b}$$

yields a magnetic field integral equation (MFIE)

$$\frac{1}{2}\mathbf{H}^{total}(\mathbf{r})|_{\tan} = \mathbf{H}^i|_{\tan} + \left\{\int_S [\,-j\omega\varepsilon_0(\sigma_m t)\mathbf{H}\Phi + (\hat{n}\times\mathbf{H})\times\nabla'\Phi]\,dS'\right\}_{\tan} \tag{4.19}$$

where $\mathbf{H}$ is the unknown to be solved. It is observed that MFIE does not have the term of $\nabla'\cdot(\hat{n}\times\mathbf{H})\nabla'\Phi$ which involves the divergence of $\hat{n}\times\mathbf{H}$. Thus, the MFIE has an advantage of numerical simplicity over the EFIE.

Both the MFIE and the EFIE are applicable to the perfectly conducting bodies coated with a thin magnetic lossy layer. It is expected that magnetic lossy coating can significantly change the scattered fields and the radar cross section of a conducting body. This is verified when the developed integral equations are applied to two-dimensional problems.

4.2.2 Integral Equations for Two-Dimensional Geometries

Equations (4.17) and (4.19) can be simplified when they are applied to two dimensional cases. Only the EFIE is taken as an example to show the derivation procedure. In a two-dimensional problem, the tangential component of **H** is related to the electric current by $\hat{n}\times\mathbf{H} = \mathbf{I}$ and the electric current $\mathbf{I}(\mathbf{r})$ is assumed to have a propagation constant β in the z direction as

$$\hat{n}\times\mathbf{H}(\mathbf{r}) = \mathbf{I}(\mathbf{r}) = \mathbf{I}(\vec{\rho})e^{-j\beta z} \tag{4.20a}$$

$$\mathbf{E}^i(\mathbf{r}) = \mathbf{E}^i(\vec{\rho})e^{-j\beta z} \tag{4.20b}$$

$$\mathbf{H}^i(\mathbf{r}) = \mathbf{H}^i(\vec{\rho})e^{-j\beta z} \tag{4.20c}$$

where

$$\vec{\rho} = x\hat{x} + y\hat{y}$$

Substituting the above two relations into the EFIE and integrating over the z variable yield:

$$\begin{aligned} -\mathbf{E}^i(\vec{\rho})e^{-j\beta z}|_{\tan} = & -\frac{1}{2}\sigma_m t\hat{n}\times\mathbf{H}(\vec{\rho})e^{-j\beta z}|_{\tan} + \Big\{\int_C \Big[-(\sigma_m t)\mathbf{H}(\vec{\rho})\times\nabla'_t\int_{-\infty}^{\infty} e^{-j\beta z'}\,\Phi(\mathbf{r},\mathbf{r}')\,dz' \\ & -(\sigma_m t)\mathbf{H}(\vec{\rho})\times\hat{z}\int_{-\infty}^{\infty} e^{-j\beta z'}\frac{\partial}{\partial z'}\Phi(\mathbf{r},\mathbf{r}')\,dz' - j\omega\mu_0\hat{n}\times\mathbf{H}(\vec{\rho})\int_{-\infty}^{\infty} e^{-j\beta z'}\Phi(\mathbf{r},\mathbf{r}')\,dz' \\ & +\frac{j}{\varepsilon_0\omega}(\nabla'_t - j\beta\hat{z})\cdot\mathbf{J}(\vec{\rho})\nabla'_t\int_{-\infty}^{\infty} e^{-j\beta z'}\Phi(\mathbf{r},\mathbf{r}')\,dz' \\ & +\frac{j}{\varepsilon_0\omega}(\nabla'_t - j\beta\hat{z})\cdot\mathbf{J}(\vec{\rho})\hat{z}\int_{-\infty}^{\infty} e^{-j\beta z'}\frac{\partial}{\partial z'}\Phi(\mathbf{r},\mathbf{r}')\,dz'\Big]\,dl'\Big\}_{\tan} \end{aligned} \tag{4.21}$$

It is well known that the two-dimensional Green's function is:

$$G = \frac{\pi}{j} H_0^{(2)}(\sqrt{(k^2 - \beta^2)}|\vec{\rho} - \vec{\rho}'|)$$
$$= \int_{-\infty}^{\infty} e^{-j\beta(z'-z)} \frac{\exp -j\beta\sqrt{|\vec{\rho} - \vec{\rho}'|^2 + (z'-z)^2}}{\sqrt{|\vec{\rho} - \vec{\rho}'|^2 + (z-z')^2}} dz' \tag{4.22}$$

and

$$\int_{-\infty}^{\infty} e^{-j\beta(z'-z)} \frac{\partial}{\partial z'} \left(\frac{\exp -j\beta\sqrt{|\vec{\rho} - \vec{\rho}'|^2 + (z'-z)^2}}{\sqrt{|\vec{\rho} - \vec{\rho}'|^2 + (z-z')^2}}\right) dz'$$
$$= e^{-j\beta(z'-z)} \left(\frac{\exp -j\beta\sqrt{|\vec{\rho} - \vec{\rho}'|^2 + (z'-z)^2}}{\sqrt{|\vec{\rho} - \vec{\rho}'|^2 + (z-z')^2}}\right|_{-\infty}^{\infty}$$
$$- \int_{-\infty}^{\infty} e^{-j\beta(z'-z)} (-j\beta) \left(\frac{\exp -j\beta\sqrt{|\vec{\rho} - \vec{\rho}'|^2 + (z'-z)^2}}{\sqrt{|\vec{\rho} - \vec{\rho}'|^2 + (z-z')^2}}\right) dz'$$
$$= j\beta \int_{-\infty}^{\infty} e^{-j\beta(z'-z)} \left(\frac{\exp -j\beta\sqrt{|\vec{\rho} - \vec{\rho}'|^2 + (z'-z)^2}}{\sqrt{|\vec{\rho} - \vec{\rho}'|^2 + (z-z')^2}}\right) dz'$$
$$= j\beta \left[\frac{\pi}{j} H_0^{(2)}(\sqrt{k^2 - \beta^2}|\vec{\rho} - \vec{\rho}'|\right] \tag{4.23}$$

The integrals over z variable in the integral equation can be represented by the two-dimensional Green's function:

$$-4\pi \mathbf{E}^i(\vec{\rho})|_{\tan} = -2\pi\sigma_m t \hat{n}\times\mathbf{H}(\vec{\rho})|_{\tan} + \left\{\int_C [-(\sigma_m t)\mathbf{H}(\vec{\rho}')\times(\nabla'_t + j\beta\hat{z}) G(\sqrt{(k^2 - \beta^2)}|\vec{\rho} - \vec{\rho}'|)\right.$$
$$- j\omega\mu_0 \hat{n}\times\mathbf{H}(\vec{\rho}') G(\sqrt{(k^2 - \beta^2)}|\vec{\rho} - \vec{\rho}'|)$$
$$\left. + \frac{j}{\varepsilon_0\omega}(\nabla'_t - j\beta\hat{z})\cdot\hat{n}\times\mathbf{H}(\vec{\rho}')(\nabla'_t + j\beta\hat{z}) G(\sqrt{(k^2 - \beta^2)}|\vec{\rho} - \vec{\rho}'|)]\, dl'\right\}_{\tan} \tag{4.24}$$

where $\mathbf{H}(\vec{\rho})$ is the unknown, but it can be related to the electric current $\mathbf{I}$ by $\mathbf{H} = -\hat{n}\times\mathbf{I}$ and $\hat{n}\times\mathbf{H} = \mathbf{I}$ since $\hat{n}\times\hat{n}\times\mathbf{H} = -\mathbf{H} + \hat{n}(\hat{n}\cdot\mathbf{H})$ and $\hat{n}\cdot\mathbf{H} = 0$. Thus the EFIE is established in terms of the electric surface current:

$$-4\pi \mathbf{E}^i(\vec{\rho})|_{\tan} = +2\pi\sigma_m t \mathbf{I}(\vec{\rho})|_{\tan} + \left\{\int_C [(\sigma_m t)\hat{n}\times\mathbf{I}(\vec{\rho})\times(\nabla'_t + j\beta\hat{z}) G(\sqrt{(k^2 - \beta^2)}|\vec{\rho} - \vec{\rho}'|)\right.$$
$$- j\omega\mu_0 \mathbf{I}(\vec{\rho}') G(\sqrt{(k^2 - \beta^2)}|\vec{\rho} - \vec{\rho}'|)$$
$$\left. + \frac{j}{\varepsilon_0\omega}(\nabla'_t - j\beta\hat{z})\cdot\mathbf{I}(\vec{\rho}')(\nabla'_t + j\beta\hat{z}) G(\sqrt{(k^2 - \beta^2)}|\vec{\rho} - \vec{\rho}'|)]\, dl'\right\}_{\tan} \tag{4.25}$$

which is an electric field integral equation for a two-dimensional arbitrarily shaped body. Compared to the pure perfect conductor case, it is seen that there is an extra term contributed by the magnetic current. The contribution from the magnetic current will give rise to a different scattering property from that of a perfect conductor without coating.

If TM polarized fields of $\mathbf{E} = \hat{z}E_z$, $\mathbf{H} = H_x\hat{x} + H_y\hat{y}$ illuminate a circular cylinder, the integral equation has only the z component

$$\mathbf{I} = \hat{n}\times\mathbf{H} = \hat{z}I \tag{4.26a}$$

Note that

$$\nabla'_t\cdot\hat{z}I_z = 0 \tag{4.26b}$$

In the cylindrical coordinates,

$$\nabla'_t G(\sqrt{(k^2-\beta^2)}|\vec{\rho}-\vec{\rho}'|) = (\hat{\theta}\frac{\partial}{\rho\partial\theta'} + \hat{\rho}\frac{\partial}{\partial\rho'})G(\sqrt{(k^2-\beta^2)}|\vec{\rho}-\vec{\rho}'|) \tag{4.27a}$$

with

$$\hat{\rho}\frac{\partial}{\partial\rho'}G(\sqrt{(k^2-\beta^2)}|\vec{\rho}-\vec{\rho}'|) = \hat{\rho}G'(\sqrt{(k^2-\beta^2)}|\vec{\rho}-\vec{\rho}'|)\sqrt{(k^2-\beta^2)}\frac{\partial}{\partial\rho'}|\vec{\rho}-\vec{\rho}'| \tag{4.27b}$$

since $|\vec{\rho}-\vec{\rho}'| = R = \sqrt{\rho^2+\rho'^2-2\rho\rho'\cos(\theta-\theta')}$, we have:

$$\frac{\partial}{\partial\rho'}|\vec{\rho}-\vec{\rho}'| = 2(\rho'-\rho\cos(\theta-\theta'))/R \tag{4.28}$$

Equation (4.25) can be decomposed into scalar components in cylindrical coordinates for a cylinder of arbitrary cross section by calculating each term as above in the integral equation. In particular if a circular cylinder is considered, then $\rho = \rho'$ and above expression can be simplified:

$$R = \rho\sqrt{1-\cos(\theta-\theta')}/\sqrt{2} \tag{4.29a}$$

and

$$\frac{\partial}{\partial\rho'}|\vec{\rho}-\vec{\rho}'| = \sqrt{2}\sqrt{(1-\cos(\theta-\theta'))} \tag{4.29b}$$

In addition

$$G'(\sqrt{(k^2-\beta^2)}|\vec{\rho}-\vec{\rho}'|) = \frac{\pi}{j}H_0^{(2)'}(\sqrt{(k^2-\beta^2)}|\vec{\rho}-\vec{\rho}'|)$$
$$= -\frac{\pi}{j}H_1^{(2)}(\sqrt{(k^2-\beta^2)}|\vec{\rho}-\vec{\rho}'|) \tag{4.30}$$

Thus for a circular cylinder, the first integrand in (4.25) is reduced to

$$(\sigma_m t)\hat{n}\times\mathbf{I}(\vec{\rho})\times(\nabla'_t + j\beta\hat{z})G(\sqrt{(k^2-\beta^2)}|\vec{\rho}-\vec{\rho}'|)$$
$$= I_z(\vec{\rho})(\hat{n}\times\hat{z}\times\hat{\rho})\frac{\partial}{\partial r'}G(\sqrt{(k^2-\beta^2)}|\vec{\rho}-\vec{\rho}'|)$$
$$= -I_z(\vec{\rho})\hat{z}\frac{\pi}{j}H_1^{(2)}(\sqrt{(k^2-\beta^2)}|\vec{\rho}-\vec{\rho}'|)\sqrt{(k^2-\beta^2)}\sqrt{(1-\cos(\theta-\theta'))}/\sqrt{2} \tag{4.31}$$

The simplified electric field integral equation in a cylindrical coordinate is obtained:

$$-4\pi E^i(\vec{\rho}) = +2\pi\sigma_m t I(\vec{\rho}) \tag{4.32}$$
$$+\pi\left\{\int_0^{2\pi}[\, j(\sigma_m t)H_1^{(2)'}(\sqrt{(k^2-\beta^2)}|\vec{\rho}-\vec{\rho}'|)\sqrt{(k^2-\beta^2)}\sqrt{(1-\cos(\theta-\theta'))}/\sqrt{2}\right.$$
$$\left.-\omega\mu_0 I(\vec{\rho}')H_0^{(2)'}(\sqrt{(k^2-\beta^2)}|\vec{\rho}-\vec{\rho}'|)]\,\rho' d\theta'\right\}$$

It is equivalent to

$$-4E^i(\vec{\rho}) = +2\sigma_m t\mathbf{I}(\vec{\rho})$$
$$+\left\{\int_0^{2\pi}[-\frac{(\sigma_m t)}{j}H_1^{(2)'}(\sqrt{(k^2-\beta^2)}|\vec{\rho}-\vec{\rho}'|)\sqrt{(k^2-\beta^2)}\sqrt{(1-\cos(\theta-\theta'))}/\sqrt{2}\right.$$
$$\left.-k_0 Z_0 I(\vec{\rho}')H_0^{(2)'}(\sqrt{(k^2-\beta^2)}|\vec{\rho}-\vec{\rho}'|)]\,r' d\theta'\right\} \tag{4.33}$$

Generally speaking, equation (4.25) can be written either in a rectangular coordinate or a cylindrical coordinate. In some cases, its representation in a rectangular coordinates is easer to use. For example, the integral equation of (4.25) applied to a rectangular cylinder with a TM polarized illumination can be written as:

$$\frac{E_z}{z_0} = \frac{\sigma t}{2z_0}I + \frac{k_0}{4}\int_C\left\{\frac{j\sigma_m t}{z_0|\vec{\rho}-\vec{\rho}'|}H_1^2(\sqrt{(k^2-\beta^2)}|\vec{\rho}-\vec{\rho}'|)sign(x-x_i')(x_i-x_i')I\right.$$

$$+ [1 - (\frac{\beta}{k})^2]H_0^2(\sqrt{(k^2 - \beta^2)}|\bar{\rho} - \bar{\rho}'|)I\Big\}dl \tag{4.34}$$

where $x_i' = x'$ and $x_i = x$ if $\bar{\rho}'$ is on the side $|y| = a$, and $x_i' = y'$ and $x_i = y$ if $\bar{\rho}'$ is on the side $|x| = b$ as depicted in Fig. 4.4. $sign(x-x_i')$ is a function which is +1 if $(x-x_i')=>0$ or −1 if $(x-x_i')=<0$. Calculation of the diagonal elements of the moment matrix for (4.33) and (4.34) needs special care for singular integrals.

In the case of TE polarization, due to the divergence of unknown I , the EFIE becomes difficult to solve numerically . An alternative approach is to use MIFE for treating the TE polarization. The proper MFIE can be summarized as follows:

$$2\pi\mathbf{H}(\bar{\rho})|_{tan} = 4\pi\mathbf{H}^i(\bar{\rho})|_{tan} + \Big\{\int_S [- j\omega\varepsilon_0(\sigma_m t)\mathbf{H}(\bar{\rho})G(\sqrt{(k^2 - \beta^2)}|\bar{\rho} - \bar{\rho}'|)$$

$$+ \hat{n}\times\mathbf{H}(\bar{\rho})\times(\nabla'_t + j\beta\hat{z})G(\sqrt{(k^2 - \beta^2)}|\bar{\rho} - \bar{\rho}'|)]\, dS'\Big\}_{tan} \tag{4.35}$$

In the case of TE polarization, $\mathbf{H}(\bar{\rho}) = \hat{z}H_z(\bar{\rho})$ and $\mathbf{E}(\bar{\rho}) = \hat{x}E_x + \hat{y}E_y$. The MFIE with TE excitation reduces to an integral equation with only z component:

$$2\pi\hat{z}H^z(\bar{\rho}) = 4\pi\hat{z}H_z^i(\bar{\rho}) + \Big\{\int_S [- j\omega\varepsilon_0(\sigma_m t)H_z(\bar{\rho})G(\sqrt{(k^2 - \beta^2)}|\bar{\rho} - \bar{\rho}'|)\hat{z}$$

$$+ H_z(\bar{\rho})\hat{n}\times\hat{z}\times(\nabla'_t)G(\sqrt{(k^2 - \beta^2)}|\bar{\rho} - \bar{\rho}'|)]\, dS'\Big\} \tag{4.36}$$

The second integrand in (4.36) is similar to the first one in (4.25), which can be conducted in a cylindrical coordinate as:

$$H_z(\bar{\rho})\hat{n}\times\hat{z}\times(\nabla'_t)G(\sqrt{(k^2 - \beta^2)}|\bar{\rho} - \bar{\rho}'|)$$

$$= - H_z(\bar{\rho})\hat{z}\frac{\pi}{j}H_1^{(2)'}(\sqrt{(k^2 - \beta^2)}|\bar{\rho} - \bar{\rho}'|)\sqrt{(k^2 - \beta^2)}\sqrt{(1 - \cos(\theta - \theta'))}/\sqrt{2} \tag{4.37}$$

The MFIE for a circular cylinder with TE excitation then becomes:

$$2H^z(\bar{\rho}) = 4H_z^i(\bar{\rho}) + \Big\{\int_S [- \omega\varepsilon_0(\sigma_m t)H_z(\bar{\rho})H_0^{(2)}(\sqrt{(k^2 - \beta^2)}|\bar{\rho}$$

$$- \bar{\rho}'|)\hat{z} + jH_z(\bar{\rho})H_1^{(2)'}(\sqrt{(k^2 - \beta^2)}|\bar{\rho} - \bar{\rho}'|)\sqrt{(k^2 - \beta^2)}\sqrt{(1 - \cos(\theta - \theta'))}/\sqrt{2}]\, dS'\Big\} \tag{4.38}$$

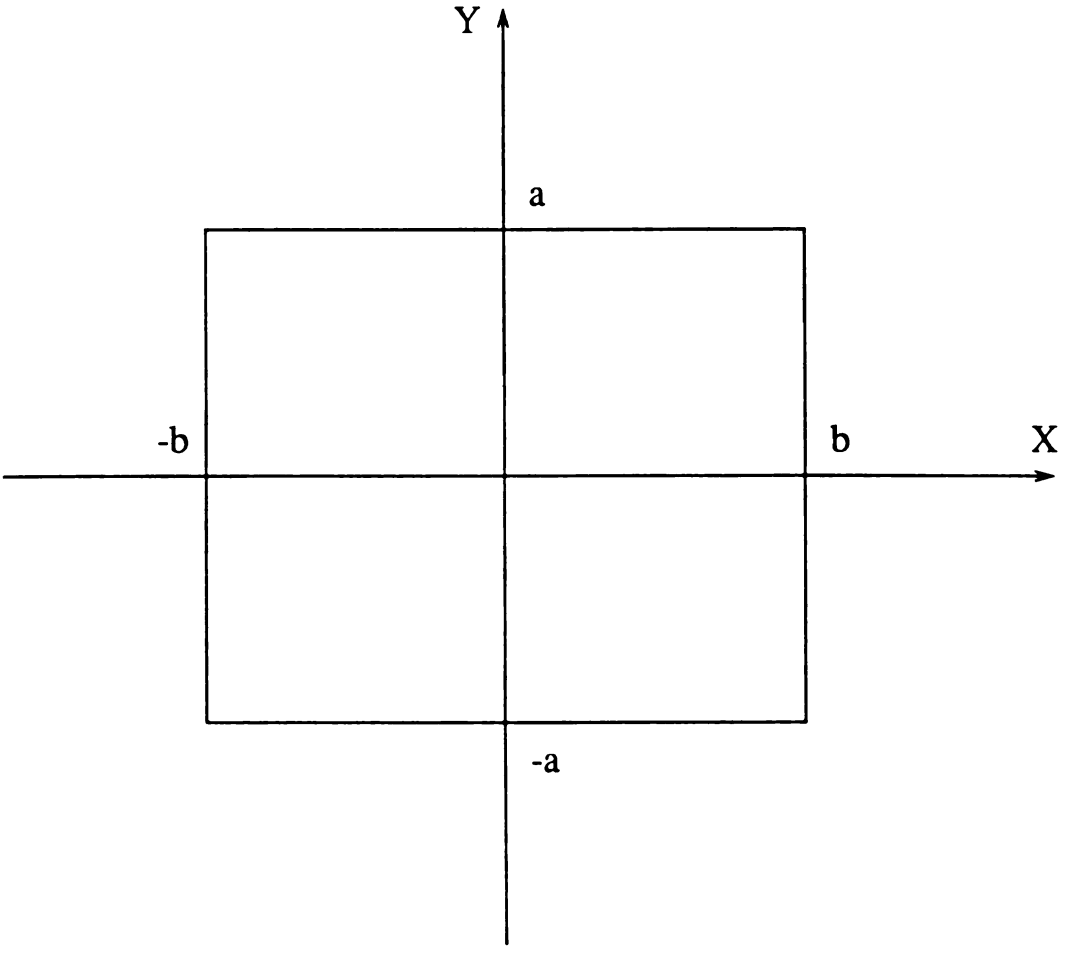

Fig. 4.4 Application of the surface E-field integral equation on the surface of a rectangular cylinder

and the MFIE for a square cylinder with TE excitation is:

$$H_z^i = -\frac{1}{2}I - \frac{jk_0}{4}\int_C \left\{ \frac{-j\sigma t_m t}{z_0} H_0^2(\sqrt{(k^2-\beta^2)}|\vec{\rho} - \vec{\rho}'|)I + sign(x-x_i')\frac{(x_i - x_i')}{|\vec{\rho} - \vec{\rho}'|} H_1^2(\sqrt{(k^2-\beta^2)}|\vec{\rho} - \vec{\rho}'|)I \right\} dl \tag{4.39}$$

which can be solved by the moment method.

When the currents are known, radar cross section can be evaluated by using the asymptotic expressions of Bessel functions.

$$H_n^{(2)}(z) \to \sqrt{2/\pi z}e^{-j(z-n\pi/2-\pi/4)} \qquad (z \to \infty) \tag{4.40}$$

For the TM case, radar cross section of a circular cylinder is represented by

$$\begin{aligned}
\sigma(\theta) &= 2\pi\rho|\frac{E_z^s}{E_z^i}|^2 \\
&= 2\pi\rho|\frac{ka}{4}\int_C [\eta_0 H_0^{(2)}(k\rho) + j\sigma_m t\cos(\theta - \theta')H_1^{(2)}(k\rho)]I(\theta')d\theta'|^2 \\
&= 2\pi\rho|-\frac{ka}{4j}\sqrt{\frac{2}{\pi k\rho}}e^{-j(k\rho - \frac{\pi}{4})}\int_C [\eta_0 + j\sigma_m t\cos(\theta - \theta')e^{j\frac{\pi}{2}}]I(\theta')d\theta'|^2 \\
&= \frac{ka^2}{4\eta_0}|\int_C [1 - \frac{\sigma_m t}{\eta_0}\cos(\theta - \theta')]I(\theta')d\theta'|^2
\end{aligned} \tag{4.41}$$

and the normalized radar cross section is by

$$\frac{\sigma(\theta)}{\lambda} = \frac{ka^2}{8\pi\eta_0}|\int_C [1 - \frac{\sigma_m t}{\eta_0}\cos(\theta - \theta')]I(\theta')d\theta'|^2 \tag{4.42}$$

The radar cross section of a rectangular cylinder is given by

$$\frac{\sigma}{\lambda} = \frac{ka^2}{8\pi}|\int_C (\frac{-\sigma_m t}{z_0}\alpha + 1)e^{jkp'\cos(\theta - \theta')}I(x',y')d(\frac{l}{a})|^2 \tag{4.43}$$

where $\alpha = \cos\theta$ is $45^0 \le |\theta| \le 135^0$, and $\alpha = \sin\theta$ if $0 \le |\theta| \le 45^0$ or $135^0 \le |theta| \le 180^0$.

For the TE case, the radar cross section of a circular cylinder is

$$\begin{aligned}
\sigma(\theta) &= 2\pi\rho|\frac{H_z^s}{H_z^i}|^2 \\
&= 2\pi\rho|\frac{ka}{4j}\int_C [\frac{\sigma_m t}{j\eta_0}H_0^{(2)}(k\rho) - \cos(\theta - \theta')H_1^{(2)}(k\rho)]I(\theta')d\theta'|^2
\end{aligned}$$

$$= 2\pi\rho\Big| - \frac{ka}{4j}\sqrt{\frac{2}{\pi k\rho}}\int_C\Big[- \frac{\sigma_m t}{j\eta_0}e^{-j(k\rho - \frac{\pi}{4})} + \cos(\theta - \theta')e^{-j(k\rho - \frac{\pi}{4} - \frac{\pi}{2})}\Big]I(\theta')d\theta'\Big|^2$$

$$= \frac{ka^2}{4\lambda}\Big|\int_C\Big[\frac{\sigma_m t}{\eta_0} + \cos(\theta - \theta')\Big]I(\theta')d\theta'\Big|^2 \qquad (4.44)$$

and the normalized radar cross section is

$$\frac{\sigma(\theta)}{\lambda} = \frac{ka^2}{8\pi}\Big|\int_C\Big[\frac{\sigma_m t}{\eta_0} + \cos(\theta - \theta')\Big]I(\theta')d\theta'\Big|^2 \qquad (4.45a)$$

While the radar cross section of a rectangular cylinder is

$$\frac{\sigma}{\lambda} = \frac{ka^2}{8\pi}\Big|\int_C (\frac{\sigma_m t}{z_0} - \alpha)e^{jk\rho'\cos(\theta - \theta')}I(x',y')d(\frac{l}{a})\Big|^2 \qquad (4.45b)$$

4.2.3 Some Properties of New Surface Integral Equations

The new surface integral equations for treating the scattering problem of a metallic object with thin magnetic coating have been derived in section 4.2 as given in the eq.(4.17) and eq.(4.19). The integral equations of (4.17) and (4.19) are of simple forms. Compared to the integral equations for a pure metallic conductor, only one extra integral, which is contributed by the magnetic thin layer, has to be evaluated. The Green's function in (4.17) and (4.19) remains the same as that in the free space without the complex argument involved. The permeability used has been assumed to be isotropic, but the integral equation can be easily extended to an anisotropic magnetic coating by introducing a dyadic permeability as $\mathbf{J}_m = j\omega(\bar{\bar{\mu}} - \mu_0)\mathbf{H} = \bar{\bar{\sigma}}_m\mathbf{H}$.

Both the EFIE of (4.17) and the MFIE of (4.19) are the second kind of Fredhelm integral equations which are normally diagonal dominant.

The strategies used in the derivation of (4.17) and (4.19) can also be applied to solve a homogeneous lossy body with either thin magnetic or electric coating. This will result in a set of coupled surface integral equations.

4.3 Eigen-mode Expansion Solution to an Infinitely Long Circular Cylinder

It is well known that an exact solution for an infinitely long conducting circular cylinder can be pursued by the eigen-mode expansion method. However, when a perfectly conducting circular cylinder is coated with a very thin layer of magnetic lossy material, the eigen mode expansion solution needs to be modified. In this section, a new approach with the eigen-mode expansion is developed for a circular cylinder with a thin coating based on Taylor series expansion of Bessel functions. The electrically large cylinders can be efficiently treated via this method.

The general solution to the wave equation in the cylindrical coordinate system can be expressed by the sum of eigenmodes, which are cylindrical harmonic functions, in different homogeneous regions. The coefficients in the expansion can be determined by matching the boundary conditions. As shown in Fig. 4.5, the space is divided into a few regions.

First the TE polarization is considered. In free space,

$$H_z^i = \sum_n \zeta_n j^{-jn} J_n(k_0\rho)\cos(n\theta) \tag{4.46a}$$

$$E_\theta^i = \frac{jk_0}{\omega\varepsilon_0}\sum_n \zeta_n j^{-jn} H_n^{(2)\prime}(k_0\rho)\cos(n\theta) \tag{4.46b}$$

$$H_z^s = \sum_n a_n H_n^{(2)_n}(k_0\rho)\cos(n\theta) \tag{4.46c}$$

$$E_\theta^s = \frac{jk_0}{\omega\varepsilon_0}\sum_n a_n H_n^{(2)\prime}(k_0\rho)\cos(n\theta) \tag{4.46d}$$

where

$$\zeta_n = \begin{cases} 1 & n = 0 \\ 2 & n \neq 0 \end{cases} \tag{4.47}$$

Inside the film,

$$H_z^s = \sum [b_n H_n^{(1)}(k\rho) + c_n H_n^{(2)}(k\rho)]\cos(n\theta) \tag{4.48a}$$

$$E_\theta^s = \frac{jk_0}{\omega\varepsilon_0}\sum [b_n H_n^{(2)\prime}(k\rho) + c_n H_n^{(2)\prime}(k\rho)]\cos(n\theta) \tag{4.48b}$$

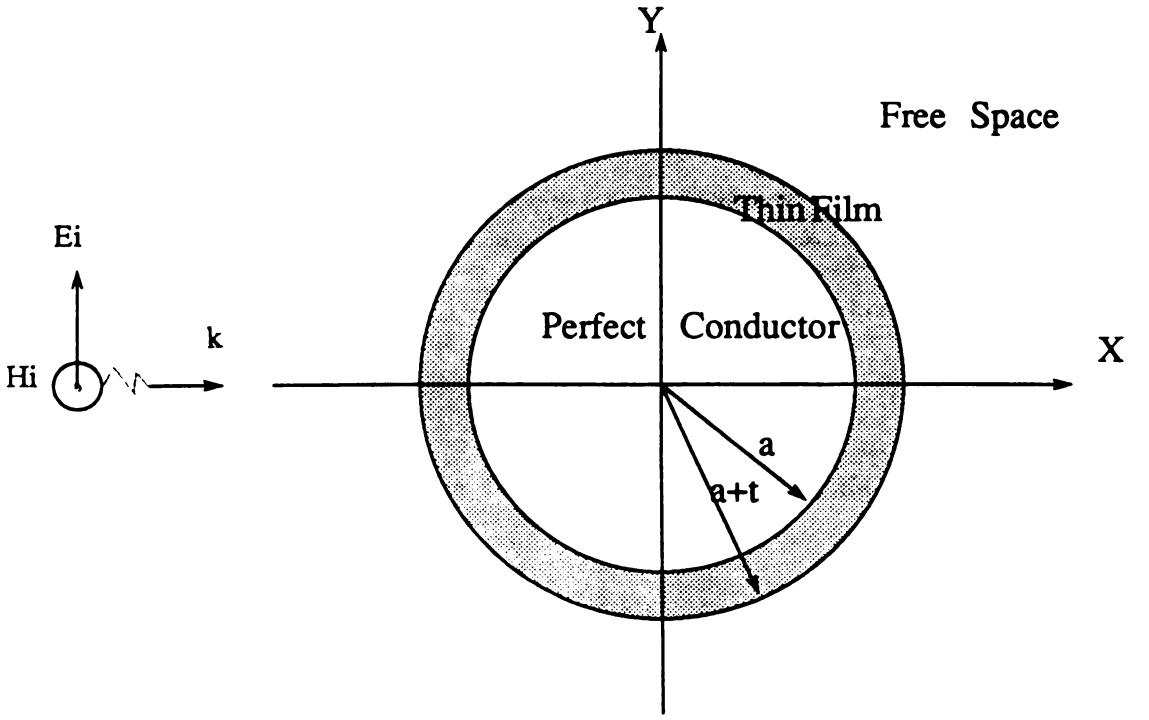

Fig. 4.5 A circular cylinder coated with a magnetically lossy layer

At surface of a perfect conductor $\rho = a$, the tangential component of electric field $E_\theta^s(\rho = a) = 0$. Using this condition and the orthogonal property of the sinusoidal functions yields:

$$b_n = - c_n \frac{H_n^{(2)\prime}(ka)}{H_n^{(1)\prime}(ka)} \tag{4.49}$$

Substituting it back into Eq.(48) for the b_n leads to:

$$H_z^s = \sum c_n [- \frac{H_n^{(2)\prime}(ka)}{H_n^{(1)\prime}(ka)} H_n^{(1)}(k\rho) + H_n^{(2)}(k\rho)] \cos(n\theta) \tag{4.50a}$$

$$E_\theta^s = \frac{jk_0}{\omega\varepsilon_0} \sum c_n [- \frac{H_n^{(2)\prime}(ka)}{H_n^{(1)\prime}(ka)} H_n^{(2)\prime}(k\rho) + H_n^{(2)\prime}(k\rho)] \cos(n\theta) \tag{4.50b}$$

At the interface between the film and the free space, the tangential components of fields are related by

$$E_\theta^i(a + t^+) + E_\theta^s(a + t^+) = E_\theta^s(a + t^-) \tag{4.51a}$$

$$H_z^i(a + t^+) + H_z^s(a + t^+) = H_z^s(a + t^-) \tag{4.51b}$$

Note that the thickness t is very thin, Bessel functions can be approximated by their first order Taylor expansions:

$$H_n^{(1)}(a + t) = H_n^{(1)}(a) + H_n^{(1)\prime}(a)\, t \tag{4.52a}$$

$$H_n^{(2)}(a + t) = H_n^{(2)}(a) + H_n^{(2)\prime}(a)\, t \tag{4.52b}$$

$$H_n^{(1)\prime}(a + t) = H_n^{(1)\prime}(a) + H_n^{(1)\prime\prime}(a)\, t \tag{4.52c}$$

$$H_n^{(2)\prime}(a + t) = H_n^{(2)\prime}(a) + H_n^{(2)\prime\prime}(a)\, t \tag{4.52d}$$

$$J_n(a + t) = J_n(a) + J_n'(a)\, t \tag{4.52e}$$

$$J_n'(a + t) = J_n'(a) + J_n''(a)\, t \tag{4.52f}$$

Using the approximations of Bessel's functions and matching the boundary condition of θ-component electric field lead to:

$$\begin{aligned}
&\frac{k_0}{\omega\varepsilon_0}\zeta_n j^{-n}[J_n'(k_0a) + J_n''(k_0a)\, k_0t] + \frac{k_0}{\omega\varepsilon_0}a_n[H_n^{(1)\prime}(k_0a) + H_n^{(1)\prime\prime}(k_0a)\, k_0t] \\
&= \frac{k}{\omega\varepsilon}c_n\left\{ - \frac{H_n^{(2)\prime}(ka)}{H_n^{(1)\prime}(ka)}[H_n^{(1)\prime}(ka) + H_n^{(1)\prime\prime}(ka)\, kt] + H_n^{(2)\prime}(ka) + H_n^{(2)\prime\prime}(ka)\, kt]\right\} \\
&= - \frac{k^2t}{\omega\varepsilon}c_n[\frac{H_n^{(2)\prime}(ka)H_n^{(1)\prime\prime}(ka) - H_n^{(1)\prime}(ka)H_n^{(2)\prime\prime}(ka)}{H_n^{(1)\prime}(ka)}]
\end{aligned} \tag{4.53}$$

It can be shown by using Wronskin's relations that

$$H_n^{(2)\nu}(ka)H_n^{(1)\nu\prime}(ka) - H_n^{(1)\nu}(ka)H_n^{(2)\nu\prime}(ka) = \frac{4j}{\pi ka}[1 - (\frac{n}{ka})^2] \tag{4.54}$$

Thus

$$\frac{k_0}{\omega\varepsilon_0}\zeta_n j^{-n}[J_n'(k_0a) + J_n''(k_0a)\ k_0t] + \frac{k_0}{\omega\varepsilon_0}a_n[H_n^{(1)\nu}(k_0a) + H_n^{(1)\nu\prime}(k_0a)\ k_0t]$$
$$= -\frac{4jkt}{\pi a\omega\varepsilon}c_n[1 - (\frac{n}{ka})^2]\frac{1}{H_n^{(1)\nu}(ka)} \tag{4.55}$$

As t approaches zero, k_0t approaches zero, but $j\omega(\mu - \mu_0)t$ remains a constant. Equation (4.55) also holds in the limit of $t \to 0$:

$$-\frac{4jkt}{\pi a\omega\varepsilon}c_n\frac{[1 - (\frac{n}{ka})]^2}{H_n^{(1)\nu}(ka)} = \eta_0[\zeta_n j^{-n}J_n'(k_0a) + a_nH_n^{(2)\nu}(k_0a)] \tag{4.56}$$

If A is defined as:

$$A = -\frac{4j\sqrt{\mu_r}t}{\pi a\sqrt{\varepsilon_r}}\frac{[1 - (\frac{n}{ka})]^2}{H_n^{(1)\nu}(ka)} \tag{4.57}$$

Then the coefficient a_n is given by:

$$a_n = \frac{Ac_n - \zeta_n j^{-n}J_n'(k_0a)}{H_n^{(2)\nu}(k_0a)} \tag{4.58}$$

Following the same arguments and Using the boundary condition of the tangential magnetic field result in another equation, which can be used to determine the coefficients a_n and c_n in (4.53) and (4.54)

$$[\zeta_n j^{-n}J_n(k_0a) + a_nH_n^{(2)}(k_0a)] = c_n[-\frac{H_n^{(2)'}(ka)}{H_n^{(1)'}(ka)}H_n^{(1)}(ka) + H_n^{(2)}(ka)]$$
$$= \frac{4jc_n}{\pi kaH_n^{(1)\nu}(ka)} = Bc_n \tag{4.59}$$

where $B = \frac{4j}{\pi kaH_n^{(1)\nu}(ka)}$ .. From (4.59), the coefficient c_n is given

$$c_n = \frac{1}{B}[\zeta_n j^{-n}J_n(k_0a) + a_nH_n^{(2)}(k_0a)] \tag{4.60}$$

Finally the solution to the coefficient a_n is obtained as

$$a_n = -\frac{[k_0 t\mu_r J_n(k_0 a) + J_n'(k_0 a)]\zeta_n j^{-n}}{H_n^{(2)'}(k_0 a) + k_0 t\mu_r H_n^{(2)}(k_0 a)} \tag{4.61}$$

Subsequently the magnetic field H_z on the surface of the film is represented in terms of the coefficients $\{ a_n \}$ as

$$\begin{aligned} H_z(a + t^+) &= H_z^i(a + t^+) + H_z^s(a + t^+) \\ &= -\sum_n \zeta_n j^{-n}[J_n(k_0 a) - \frac{[k_0 t\mu_r J_n(k_0 a) + J_n'(k_0 a)]\zeta_n j^{-n}}{H_n^{(2)'}(k_0 a) + k_0 t\mu_r H_n^{(2)}(k_0 a)} H_n^{(2)}(k_0 a)]\cos(n\theta) \\ &= \sum_n \zeta_n j^{-n} \frac{-j2}{\pi k_0 a} \frac{1}{H_n^{(2)'}(k_0 a) + k_0 t\mu_r H_n^{(2)}(k_0 a)} \cos(n\theta) \end{aligned} \tag{4.62}$$

where the Wronskin's relation is used. The surface electric current is represented by:

$$\begin{aligned} I_\theta &= -H_z \\ &= -\sum_n \zeta_n j^{-n} \frac{-j2}{\pi k_0 a} \frac{1}{H_n^{(2)'}(k_0 a) + k_0 t\mu_r H_n^{(2)}(k_0 a)} \cos(n\theta) \end{aligned} \tag{4.63}$$

The radar cross section can be evaluated by using the asymptotic expressions of Bessel functions when the arguments are large.

$$\sigma = 2\pi\rho \left| \frac{H_z^s}{H^i} \right|^2 \tag{4.64}$$

$$\sigma = 2\pi\rho \left| \sum_n a_n \sqrt{\frac{2}{\pi k_0 \rho}} e^{-j(k\rho - \frac{n\pi}{2} - \frac{\pi}{4})} \cos(n\theta) \right|^2$$

$$= \frac{4}{k_0} \left| \sum_n a_n e^{j\frac{n\pi}{2}} \cos(n\theta) \right|^2$$

$$\frac{\sigma}{\lambda} = \frac{2}{\pi} \left| \sum_{n=0}^{\infty} a_n j^n \cos(n\theta) \right|^2 \tag{4.65}$$

The same procedure can be followed to find the solution to the case of TM polarization. In the case of TM polarization,

$$\mathbf{E} = \hat{z} E_z , \qquad \mathbf{H} = \hat{\theta} H_\theta + \hat{\rho} H_\rho$$

In free space:

$$E_z^i = \eta_0 \sum \zeta_n j^{-jn} J_n(k_0 \rho) \cos(n\theta) \tag{4.66a}$$

$$H_\theta^i = -j\sum \zeta_n j^{-n} J_n'(k_0\rho)\cos(n\theta) \tag{4.66b}$$

$$E_z^s = \eta_0 \sum a_n H_n^{(2)}(k_0\rho)\cos(n\theta) \tag{4.66c}$$

$$H_\theta^s = -j\sum a_n H_n^{(2)\prime}(k_0\rho)\cos(n\theta) \tag{4.66d}$$

Inside the film,

$$E_z^s = \eta\sum [b_n H_n^{(2)}(k\rho) + c_n H_n^{(1)}(k\rho)]\cos(n\theta) \tag{4.67a}$$

$$H_\theta^s = -j\sum [b_n H_n^{(2)\prime}(k\rho) + c_n H_n^{(1)}{}'(k\rho)]\cos(n\theta) \tag{4.67b}$$

By approximating Bessel functions with their first order Taylor expansions and matching the boundary conditions, a_n , b_n , and c_n are determined as

$$b_n = -\frac{H_n^{(1)}(ka)}{H_n^{(2)}(ka)} c_n \tag{4.68}$$

$$c_n \frac{4j}{\pi k a H_n^{(2)}(ka)} = \zeta_n j^{-n} J_n'(k_0 a) + a_n H_n^{(2)\prime}(k_0 a) \tag{4.69}$$

with

$$a_n = \zeta_n j^{-n} \frac{k_0 t\mu_r J_n'(k_0 a) - J_n(k_0 a)}{H_n^{(2)}(k_0 a) - k_0 t\mu_r H_n^{(2)\prime}(k_0 a)} \tag{4.70}$$

The surface current is determined by

$$I_z = H_\theta(\rho = a) \tag{4.71}$$

$$= \sum_n -j\zeta_n j^{-n}\left[\frac{k_0 t\mu_r J_n'(k_0 a) - J_n(k_0 a)}{H_n^{(2)}(k_0 a) - k_0 t\mu_r H_n^{(2)\prime}(k_0 a)} H_n^{(2)\prime}(k_0 a) + J_n'(k_0 a)\right]\cos(n\theta)$$

and the radar cross section is by

$$\frac{\sigma}{\lambda} = \frac{2}{\pi}\left|\sum_n a_n j^{n-1}\cos(n\theta)\right|^2 \tag{4.72}$$

The numerical results based on this method will be shown in Section 4.5 to serve as a comparison with the results by the MoM or the FD-TD method.

4.4 Finite Difference Time Domain Method

In the proceeding sections, the integral equations and the eigen mode expansion have been used to solve the scattering problems of a perfectly conducting cylinder

coated with a thin film. When the body is electrically large, the integral equation technique becomes inefficient due to the matrix inversion required by the moment method. In this section, the FD-TD method is introduced to solve the same problem and to provide an alternative approach to validate the integral equations derived. As an example of the FD-TD method, only two dimensional metallic objects coated with layers of thin lossy magnetic materials are studied in this section.

The basic used algorithm of the FD-TD method is developed from that discussed in Chapter 3. As shown in Fig. 4.6, an infinite two dimensional space is truncated into a finite region, and Mur's second order radiation boundary condition is applied to the truncated surfaces. The truncated region is then divided into the scattered field region and the total field region to ease the application of the radiation boundary condition in the presence of an incident wave. Two dimensional Yee's model is used for interior points.

The thin magnetic coating is taken into account by using the integral form of Maxwell's curl equations, which leads to a modification of Yee's difference scheme. It will be discussed in detail for the cases of TM polarization and TE polarization respectively.

The Farady's law can be represented by an integral form as:

$$\int_C \mathbf{E}\cdot d\vec{l} = -\int_S \mu_0 \frac{\partial}{\partial t}\mathbf{H}\cdot d\vec{S} - \int_S (\mu - \mu_0)\frac{\partial}{\partial t}\mathbf{H}\cdot d\vec{S} - \int_S \mathbf{J}_m \cdot d\vec{S} \tag{4.73}$$

where $\mathbf{J}_m$ is magnetic conducting current. Hereafter the magnetic current is related to the magnetic field by $\mathbf{J}_m = \sigma_m \mathbf{H}$ as the electric current is related to electric field by $\mathbf{J}_e = \sigma \mathbf{E}$. In the time domain, σ_m represents the magnetic loss of magnetic material which is equivalent to the imaginary part of complex permeability (μ_r,μ_i) in the frequency domain by a relation of $\sigma_m = \omega\mu_i$ when the excitation wave is harmonic in time.

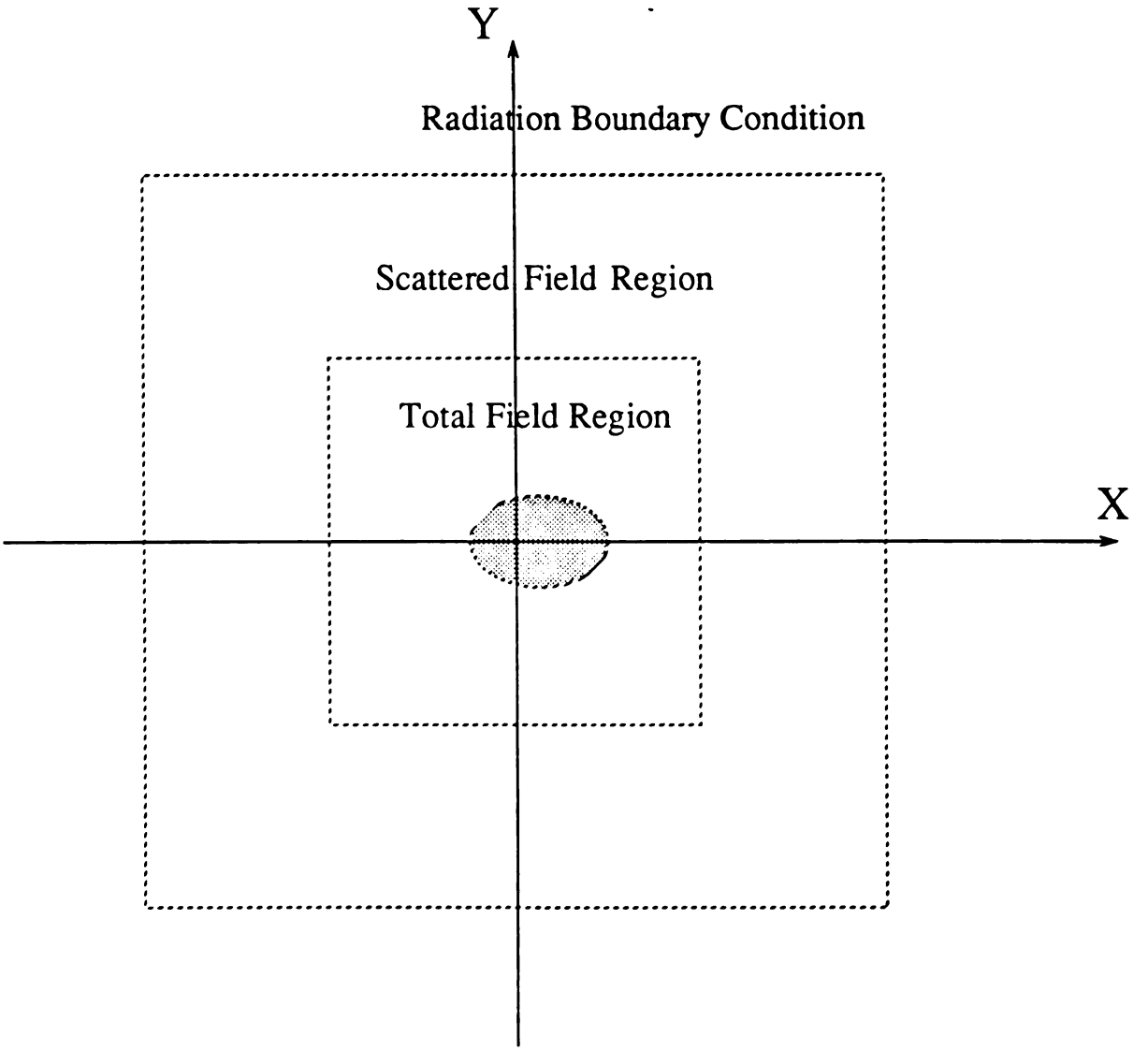

Fig. 4.6 Truncation of an infinite two-dimensional space into a finite region

Shown in Fig. 4.7 is one cell of Yee's model in the case of TM polarization near the coating of a square cylinder. To update the x component of magnetic field H_x, for example, Farady's law is applied. According to the model in Fig.4.7, the left hand side of Farady's law in (4.73) can be approximated as:

$$\int_C \mathbf{E}\cdot d\vec{l} = [E_z^n(i, j+1) - E_z^n(i, j)]\,\Delta z \tag{4.74a}$$

The third term on the right side in (4.73) is discretized as

$$\int_S \mathbf{J}_m\cdot d\vec{S} = 0.5(\sigma_m t)\Delta z[H_x^{n+\frac{1}{2}}(i, j+\frac{1}{2}) + H_x^{n-\frac{1}{2}}(i, j+\frac{1}{2})] \tag{4.74b}$$

where t is the thickness of the thin layer. The first and the second terms on the right hand side of (4.73) are approximated as:

$$\int_S \mu_0\frac{\partial}{\partial t}\mathbf{H}\cdot d\vec{S} + \int_S (\mu - \mu_0)\frac{\partial}{\partial t}\mathbf{H}\cdot d\vec{S} = \tag{4.74c}$$

$$\mu_0\Delta z\Delta y/\Delta t[H_x^{n+\frac{1}{2}}(i, j+\frac{1}{2}) - H_x^{n-\frac{1}{2}}(i, j+\frac{1}{2})]$$

$$+ (\mu - \mu_0)t\Delta z/\Delta t[H_x^{n+\frac{1}{2}}(i, j+\frac{1}{2}) - H_x^{n-\frac{1}{2}}(i, j+\frac{1}{2})]$$

By rearranging (4.73-4.74), we can obtain a modified Yee's difference scheme suitable for the 2D scattering problem with TM polarization.

$$H_x^{n+\frac{1}{2}}(i, j+\frac{1}{2}) = -\frac{CA}{CB}H_x^{n-\frac{1}{2}}(i, j+\frac{1}{2}) - \frac{c_0\Delta t}{z_0 CB}[E_z^n(i, j+1) - E_z^n(i, j)] \tag{4.75}$$

where CA and CB are defined as

$$CA = 0.5\sigma_m t c_0\Delta t/z_0 - (\mu_r - 1)t - \Delta y \tag{4.76a}$$

$$CB = 0.5\sigma_m t c_0\Delta t/z_0 + (\mu_r - 1)t + \Delta y \tag{4.76b}$$

This modified formulation is for updating H_x in the cells adjacent to the square cylinder walls which cross the y-axis at $y = -n_1 dy$ and $y = n_1 dy$. Similarly, a formulation for updating H_y in the cells adjacent to the walls which cross the x-axis at $x = -n_1 dx$ and $x = n_1 dx$ can also be derived by using the Farady's law.

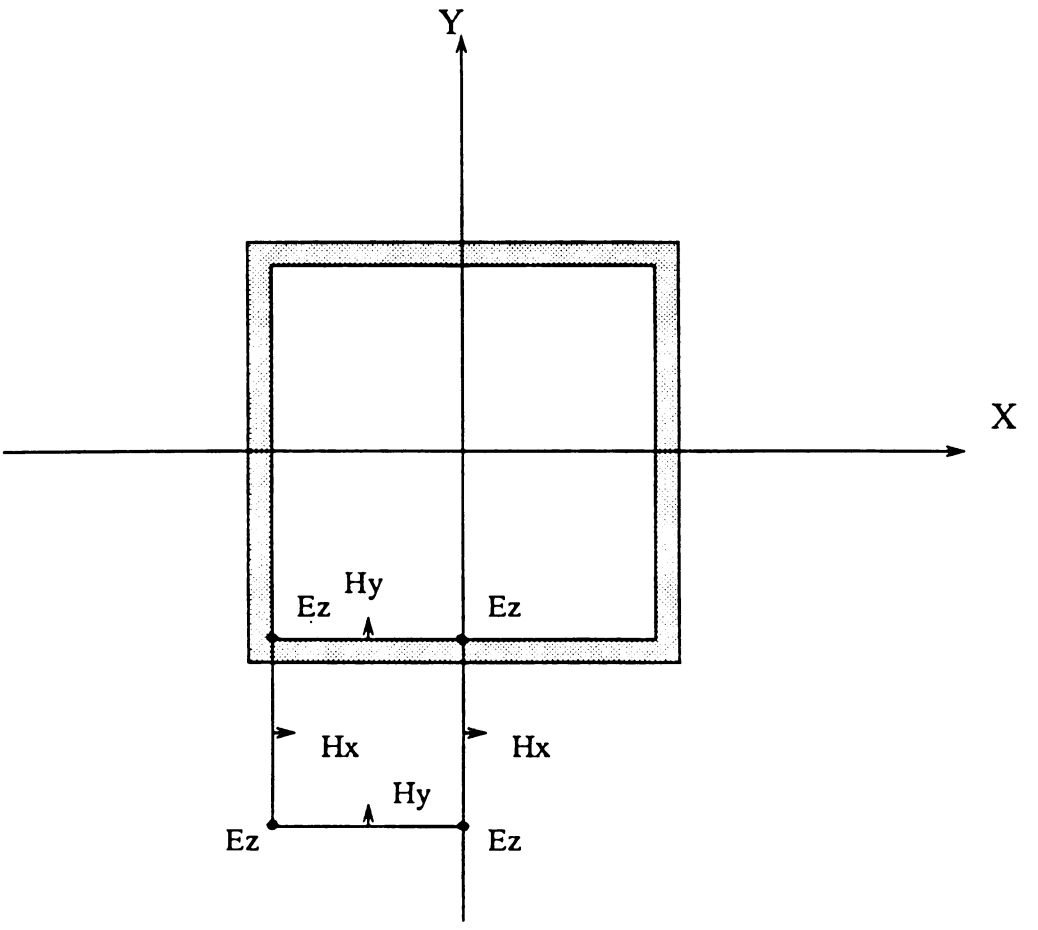

Fig. 4.7 A basic cell of Yee's model adjacent to the coating in the case of the TM excitation

Next, consider the case of TE polarization, and focus on the cell as shown in Fig. 4.8. To update the z component of magnetic field, Farady's law is used again. On left hand side of the Farady's law, the contour integral yields:

$$\int_C \mathbf{E}\cdot\vec{dl} = -[E_x^n(i, j+\frac{1}{2}) - E_x^n(i, j-\frac{1}{2})]\Delta x + [E_y^n(i+\frac{1}{2}, j) - E_y^n(i-\frac{1}{2}, j)]\Delta y \qquad (4.77a)$$

On the right hand side of the Farady's law, the flux integral of the magnetic conducting current and the magnetic polarization current are those included by the contour integral path. From the third integral of (4.73):

$$\int_S \mathbf{J}_m\cdot\vec{dS} = 0.5\sigma t[H_z^{n+\frac{1}{2}}(i, j) + H_z^{n-\frac{1}{2}}(i, j)]\beta\Delta x \qquad (4.77b)$$

where β is equal to 0.5 if H_z is on the corners of square cylinder, otherwise $\beta = 1$. The second integral of (4.73) can be written as

$$\int_S (\mu - \mu_0)\frac{\partial}{\partial t}\mathbf{H}\cdot\vec{dS} = (\mu - \mu_0)t/\Delta t[H_z^{n+\frac{1}{2}}(i, j) - H_z^{n-\frac{1}{2}}(i, j)]\beta\Delta x \qquad (4.77c)$$

where β is the same as defined in (4.77b). The first term of (73) is written as

$$\int_S \mu_0\frac{\partial}{\partial t}\mathbf{H}\cdot\vec{dS} = \mu_0\Delta x\Delta y/\Delta t[H_z^{n+\frac{1}{2}}(i, j) - H_z^{n-\frac{1}{2}}(i, j)] \qquad (4.77d)$$

By adding (4.77) together and rearranging terms, a formulation for updating H_z becomes:

$$H_z^{n+\frac{1}{2}}(i, j) = -\frac{CA}{CB}H_z^{n-\frac{1}{2}}(i, j) + \frac{c_0\Delta t}{z_0 CB}\left\{[E_x^n(i, j+\frac{1}{2}) - E_x^n(i, j-\frac{1}{2})]\Delta x - [E_y^n(i+\frac{1}{2}, j) - E_y^n(i-\frac{1}{2}, j)]\Delta y\right\} \qquad (4.78)$$

with

$$CA = 0.5\sigma_m t c_0\Delta t/z_0 - (\mu_r - 1)t - \Delta y \qquad (4.79a)$$

$$CB = 0.5\sigma_m t c_0\Delta t/z_0 + (\mu_r - 1)t + \Delta y \qquad (4.79b)$$

The same strategies can be followed to treat the cylinders with an arbitrary cross section. The irregular boundaries can also be modeled by using Farady's law and

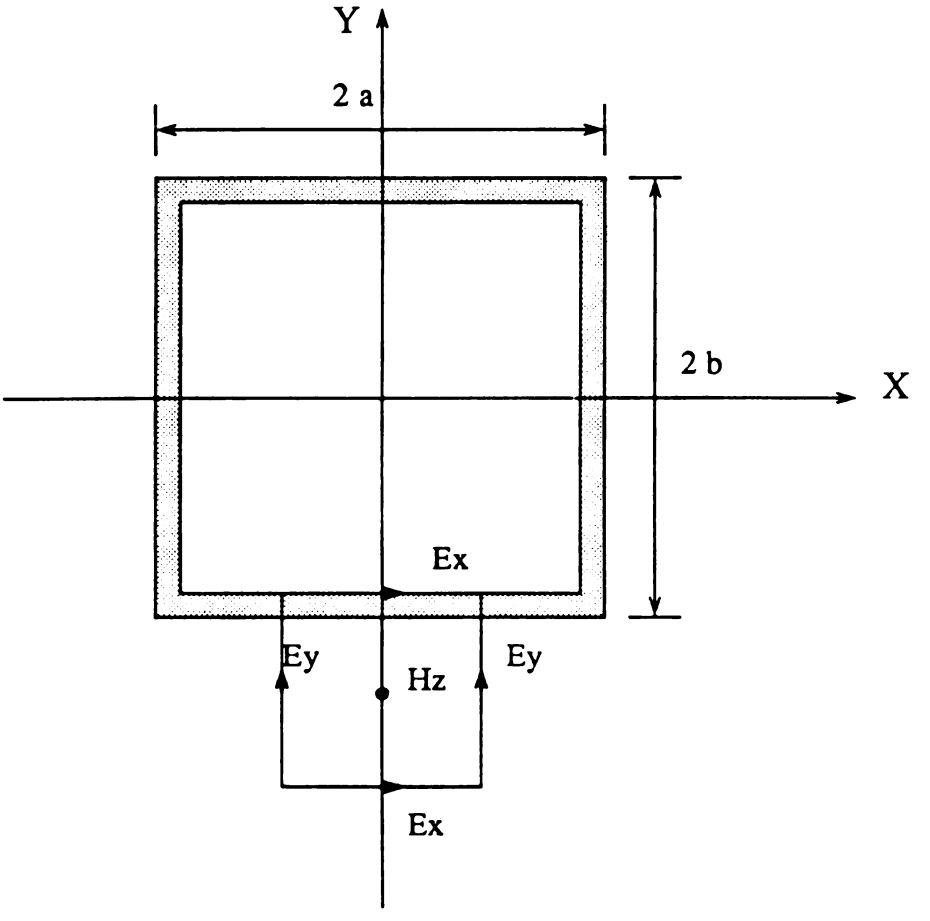

Fig. 4.8 A basic cell of Yee's model adjacent to the coating of a retangular cylinder in the case of the TE excitation

Ampere's law to conform the integral paths.

Numerical results have been obtained by using the schemes discussed in this section for the TM or the TE case. They will be compared with those generated by the integral equation method and the eigen mode expansion method in the next section.

4.5 Numerical Results

Now we have three different methods for solving the scattering problems involving a metallic object coated with thin layers of magnetic materials: the new surface integral equation has been developed for an arbitrarily shaped metallic object coated with a thin layer of magnetic material; the solution with eigen mode expansion for a circular cylinder has also derived for a circular cylinder case; a modified scheme of the FD-TD method has been developed for a cylinder with an arbitrarily shaped cross section. Based on these three indepedent methods, numerical results are obtained, respectively. To validate the new surface integral equations, the current distribution and the radar cross section of a circular cylinder are calculated and compared with that from the eigen mode expansion method. To study the singularity behavior of sharp corners, square cylinders are chosen and the results from the integral equation technique and the FD-TD method are compared. The excellent agreement is obtained. The effects of both complete coating and partial coating on radar cross section are investigated for a circular cylinder and a square cylinder.

4.5.1 Perfectly Conducting Circular Cylinder Coated with Magnetic Thin Layer

a. Completely Coated Cylinder

Consider an infinitely long, perfectly conducting circular cylinder with $k_0 a = 5\pi$ where a is the radius of the circular cylinder. The perfectly conducting cylinder is completely coated with a magnetic thin layer which has a parameter of

$u_r t/a = 0.01 - j0.03$. A plane wave is incident on the cylinder along the direction of increasing x. For the TE excitation, the current distributions and the radar cross sections by the MoM and the eigen mode expansion method are plotted in Fig. 4.9-4.10. As shown in Fig. 4.9-4.10, the results by the MoM based on the new surface integral equations for both the current distribution and the radar cross section have excellent agreement with that of the exact solutions of eigenmode expansion. The comparison of the current and the radar cross section between the cases of coated cylinder and non-coated cylinder is also plotted in Fig. 4.9-4.10, and significant reduction in the radar cross section is obtained if a magnetic thin layer is coated on the cylinder. The back scattered filed is reduced by more than 10 db.

Figures 4.11 and 4.12 show the currents and the radar cross section of a coated and uncoated cylinder with $k_0 a = 2\pi$ under a TM excitation. Both results from the MoM and the exact solution also have an excellent agreement. The back scattered filed is reduced by 3 db. If the size of the cylinder is increased to $k_0 a = 5\pi$, the back scattered field is decreased by 7 db as shown in Fig. 4.13-4.14.

Comparing the results with the TM and the TE excitation as shown in Fig. 4.9-4.14, we see that magnetic coating on the reduction of radar cross section is more effective for the TE excitation than for the TM excitation.

b. Partially Coated Cylinder

A perfectly conducting circular cylinder of $k_0 a = 2\pi$ is partially coated with a thin layer of $u_r t/a = 0.01 - j0.03$ which covers 25% of the circumference within $180^0 - 45^0 \leq \theta \leq 180^0 + 45^0$.

With the TM excitation, the radar cross section and the current on the fully coated, partially coated or bare cylinder are plotted in Figs. 4.15-4.16. The current distribution of partially coated cylinder exhibits a singular behavior at the edges of the

coating. On the coated surface the current is very close to that of fully coated cylinder except for at edges. On the remaining portion without coating, the current is almost the same as that of the uncoated cylinder. The radar cross section of a partially coated cylinder is some value between that of fully coated and bare cylinders except for around 180^0 degree.

Figures 4.17 and 4.18 show the currents and the radar cross sections of a cylinder with $k_0a = 2\pi$ under the TE excitation for fully coated, partially coated and uncoated cylinders. The current distribution in the TE case does not have the strong singularity as observed in the TM case.

4.5.2 Perfectly Conducting Square Cylinder Coated with Magnetic Thin Layer

Next we examine an infinitely long square cylinder with $k_0a = 2\pi$ where a is the length of one side. The plane wave is propagating along the x-axis at 0^0 degree and the parameter of magnetic coating is $\mu_r = t/a = 0.01 - j0.03$. The curves in Figs. 4.19, 4.20 and 4.21 are the numerical results obtained by the MoM, based on the integral equations, and the FD-TD method.

Figure 4.19 shows current distributions of a perfectly conducting square cylinder without coating based on the MoM and the FD-TD method. Fig. 4.20 exhibits current distributions on the fully coated square cylinder. The current distributions on the partially coated square cylinder are also plotted in Fig. 4.21. The magnetic films with one half of side length are symmetrically coated on the two corners at 135^0 and 225^0 degrees. The numerical results have shown good consistence between the MoM and the FD-TD method, even including singularity behaviors.

As the last example, consider a plane wave propagating along the direction of 45^0 degree. Figs. 4.22-4.25 depict the variations of current distributions on the square cylinder for the TM and the TE cases. Figs. 4.23 and 4.25 are the radar cross sections

associated with the current distributions in Figs. 4.22 and 4.24.

4.6 Extension to Three Dimensional Case

The integral equation method and the FD-TD method used in this chapter can be extended to the three dimensional problems. To use the integral equation method for a 3D problem, numerical algorithm developed in Chapter 2 can be applied. The moment method with vector basis functions would be an appropriate choice. The eigen mode expansion method can be used to solve the problem of a perfectly conducting sphere with thin magnetic coating. The FD-TD scheme for 3D problems can be developd in a similar procedure as described in this chapter.

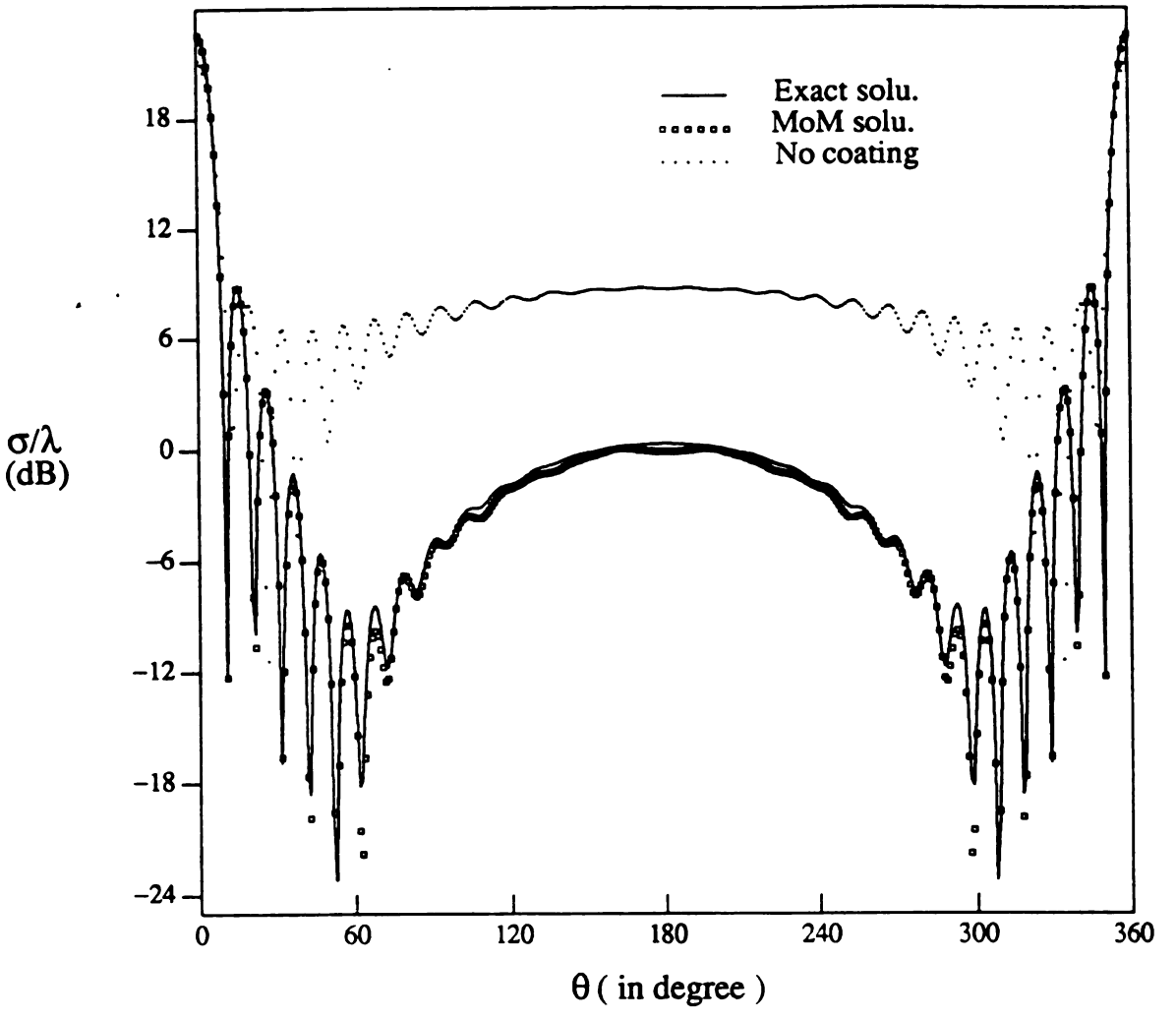

Figure 4.9 Radar cross sections of an infinitely long conducting circular cylinder with or without a magnetic coating in the case of TE excitation ($k_0 a = 5\pi$, $\mu_r t/a = 0.01 - j0.03$)

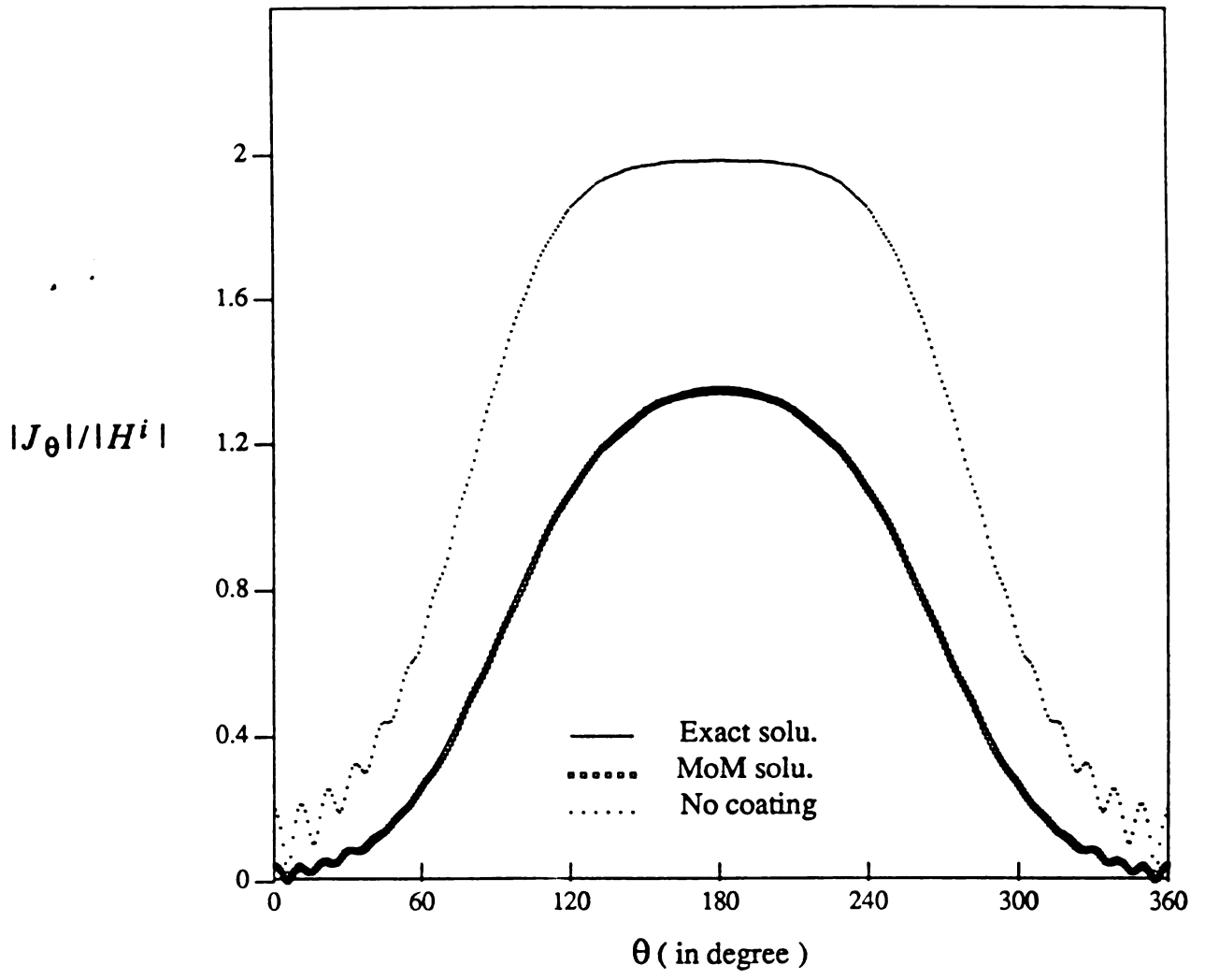

Figure 4.10 Amplitude distribution of the θ-component current on the surface of an infinitely long conducting circular cylinder with or without a magnetic coating in the case of TE excitation ($k_0 a = 5\pi$, $\mu_r t/a = 0.01 - j0.03$)

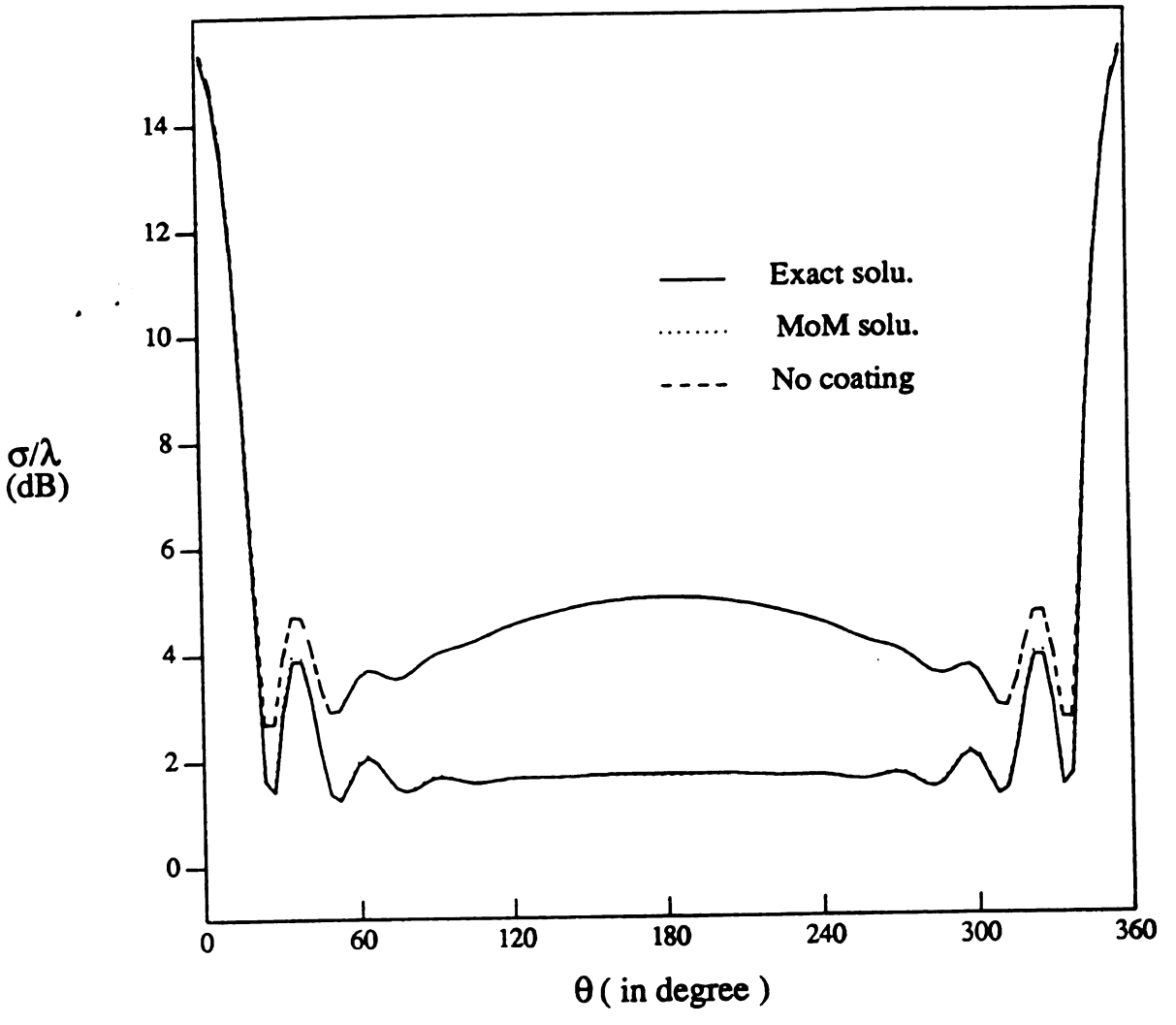

Figure 4.11 Radar cross sections of an infinitely long conducting circular cylinder with or without a magnetic coating in the case of TM excitation ($k_0 a = 2\pi$, $\mu_r t/a = 0.01 - j0.03$)

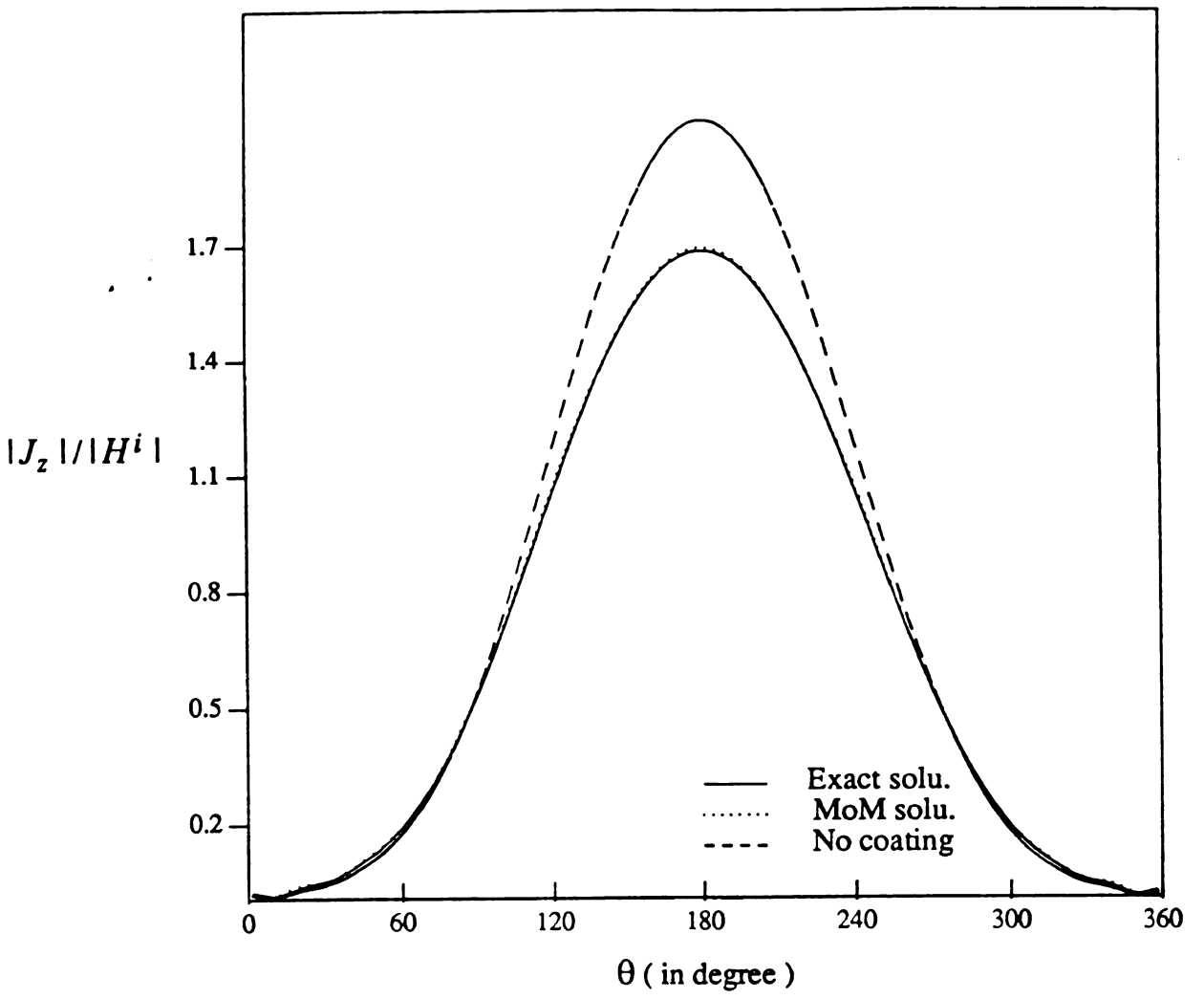

Figure 4.12 Amplitude distribution of the z-component current on the surface of an infinitely long conducting circular cylinder with or without a magnetic coating in the case of TM excitation ($k_0 a = 2\pi$, $\mu_r t/a = 0.01 - j0.03$)

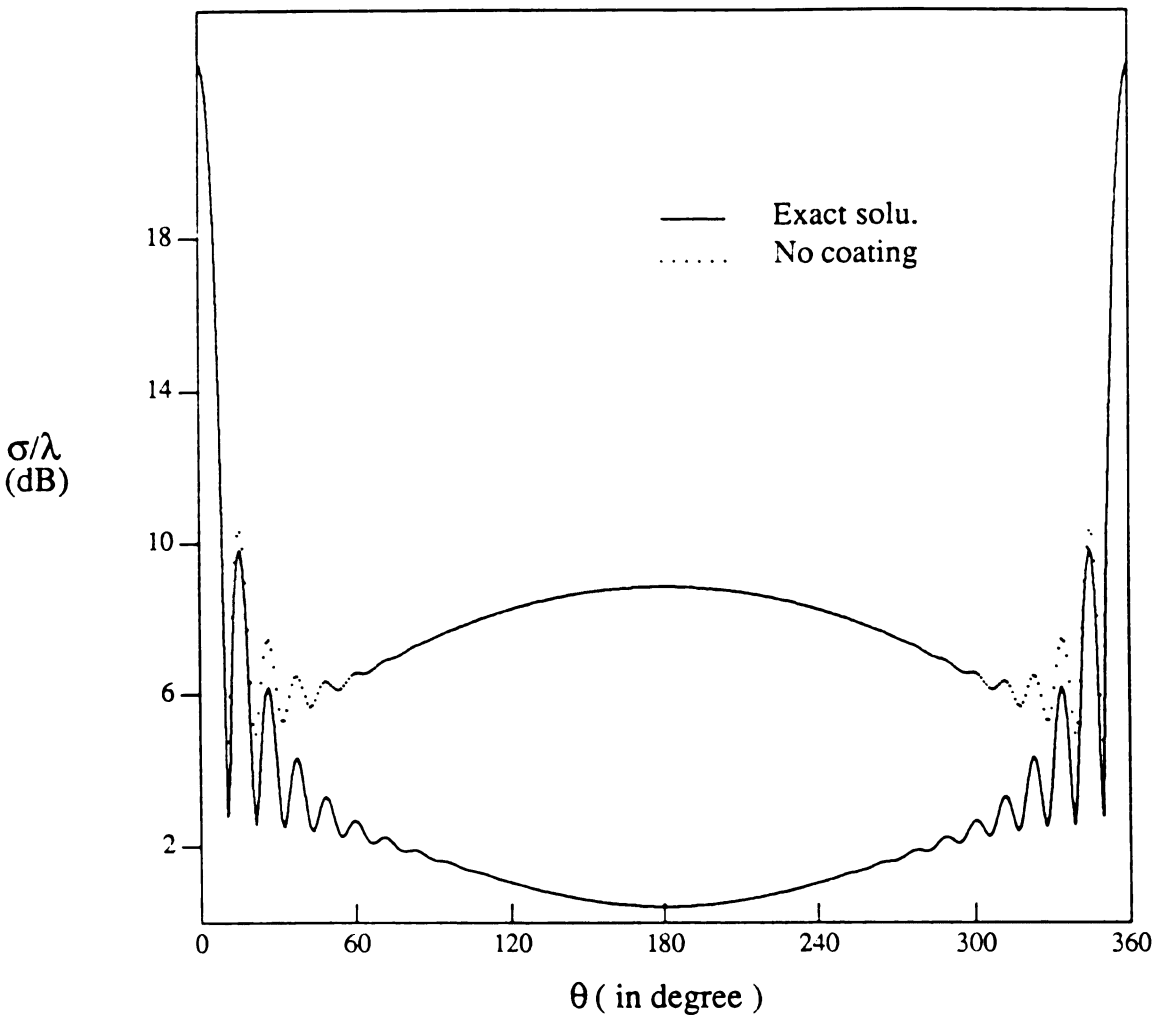

Figure 4.13 Radar cross sections of an infinitely long conducting circular cylinder with or without a magnetic coating in the case of TM excitation ($k_0 a = 5\pi$, $\mu_r t/a = 0.01 - j0.03$)

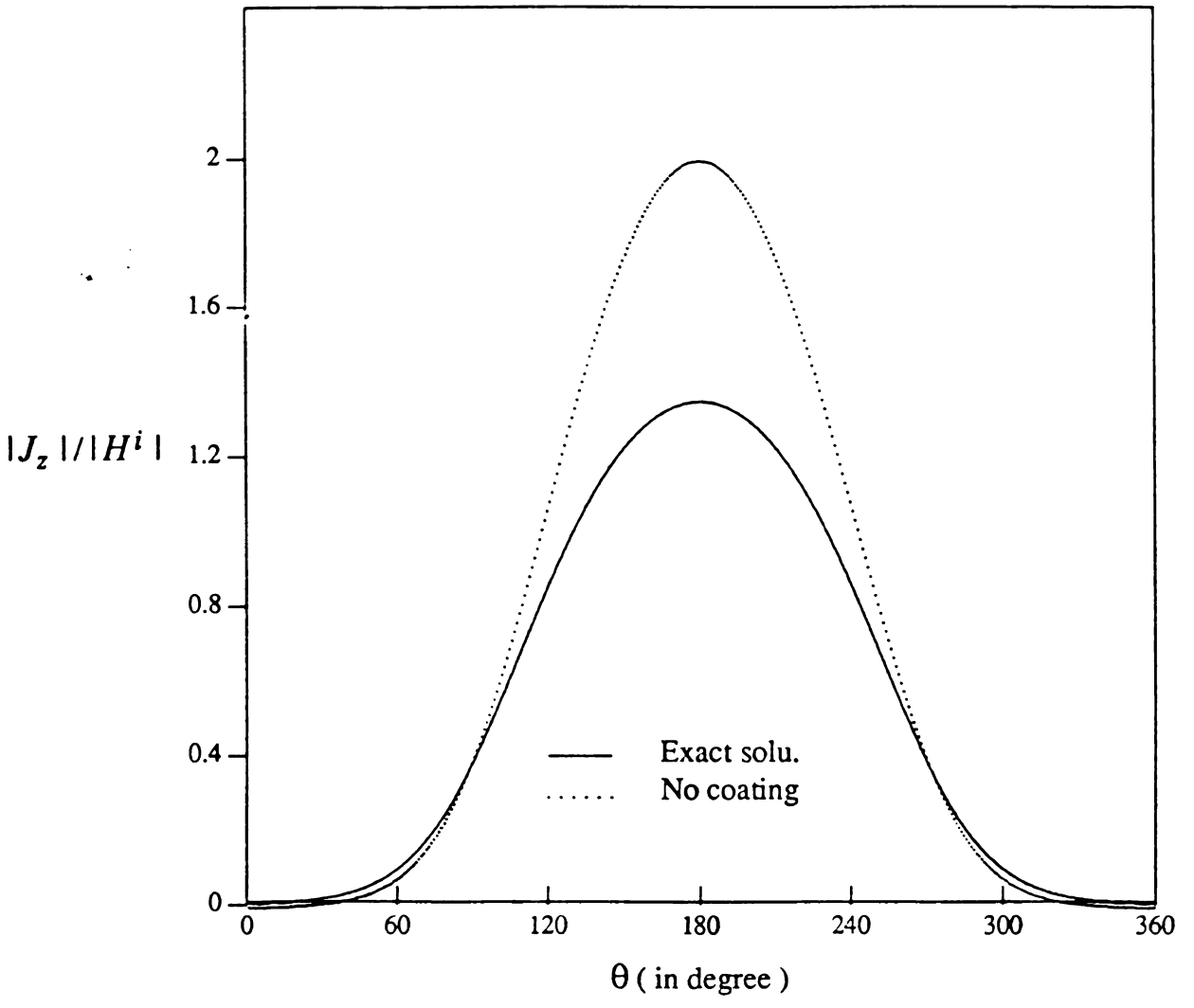

Figure 4.14 Amplitude distribution of the z-component current on the surface of an infinitely long conducting circular cylinder with or without a magnetic coating in the case of TM excitation ($k_0 a = 5\pi$, $\mu_r t/a = 0.01 - j0.03$)

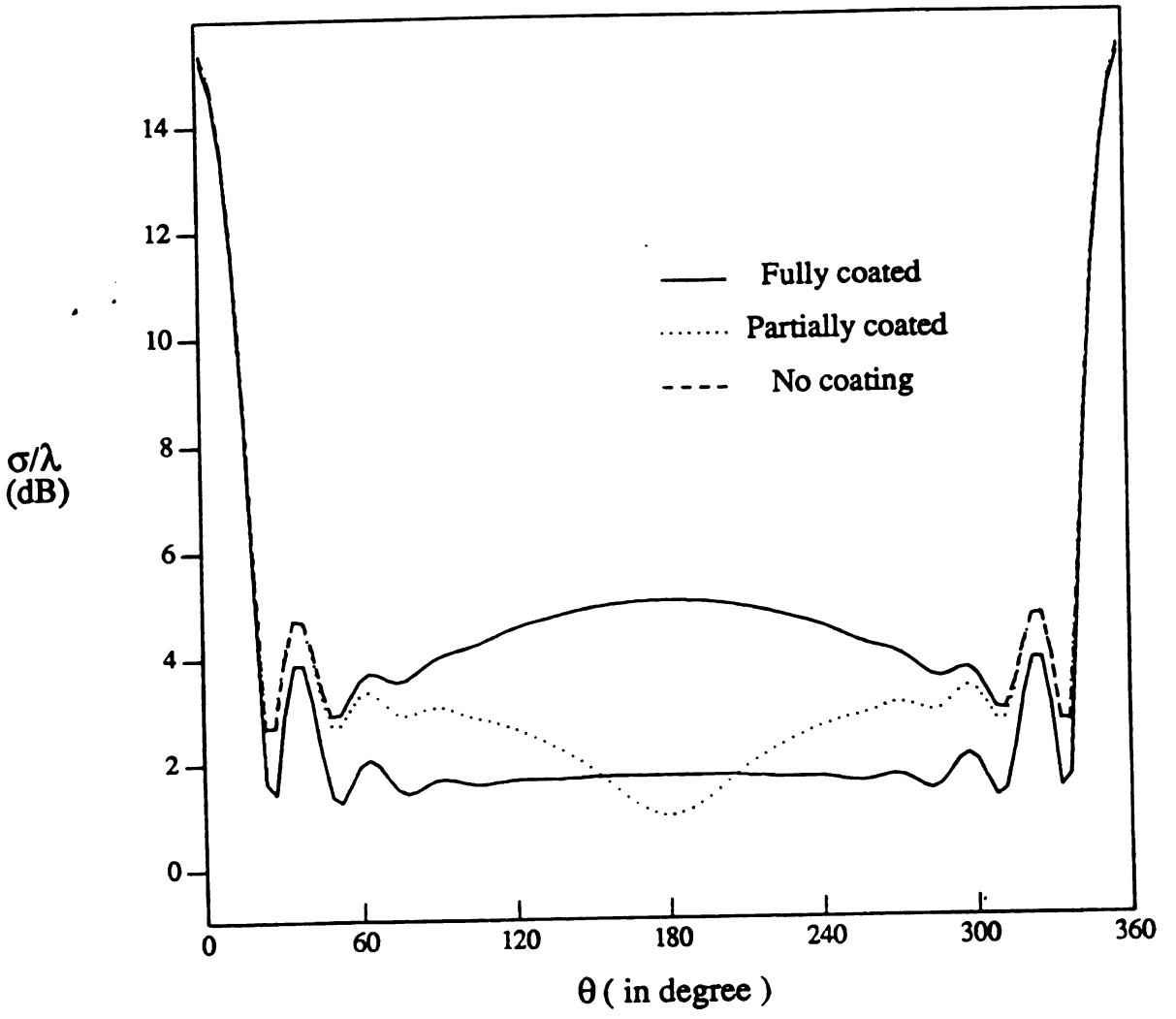

Figure 4.15 Radar cross sections of an infinitely long conducting circular cylinder partially coated with a magnetically lossy thin layer in the case of TM excitation ($k_0 a = 2\pi$, $\mu_r t/a = 0.01 - j0.03$)

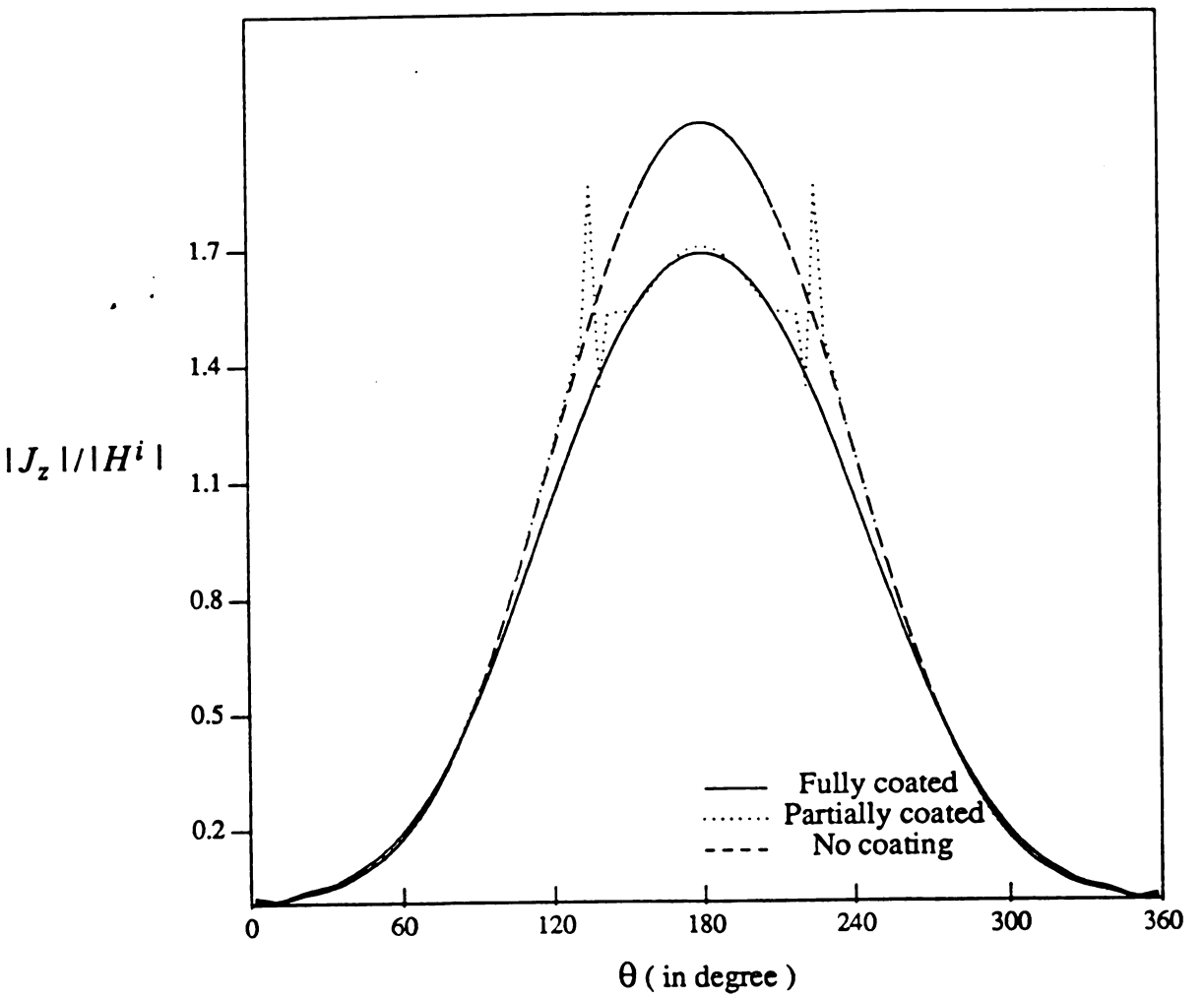

Figure 4.16 Amplitude distribution of the z-component current on the surface of an infinitely long conducting circular cylinder partially coated with a magneticallt lossy thin layer in the case of TM excitation ($k_0 a = 2\pi$, $\mu_r t/a = 0.01 - j0.03$)

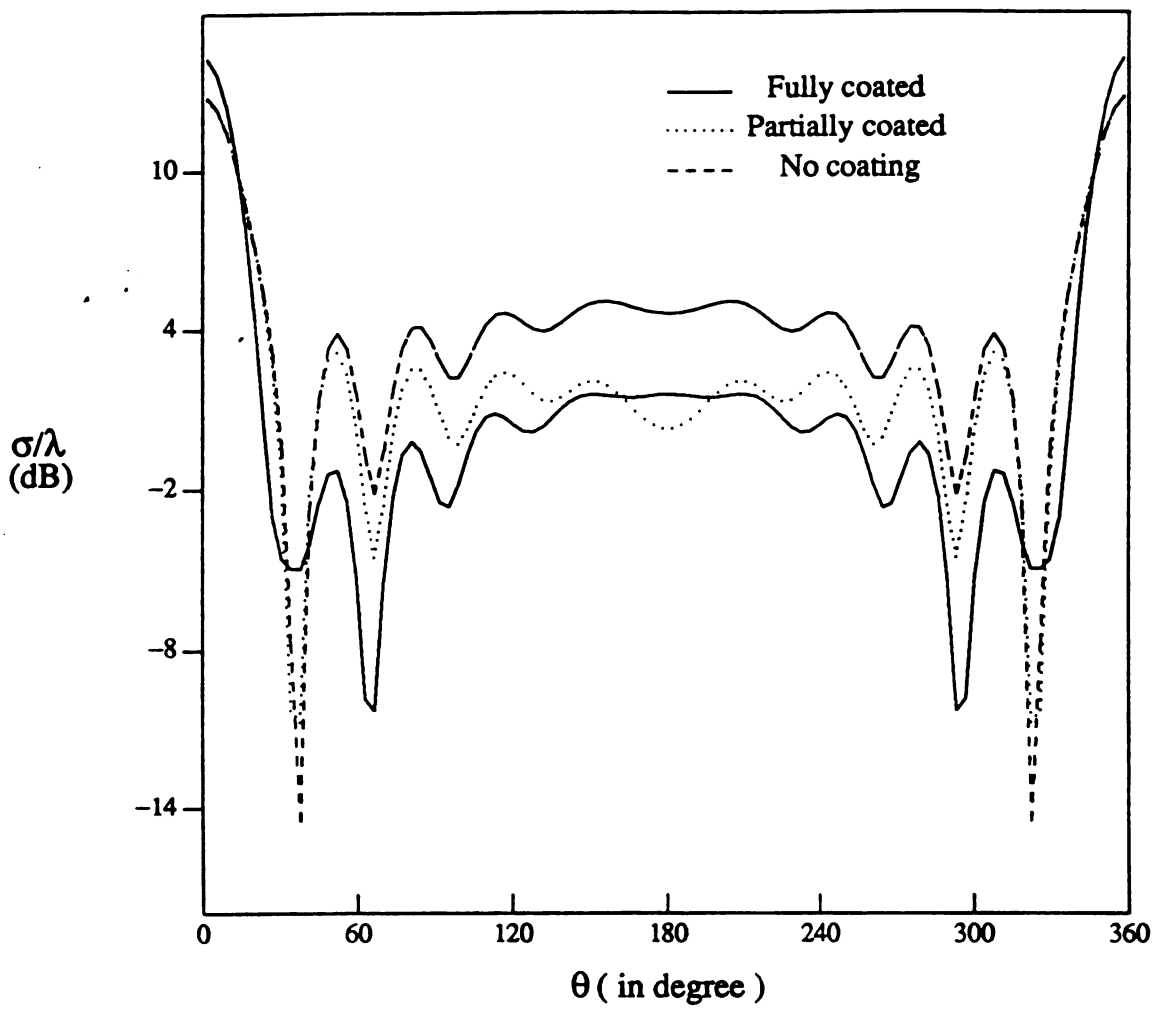

Figure 4.17 Radar cross sections of an infinitely long conducting circular cylinder partially coated with a magnetically lossy thin layer in the case of TE excitation ($k_0 a = 2\pi$, $\mu_r t/a = 0.01 - j0.03$)

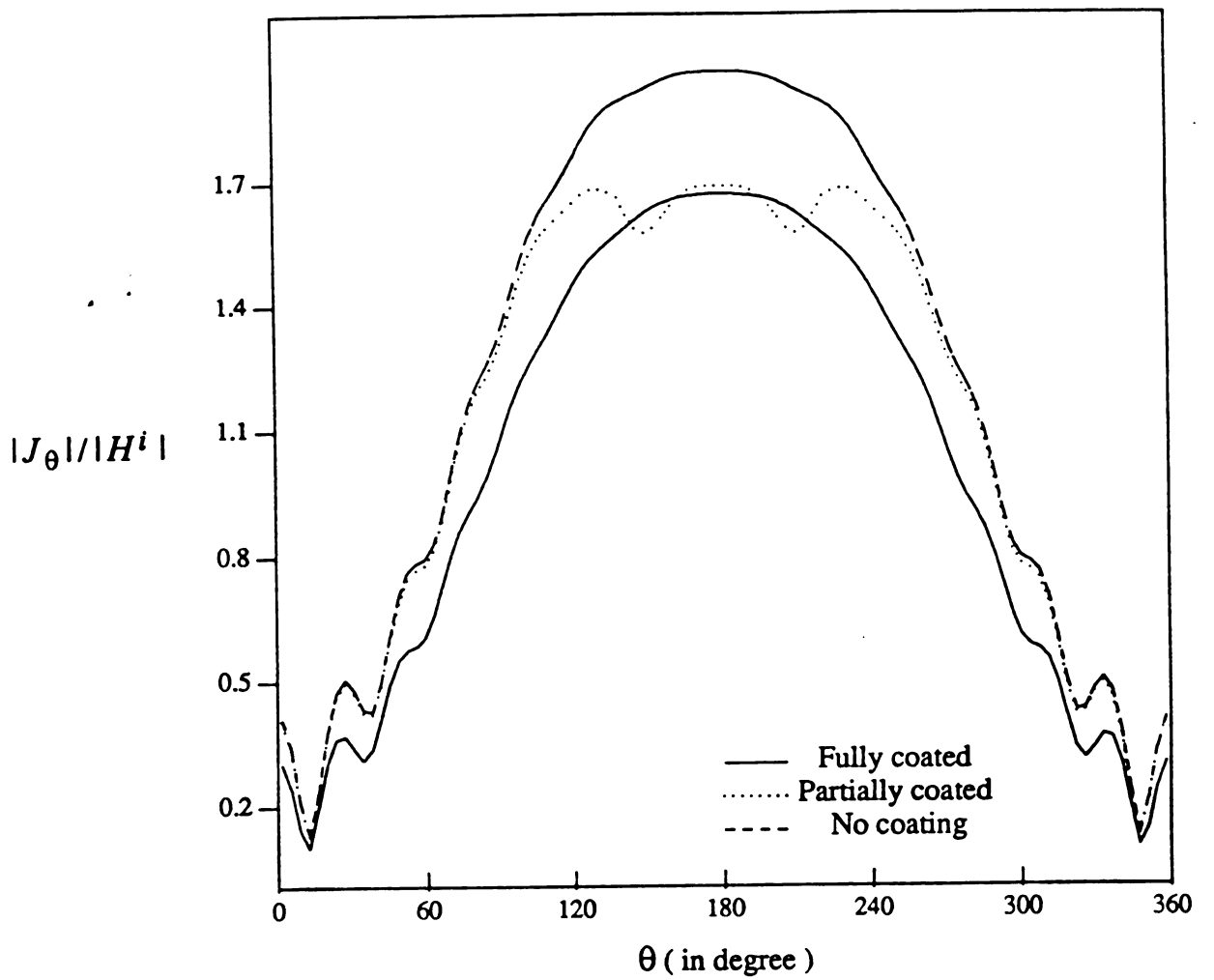

Figure 4.18 Amplitude distribution of the θ-component current on the surface of an infinitely long conducting circular cylinder partially coated with a magneticallt lossy thin layer in the case of TE excitation ($k_0 a = 2\pi$, $\mu_r t/a = 0.01 - j0.03$)

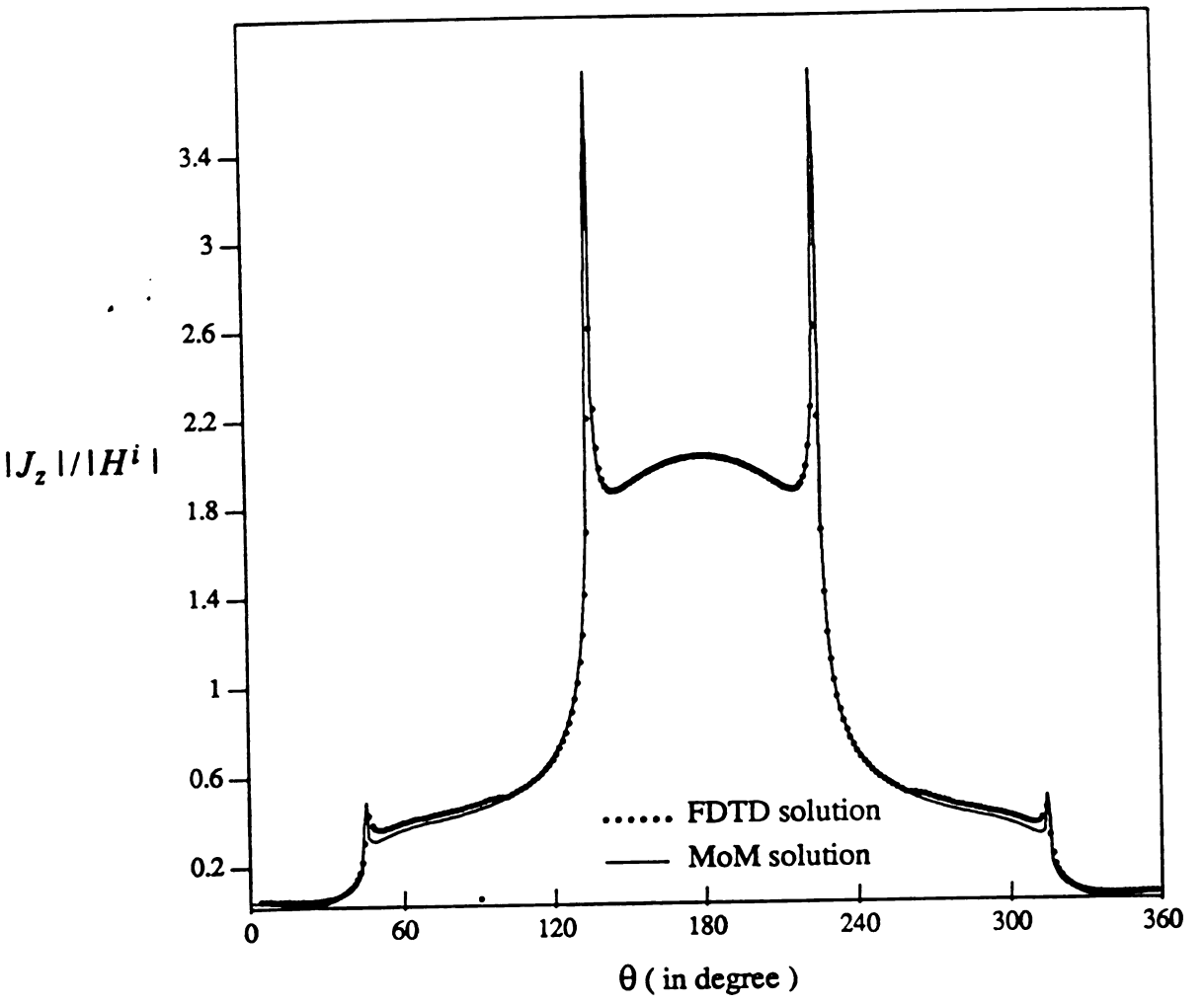

Figure 4.19 Amplitude distribution of the z-component current on the surface of an infinitely long conducting rectangular cylinder in the case of TM excitation ($k_0 a = 2\pi$, $\mu_r t/a = 0.0$)

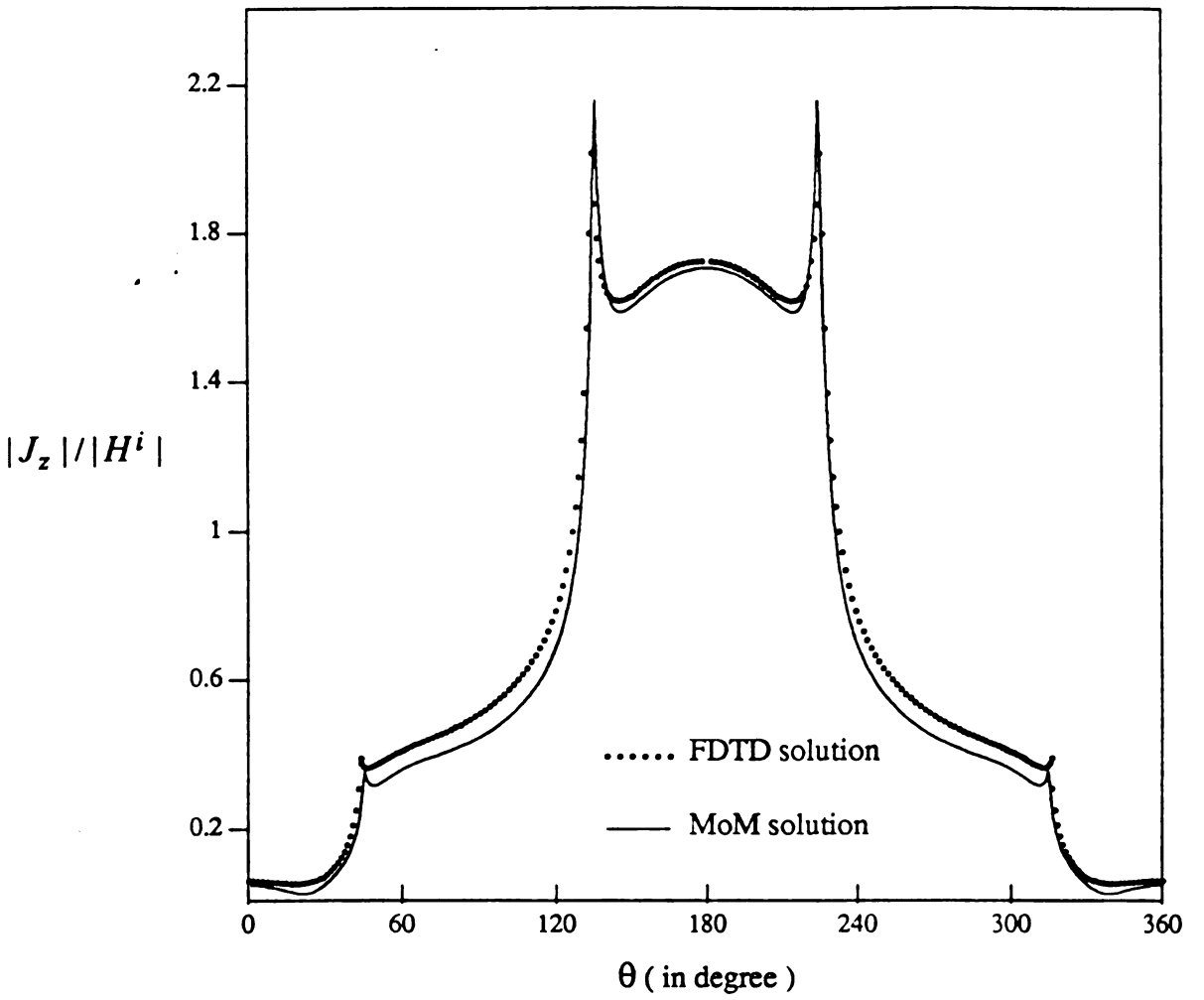

Figure 4.20 Amplitude distribution of the z-component current on the surface of an infinitely long conducting rectangular cylinder coated with a magnetically lossy thin layer in the case of TM excitation ($k_0 a = 2\pi$, $\mu_r t/a = 0.01 - j0.03$)

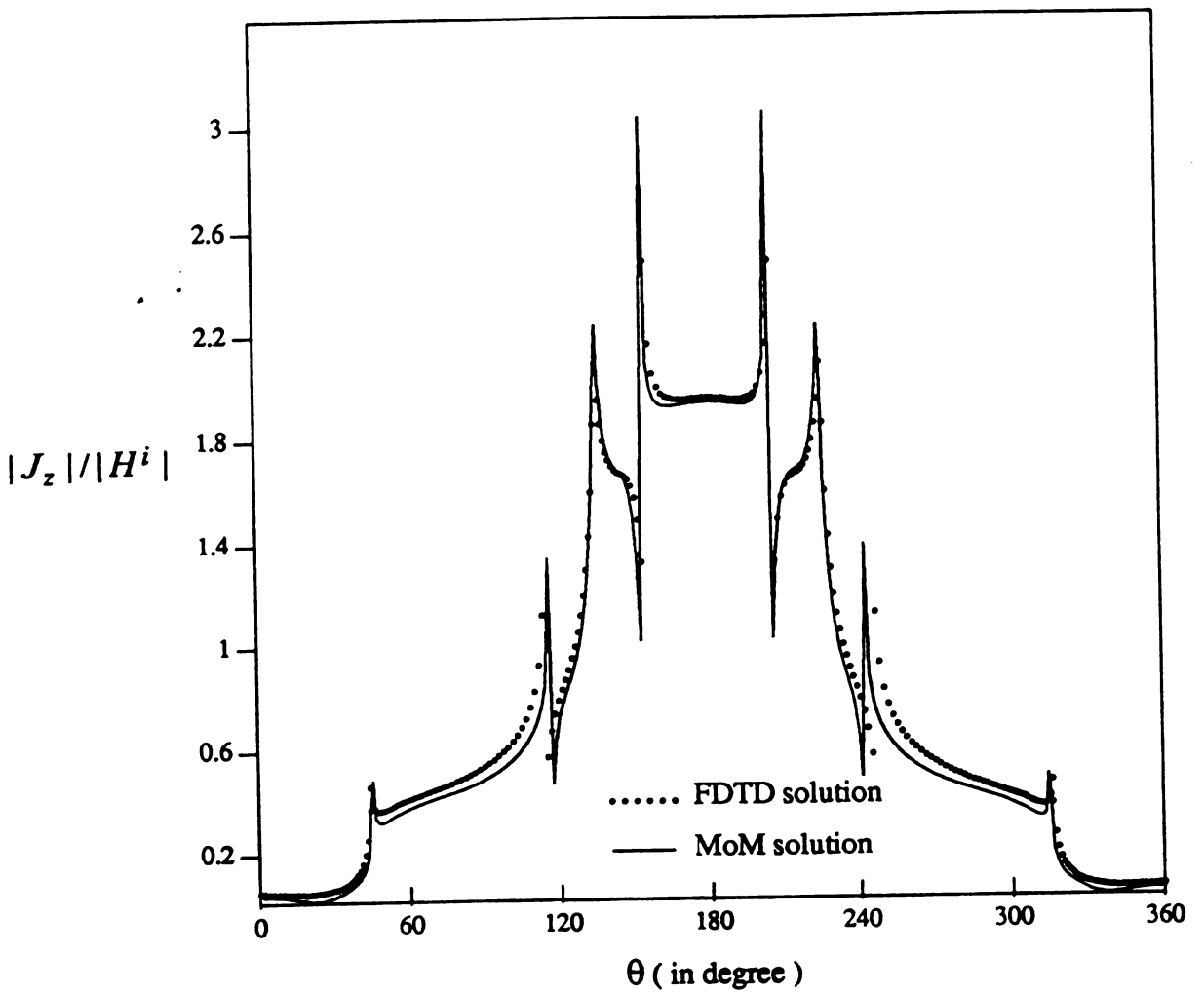

Figure 4.21 Amplitude distribution of the z-component current on the surface of an infinitely long conducting rectangular cylinder partially coated with a magnetically lossy thin layer in the case of TM excitation ($k_0 a = 2\pi$, $\mu_r t/a = 0.01 - j0.03$)

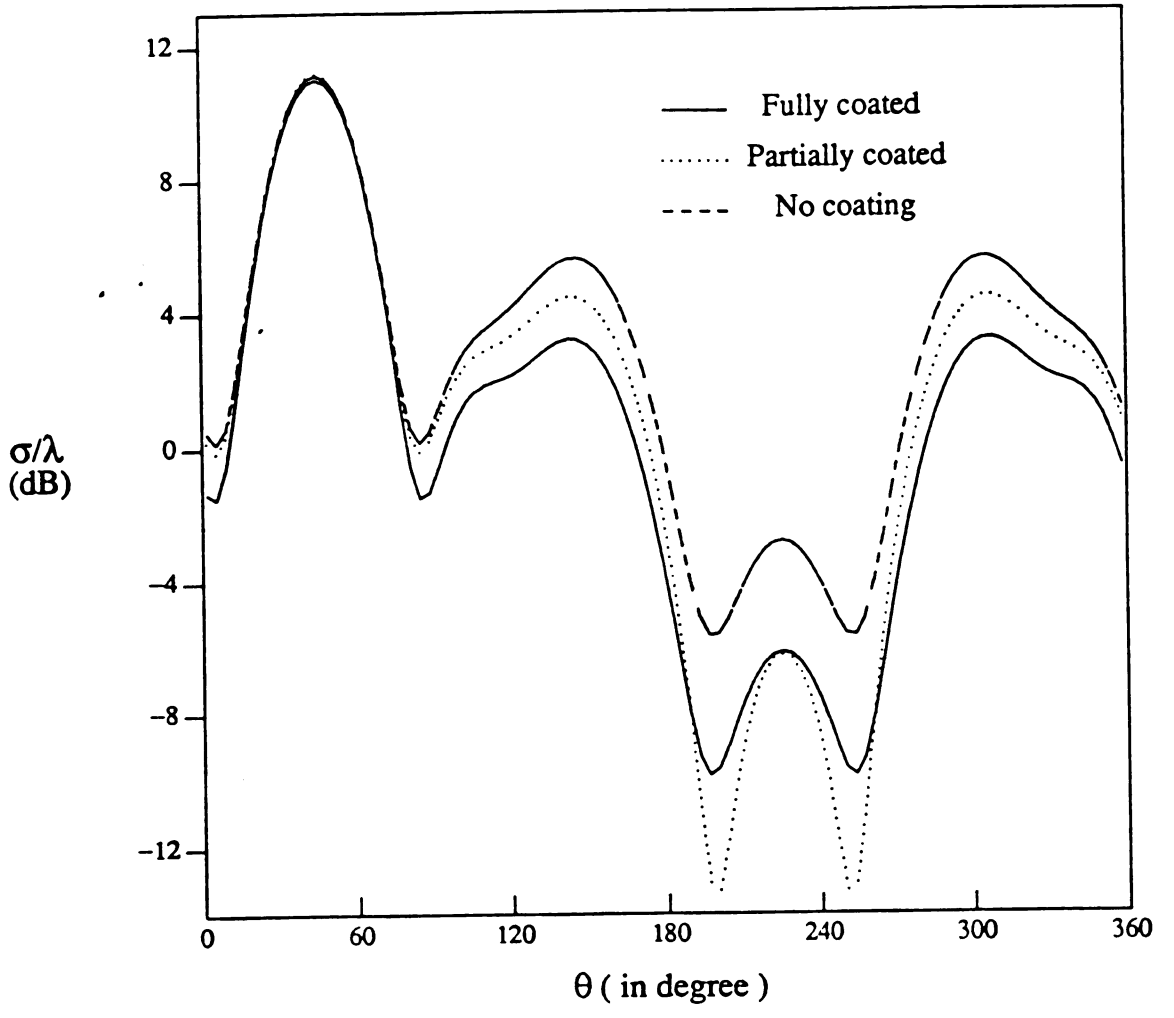

Figure 4.22 Radar cross sections of an infinitely long conducting rectangular cylinder partially coated with a magnetically lossy thin layer in the case of TM excitation ($k_0 a = 2\pi$, $\mu_r t/a = 0.01 - j0.03$)

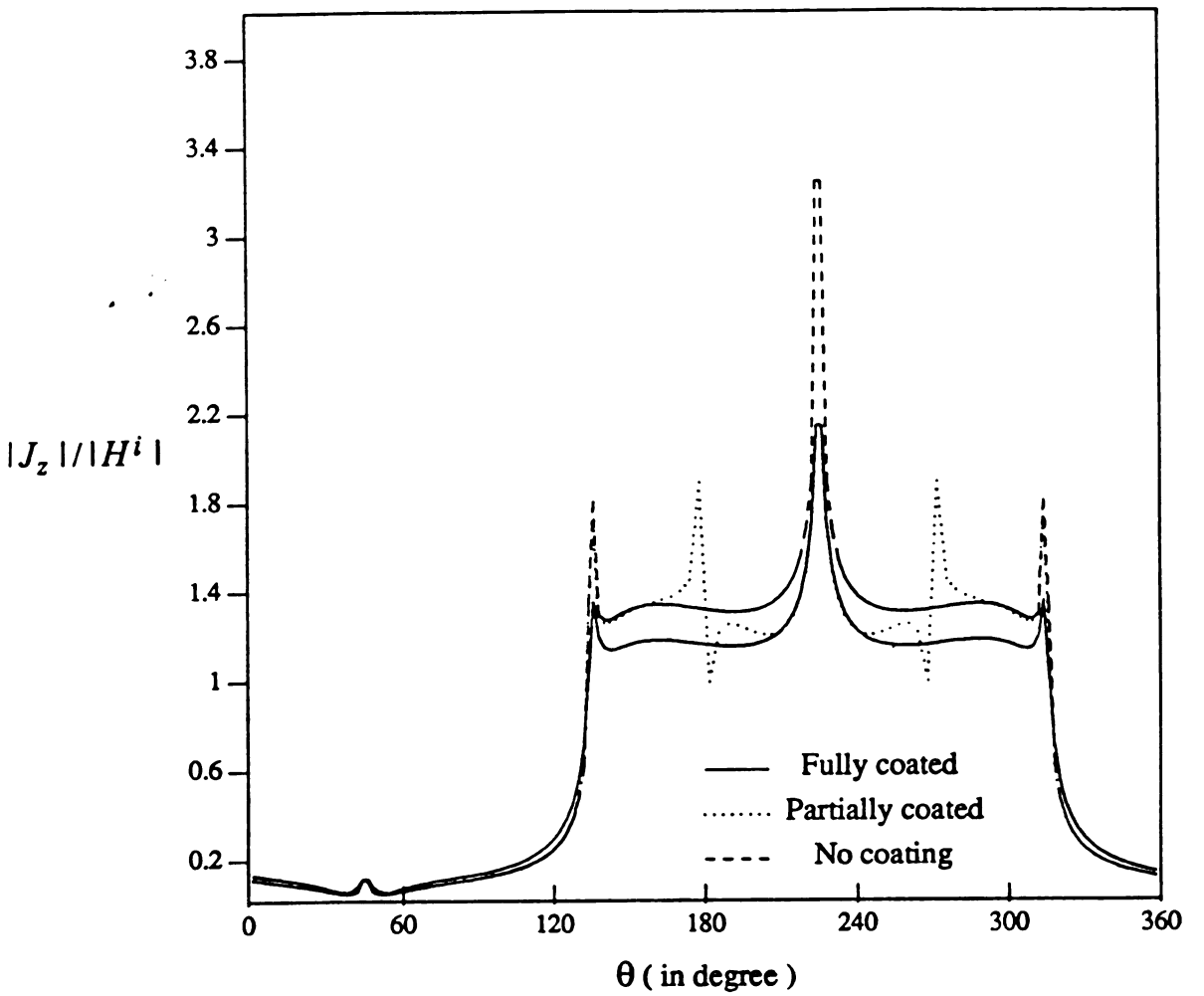

Figure 4.23 Amplitude distribution of the z-component current on the surface of an infinitely long conducting rectangular cylinder partially coated with a magnetically lossy thin layer in the case of TM excitation ($k_0 a = 2\pi$, $\mu_r t/a = 0.01 - j0.03$)

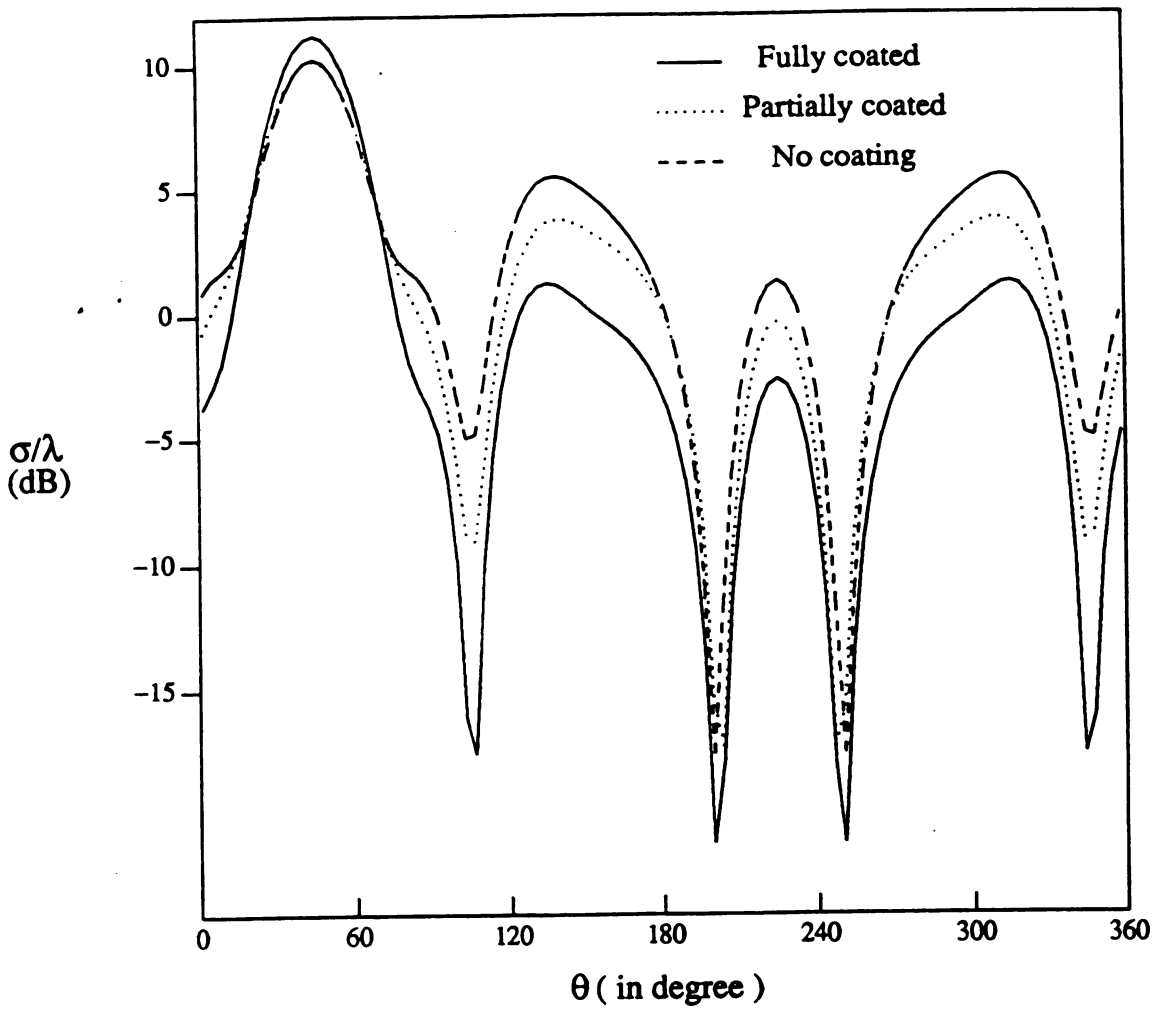

Figure 4.24 Radar cross sections of an infinitely long conducting rectangular cylinder partially coated with a magnetically lossy thin layer in the case of TE excitation ($k_0 a = 2\pi$, $\mu_r t/a = 0.01 - j0.03$)

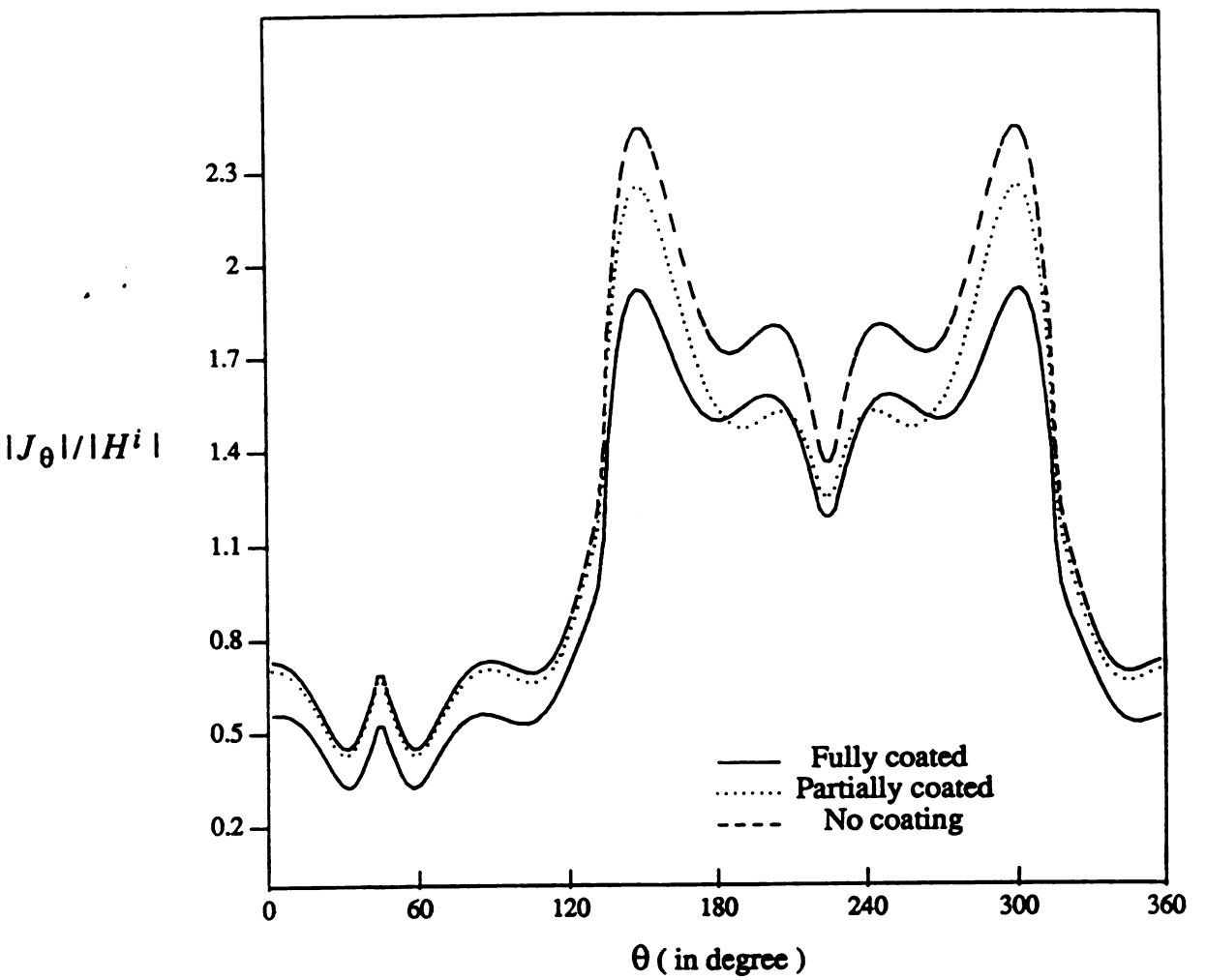

Figure 4.25 Amplitude distribution of the θ-component current on the surface of an infinitely long conducting rectangular cylinder partially coated with a magnetically lossy thin layer in the case of TE excitation ($k_0 a = 2\pi$, $\mu_r t/a = 0.01 - j0.03$)

CHAPTER V

EFFECTS OF AN IMPEDANCE SHEET ON THE CHARACTERISTIC PROPERTIES OF CAVITY BACKED ANTENNA BY FINITE DIFFERENCE TIME DOMAIN METHOD

5.1 Introduction

In some military applications, it is desirable to hide an airplane from the detection of radar systems. To achieve this goal, the scattered electromagnetic fields from the airplane need to be substantially reduced. Since an antenna on an airplane is an efficient scatterer, it is necessary to cover the antenna with a lossy layer to reduce its radar cross section. However, by doing so, the receiving characteristics of the antenna may be hampered. In this chapter, we will study the effects of an impedance sheet, covering a cavity backed antenna, on the scattering and receiving characteristics of the antenna.

The antenna system to be analyzed is a cavity-backed antenna as depicted in Fig. 5.1. Its receiving and scattering characteristics will be investigated by the finite difference time domain method. As shown in Fig 5.1, an open rectangular cavity is situated on an infinite ground plane, and an impedance sheet covers the aperture of the cavity. Intuitively, it is expected that the impedance sheet will attenuate the scattered fields more than it will do to the incident field of the antenna, because the back-scattered wave crosses through the impedance sheet twice but the incident wave to the antenna crosses through the sheet only once. Since the interaction of an EM wave with a cavity backed antenna covered by an impedance sheet involves complicated phenomena, quantitative information on the characteristics of this antenna can be obtained after a complete solution is obtained.

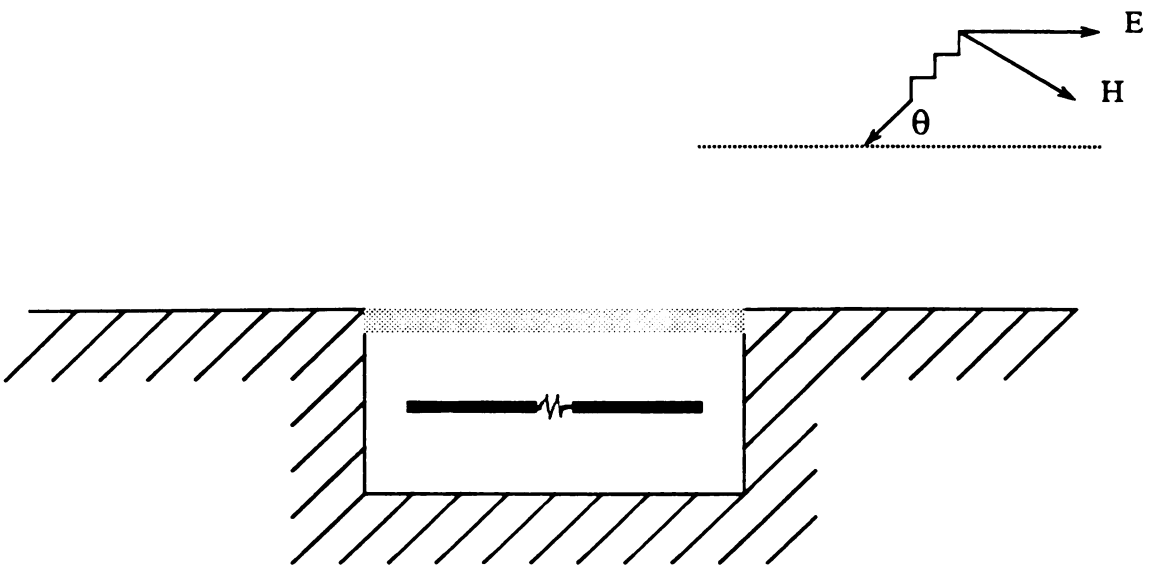

Fig. 5.1 Cavity backed antenna with an impedance sheet on the aperture

The integral equation technique is difficult to apply to this problem due to its complex geometry and the infinite conducting surface involved. Therefore, the finite difference time domain method is applied due to its simplicity and efficiency in treating complex problems. Based on the fundamental theory described in Chapter III, the Yee's model is modified for treating an infinitely thin impedance sheet. The radiation boundary condition is changed to adapt the infinite structure. The backscattered field and the current distribution on the antenna are obtained by the FD-TD method.

5.2 Basic Finite Difference Time Domain Scheme

The basic algorithm used in this chapter is similar to that discussed in Chapter III. The Yee's model is used to discretize the Maxwell's equations for the interior points as shown in Fig 5.2. The Mur's second order radiation boundary condition is used to truncate the infinite space into a finite one. The total field region and the scattered field region are also defined. However, several modifications have to be made when the basic algorithms are applied to this specific problem. First, the Yee's model is reconstructed from the integral form of Maxwell's curl equations to facilitate the dealing of the infinite thin sheet. Second, the Mur's second order radiation boundary condition is applied to the infinite ground plane by using the image theory. And last, to reserve the applicability of the radiation boundary condition in the scattered field region, the total field is decomposed into a part generated with the aperture absent and another part contributed by the equivalent sources on the aperture.

5.3 Integral Interpolation of Maxwell's Curl Equation

The differential forms of Maxwell's curl equations are easily discretized into rectangular or cubic cells of finite differences. In practice, a complex geometry or constituents of materials need a better modeling of the curvature of smooth surface or

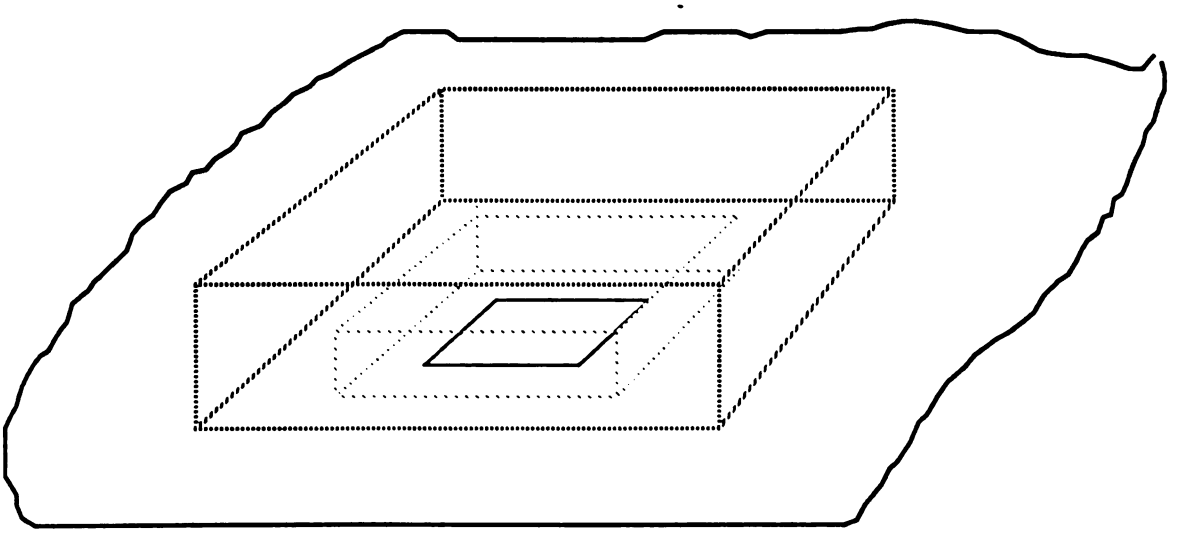

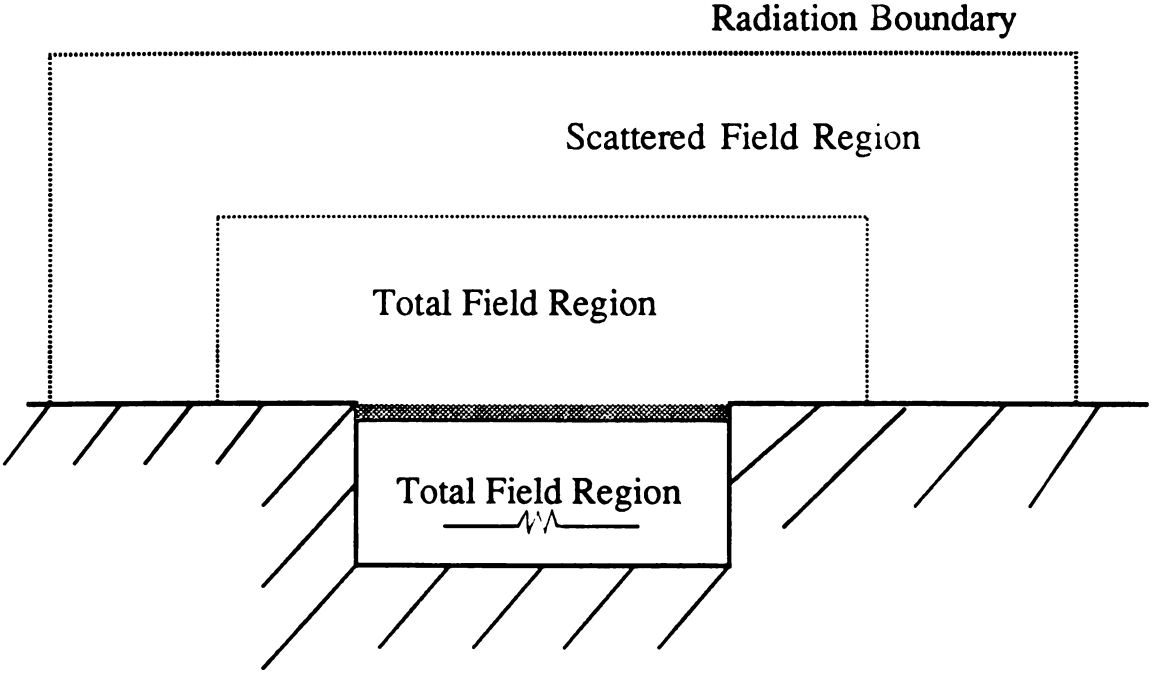

Fig. 5.2 Radiation Boundary And Boundary Seperating
Total Field and Scattering Field

irregular inhomogeneity than the staircase modeling. The integral interpolation of Maxwell's equations provides a simple but efficient method to overcome the shortcoming of the classic finite difference method. By using the integral interpolation, curvature can be handled by conforming the paths of integration and inhomogeneity which need not to be some units of the cells, such as the case of thin layers, thin wires etc. In this section, as an important application, integral interpolation is used to treat an infinitely thin sheet covering a cavity.

A Yee's model with an impedance sheet is shown in Fig 5.3. The idea of handling the thin sheet is based on the integral forms of Maxwell's equations which are stated as follows:

Farady's Law is

$$\int_C \mathbf{E}\cdot d\vec{l} = -\int_S \mathbf{J}_m\cdot d\vec{S} - \int_S \mu\frac{\partial}{\partial t}\mathbf{H}\cdot d\vec{S} \tag{5.3.1a}$$

Ampere's Law is

$$\int_C \mathbf{H}\cdot d\vec{l} = \int_S \mathbf{J}_e\cdot d\vec{S} + \int_S \varepsilon\frac{\partial}{\partial t}\mathbf{E}\cdot d\vec{S} \tag{5.3.1b}$$

where $\mathbf{J}_m = \sigma_m\mathbf{H}$, $\mathbf{J}_e = \sigma\mathbf{E}$, C is the contour path of integration and S is the surface area surrounded by the contour C . When a magnetic field is to be updated, Farady's law is employed. While Ampere's law is used to update an electric field. As an example, to update H_x , the contour integrations of electric fields E_z and E_y, which surround the H_x as shown in Fig.5.3, are conducted.

The integral equations of (5.3.1a) and (5.3.1b) can be equivalently written into the forms of

$$\int_C \mathbf{E}\cdot d\vec{l} = -\int_S \mathbf{J}_m\cdot d\vec{S} - \int_S (\mu-\mu_0)\frac{\partial}{\partial t}\mathbf{H}\cdot d\vec{S} - \int_S \mu_0\frac{\partial}{\partial t}\mathbf{H}\cdot d\vec{S} \tag{5.3.2a}$$

$$\int_C \mathbf{H}\cdot d\vec{l} = \int_S \mathbf{J}_e\cdot d\vec{S} + \int_S (\varepsilon-\varepsilon_0)\frac{\partial}{\partial t}\mathbf{E}\cdot d\vec{S} + \int_S \varepsilon_0\frac{\partial}{\partial t}\mathbf{E}\cdot d\vec{S} \tag{5.3.2b}$$

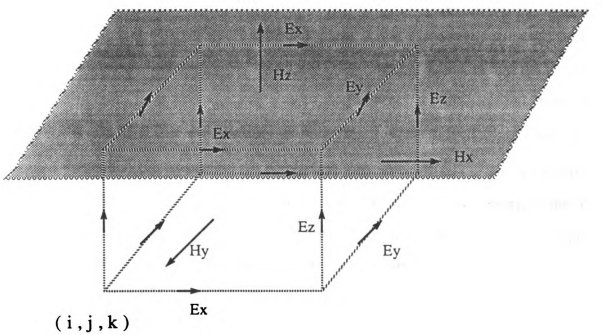

Fig. 5.3 Yee's Model Near The Impedence Sheet

The equivalent sources can be defined as:

$$\mathbf{J}_m^{eq} = \mathbf{J}_m + (\mu - \mu_0)\frac{\partial}{\partial t}\mathbf{H} \tag{5.3.3a}$$

$$\mathbf{J}_e^{eq} = \mathbf{J}_e + (\varepsilon - \varepsilon_0)\frac{\partial}{\partial t}\mathbf{E} \tag{5.3.3b}$$

or

$$\mathbf{J}_m^{eq} = \sigma_m\mathbf{H} + (\mu - \mu_0)\frac{\partial}{\partial t}\mathbf{H} \tag{5.3.4a}$$

$$\mathbf{J}_e^{eq} = \sigma\mathbf{E} + (\varepsilon - \varepsilon_0)\frac{\partial}{\partial t}\mathbf{E} \tag{5.3.4b}$$

The equivalent magnetic current consists of two parts: magnetic conducting current $\mathbf{J}_m = \sigma_m\mathbf{H}$ comparable to the electric conducting current, and magnetic polarization current. σ_m represents the magnetic loss of material which is represented by the imaginary part of complex permeability in the frequency domain. σ_m can be related to the complex $\mu^* = (\mu_r - j\mu_i)$ by $\sigma_m = \omega\mu_i$ when the excitation wave is time harmonic.

In the thin film structure, the sheet current manifests if the thickness t approaches zero but $\sigma_m t$ or $\omega(\mu - \mu_0)t$ and σt or $\omega(\varepsilon - \varepsilon_0)t$ remain finite. According to the Yee's model as shown in Fig 5.3, the integration of (5.3.2) is performed. For simplicity, we first assume that $\sigma_m = 0$ and $\mu = \mu_0$ so that only the electric current exists on the sheet. By using (5.3.2b) and integrating along the contour shown in Fig 5.4(a), the integral equation (5.3.2b) can be interpolated as:

$$\begin{aligned}
&[H_z^{n+\frac{1}{2}}(i+\tfrac{1}{2}, j+\tfrac{1}{2}, k) - H_z^{n+\frac{1}{2}}(i+\tfrac{1}{2}, j-\tfrac{1}{2}, k)]\Delta z \\
&- [H_y^{n+\frac{1}{2}}(i+\tfrac{1}{2}, j, k+\tfrac{1}{2}) - H_y^{n+\frac{1}{2}}(i+\tfrac{1}{2}, j, k-\tfrac{1}{2})]\Delta y \\
&= \sigma t\Delta y 0.5[E_x^{(n+1)}(i+\tfrac{1}{2}j, k) + E_x^{(n)}(i+\tfrac{1}{2}j, k)] \\
&+ (\varepsilon - \varepsilon_0)t\Delta y/\Delta t[E_x^{(n+1)}(i+\tfrac{1}{2}j, k) - E_x^{(n)}(i+\tfrac{1}{2}j, k)] \\
&+ \varepsilon_0\Delta y\Delta z/\Delta t[E_x^{(n+1)}(i+\tfrac{1}{2}j, k) - E_x^{(n)}(i+\tfrac{1}{2}j, k)]
\end{aligned} \tag{5.3.5}$$

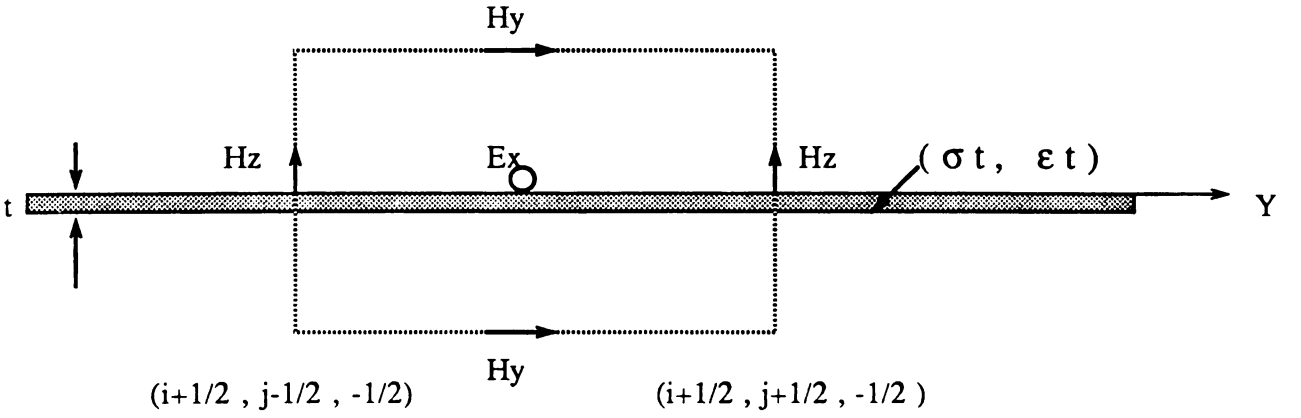

Fig. 5. 4.a Integral Path For Ex

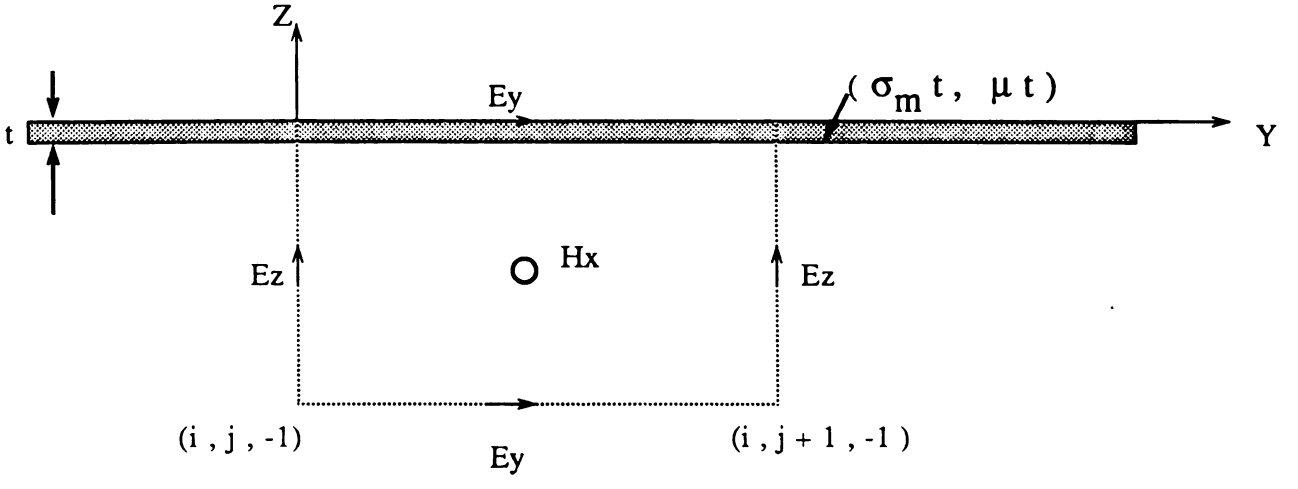

Fig. 5.4.b Integral Path For Hx

where the first and the second terms on the right hand side are contributed by the conducting and the polarization sheet currents. Equation (5.3.5) can be further simplified to

$$
\begin{aligned}
&[H_z^{n+\frac{1}{2}}(i+\frac{1}{2}, j+\frac{1}{2}, k) - H_z^{n+\frac{1}{2}}(i+\frac{1}{2}, j+\frac{1}{2}, k)]\Delta z \\
&- [H_y^{n+\frac{1}{2}}(i+\frac{1}{2}, j, k+\frac{1}{2}) - H_y^{n+\frac{1}{2}}(i+\frac{1}{2}, j, k-\frac{1}{2})]\Delta y \\
&= [\sigma t \Delta y 0.5 + (\varepsilon - \varepsilon_0) t DELTAy/\Delta t + \varepsilon_0 \Delta y \Delta z/\Delta t] E_x^{(n+1)}(i+\frac{1}{2} j, k) \\
&+ [\sigma t \Delta y 0.5 - (\varepsilon - \varepsilon_0) t \Delta y/\Delta t - \varepsilon_0 \Delta y \Delta z/\Delta t] E_x^{(n)}(i+\frac{1}{2} j, k)
\end{aligned} \tag{5.3.6}
$$

The modified Yee's scheme is then obtained as

$$
\begin{aligned}
E_x^{(n+1)}(i, j+\frac{1}{2}, k) = &- \frac{CB}{CA} E_x^{(n)}(i, j+\frac{1}{2}, k) \\
&+ \frac{c_0 \Delta t z}{\Delta y \Delta z CA} \Big\{ [H_z^{n+\frac{1}{2}}(i+\frac{1}{2}, j+\frac{1}{2}, k) - H_z^{n+\frac{1}{2}}(i+\frac{1}{2}, j-\frac{1}{2}, k)]\Delta z \\
&- [H_y^{n+\frac{1}{2}}(i+\frac{1}{2}, j, k+\frac{1}{2}) - H_y^{n+\frac{1}{2}}(i+\frac{1}{2}, j, k-\frac{1}{2})]\Delta y \Big\}
\end{aligned} \tag{5.3.7}
$$

where coefficients CA and CB are defined as

$$CA = [c_0 \Delta t z_0 \sigma t/\Delta z 0.5 + (\varepsilon_r - 1) t/\Delta z + 1] \tag{5.3.8a}$$

$$CB = [c_0 \Delta t z_0 \sigma t/\Delta z 0.5 - (\varepsilon_r - 1) t/\Delta z - 1] \tag{5.3.8b}$$

Note that **E** is continuous across the sheet, only averaged value of **E** was used to approximate the fields on the area closed by the integral contour.

In a similar way, a modified scheme for E_y can also be derived:

$$
\begin{aligned}
E_y^{(n+1)}(i, j+\frac{1}{2}, k) = &- \frac{CB}{CA} E_y^{(n)}(i, j+\frac{1}{2}, k) \\
&- \frac{c_0 \Delta t z}{\Delta x \Delta z CA} \Big\{ [H_z^{n+\frac{1}{2}}(i+\frac{1}{2}, j+\frac{1}{2}, k) - H_z^{n+\frac{1}{2}}(i-\frac{1}{2}, j+\frac{1}{2}, k)]\Delta z \\
&- [H_x^{n+\frac{1}{2}}(i, j+\frac{1}{2}, k+\frac{1}{2}) - H_x^{n+\frac{1}{2}}(i, j+\frac{1}{2}, k-\frac{1}{2})]\Delta x \Big\}
\end{aligned} \tag{5.3.9}
$$

where

$$CA = [c_0\Delta t z_0 \sigma t/\Delta z 0.5 + (\varepsilon_r - 1)t/\Delta z + 1] \tag{5.3.10a}$$

$$CB = [c_0\Delta t z_0 \sigma t/\Delta z 0.5 - (\varepsilon_r - 1)t/\Delta z - 1] \tag{5.3.10b}$$

As discussed in Chapter IV, the scattered fields can be significantly modified when a magnetic material is introduced in the sheet. If $\sigma = 0$ and $\varepsilon = \varepsilon_0$, we have a magnetically lossy sheet, which is characterized by the parameter of σ_m or $\mu_r - 1$, over the cavity on $k = 0$ plane as shown in Fig 5.4(b). Then the finite difference schemes for magnetic fields are created in a similar way as we did previously for electric fields with an electrically lossy sheet. Since equivalent electric current $\mathbf{J}_e^{eq}$ is zero when $\sigma = 0$ and $\varepsilon = \varepsilon_0$, the magnetic fields are continuous across the sheet. By using Farady' law of (5.3.2a) and integral along the contour shown in Fig 5.4(b), a difference scheme for the magnetic field H_x can be constructed as follows:

$$\begin{aligned}
&[E_z^n(i, j+1, k+\tfrac{1}{2}) - E_z^n(i, j, k+\tfrac{1}{2})]\Delta z - [E_y^n(i, j+\tfrac{1}{2}, k+1) - E_y^n(i, j+\tfrac{1}{2}, k)]\Delta y = \\
&\quad - \sigma_m t\Delta y 0.5[H_x^{(n+\frac{1}{2})}(i, j+\tfrac{1}{2}, k+\tfrac{1}{2}) + H_x^{(n-\frac{1}{2})}(i, j+\tfrac{1}{2}, k+\tfrac{1}{2})] \\
&\quad - (\mu - \mu_0)t\Delta y/\Delta t[H_x^{(n+\frac{1}{2})}(i, j+\tfrac{1}{2}, k+\tfrac{1}{2}) - H_x^{(n-\frac{1}{2})}(i, j+\tfrac{1}{2}, k+\tfrac{1}{2})] \\
&\quad - \mu_0\Delta z\Delta y/\Delta t[H_x^{(n+\frac{1}{2})}(i, j+\tfrac{1}{2}, k+\tfrac{1}{2}) - H_x^{(n-\frac{1}{2})}(i, j+\tfrac{1}{2}, k+\tfrac{1}{2})]
\end{aligned} \tag{5.3.11}$$

Physically, the first and the second terms on the right hand side of (5.3.11) are contributed by the equivalent magnetic currents. Rearranging (5.3.11) yields

$$\begin{aligned}
H_x^{(n+\frac{1}{2})}(i, j+\tfrac{1}{2}, k+\tfrac{1}{2}) = &- \frac{CB}{CA} H_x^{(n-\frac{1}{2})}(i, j+\tfrac{1}{2}, k+\tfrac{1}{2}) - \frac{c_0\Delta t}{CA\Delta z\Delta y z_0} \\
&\left\{[E_z^n(i, j+1, k+\tfrac{1}{2}) - E_z^n(i, j, k+\tfrac{1}{2})]\Delta z - [E_y^n(i, j+\tfrac{1}{2}, k+1) - E_y^n(i, j+\tfrac{1}{2}, k)]\Delta y\right\}
\end{aligned} \tag{5.3.12}$$

where

$$CA = \sigma_m t c_0 \Delta t 0.5/(z_0\Delta z) + (\mu_r - 1)t/\Delta z + 1 \tag{5.3.13a}$$

$$CB = \sigma_m t c_0 \Delta t 0.5/(z_0\Delta z) - (\mu_r - 1)t/\Delta z - 1 \tag{5.3.13b}$$

Similarly, the y component of magnetic field can be updated by

$$H_y^{(n+\frac{1}{2})}(i+\frac{1}{2}, j, k+\frac{1}{2}) = -\frac{CB}{CA}H_y^{(n-\frac{1}{2})}(i+\frac{1}{2}, j, k+\frac{1}{2})] - \frac{c_0\Delta t}{CA\Delta z\Delta x z_0}$$

$$\left\{[E_z^n(i+1, j, k+\frac{1}{2})-E_z^n(i, j, k+\frac{1}{2})]\Delta z-[E_x^n(i+\frac{1}{2}, j, k+1)-E_x^n(i+\frac{1}{2}, j, k)]\Delta x\right\} \quad (5.3.14)$$

Both the electrically lossy sheet and the magnetically lossy sheet have been considered separately, and the Yee's difference schemes have been modified for these two special cases. However, most practical materials have both electrically and magnetically lossy properties. Thus, the electric current and the magnetic current are presented simultaneously. In this general case, the formulations for the two special cases discussed before can be combined and modified. It is informative to note that the tangential components of the electric fields and the magnetic fields are no longer continuous across the covered sheet when both the magnetic and the electric losses exist. Therefore, the difference equations for updating both the electric fields and the magnetic fields comprise both electric and magnetic sheet currents.

By the Ampere's Law, we have

$$\int_C \mathbf{H}\cdot\vec{dl} = \int_S \mathbf{J}_e\cdot\vec{dS} + \int_S (\varepsilon - \varepsilon_0)\frac{\partial}{\partial t}\mathbf{E}\cdot\vec{dS} + \int_S \varepsilon_0\frac{\partial}{\partial t}\mathbf{E}\cdot\vec{dS}$$

The discontinuity of electric fields across the sheet can be compensated by a magnetic sheet current of $\mathbf{J}_m^{eq}t$. Inside the sheet, electric fields can be approximated by the average value of the electric fields on both sides of the sheet. As shown in Fig 5.4(c), if

$$E_x(i+\frac{1}{2}j, 0^+)$$

or

$$E_y(i,j+\frac{1}{2}, 0^+)$$

is above the sheet, then the electric field inside the sheet is approximated by

$$E_x(i+\frac{1}{2}j, 0^+) + 0.5J_{my}^{eq}t$$

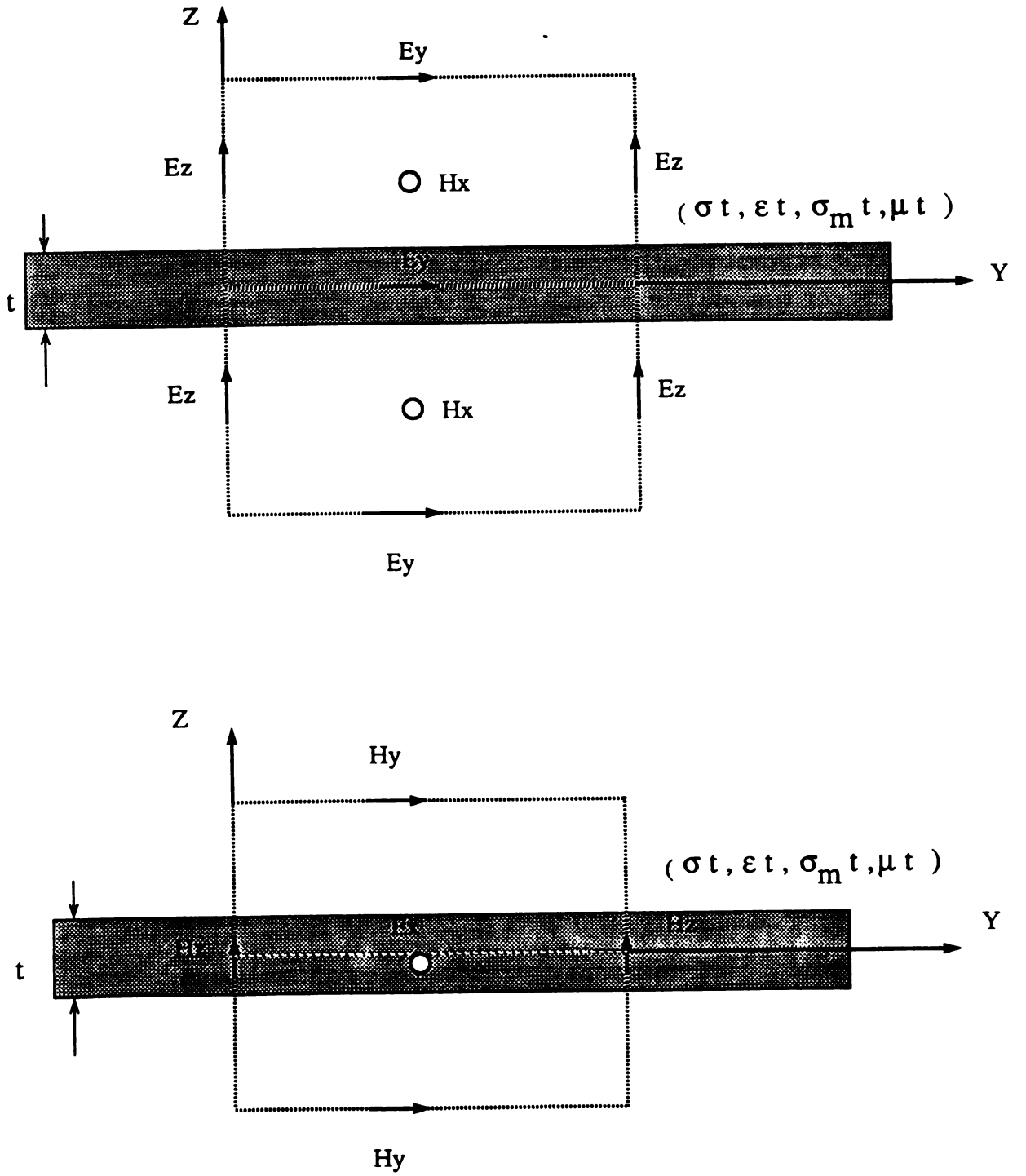

Fig. 5.4 (c) Integral Paths

or

$$E_y(i,j+\frac{1}{2},\,0^+) - 0.5J_{mx}^{eq}t\ ,$$

where

$$\mathbf{J}_m^{eq} = \sigma_m\mathbf{H}(i+\frac{1}{2}j,\,0) + (\mu-\mu_0)\frac{\partial}{\partial t}\mathbf{H}(i+\frac{1}{2}j,\,0)$$

While the electric fields are below the sheet, they can be evaluated by a difference of magnetic sheet currents as

$$E_x(i+\frac{1}{2}j,\,0^-) = E_x(i+\frac{1}{2}j,\,0^+) + \sigma_m t H_y(i+\frac{1}{2}j,\,0) + (\mu-\mu_0)t\frac{\partial}{\partial t}H_y(i+\frac{1}{2}j,\,0)$$

or

$$E_y(i,j+\frac{1}{2},\,0^-) = E_y(i,j+\frac{1}{2},\,0^+) - \sigma_m t H_x(i,j+\frac{1}{2},\,0) - (\mu-\mu_0)t\frac{\partial}{\partial t}H_x(i,j+\frac{1}{2},\,0)\ .$$

It is seen that the right hand side of the Ampere's law can be completed by finite differences. Unfortunately, it is found that those approximations will fail if any time derivative is involved. The difficulty can be viewed from the example of the third integral on the right hand side of the Ampere's law as shown in Fig.(5.4c).

The third integral ($\int_S \varepsilon_0\frac{\partial}{\partial t}\mathbf{E}\cdot d\vec{S}$) is approximated by

$$\frac{\partial}{\partial t}\left\{\frac{1}{2}\Delta S\varepsilon_0\left[E_x^{(n+\frac{1}{2})}(i+\frac{1}{2}j,\,0^+) + (E_x^{(n+\frac{1}{2})}(i+\frac{1}{2}j,\,0^+) + \right.\right.$$
$$\left.\left.\sigma_m t H_y^{(n+\frac{1}{2})}(i+\frac{1}{2}j,\,0) + (\mu-\mu_0)t\frac{\partial}{\partial t}H_y^{(n+\frac{1}{2})}(i+\frac{1}{2}j,\,0)\right)\right]\right\} \qquad (5.3.15)$$

and the derivative in time domain leads to:

$$\Delta S\varepsilon_0/\Delta t\left\{E_x^{(n+1)}(i+\frac{1}{2}j,\,0^+) - E_x^{(n)}(i+\frac{1}{2}j,\,0^+) + 0.5\sigma_m t[H_y^{(n+1)}(i+\frac{1}{2}j,\,0) - H_y^{(n)}(i+\frac{1}{2}j,\,0)]\right.$$
$$\left. + (\mu-\mu_0)t/\Delta t^2[H_y^{(n+1)}(i+\frac{1}{2}j,\,0) - 2H_y^{(n+\frac{1}{2})}(i+\frac{1}{2}j,\,0) + H_y^{(n)}(i+\frac{1}{2}j,\,0)]\right\} \qquad (5.3.16)$$

However, the left hand side of the Ampere's law $\int_C \mathbf{H}\cdot d\vec{l}$ yields:

$$\int_C \mathbf{H}\cdot d\vec{l} = [H_z^{(n+\frac{1}{2})}(i+\frac{1}{2}, j+\frac{1}{2},0) - H_z^{(n+\frac{1}{2})}(i+\frac{1}{2}, j-\frac{1}{2},0)]\Delta z -$$

$$[H_y^{(n+\frac{1}{2})}(i+\frac{1}{2}, j, \frac{1}{2}) - H_y^{(n+\frac{1}{2})}(i+\frac{1}{2}, j, -\frac{1}{2})]\Delta y \qquad (5.3.17)$$

The iteration of H_y needs its information at time steps of n+1 and n on the right hand side of the Ampere's law, but time step of $n+\frac{1}{2}$ on the left hand side. To overcome this difficulty, the electric field $E_x(i+\frac{1}{2}j, 0)$ or $E_y(ij+\frac{1}{2}, 0)$ is assumed to be the field inside the sheet. Then, the integration over the area as shown in Fig 5.4(c) is equivalent to taking the electric field inside the film as an averaged value. With this assumption, the representation for the Ampere's law remains the same, but that for the Falady's law is changed as shown in Fig 5.4(c). By the Farady's law

$$\int_C \mathbf{E}\cdot d\vec{l} = -\int_S \mathbf{J}_m\cdot d\vec{S} - \int_S (\mu - \mu_0)\frac{\partial}{\partial t}\mathbf{H}\cdot d\vec{S} - \int_S \mu_0\frac{\partial}{\partial t}\mathbf{H}\cdot d\vec{S}$$

Consider the electric field inside the film, the total current closed by the integral contour is $\frac{1}{2}\sigma_m t dy H_x$ or $\frac{1}{2}\sigma_m t dy H_x$. After some manipulations, the updating formulas for magnetic fields become

$$H_x^{(n+\frac{1}{2})}(i, j+\frac{1}{2}, k+\frac{1}{2}) = -\frac{CB}{CA}H_x^{(n-\frac{1}{2})}(i, j+\frac{1}{2}, k+\frac{1}{2}) - \frac{c_0\Delta t}{CA\Delta z\Delta y z_0}$$

$$\left\{[E_z^n(i, j+1, k+\frac{1}{2}) - E_z^n(i, j, k+\frac{1}{2})]\Delta z - [E_y^n(i, j+\frac{1}{2}, k+1) - E_y^n(i, j+\frac{1}{2}, k)]\Delta y\right\} \qquad (5.3.18)$$

and

$$H_y^{(n+\frac{1}{2})}(i+\frac{1}{2}, j, k+\frac{1}{2}) = -\frac{CB}{CA}H_y^{(n-\frac{1}{2})}(i+\frac{1}{2}, j, k+\frac{1}{2})] - \frac{c_0\Delta t}{CA\Delta z\Delta x z_0}$$

$$\left\{[E_z^n(i+1, j, k+\frac{1}{2}) - E_z^n(i, j, k+\frac{1}{2})]\Delta z - [E_x^n(i+\frac{1}{2}, j, k+1) - E_x^n(i+\frac{1}{2}, j, k)]\Delta x\right\} \qquad (5.3.19)$$

where

$$CA = \sigma_m t c_0 \Delta t 0.25/(z_0\Delta z) + (\mu_r - 1)t/\Delta z + 1 \qquad (5.3.20a)$$

$$CB = \sigma_m t c_0 \Delta t 0.25/(z_0 \Delta z) - (\mu_r - 1)t/\Delta z - 1 \qquad (5.3.20b)$$

Equations (5.3.18) and (5.3.19) hold also for $k = -1$ and $k = 0$ where the magnetic field components are just above or below the sheet. For example, $H_y^{(n+\frac{1}{2})}(i+\frac{1}{2}, j, -\frac{1}{2})$ or $H_y^{(n+\frac{1}{2})}(i+\frac{1}{2}, j, \frac{1}{2})$ is below or above the sheet which is located at plane $k = 0$. The formulas of (5.3.18) and (5.3.19) evaluated at $k = -1$ and $k = 0$ are almost the same except for some changes in the coefficients of CA and CB .

5.4 Modification of Radiation Boundary Condition

For the geometry shown in Fig 5.1, a radiation boundary condition needs to be applied to truncate the half space into a finite one. The outer surface of the truncated space is depicted in Fig 5.2 where the infinite ground plane is included. Because both the second order and the first order radiation boundary conditions use the points below the ground plane, it is necessary to use the image theory. By the image theory, the second order radiation boundary condition can be kept for the corner points on the ground plane while the stability criterion is unchanged.

As discussed in Chapter III, with the Yee's model only the components of electric fields are determined from the field values at points outside the considered region if the outmost surface is placed as in Fig.5.6. Thus, the radiation boundary condition is only applied to the electric field components on the truncation surface. The Mur's second order radiation boundary condition for a three dimensional problem as stated in Eq. (3.3.35a) of Chapter III can be illustrated in Fig. 5.5. If the outmost truncated surface is assumed to be on the $x = 0$ plane, then $x>0$ region belongs to the interior region. The field at point $(0, j, k)$ is determined by all its adjacent points as shown in Fig.5.5.

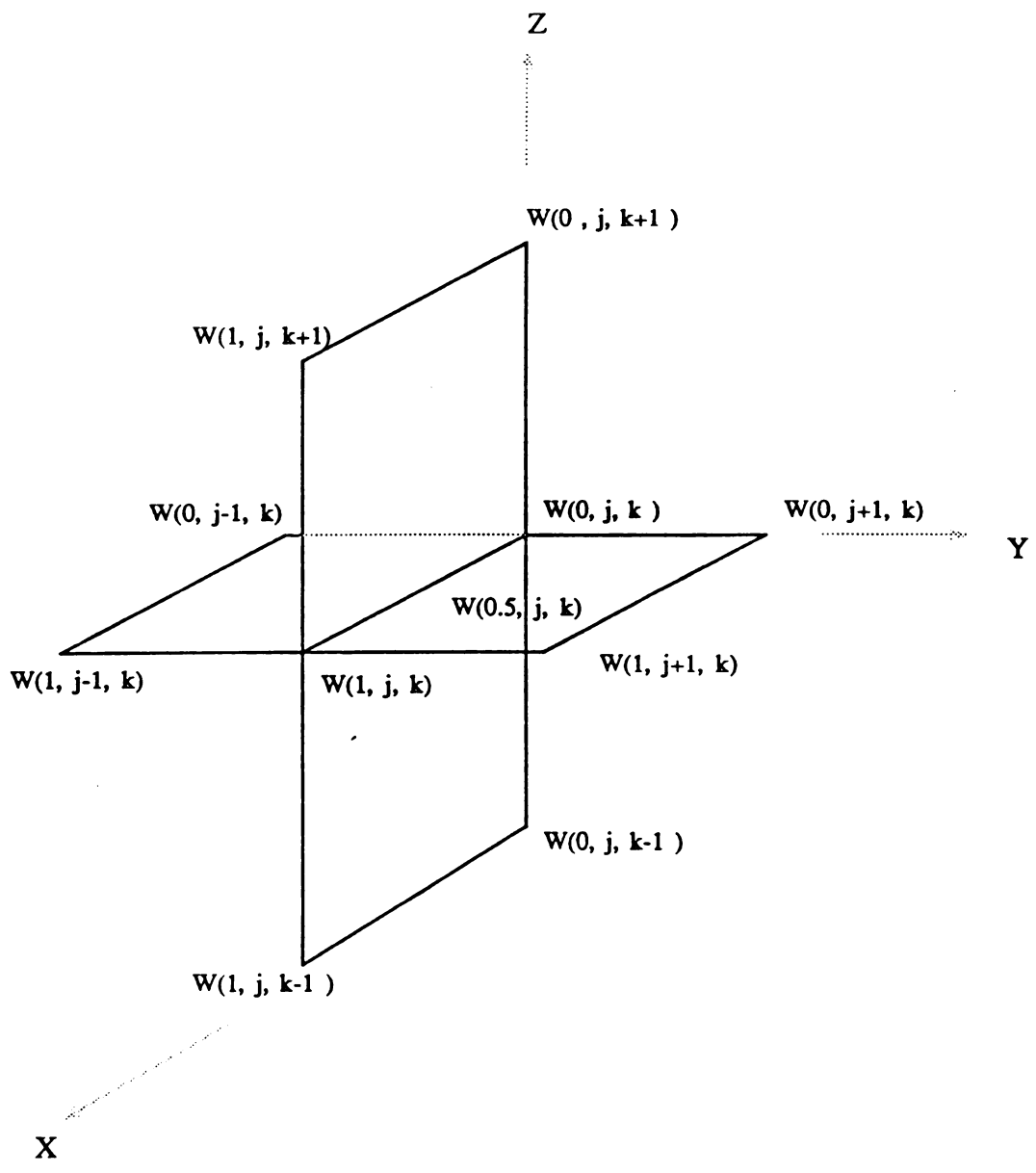

Fig. 5 .5 Points Used in the Mur's Second Order Approximation

Figure 5.6 illustrates a radiation boundary condition for a structure with an infinite ground plane. W represents any components of electric fields at a proper position in the Yee's model. It is assumed that the ground plane is located at $k = 0$ plane. Since E_x and E_y at $k = 0$ are tangential components which lead to zero, the Mur's second order approximation and the first order approximationcan be directly applied to them.

To update the normal component of electric field above the ground plane, E_z component at $k = \frac{1}{2}$, the knowledge of field below the ground plane is necessary. Fortunately, the image theory can be used and the fields produced by the sources and their images are intuitively illustrated in the Fig. 5.7. The real sources above the ground and their images provides the actual solution in the space over the ground plane. The tangential components of electric field produced by the sources and their images are antisymmetric w.r.t. the ground plane, while the normal components of electric field are symmetric w.r.t. the ground plane.

In our specified problem, the aperture fields can be regarded as equivalent sources on the ground plane, so the same image theory can be applied to analyze their symmetry properties. For example, to update $E_z(i, j, \frac{1}{2})$, the normal component of electric field $E_z(i, j, -\frac{1}{2})$ in the radiation boundary condition is replaced by the field $E_z(i, j, \frac{1}{2})$ according to the field symmetry from the image theory. This technique is applicable to the second and the first order approxiamtions on the points at the intersection of the ground plane with the outermost plane. It can be shown that the resulted scheme is stable. As an exmaple, the radiation boundary condition for E_z at points $(i, j, k+\frac{1}{2})$ on the plane $x = 0$ is represented by:

$$E_z^{n+1}(0, j, k+\frac{1}{2}) = -E_z^{n-1}(1, j, k+\frac{1}{2}) + \frac{c_0\Delta t-\Delta x}{c_0\Delta t+\Delta x}[E_z^{n+1}(1, j, k+\frac{1}{2}) +$$

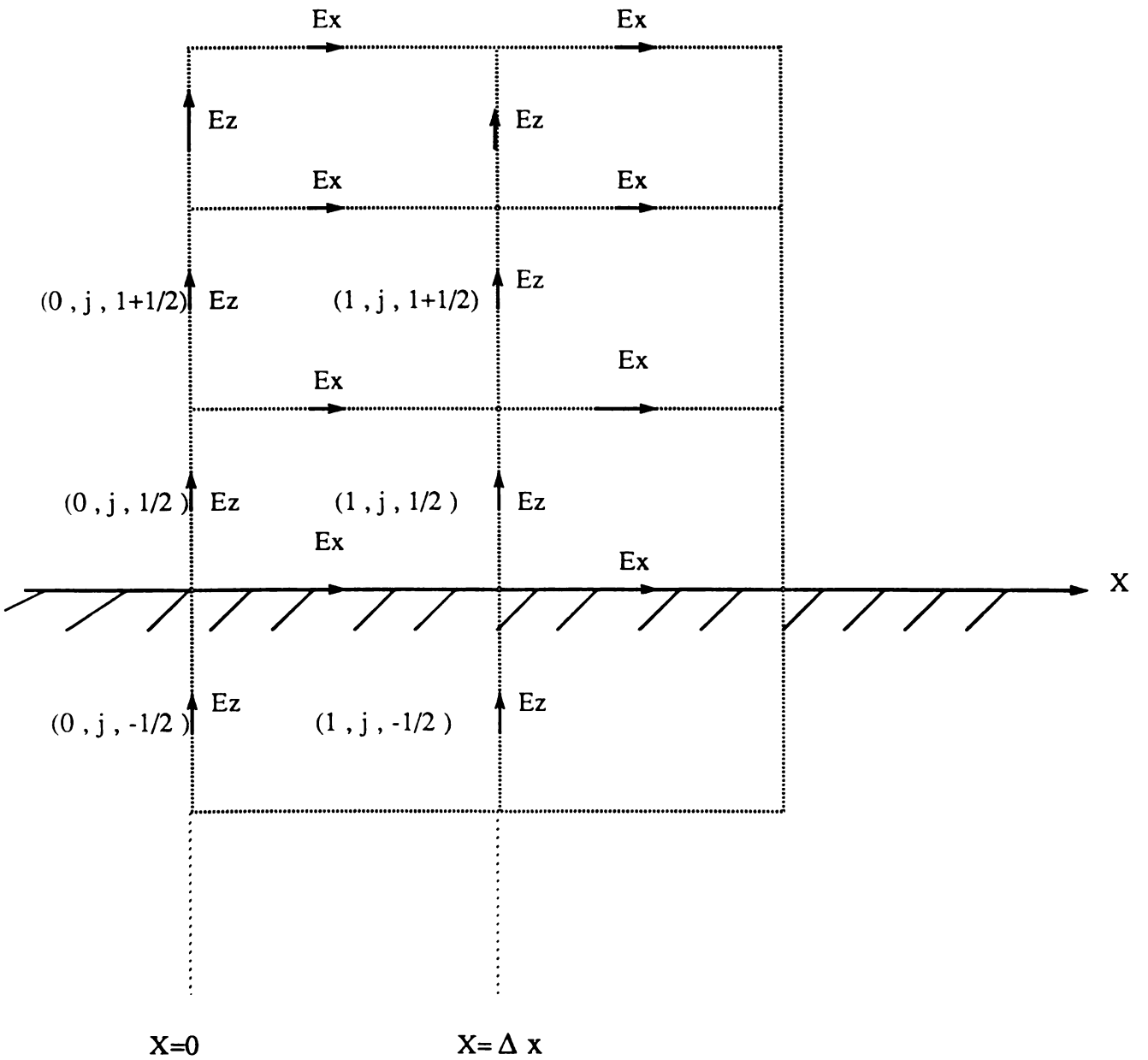

Fig. 5.6 Mur's Difference Scheme Near Ground Plane

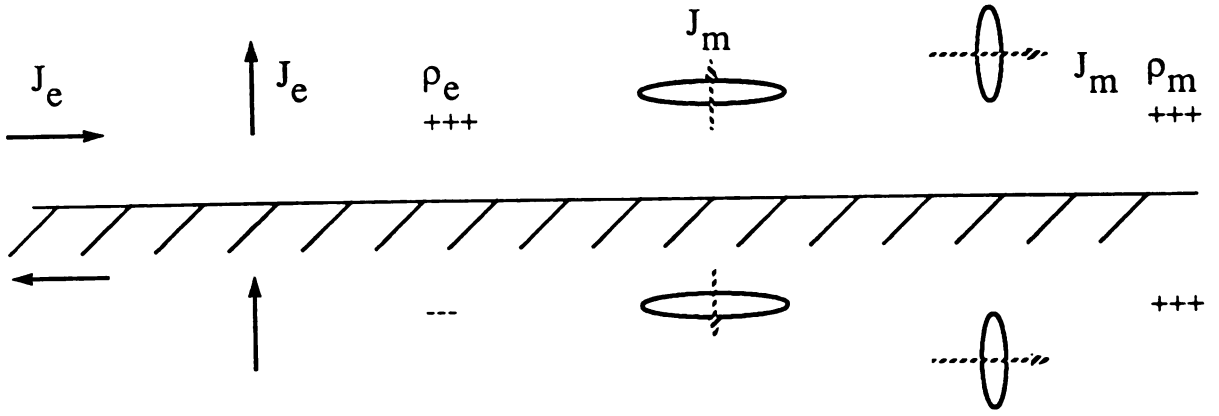

Fig. 5.7 Sources and Their Images

$$E_z^{n-1}(0, j, k+\frac{1}{2})] + \frac{2\Delta x}{c_0\Delta t+\Delta x}[E_z^n(1, j, k+\frac{1}{2}) + E_z^n(0, j, k+\frac{1}{2})]$$

$$+ \frac{(c_0\Delta t)^2\Delta x}{2\Delta y^2(c_0\Delta t+\Delta x)}[E_z^n(0, j+1, k+\frac{1}{2}) - 2E_z^n(0, j, k+\frac{1}{2}) + E_z^n(0, j-1, k+\frac{1}{2})$$

$$+ E_z^n(1, j+1, k+\frac{1}{2}) - 2E_z^n(1, j, k+\frac{1}{2}) + E_z^n(1, j-1, k+\frac{1}{2})]$$

$$\frac{(c_0\Delta t)^2\Delta x}{2\Delta z^2(c_0\Delta t+\Delta x)}[E_z^n(0, j, k+1+\frac{1}{2}) - 2E_z^n(0, j, k+\frac{1}{2}) + E_z^n(0, j, k-\frac{1}{2}) +$$

$$E_z^n(1, j, k+1+\frac{1}{2}) - 2E_z^n(1, j, k+\frac{1}{2}) + E_z^n(1, j, k-\frac{1}{2})] \qquad (5.4.1)$$

Equation (5.4.1) is the Mur's second order formulation at $x = 0$ for the wave propagating against the x-axis direction. It is exactly the same as (3.3.35a) if E_z is interchanged with W .

When $k = 0$, $E_z(0, j, +\frac{1}{2})$ is the field just above the ground plane, but $E_z^n(0, j, -\frac{1}{2})$ or $E_z^n(1, j, -\frac{1}{2})$ in (5.4.1) are the fields below the ground plane which should be substituted by $E_z^n(0, j, +\frac{1}{2})$ or $E_z^n(0, j, +\frac{1}{2})$. Therefore (5.4.1) becomes

$$E_z^{n+1}(0, j, +\frac{1}{2}) = -E_z^{n-1}(1, j, \frac{1}{2}) + \frac{c_0\Delta t-\Delta x}{c_0\Delta t+\Delta x}[E_z^{n+1}(1, j, \frac{1}{2}) + E_z^{n-1}(0, j, \frac{1}{2})]$$

$$+ \frac{2\Delta x}{c_0\Delta t+\Delta x}[E_z^n(1, j, \frac{1}{2}) + E_z^n(0, j, \frac{1}{2})]$$

$$+ \frac{(c_0\Delta t)^2\Delta x}{2\Delta y^2(c_0\Delta t+\Delta x)}[E_z^n(0, j+1, +\frac{1}{2}) - 2E_z^n(0, j, +\frac{1}{2}) + E_z^n(0, j-1, \frac{1}{2})$$

$$+ E_z^n(1, j+1, \frac{1}{2}) - 2E_z^n(1, j, \frac{1}{2}) + E_z^n(1, j-1, \frac{1}{2})]$$

$$\frac{(c_0\Delta t)^2\Delta x}{2\Delta z^2(c_0\Delta t+\Delta x)}[E_z^n(0, j, 1+\frac{1}{2}) - E_z^n(0, j, \frac{1}{2})) +$$

$$E_z^n(1, j, 1+\frac{1}{2}) - E_z^n(1, j, \frac{1}{2}))] \qquad (5.4.2)$$

5.5 Fields in the Scattered Field Region

In the scattered field region, only outgoing waves are considered so that one can apply the radiation boundary condition. As shown in Fig.5.8, the total fields can be decomposed into incident field $\mathbf{E}^i$, reflected field $\mathbf{E}^r$ with the aperture absent, and scattered field produced by the aperture field $\mathbf{E}^s$. It is easy to see that the field produced by aperture field is an outgoing wave exiting the outermost truncated surface, and the incident field and the reflected field are known. The total fields then can be represented by:

$$\mathbf{E}^{total}(\mathbf{r}) = \mathbf{E}^i(\mathbf{r}) + \mathbf{E}^r(\mathbf{r}) + \mathbf{E}^s(\mathbf{r}) \tag{5.5.1}$$

where $\mathbf{E}^i(\mathbf{r}) + \mathbf{E}^r(\mathbf{r})$ are known functions and E^s is an outgoing wave exiting the truncated region. A radiation boundary condition now can be applied to the $\mathbf{E}^s$ in the scattered field region.

5.6 Backscattered Fields

When an excitation or driving force is a sinusoidal function, a steady state is reached after a certain period of time. The fields at any points in the truncated region can be obtained after sufficient iterations. To calculate the far zone scattered fields or radiation fields, it is easer to use equivalent surface sources based on the equivalence principle as shown in Fig 5.9(a).

On the aperture S_p , $\hat{n}\times\mathbf{E} \neq 0$ and $\hat{n}\times\mathbf{H} \neq 0$. On the ground screen S_0 , $\hat{n}\times\mathbf{E} = 0$ but $\hat{n}\times\mathbf{H} \neq 0$. The scattered fields are evaluated as

$$\mathbf{E}^s(\mathbf{r}) = \frac{1}{4\pi}\int_{S_0+S_p}\left[(\hat{n}'\times\mathbf{E})\times\nabla'\Phi + (\hat{n}'\cdot\mathbf{E})\nabla'\Phi - j\omega\mu(\hat{n}'\times\mathbf{H})\Phi\right] dS' \tag{5.6.1a}$$

$$\mathbf{H}^s(\mathbf{r}) = \frac{1}{4\pi}\int_{S_0+S_p}\left[(\hat{n}'\times\mathbf{H})\times\nabla'\Phi + (\hat{n}'\cdot\mathbf{H})\nabla'\Phi + j\omega\mu(\hat{n}'\times\mathbf{E})\Phi\right] dS' \tag{5.6.1b}$$

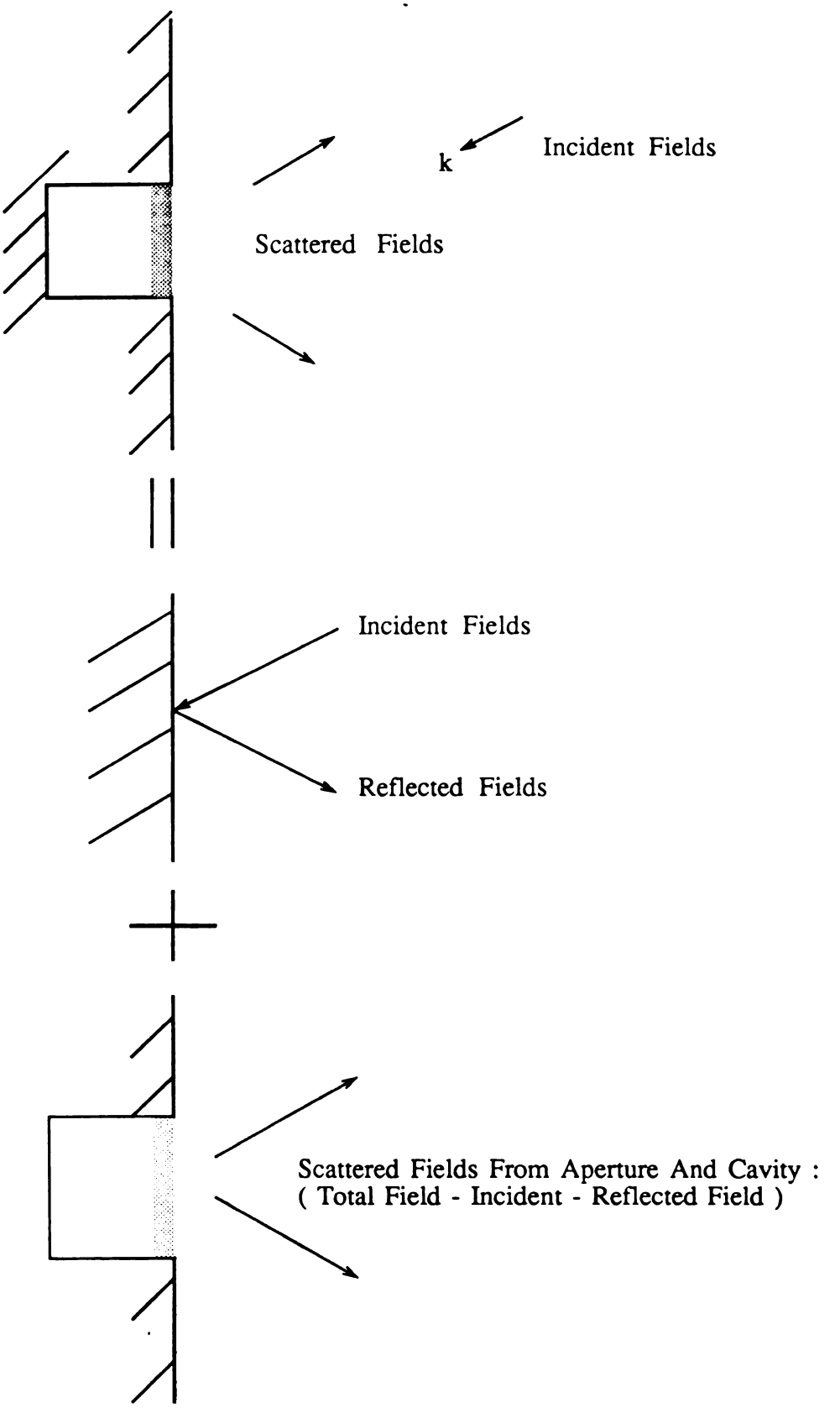

Fig. 5.8 Decomposion of Total Fields in the Scattered Field Region

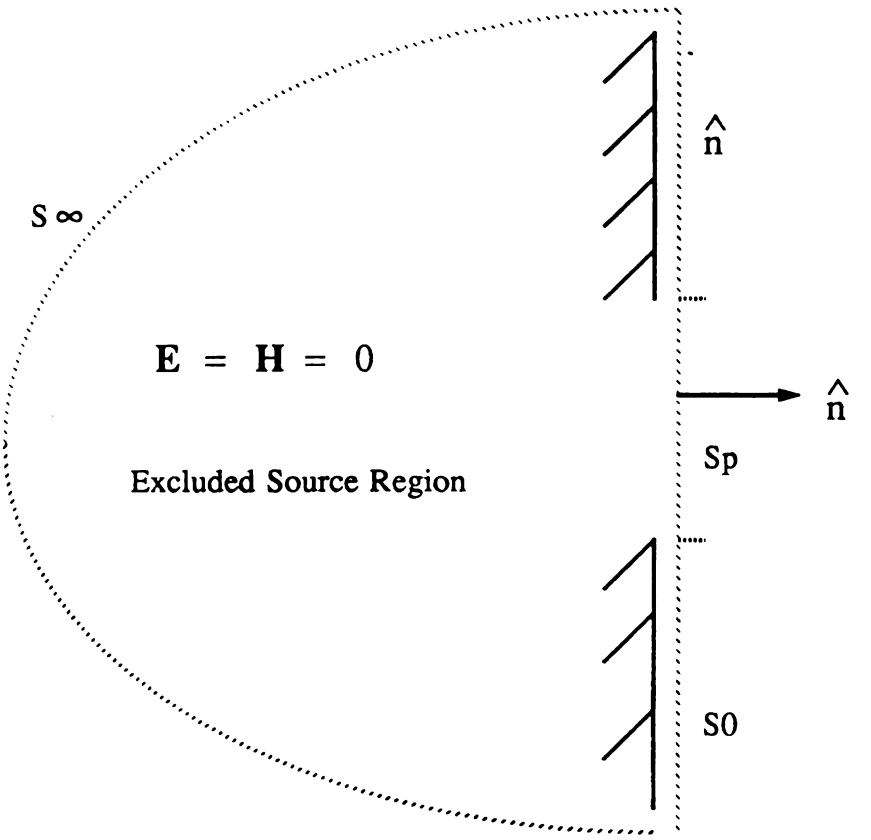

(a)

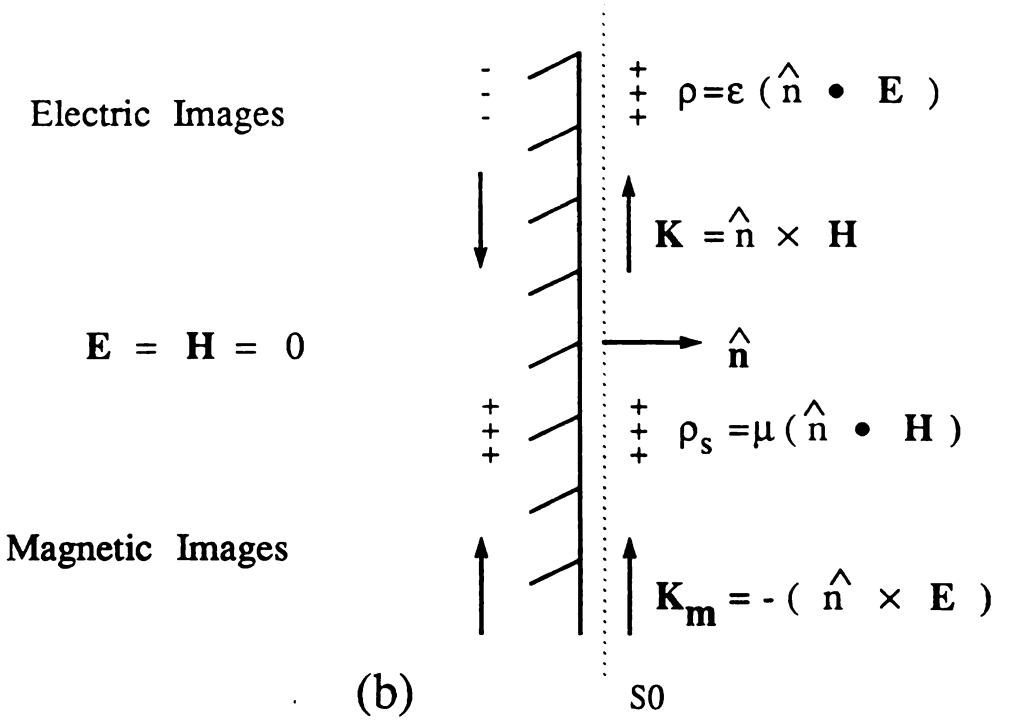

(b)

Fig. 5.9 Aperture Fields and Their Images

where the integration is over the aperture and the entire ground plane. Since equivalent surface currents are only known on the finite aperture region, it is desirable to eliminate the contribution of $n\times\mathbf{H}$ and $\hat{n}\cdot\mathbf{E}$ over the ground plane. Because the surface fields maintain the null field within the excluded region, then nothing is changed if that region is backed by a perfect conductor. The resulted image system is indicated in Fig.5.9(b):

By the image theory, electric sources are annulled by their images while the magnetic source and their images are additive in effect. This leads to the conclusion that $\hat{n}\times\mathbf{E}$ is the only effective surface current such that:

$$\mathbf{E}^s(\mathbf{r}) = \frac{1}{2\pi}\int_{S_p} (\hat{n}'\times\mathbf{E})\times\nabla'\Phi \, dS' \tag{5.6.2a}$$

$$\mathbf{H}^s(\mathbf{r}) = \frac{1}{2\pi}\int_{S_p}\left[(\hat{n}'\cdot\mathbf{H})\nabla'\Phi + j\omega\mu(\hat{n}'\times\mathbf{E})\Phi\right] dS' \tag{5.6.2b}$$

where $\Phi = \dfrac{e^{-jkR}}{R}$ and $R = |\mathbf{r} - \mathbf{r}'|$. Under far zone approximation:

$$\nabla'\Phi \approx \hat{r}jk\frac{e^{-jkr}}{r}e^{jk\hat{r}\cdot\hat{r}'} \tag{5.6.3}$$

when $|\mathbf{r}|\gg|\mathbf{r}'|$ and $kR\gg 1$. The radiated fields are:

$$\mathbf{E} \approx \frac{-jk}{2\pi}\frac{e^{-jkr}}{r}\hat{r}\times\int_{S_p}(\hat{n}'\times\mathbf{E})\, e^{jk\hat{r}\cdot\hat{r}'} dS' \tag{5.6.4a}$$

$$\mathbf{H} = (\hat{r}\times\mathbf{E})/\eta \tag{5.6.4b}$$

and radar cross section is given by

$$\sigma = 2\pi r^2\left|\frac{\mathbf{E}^s(\mathbf{r})}{\mathbf{E}^0}\right|^2 \tag{5.6.5}$$

As r approaches ∞ (5.6.5) becomes:

$$\sigma = \frac{k^2}{2\pi}\left|\int_{S_0}(\hat{n}\times\frac{\mathbf{E}}{\mathbf{E}_0})\times\hat{r}\, e^{jk\hat{r}\cdot\hat{r}'} dS'\right|^2 \tag{5.6.6}$$

or

$$\frac{\sigma}{\lambda^2} = \frac{k^4}{8\pi^3}\left|\int_{S_0}(\hat{n}\times\frac{\mathbf{E}}{\mathbf{E}_0})\times\hat{r}\, e^{jk\hat{r}\cdot\hat{r}'} dS'\right|^2 \tag{5.6.7}$$

In the y-z plane, the unit vector $\hat{r} = \cos\theta\hat{z} + \sin\theta\hat{y}$, $\vec{r'} = x'\hat{x} + y'\hat{y}$ and $\hat{n}\times\mathbf{E} = E_x\hat{y} - E_y\hat{x}$. Radar cross section in y-z plane becomes:

$$\frac{k^4}{8\pi^3}\left|\int_{S_0}(E_x\hat{x}\cos\theta + E_y\hat{y}\cos\theta - E_y\hat{z}\sin\theta)e^{jky'\sin\theta}dS'\right|^2 \tag{5.6.8}$$

Similarly in the x-z plane, $\hat{r} = \cos\theta\hat{z} + \sin\theta\hat{x}$, $\vec{r'} = x'\hat{x} + y'\hat{y}$ and $\hat{n}\times\mathbf{E} = E_x\hat{y} - E_y\hat{x}$. Radar cross section in y-z plane is given by

$$\frac{k^4}{8\pi^3}\left|\int_{S_0}(E_x\hat{x}\cos\theta + E_y\hat{y}\cos\theta - E_x\hat{z}\sin\theta)e^{jkx'\sin\theta}dS'\right|^2 \tag{5.6.9}$$

5.7 Numerical Results

5.7.1 Open Cavity situated in the Ground Plane

Use the algorithms discussed in proceeding sections, fields at any points in the truncated region can be calculated. First consider an open cavity situated in the ground plane without an antenna inside. The field distributions inside the cavity and on the aperture, and the radar cross section are calculated when a plane wave is incident on the cavity. The effects of an impedance sheet on the radar cross section and field distributions are also studied.

As shown in Fig.(5.10), each side of the aperture is one wavelength long, and the depth of the cavity is also one wavelength long. A plane wave is normally incident on the ground screen. In the FD-TD computer code used for all the following numerical data, each side of the cavity is divided into twenty-one cells and the radiation boundary is set about fifteen cells away from the aperture. Two cases are considered which are an open cavity with empty aperture and an open cavity with its aperture covered by an electrically lossy film. Figs. (5.10a) and (5.11a) show the distribution of the tangential components of electric field E^s on the aperture without film covered, and Figs. (5.10b) and (5.11b) show that when the aperture is covered by an infinitely thin,

electrically lossy sheet of $\sigma t = 0.01$. By comparing these two cases, the difference between field distributions can be seen. Fig. (5.12) shows the radar cross section in the X-Z plane and the Y-Z plane for the two cases. The radar cross section is reduced by 10 db in Fig.(5.13) when a resistive film is presented.

When aperture is empty, Figs.(5.10a), (5.11a) and Fig. (5.14) exhibit three components of the electric field $\mathbf{E}_s$ on the aperture and E_z is plotted half cell above, E_z^s, and half cell below, E_z^{total}, the plane of aperture according to the location of Yee's model. It can be seen that the x component is much greater than the y component of electric field and E_z component is changed greatly across the aperture plane.

When the aperture is empty, the total fields inside the cavity at the plane of $z = -d+5*dz$ which is 5 cells away from the bottom are plotted in Figs. (5.15-5.16). It is also interesting to see the variation of the total field distributions along the z direction in both the x-z plane and the y-z plane as shown in Figs. (5.17-5.21). The fields of E_x and H_y are two dominant components which are also plotted for the case of an electrically lossy impedance sheet with $\sigma t = 0.01$ covering over the aperture as shown in Figs. (5.40-5.44). Comparison of Figs. (5.20-5.21) with Figs. (5.17-5.18) indicates that the structures of field distributions are the same while the amplitudes of the fields are reduced as an impedance sheet is covered over the aperture.

5.7.2 Cavity Backed Antenna

Receiving Characteristics

Figure (5.22) shows a cavity backed antenna where cavity size is the same as described above. The antenna is placed parallel to the incident electric field. The plane wave is normally incident on the cavity. The antenna is about half wavelength long and one cell size thick. It is centrally fed by 50 ohm. The antenna is located

17/20 wavelength away from the bottom of the cavity where the x component of electric field reaches maximum in the absence of the antennna as shown in Fig.(5.20). The loaded impedance is accounted by taking the conductivity of central cell of the antenna to be $\sigma = \frac{\Delta x}{\Delta z \Delta y Z_m}$ where $Z_m = 50 ohm$.

The aperture fields are shown in Figs. (5.22-5.23) and the radar cross sections are plotted in Fig. (5.24). We didn't see a significant difference in the field distributions for the case of an open cavity and the case of a cavity-backed antenna for this size of cavity. The radar cross section is reduced more than 10db if an infinite thin film with $\sigma t = 0.01$ is placed over the aperture.

As shown in Figs. (5.25-5.26), the field distributions inside the cavity are greatly changed when the film is on the aperture. The discontinuities of the fields at both ends and the center of the antenna are observed. The boundary conditions on both the walls and the antenna are seen to be satisfied.

A comparison of current distributions on the antenna is given in Fig. (5.27) which shows the effect of an electrically lossy sheet on the antenna. The received power of the antenna without a film covered is -54.4 db, while it is reduced to -65.6 db when the film is covered. Unfortunately, the received power is also reduced about 10 db, which is almost the same as the radar cross section. This is not what we expected. We expect to reduce the radar cross section of an airborne antenna but not to degrade its receiving property by covering the antenna with an impedance sheet.

The comparison between the open cavity and the cavity backed antenna on the ground plane shows that the reductions in their radar cross sections when the film is on the aperture are almost the same, which is about 10 db, for the geometry chosen.

The unsatisfactory reduction in the radar cross section may be due to the fact that the scattering properties are strong functions of cavity parameters. In our numerical

example, the cavity is at resonance. The scattered fields produced by the aperture and the cavity are dominant, which is much stronger than that produced by the antenna.

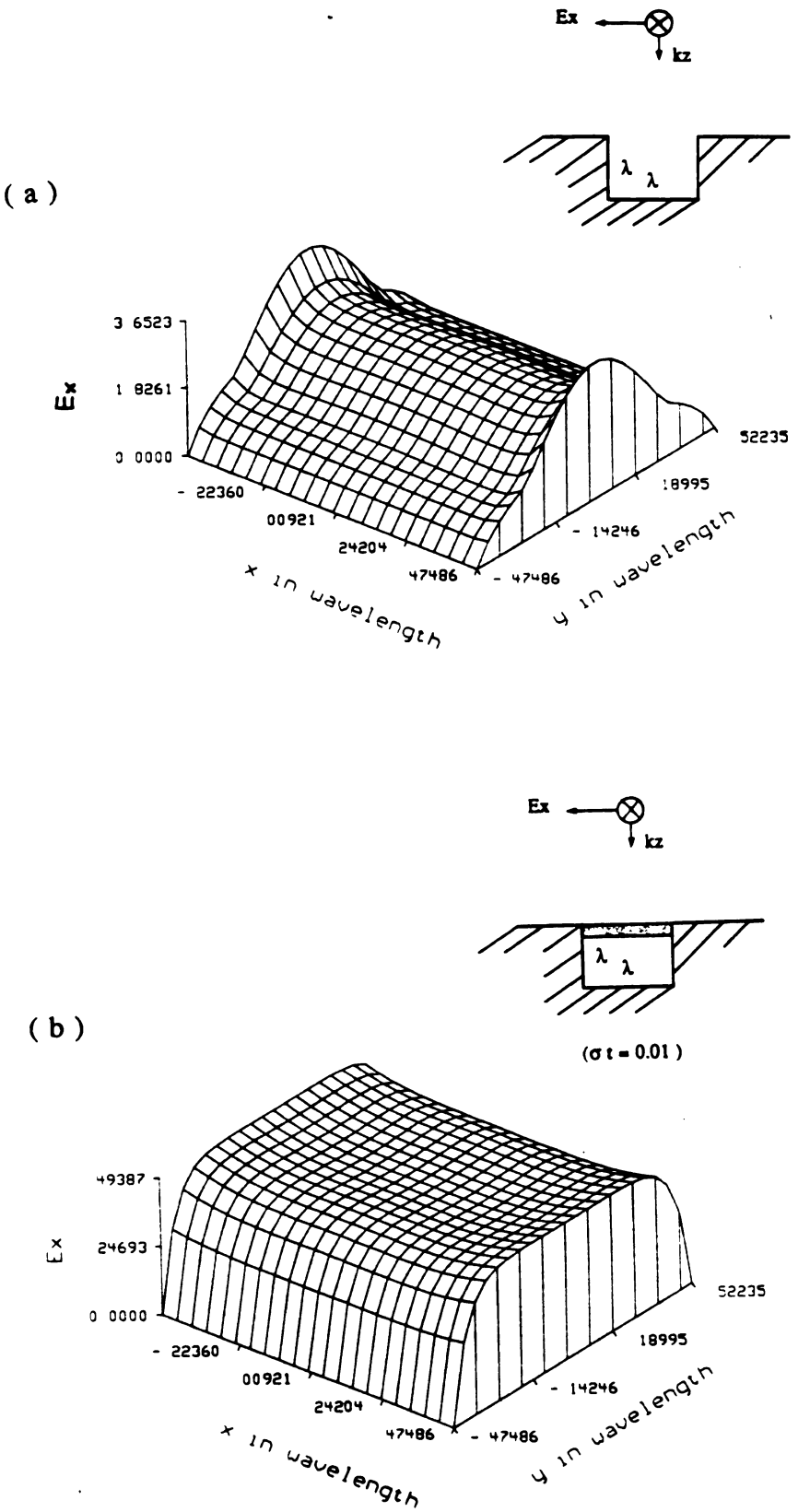

Figure 5.10 (a) x-component of scattered electric field on the empty aperture of an opened cavity in the ground screen; (b) x-component of scattered electric field on the aperture covered with an impedance sheet.

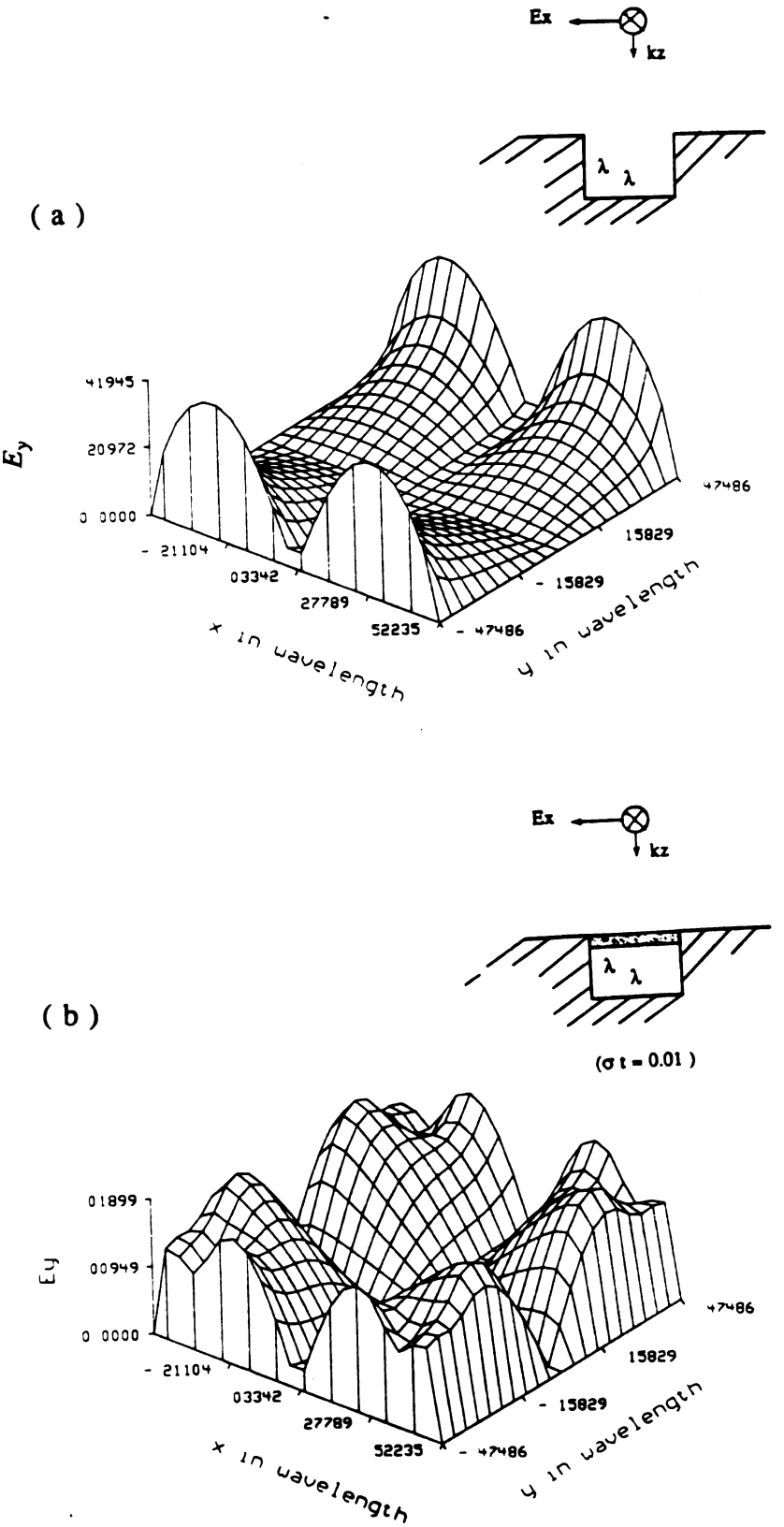

Figure 5.11 (a) y-component of scattered electric field on the empty aperture of an opened cavity in the ground screen; (b) y-component of scattered electric field on the aperture covered with an impedance sheet.

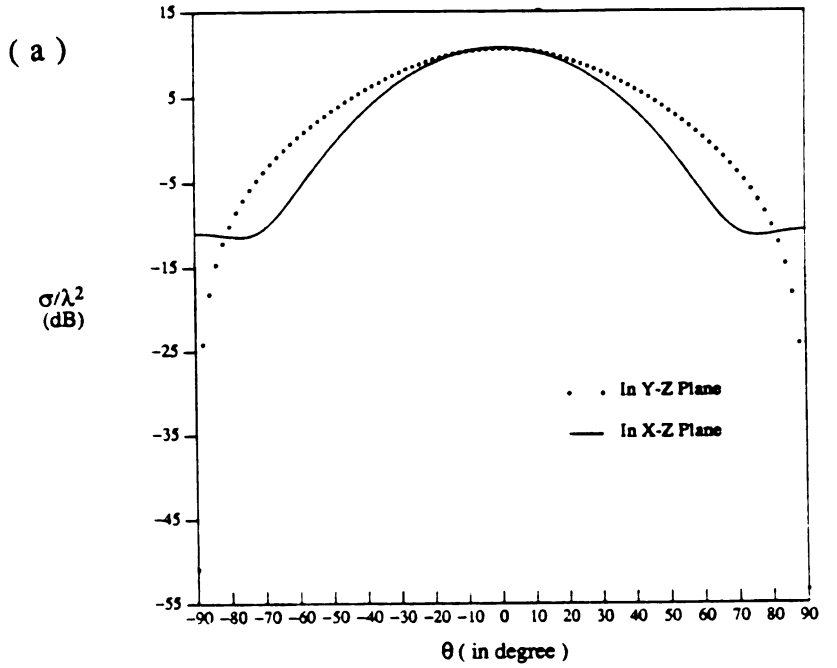

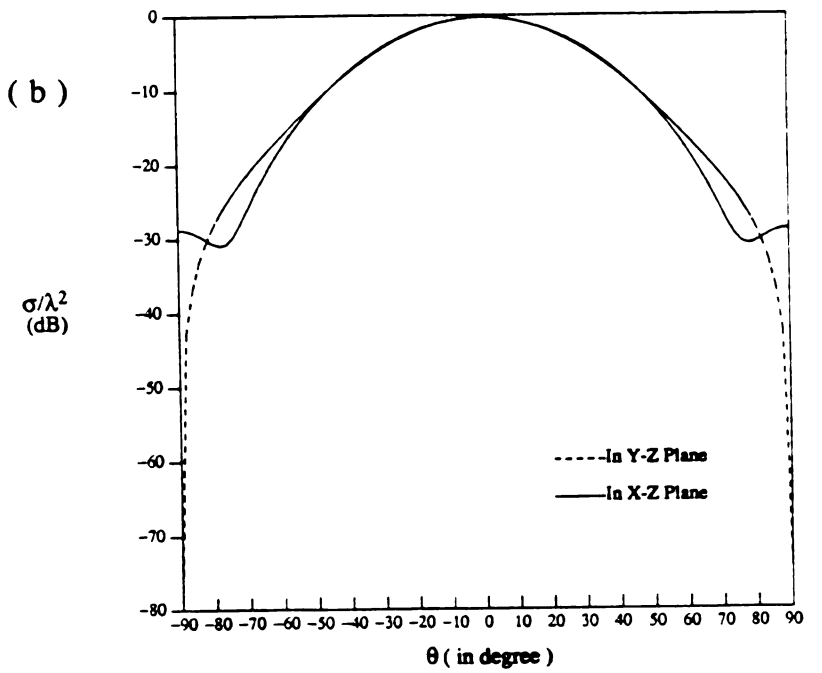

Figure 5.12 Radar cross section of an opened cavity ($k_0a = 2\pi$, $d/\lambda = 1$) when a plane wave is normally incident on it ($\theta = 0.0$): (a) an opened cavity with its aperture empty; (b) an opened cavity with its aperture covered by a thin film ($\sigma t = 0.01$).

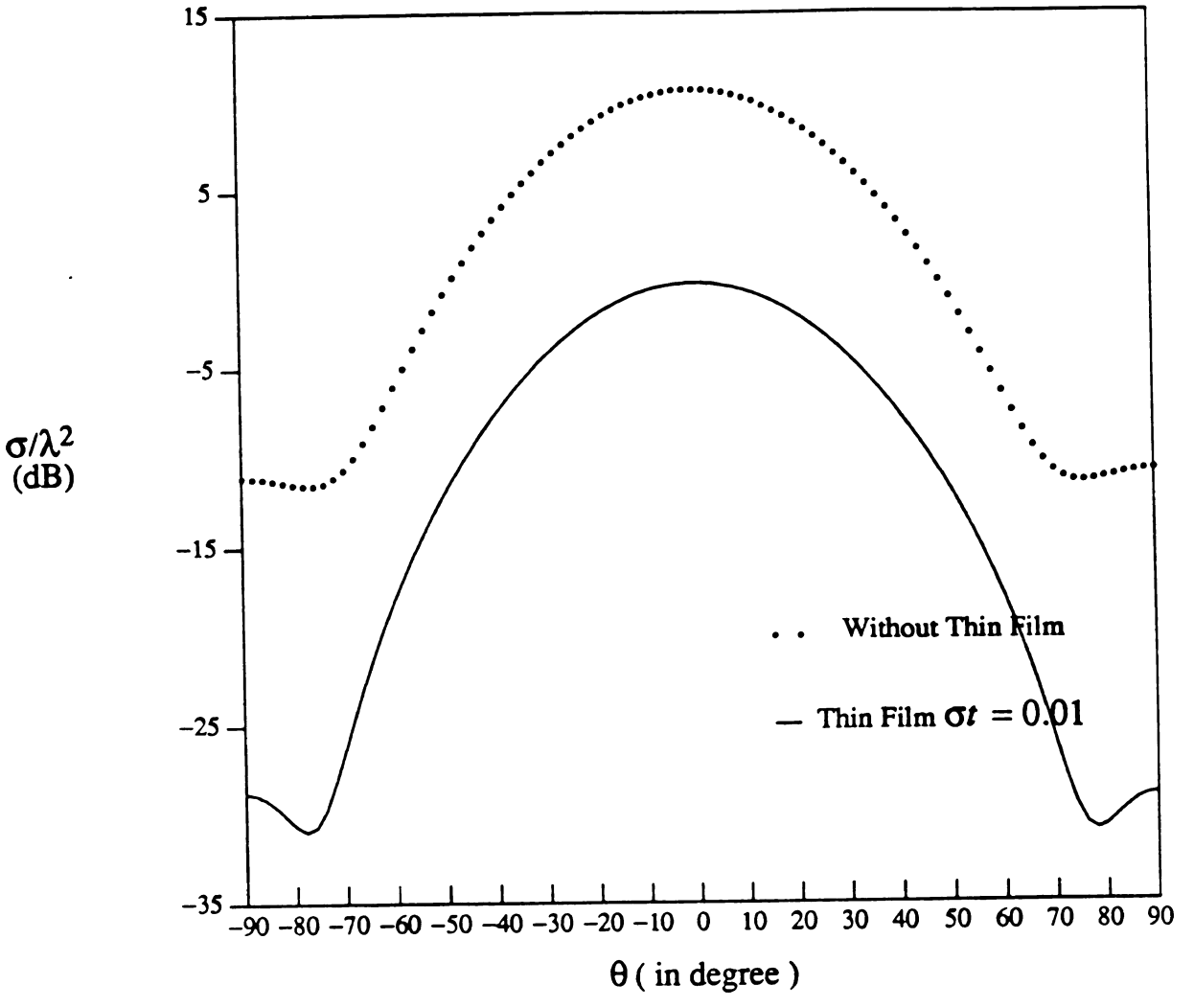

Figure 5.13 Comparison of radar cross sections in the X-Z plane of an opened cavity ($k_0a = 2\pi$, $d/\lambda = 1$) when a plane wave is normally incident on it ($\theta = 0.0$).

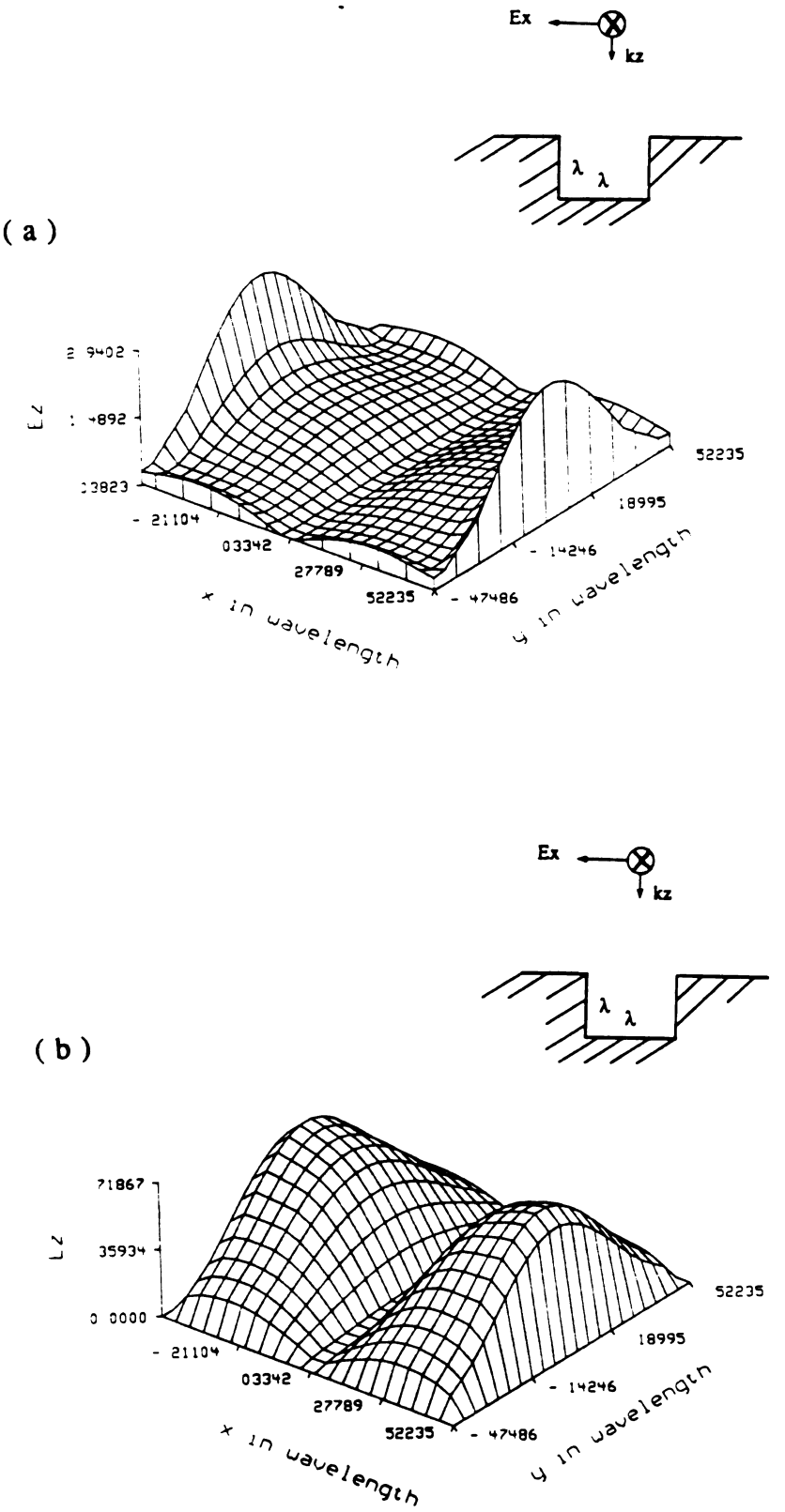

Figure 5.14 z-component of electric field on the empty aperture of an opened cavity in the ground screen: (a) E_z at half cell above the aperture; (b) E_z at half cell below the aperture.

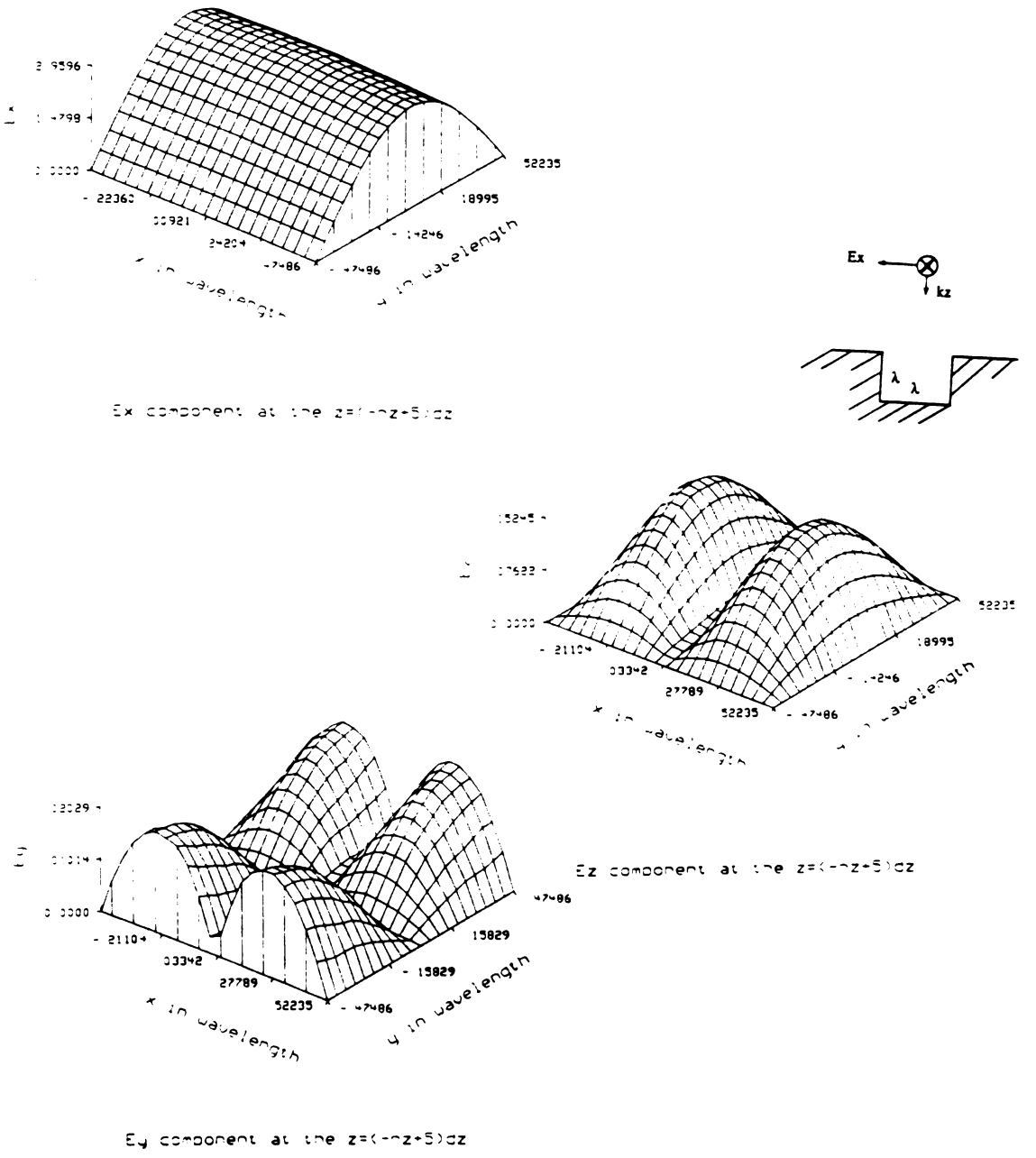

Figure 5.15 Total electric field distribution at the plane $z = -d + 5dz$ which is 5 cells away from the bottom of the cavity ($k_0a = 2\pi$, $d/\lambda = 1$) when a plane wave is normally incident on it ($\theta = 0.0$) and no film is covered on the aperture.

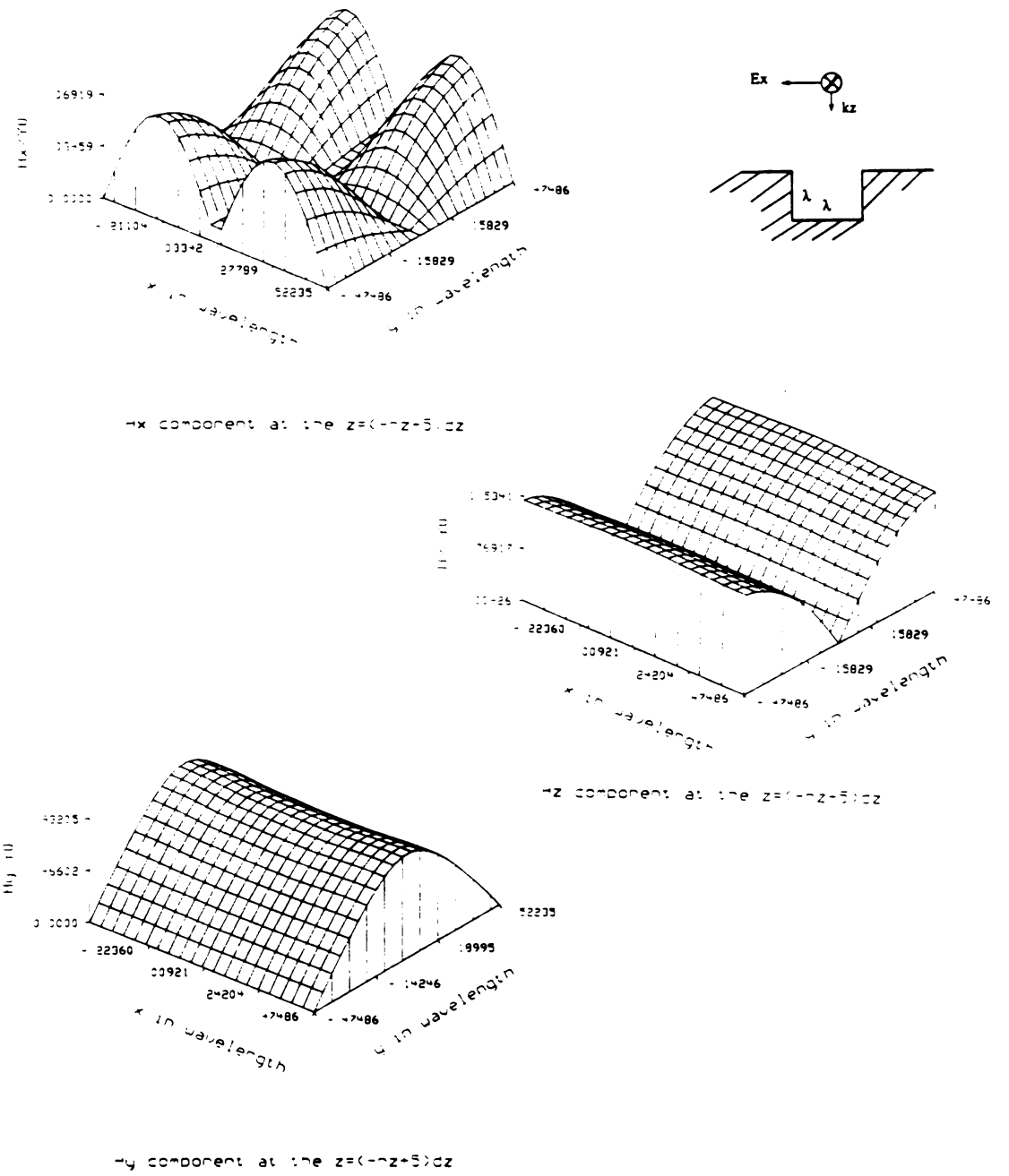

Figure 5.16 Total magnetic field distribution at the plane $z = -d + 5dz$ which is 5 cells away from the bottom of the cavity ($k_0a = 2\pi$, $d/\lambda = 1$) when a plane wave is normally incident on it ($\theta = 0.0$) and no film is covered on the aperture.

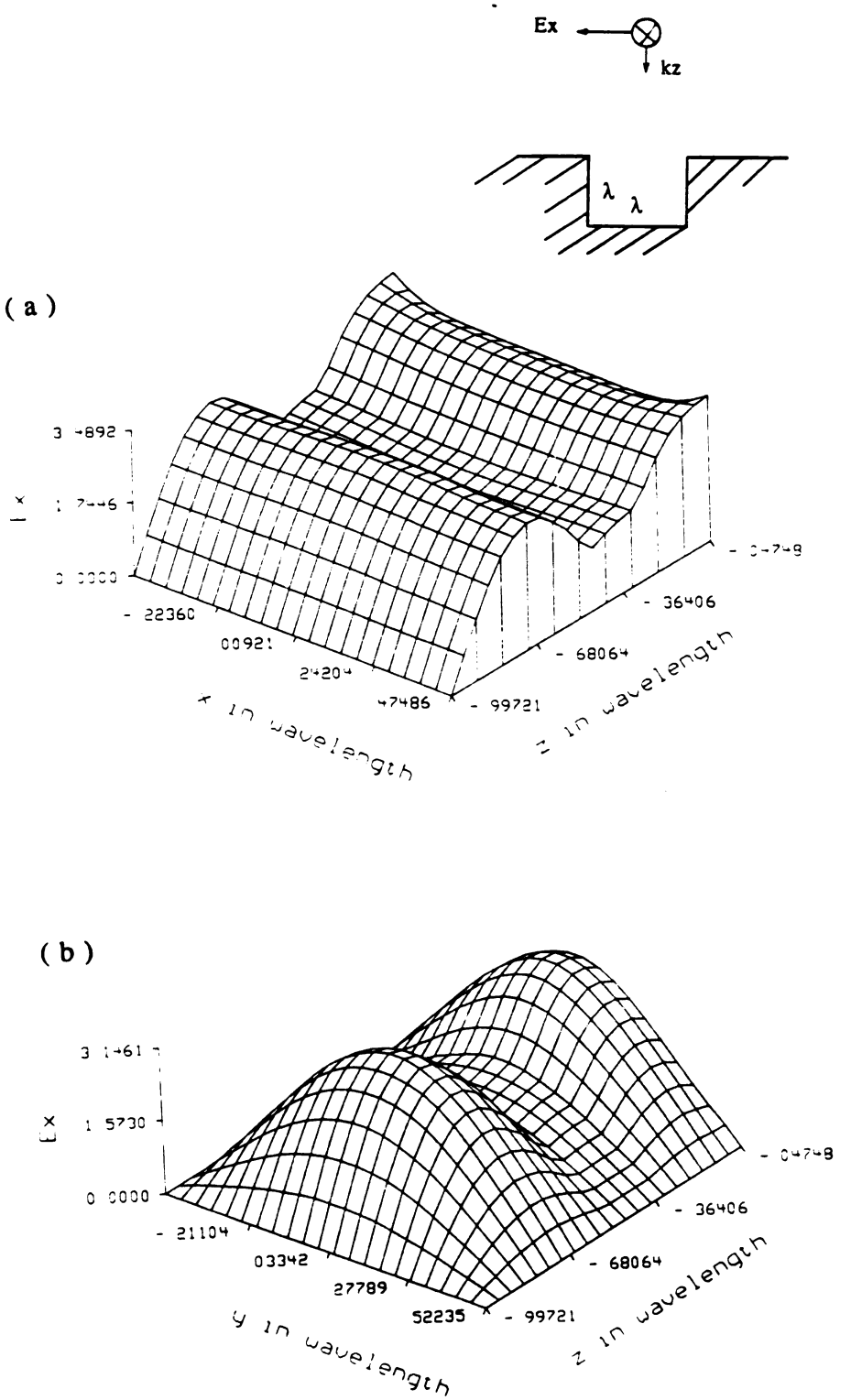

Figure 5.17 (a) x-component of total electric field in the X-Z plane inside the cavity with its aperture empty; (b) x-component of total electric field in the Y-Z plane inside the cavity with its aperture empty.

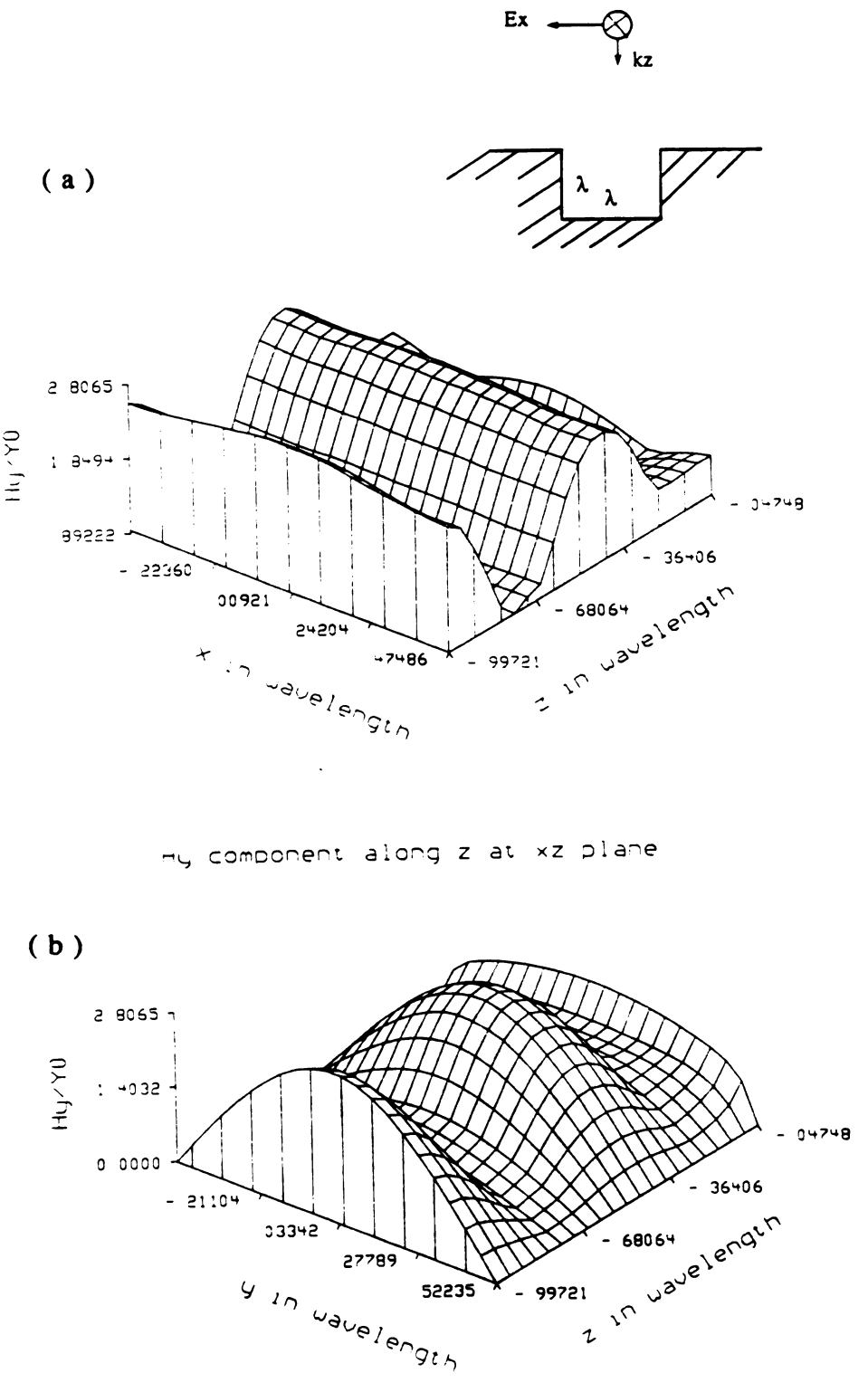

Figure 5.18 (a) *y*-component of total magnetic field in the X-Z plane inside the cavity with its aperture empty; (b) *y*-component of total magnetic field in the Y-Z plane inside the cavity with its aperture empty.

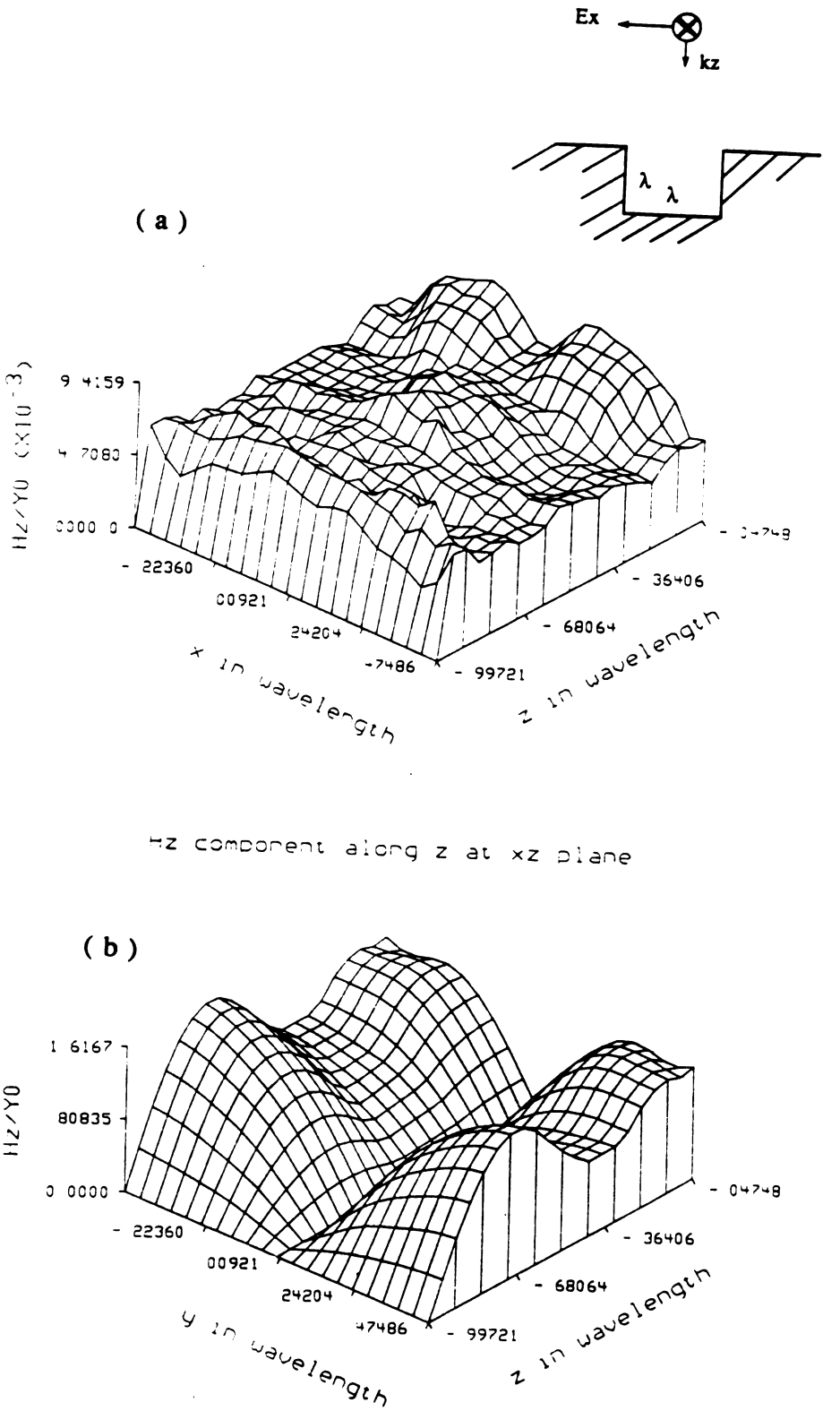

Figure 5.19 (a) z-component of total magnetic field in the X-Z plane inside the cavity with empty aperture; (b) z-component of total magnetic field in the Y-Z plane inside the cavity with its aperture empty.

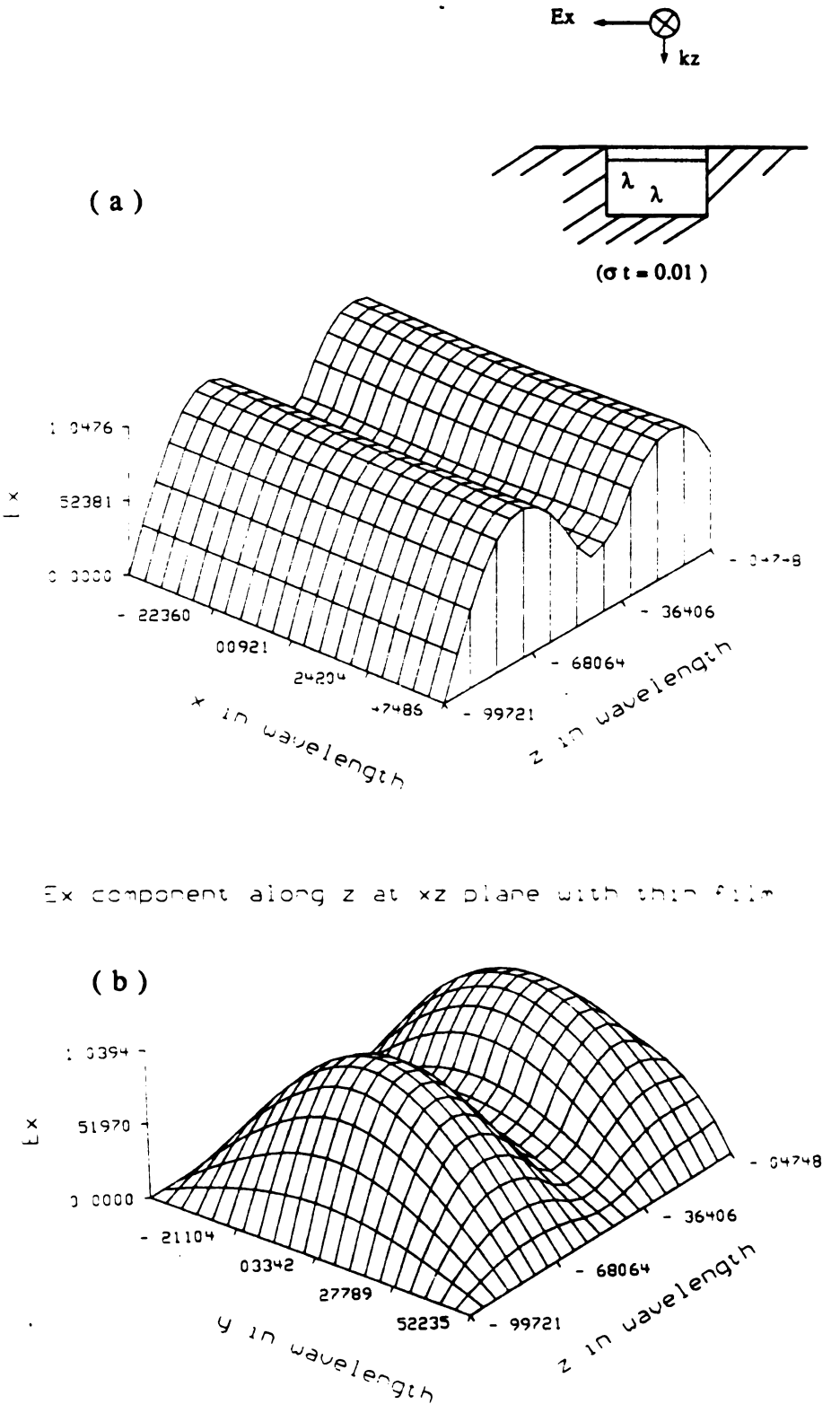

Figure 5.20 (a) x-component of total electric field in the X-Z plane inside the cavity with its apertutre covered by an impedance film; (b) x-component of total electric field in the Y-Z plane inside the cavity with its aperture covered by an impedance film.

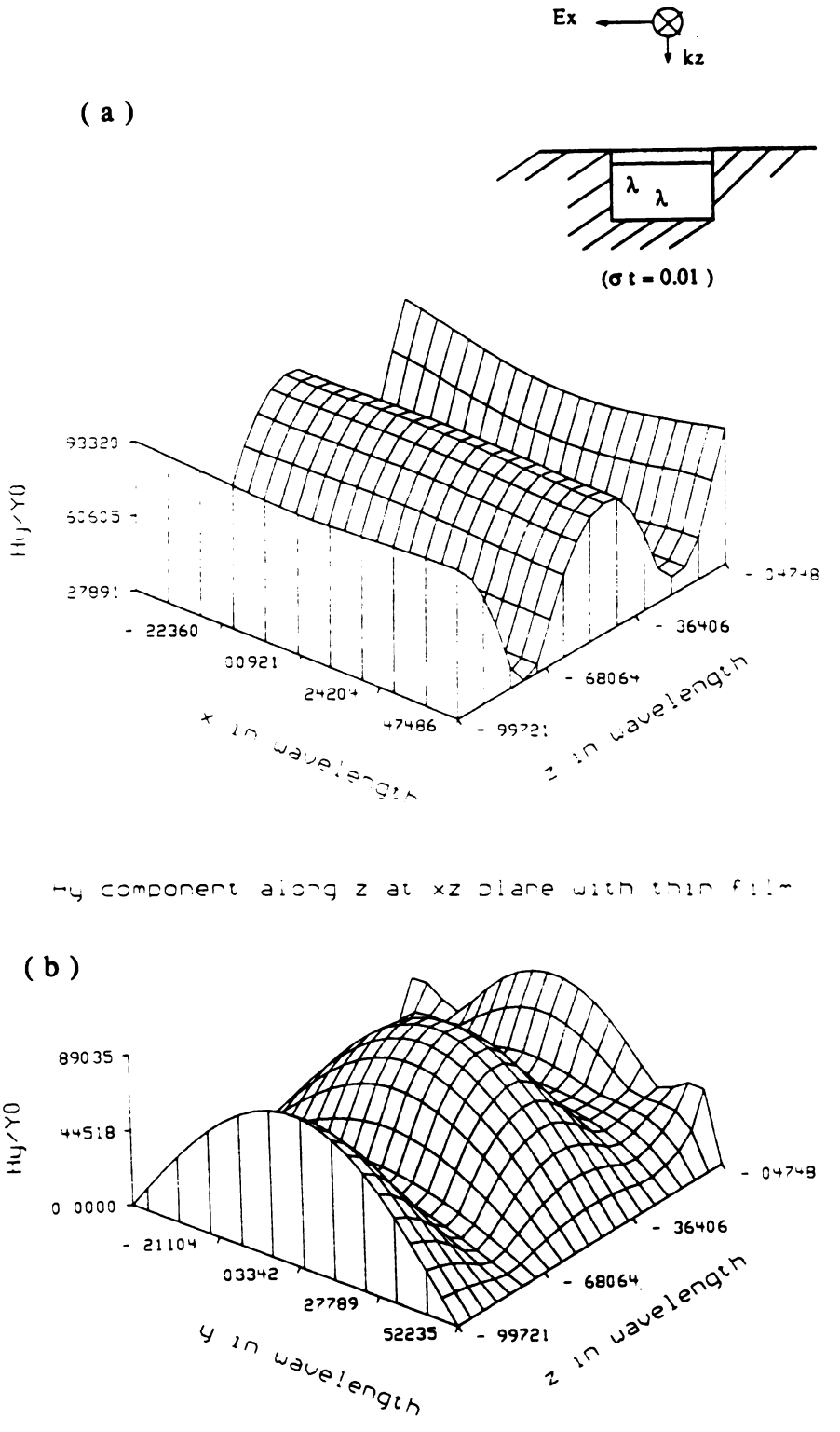

Figure 5.21 (a) *y*-component of total magnetic field in the X-Z plane inside the cavity with its aperture covered by an impedance film; (b) *y*-component of total magnetic field in the Y-Z plane inside the cavity with its aperture covered by an impedance film.

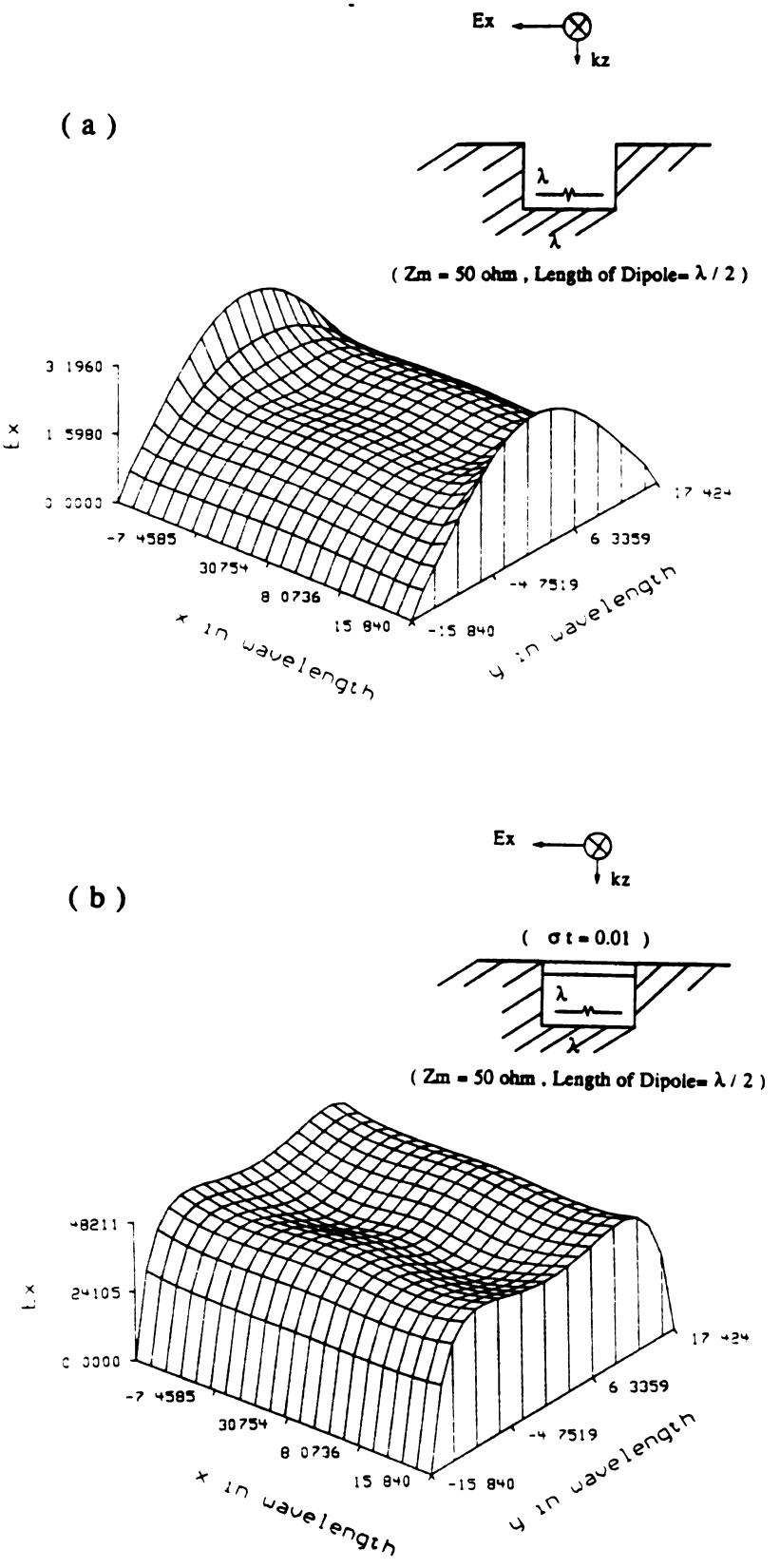

Figure 5.22 (a) x-component of scattered electric field on the empty aperture of a cavity-backed antenna; (b) x-component of electric field on the impedance-film covered aperture of a cavity-backed antenna.

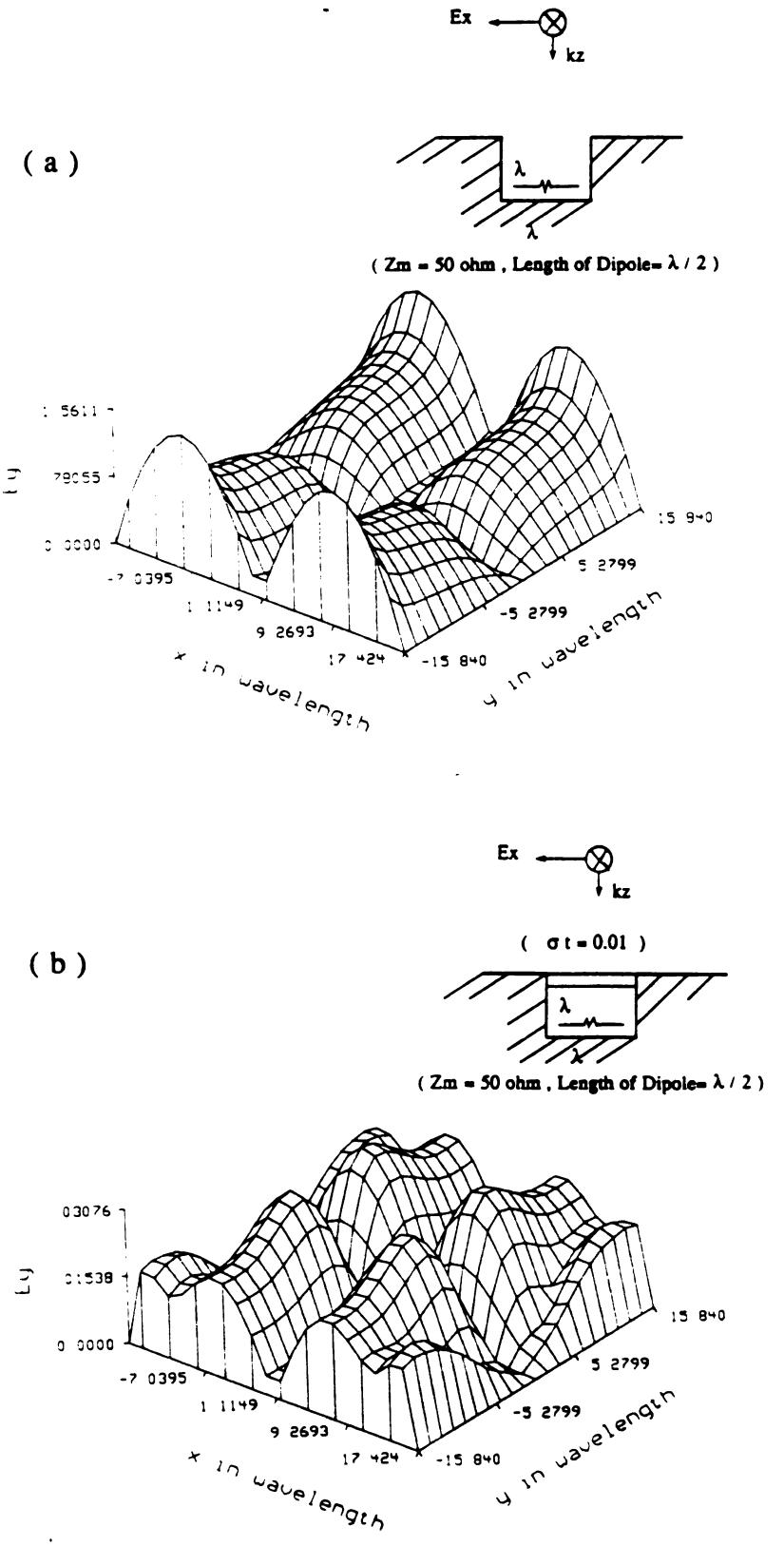

Figure 5.23 (a) y-component of scattered electric field on the empty aperture of a cavity-backed antenna; (b) y-component of electric field on the impedance-film covered aperture of a cavity-backed antenna.

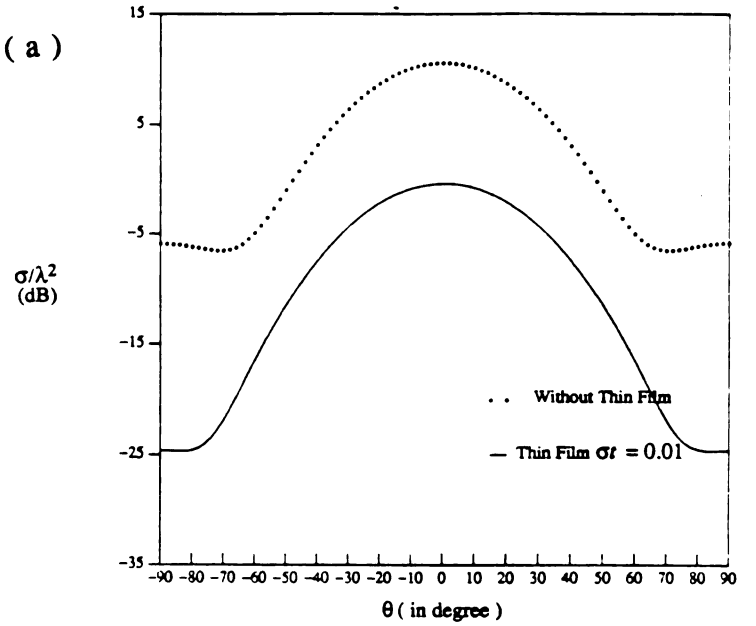

Figure 5.24 Comparison of radar cross sections of a cavity-backed antenna ($k_0a = 2\pi$, $d/\lambda = 1$, location of the antenna $h/\lambda = 17/21$, $Z_m = 50$ *ohms*) when a plane wave is normally incident on it ($\theta = 0.0$): (a) Radar cross section in the X-Z plane; (b) Radar cross section in the Y-Z plane.

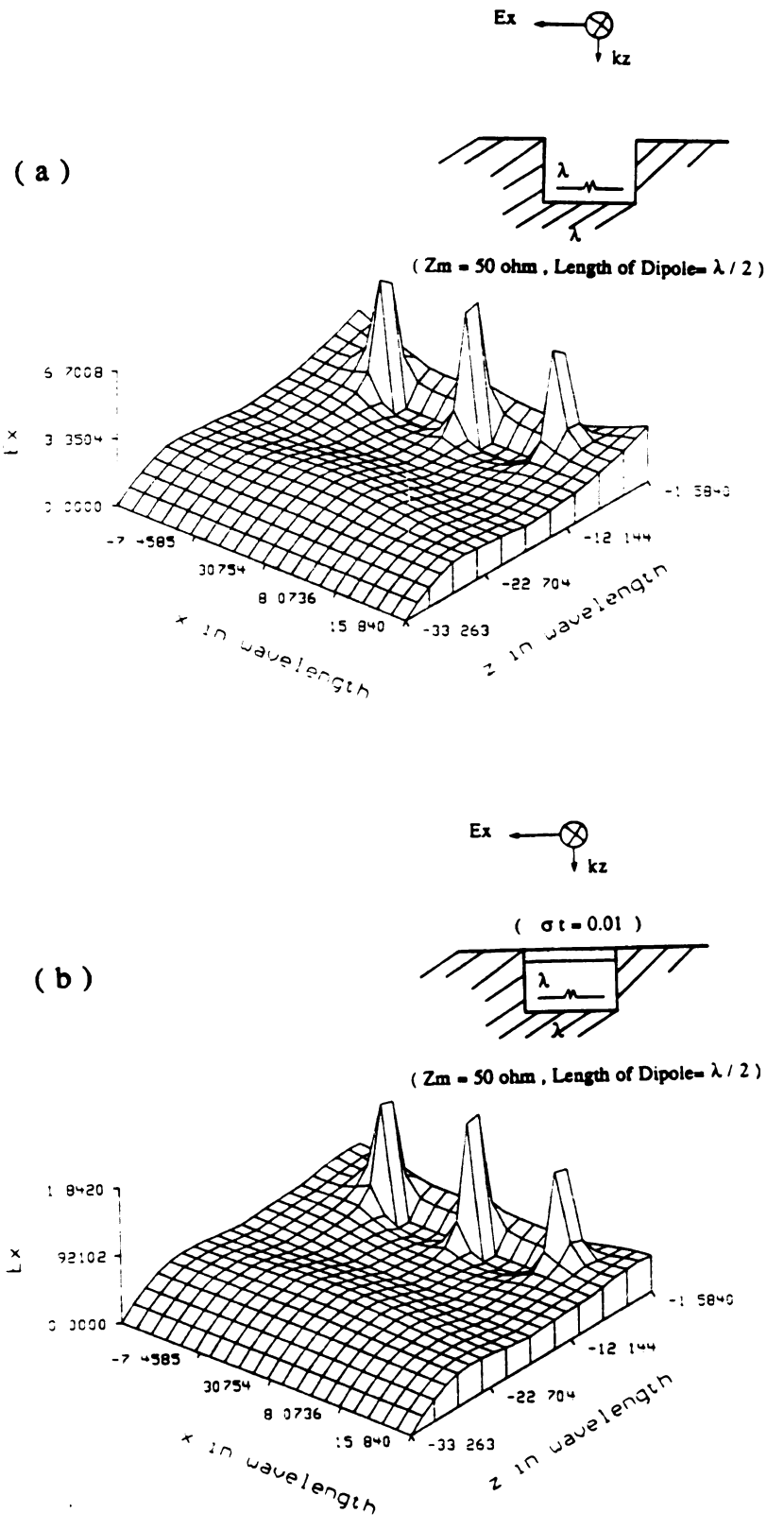

Figure 5.25 (a) x-component of total electric field in the X-Z plane inside the cavity produced by a cavity-backed antenna with its aperture empty; (b) x-component of total electric field in the X-Z plane inside the cavity produced by a cavity-backed antenna with its aperture covered by an impedance film.

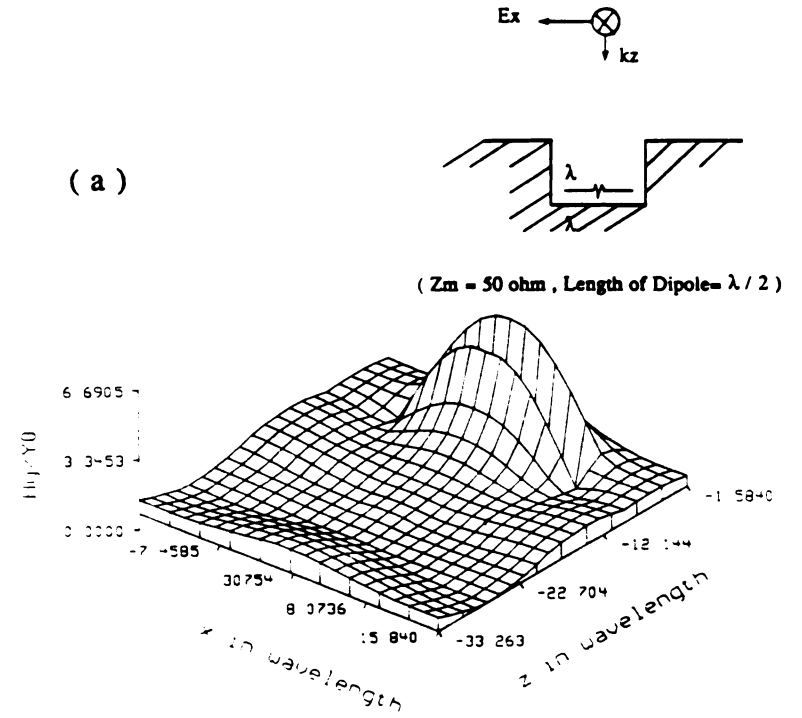

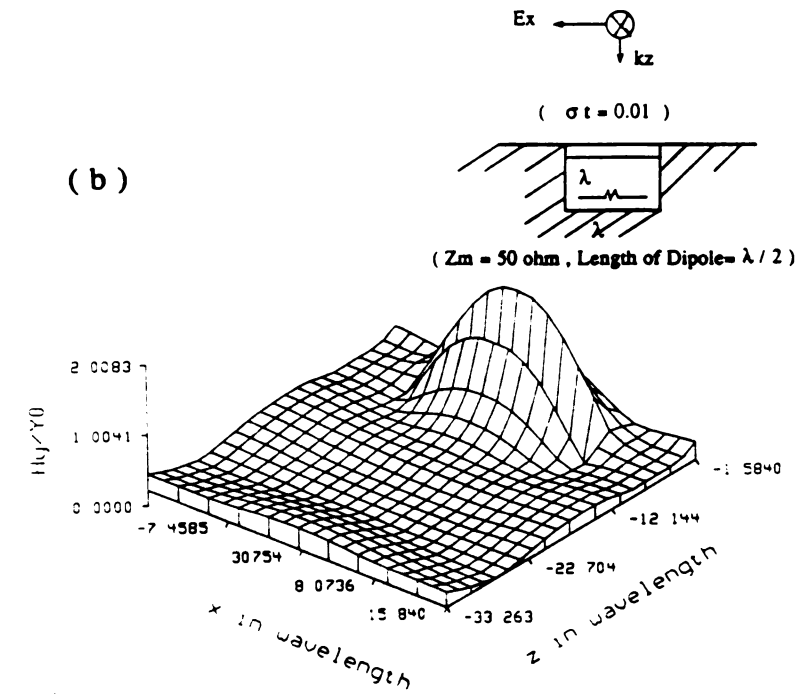

Figure 5.26 (a) y-component of total magnetic field in the X-Z plane inside the cavity produced by a cavity-backed antenna with its aperture empty; (b) y-component of total magnetic field in the X-Z plane inside the cavity produced by a cavity-backed antenna with its aperture covered by an impedance film.

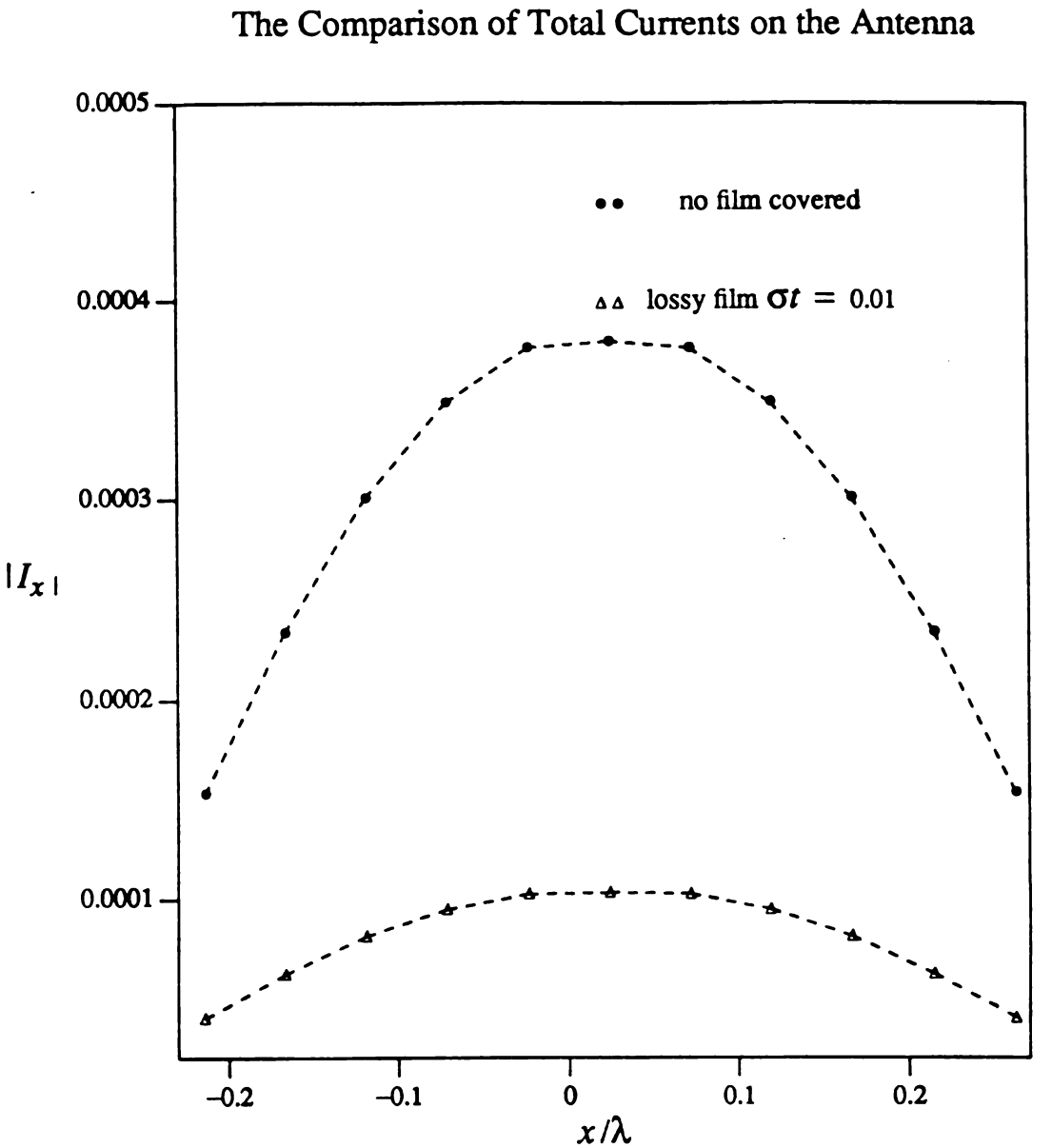

Figure 5.27 Comparison of the total current density distribution on the cavity-backed antenna :

(centra fed impedance Z_m = 50 *ohms*; the antenna is l/λ = 17/21 from the bottom of the cavity; receiving power in the case of no film covered $P = -54.4085$ *db*; receiving power in the case of an impedance covered aperture $P = -65.6098$ *db*)

CHAPTER VI

SUMMARY

A new set of coupled surface integral equations, which are capable of handling arbitrarily shaped heterogeneous bodies either with or without a perfectly conducting body inside, has been derived based on the equivalent electric and magnetic currents on the interfaces of the body. Its numerical solution for the equivalent surface currents on the interfaces via the method of moments with vector basis functions has been conducted. The numerical procedures developed have been tested by applying them to concentric spheres and the results are in very good agreement with the exact solutions. The absence of numerical anomalies in the procedures used is atributed primarily to the use of basis functions which are free of ficticous line or point charges and in which the expansion coefficients are not associated with current flowing parallel to boundary edges.

The effects of a thin magnetic layer coating a metallic object on the radar cross section of the object have been investigated. An efficient integral equation formulation for this extreme case of thin coating has been proposed. To validate the new integral equations, an alternative method based on the eigenmode expansion for an infinite circular cylinder coated with a thin, lossy magnetic layer has also been derived. The agreement between the two approaches is excellent.

A new algorithm for the finite difference time-domain method has been developed based on the integral forms of Maxwell's equations for treating the problems of scattering by a cylinder coated with thin magnetic films. In addition, the effect of the impedance sheet, covering a cavity backed antenna, on the scattering and receiving characteristics of the antenna have been studied by the finite difference time domain method. Yee's model and the radiation boundary condition have been modified and

then applied to the infinitely thin impedance sheet and the infinite ground plane structure. A systematic approach of analyzing the stability of the FD-TD method has also been introduced and illustrated through examples of several different FD-TD schemes. Conclusions about the stability of several popular FD-TD schemes have been made, which are the same as numerical empiricism.

APPENDIX A

In this Appendix, we will prove the following relations:

$$\hat{n}\cdot\mathbf{E} = \frac{j}{\omega\varepsilon}\nabla\cdot(\hat{n}\times\mathbf{H}) \tag{A1}$$

$$\hat{n}\cdot\mathbf{H} = \frac{1}{j\omega\mu}\nabla\cdot(\hat{n}\times\mathbf{E}) \tag{A2}$$

By the Maxwell's equation, we have:

$$\nabla\times\mathbf{H} = j\omega\varepsilon\mathbf{E} \tag{A3}$$

$$\nabla\times\mathbf{E} = -j\omega\mu\mathbf{H} \tag{A4}$$

Taking the inner product of the unit normal vector $\hat{n}$ of the surface with both sides of Maxwell's curl equation yields

$$\hat{n}\cdot\nabla\times\mathbf{H} = j\omega\varepsilon\hat{n}\cdot\mathbf{E} \tag{A5}$$

$$\hat{n}\cdot\nabla\times\mathbf{E} = -j\omega\mu\hat{n}\cdot\mathbf{H} \tag{A6}$$

Using the vector identity:

$$\nabla\cdot(\mathbf{A}\times\mathbf{B}) = \mathbf{B}\cdot(\nabla\times\mathbf{A}) - \mathbf{A}\cdot(\nabla\times\mathbf{B}) \tag{A7}$$

we have:

$$\nabla\cdot(\hat{n}\times\mathbf{E}) = \mathbf{E}\cdot(\nabla\times\hat{n}) - \hat{n}\cdot(\nabla\times\mathbf{E}) \tag{A8}$$

$$\nabla\cdot(\hat{n}\times\mathbf{H}) = \mathbf{H}\cdot(\nabla\times\hat{n}) - \hat{n}\cdot(\nabla\times\mathbf{H}) \tag{A9}$$

Next, on any smooth surfaces, we want to show that $\nabla\times\hat{n} = 0$:

$$\nabla\times\hat{n} = (\nabla_s + \hat{n}\frac{\partial}{\partial n})\times\hat{n} = \nabla_s\times\hat{n} \tag{A10}$$

where $\nabla_s\times$ denotes surface curl and $\nabla_s\times\hat{n} = 0$ from reference [35]. $\nabla_s\times\hat{n} = 0$ can be easily proved by the defination of surface curl [35].

Since $\nabla_s\times\hat{n} = 0$, equations (A8) & (A9) become:

$$\nabla\cdot(\hat{n}\times\mathbf{E}) = -\hat{n}\cdot(\nabla\times\mathbf{E}) \tag{A11}$$

$$\nabla\cdot(\hat{n}\times\mathbf{H}) = -\hat{n}\cdot(\nabla\times\mathbf{H}) \tag{A12}$$

Putting (A11) & (A12) back into (A5) & (A6), we have:

$$-\nabla\cdot(\hat{n}\times\mathbf{H}) = j\omega\varepsilon\hat{n}\cdot\mathbf{E} \tag{A16}$$

$$\nabla\cdot(\hat{n}\times\mathbf{E}) = j\omega\mu\hat{n}\cdot\mathbf{H} \tag{A17}$$

Finally, we have the relations:

$$\hat{n}\cdot\mathbf{E} = \frac{j}{\omega\varepsilon}\nabla\cdot(\hat{n}\times\mathbf{H})$$

$$\hat{n}\cdot\mathbf{H} = \frac{1}{j\omega\mu}\nabla\cdot(\hat{n}\times\mathbf{E})$$

APPENDIX B

In oder to evaluate the various elements of matrix equations in Chapter 2, calculation of the following three integrals (2.3.16) is required.

$$\int_{T^p} \mathbf{f}_m \cdot \mathbf{A}^q \, dS = \int_{T^p} dS \, \mathbf{f}_m(\mathbf{r}) \cdot \int_{T^q} \mathbf{f}_n(\mathbf{r}') \frac{e^{-jkR^p}}{R^p} \, dS' \tag{B1}$$

$$-\int_{T^p} \mathbf{f}_m \cdot \nabla V \, dS = \int_{T^p} \mathbf{f}_m \cdot \int_{T^q} \nabla_s' \cdot \mathbf{f}_n(\mathbf{r}') \nabla' \Phi \, d S' \tag{B2}$$

$$P_{mn}^{\pm} = \frac{l_m}{2A_m^{\pm}} \int\int_{T^p} \rho_m^{\pm} \cdot \left[\int\int_{T^q} \mathbf{f}_n(\mathbf{r}') \times \nabla' \Phi(\mathbf{r}^p, \mathbf{r}') dS' \right] dS \tag{B3}$$

with $R^p = |\mathbf{r}^p - \mathbf{r}'|$ and $\Phi = \dfrac{e^{-jkR}}{R}$

The first two integrals are easy to be performed in a local coordinate system

First, we consider integration of Eq. (B2).

$$\int_{T^p} \mathbf{f}_m \cdot \int_{T^q} \nabla_s' \cdot \mathbf{f}_n(\mathbf{r}') \nabla' \Phi \, d S' = -\int_{T^p} \mathbf{f}_m \cdot \nabla \int_{T^q} \nabla_s' \cdot \mathbf{f}_n(\mathbf{r}') \Phi \, d S' \tag{B4}$$

$$= \int_{T^p} dS \, \nabla \cdot \mathbf{f}_m \cdot \int_{T^q} \nabla_s' \cdot \mathbf{f}_n(\mathbf{r}') \Phi \, d S'$$

$$= \int_{T^p} \pm\left(\frac{l_m}{A^p}\right) \int_{T^q} \pm\left(\frac{l_n}{A^q}\right) \frac{e^{-jkR^p}}{R^p} \, dS'$$

$$= \pm 4 l_m \pm l_n \int_0^1 \int_0^{1-\eta} d\xi \, d\eta \int_0^1 \int_0^{1-\eta'} \frac{e^{-jkR^p}}{R^p} \, d\xi' \, d\eta'$$

$$= \pm 4 l_m \pm l_n \int_0^1 \int_0^{1-\eta} d\xi \, d\eta \, I_1$$

Consider Eq. (B1), we first attempt to evaluate $\mathbf{A}_{mn}$:

$$\mathbf{A}_{mn} = l_n \int_0^1 \int_0^{1-\eta} \rho_n \frac{e^{-jkR^p}}{R^p}\, d\xi\, d\eta \tag{B5}$$

$$= \pm l_n^i \int_0^1 \int_0^{1-\eta} (\mathbf{r}' - \mathbf{r}^i) \frac{e^{-jkR^p}}{R^p}\, d\xi\, d\eta$$

$$= \pm l_n^i \left[\mathbf{r}_1 I_{1\xi}^{pq} + \mathbf{r}_2 I_{1\eta}^{pq} + \mathbf{r}_3 I_{1\xi}^{pq} - \mathbf{r}_i I_1^{pq} \right]$$

$$= \pm l_n^i \left[(\mathbf{r}_1 - \mathbf{r}_2) I_{1\xi}^{pq} + (\mathbf{r}_2 - \mathbf{r}_3) I_{1\eta}^{pq} + (\mathbf{r}_3 - \mathbf{r}_i) I_1^{pq} \right]$$

The two integrals have be represented as the functions of the following three single integrals:

$$I_1 = \int_{\eta=0}^{1} \int_{\xi=0}^{1-\eta} \frac{e^{-jkR}}{R}\, d\xi d\eta \tag{B6}$$

$$I_{1\xi} = \int_{\eta=0}^{1} \int_{\xi=0}^{1-\eta} \xi \frac{e^{-jkR}}{R}\, d\xi d\eta \tag{B7}$$

$$I_{1\eta} = \int_{\eta=0}^{1} \int_{\xi=0}^{1-\eta} \eta \frac{e^{-jkR}}{R}\, d\xi d\eta \tag{B8}$$

and these three integrals have been referred in the Appendix C of [10].

Next, the integral $\int_{T^p} \mathbf{f}_m \cdot \mathbf{A}_{mn}^q\, dS$ is conducted as follows:

$$\int_{T^p} \mathbf{f}_m \cdot \mathbf{A}_{mn}^q\, dS = \int_{T^p} \mathbf{f}_m \cdot \pm l_n^i \left[(\mathbf{r}_1 - \mathbf{r}_2) I_{1\xi}^{pq} + (\mathbf{r}_2 - \mathbf{r}_3) I_{1\eta}^{pq} + (\mathbf{r}_3 - \mathbf{r}_i) I_1^{pq} \right] \tag{B9}$$

$$= \pm l_m^j \pm l_n^i \int_0^1 \int_0^{1-\eta} d\xi\, d\eta (\mathbf{r}_m - \mathbf{r}_{mj}) \cdot \left[(\mathbf{r}_1 - \mathbf{r}_2) I_{1\xi}^{pq} + (\mathbf{r}_2 - \mathbf{r}_3) I_{1\eta}^{pq} + (\mathbf{r}_3 - \mathbf{r}_i) I_1^{pq} \right]$$

After some manipulation, we can obtain:

$$= \pm\mu_m^j \pm l_n^i \Big\{ (\mathbf{r}_{m1} - \mathbf{r}_{m3}) \cdot [(\mathbf{r}_1 - \mathbf{r}_3) I^5 + (\mathbf{r}_2 - \mathbf{r}_3) I^8 + (\mathbf{r}_3 - \mathbf{r}_i) I^2] +$$

$$= (\mathbf{r}_{m2} - \mathbf{r}_{m3}) \cdot [(\mathbf{r}_1 - \mathbf{r}_3) I^6 + (\mathbf{r}_2 - \mathbf{r}_3) I^9 + (\mathbf{r}_3 - \mathbf{r}_i) I^3] +$$

$$= (\mathbf{r}_{m3} - \mathbf{r}_{mj}) \cdot [(\mathbf{r}_1 - \mathbf{r}_3) I^4 + (\mathbf{r}_2 - \mathbf{r}_3) I^7 + (\mathbf{r}_3 - \mathbf{r}_i) I^1] +$$

where $I^1 \cdots I^9$ are defined as:

$$I^1 = \int_0^1 \int_0^{1-\eta} I_1 d\xi \, d\eta \tag{B10}$$

$$I^2 = \int_0^1 \int_0^{1-\eta} \xi \, I_1 d\xi \, d\eta \tag{B11}$$

$$I^3 = \int_0^1 \int_0^{1-\eta} \eta \, I_1 d\xi \, d\eta \tag{B12}$$

$$I^4 = \int_0^1 \int_0^{1-\eta} I_{1\xi} d\xi \, d\eta \tag{B13}$$

$$I^5 = \int_0^1 \int_0^{1-\eta} \xi \, I_{1\xi} d\xi \, d\eta \tag{B14}$$

$$I^6 = \int_0^1 \int_0^{1-\eta} \eta \, I_{1\xi} d\xi \, d\eta \tag{B15}$$

$$I^7 = \int_0^1 \int_0^{1-\eta} I_{1\eta} d\xi \, d\eta \tag{B16}$$

$$I^8 = \int_0^1 \int_0^{1-\eta} \xi \, I_{1\eta} d\xi \, d\eta \tag{B17}$$

$$I^9 = \int_0^1 \int_0^{1-\eta} \eta \, I_{1\eta} d\xi \, d\eta \tag{B18}$$

Now we consider the third integral

$$P_{mn}^{\pm} = \frac{l_m}{2A_m^{\pm}} \iint_{T^p} \rho_m^{\pm} \cdot \left[\iint_{T^q} \mathbf{f}_n(\mathbf{r}') \times \nabla' \Phi_i(\mathbf{r}^p, \mathbf{r}') dS' \right]$$

in (B3) , where

$$\nabla' \Phi(\mathbf{r}, \mathbf{r}') = (\mathbf{r} - \mathbf{r}')(1 + jkR) \frac{e^{-jkR}}{R^3}$$

What we need to do is the double integrations over T^p and T^q . First, we evaluate the following $\mathbf{P}_i^{pq}$, the integral over T^q with observation point at $\mathbf{r}$ in triangle T^p .

$$\mathbf{P}_{mn} = \int_{T^q} \frac{l_n^i}{2A_q} \rho_i \times (\mathbf{r}_m^{\pm} - \mathbf{r}')(1 + jkR^{\pm}) \frac{e^{-jkR^{\pm}}}{(R^{\pm})^3} \, dS \tag{B19}$$

Then, we calculate $P_{imn}^{\pm}$ by

$$P_{mn}^{\pm} = \frac{l_m}{2A_m^{\pm}} \iint_{T^p} \rho_m^{\pm} \cdot \mathbf{P}_{mn}^{pq} \tag{B20}$$

Starting from $\mathbf{P}_{mn}^{pq}$ and Changing varibles by using area coordinate: $\mathbf{r}' = \xi \mathbf{r}_1 + \eta \mathbf{r}_2 + (1 - \xi - \eta)\mathbf{r}_3$ result in $\rho_i = \mathbf{r}' - \mathbf{r}^i = \xi \mathbf{r}_1 + \eta \mathbf{r}_2 + (1 - \xi - \eta)\mathbf{r}_3 - \mathbf{r}^i$

Then

$$\mathbf{P}_{mn} = \pm l_n^i \int_0^1 \int_0^{1-\eta} \left(\xi \mathbf{r}_1 + \eta \mathbf{r}_2 + (1 - \xi - \eta)\mathbf{r}_3 - \mathbf{r}^i \right) \times \tag{B21}$$

$$\left(\mathbf{r}_m^{\pm} - (\xi \mathbf{r}_1 + \eta \mathbf{r}_2 + (1 - \xi - \eta)\mathbf{r}_3) \right) (1 + jkR^{\pm}) \frac{e^{-jkR^p}}{R^p} \, d\xi \, d\eta$$

$$= \pm l_n^i \int_0^1 \int_0^{1-\eta} \left[(\xi \mathbf{r}_1 + \eta \mathbf{r}_2 + (1 - \xi - \eta)\mathbf{r}_3) \times (\mathbf{r}_m^{\pm} - \mathbf{r}^i) + (\mathbf{r}_m^{\pm} \times \mathbf{r}^i) \right] (1 + jk_i R^{\pm}) \frac{e^{-jkR^p}}{R^p} \, d\xi \, d\eta$$

$$= \pm l_n^i \left[I_{2\xi} \mathbf{r}_1 \times (\mathbf{r}_m^{\pm} - \mathbf{r}^i) + I_{2\eta}^{pq} \mathbf{r}_2 \times (\mathbf{r}_m^{\pm} - \mathbf{r}^i) + I_{2\xi}^{pq} \mathbf{r}_3 \times (\mathbf{r}_m^{\pm} - \mathbf{r}^i) + \mathbf{r}_m^{\pm} \times \mathbf{r}^i I_2^{pq} \right]$$

Where

$$I_2^{pq} = \int_0^1 \int_0^{1-\eta} (1 + jkR^{\pm}) \frac{e^{-jkR^p}}{R^p} \, d\xi \, d\eta \tag{B22}$$

$$I_{2\xi}^{pq} = \int_0^1 \int_0^{1-\eta} \xi(1 + jkR^{\pm}) \frac{e^{-jkR^p}}{R^p} \, d\xi \, d\eta \tag{B23}$$

$$I_{2\eta}^{pq} = \int_0^1 \int_0^{1-\eta} \eta(1 + jkR^{\pm}) \frac{e^{-jkR^p}}{R^p} \, d\xi \, d\eta \tag{B24}$$

$$I_{2\xi} = I_2^{pq} - I_{2\xi}^{pq} - I_{2\eta}^{pq} \tag{B25}$$

Note that these three integrals $I_2^{pq}, I_{2\xi}^{pq}, I_{2\eta}^{pq}$ are independent integrals

Second, substituting Eq. (B21) into Eq. (B20) for P_{mn} we have:

$$P_{mn} = \frac{l_m}{2A_m^{\pm}} \int_{T_m^{\pm}} \rho_m^{\pm} \cdot \left[\int_{T_n} \frac{l_i}{2A_q} \rho_i \times (\mathbf{r}_m^{\pm} - \mathbf{r}') (1 + jkR^{\pm}) \frac{e^{-jkR^{\pm}}}{(R^{\pm})^3} \, dS' \right] dS \tag{B26}$$

$$\rho_m = \pm(\mathbf{r}_m^{\pm} - \mathbf{r}_m^i) \tag{B27}$$

$$P_{mn} = \pm l_m^j \int_0^1 \int_0^{1-\eta} d\xi \, d\eta \, (\mathbf{r}_m^{\pm} - \mathbf{r}_{m_j}) \cdot \pm l_i \Big[I_{2\xi} \mathbf{r}_1 \times (\mathbf{r}_m^{\pm} - \mathbf{r}^i) \tag{B28}$$

$$+ I_{2\eta}^{pq} \mathbf{r}_2 \times (\mathbf{r}_m^{\pm} - \mathbf{r}_i) + I_{2\zeta}^{pq} \mathbf{r}_3 \times (\mathbf{r}_m^{\pm} - \mathbf{r}_i) + \mathbf{r}_m^{\pm} \times \mathbf{r}_i I_2^{pq} \Big]$$

$$= \pm l_m^j \int_0^1 \int_0^{1-\eta} d\xi \, d\eta \, \pm l_n^i \Big[I_{2\xi} \mathbf{r}_m^i \cdot (\mathbf{r}_1 \times \mathbf{r}_i) + I_{2\eta}^{pq} \mathbf{r}_{m_j} \cdot (\mathbf{r}_2 \times \mathbf{r}_i) + I_{2\zeta}^{pq} \mathbf{r}_{m_j}$$

$$\cdot (\mathbf{r}_3 \times \mathbf{r}_i) + \mathbf{r}_{m_j} \cdot (\mathbf{r}_i \times \mathbf{r}_m^{\pm}) I_2^{pq} - I_{2\xi} \mathbf{r}_m^{\pm} \cdot (\mathbf{r}_1 \times \mathbf{r}_i) - I_{2\eta}^{pq} \mathbf{r}_m^{\pm} \cdot (\mathbf{r}_2 \times \mathbf{r}_i) - I_{2\zeta}^{pq} \mathbf{r}_m^{\pm}$$

$$\cdot (\mathbf{r}_3 \times \mathbf{r}_i) - I_{2\xi} \mathbf{r}_{m_j} \cdot (\mathbf{r}_1 \times \mathbf{r}_m^{\pm}) - I_{2\eta}^{pq} \mathbf{r}_{m_j} \cdot (\mathbf{r}_2 \times \mathbf{r}_m^{\pm}) - I_{2\zeta}^{pq} \mathbf{r}_{m_j} \cdot (\mathbf{r}_3 \times \mathbf{r}_m^{\pm}) \Big]$$

since:

$$\mathbf{r}_{m_j}\cdot(\mathbf{r}_i\times\mathbf{r}_m^{\pm}) = \mathbf{r}_m^{\pm}\cdot(\mathbf{r}_{m_j}\times\mathbf{r}_i) \tag{B29}$$

$$P_{mn} = \pm l_m^j \pm l_n^i \int_0^1 \int_0^{1-\eta} d\,\xi\, d\,\eta \left[I_{2\xi}^{pq}\mathbf{r}_m^{\pm}\cdot((\mathbf{r}_i - \mathbf{r}_{m_j})\times\mathbf{r}_1) + I_{2\eta}^{pq}\mathbf{r}_m^{\pm}\cdot((\mathbf{r}_i - \mathbf{r}_{m_j})\right.$$

$$\left.\times\mathbf{r}_2) + I_{2\zeta}^{pq}\mathbf{r}_m^{\pm}\cdot((\mathbf{r}_i - \mathbf{r}_{m_j})\times\mathbf{r}_3) + \mathbf{r}_m^i\cdot(\mathbf{r}_1 I_2\xi + \mathbf{r}_2 I_{2\eta} + \mathbf{r}_3 I2_\zeta)\times\mathbf{r}_i + \mathbf{r}_{m_j}\cdot(\mathbf{r}_i\times\mathbf{r}_m^{\pm})I_2\right]$$

$$= \pm l_m^j \pm l_n^i \int_0^1 \int_0^{1-\eta} d\,\xi d\,\eta \left[I_{2\xi}^{pq}\mathbf{r}_m^{\pm}\cdot((\mathbf{r}_i - \mathbf{r}_{m_j})\times(I_{2\xi}^{pq}\mathbf{r}_1 + I_{2\eta}^{pq}\mathbf{r}_2 + I_{2\zeta}^{pq}\mathbf{r}_3) + \right.$$

$$\left.\mathbf{r}_{m_j}\cdot(\mathbf{r}_1 I_2\xi + \mathbf{r}_2 I_{2\eta} + \mathbf{r}_3 I2_\zeta)\times\mathbf{r}_i + \mathbf{r}_m^{\pm}\cdot(\mathbf{r}_{m_j}\times\mathbf{r}_i)I_2^{pq}\right] \tag{B30}$$

where

$$\mathbf{r}_m^{\pm} = (\mathbf{r}_{m_1}\xi + \mathbf{r}_{m_2}\eta + \mathbf{r}_{m_3}\zeta) \tag{B31}$$

Finally, we have an expression for P_{mn}:

$$P_{mn} = \pm l_m^j \pm l_n^i \int_0^1 \int_0^{1-\eta} d\,\xi d\,\eta \left[(\mathbf{r}_{m_1}\xi + \mathbf{r}_m^2\eta + \mathbf{r}_{m_3}(1 - \xi - \eta))\cdot((\mathbf{r}_i - \mathbf{r}_{m_j})\times\right. \tag{B32}$$

$$(I_{2\xi}^{pq}\mathbf{r}_1 + I_{2\eta}^{pq}\mathbf{r}_2 + I_{2\zeta}^{pq}\mathbf{r}_3)$$

$$\left. + \mathbf{r}_{m_j}\cdot(\mathbf{r}_1 I_2\xi + \mathbf{r}_2 I_{2\eta} + \mathbf{r}_3(I_2^{pq} - I_{2\xi}^{pq} - I_{2\eta}^{pq}))\times\mathbf{r}^i + (\mathbf{r}_{m_1}\xi + \mathbf{r}_{m_2}\eta + \mathbf{r}_{m_3}(1 - \xi - \eta))\cdot(\mathbf{r}_{m_j}\times\mathbf{r}_i)I_2^{pq}\right]$$

$$= \pm l_m^j \pm l_n^i \int_0^1 \int_0^{1-\eta} d\,\xi\, d\,\eta \left[\left[(\mathbf{r}_{m_1} - \mathbf{r}_{m_3})\xi + (\mathbf{r}_{m_2} - \mathbf{r}_{m_3})\eta + \mathbf{r}_{m_3}\right]\cdot(\mathbf{r}_i - \mathbf{r}_{m_j})\times\right.$$

$$(I_{2\xi}^{pq}(\mathbf{r}_1 - \mathbf{r}^3) + I_{2\eta}^{pq}(\mathbf{r}_2 - \mathbf{r}_3) + I_2^{pq}\mathbf{r}_3) + \mathbf{r}_{m_j}\cdot(I_{2\xi}^{pq}(\mathbf{r}_1 - \mathbf{r}^3) + I_{2\eta}^{pq}(\mathbf{r}_2 - \mathbf{r}_3) +$$

$$\left. I_2^{pq}\mathbf{r}_3)\times\mathbf{r}_i + \left[(\mathbf{r}_{m_1} - \mathbf{r}_{m_3})\xi + (\mathbf{r}_{m_2} - \mathbf{r}_{m_3})\eta + \mathbf{r}_{m_3}\right]\cdot(\mathbf{r}_m^i\times\mathbf{r}_i)I_2^{pq}\right]$$

$$= \pm l_m^j \pm l_n^i \int_0^1 \int_0^{1-\eta} d\,\xi\, d\,\eta \left\{ (\mathbf{r}_{m_1} - \mathbf{r}_{m_3}) \cdot ((\mathbf{r}_i - \mathbf{r}_{m_j}) \times (\xi I_{2\xi}^{pq}(\mathbf{r}_1 - \mathbf{r}_3) \right.$$

$$+ \xi I_{2\eta}^{pq}(\mathbf{r}_2 - \mathbf{r}_3) + \xi I_2^{pq}\mathbf{r}_3) + (\mathbf{r}_{m_2} - \mathbf{r}_{m_3}) \cdot ((\mathbf{r}_i - \mathbf{r}_{m_j}) \times (\eta I_{2\xi}^{pq}(\mathbf{r}_1 - \mathbf{r}_3) + \eta I_{2\eta}^{pq}(\mathbf{r}_2 - \mathbf{r}_3) + \eta I_2^{pq}\mathbf{r}_3)$$

$$+ \mathbf{r}_{m_3} \cdot (\mathbf{r}_i - \mathbf{r}_{m_j}) \times (I_{2\xi}^{pq}(\mathbf{r}_1 - \mathbf{r}_3) + I_{2\eta}^{pq}(\mathbf{r}_2 - \mathbf{r}_3) + I_2^{pq}\mathbf{r}_3) + \mathbf{r}_{m_j} \cdot (I_{2\xi}^{pq}(\mathbf{r}_1 - \mathbf{r}_3) +$$

$$\left. I_{2\eta}^{pq}(\mathbf{r}_2 - \mathbf{r}_3) + I_2^{pq}\mathbf{r}_3) \times \mathbf{r}_i + \left[(\mathbf{r}_{m_1} - \mathbf{r}_{m_3})\xi + (\mathbf{r}_{m_2} - \mathbf{r}_{m_3})\eta + \mathbf{r}_{m_3} \right] \cdot (\mathbf{r}_{m_i} \times \mathbf{r}_i) I_2^{pq} \right\}$$

If the observation point $\mathbf{r}$ and field point $\mathbf{r}'$ are within the same triangle, then R will be zero for some value of ξ,η,ξ',η' and the integrals $I_2^{pq}, I_{2\xi}^{pq}, I_{2\eta}^{pq}$ will be singular. Fortunately, P_{mn} equals to zero when $\mathbf{r}$ and $\mathbf{r}'$ are in the same triangle. The above integral can be numerically calculated by seven-point quadrature rule.

APPENDIX C

In Appendix C, we demonstrate that **E** on the left hand side of Eq. (4.13) is the electric field on the out surface of a lossy layer, if the thickness of the layer approaches zero. The proper boundary condition posed for the Eq. (4.13a) is $\hat{n}\times\mathbf{E} = -\mathbf{J}_m t$ where t is the thickness of the layer. To justify this statement, it is necessary to check the singular integral around a field point.

Using a vector identity and Maxwell's equations [37] leads to

$$\int_V \left[- j\omega\mu \mathbf{J}\Phi - BoldJ_m\times\nabla'\Phi + \frac{\rho}{\varepsilon}\nabla'\Phi \right] dS' \tag{C1}$$

$$= \int_S \left[- j\omega\mu(\hat{n}\times\mathbf{H})\Phi + (\hat{n}\times\mathbf{E})\times\nabla'\Phi + (\hat{n}\cdot\mathbf{E})\nabla'\Phi \right] dS'$$

Equation (C1) holds in any singularity-excluded region . Refer to Fig. C1, the observed point is excluded by a semisphere S_a and S is composed by $S_\infty + S_1 + S_a$. The integration on S_∞ is zero by the Sommonfeld radiation boundary condition.

Performing the integration around the observed point on S_a yields:

$$\int_{S_a} \left[- j\omega\mu(\hat{n}\times\mathbf{H})\Phi + (\hat{n}\times\mathbf{E})\times\nabla'\Phi + (\hat{n}\cdot\mathbf{E})\nabla'\Phi \right] dS' \tag{C2}$$

The first term of the surface integral in (C2) is:

$$\int form S_a \left[- j\omega\mu(\hat{n}\times\mathbf{H})\Phi \right] dS' \tag{C3}$$

$$= - j\omega\mu(\hat{n}\times\mathbf{H}) \lim\left[\frac{e^{-j\beta R}}{R} 4\pi R^2 \right] = 0$$

The second and the third terms of the surface integral can be combined:

$$\int_{S_a} \left[(\hat{n}\times\mathbf{E}(\mathbf{r}))\times\nabla'\Phi + (\hat{n}\cdot\mathbf{E}(\mathbf{r}))\nabla'\Phi\right]dS' \tag{C4}$$

$$= \int_{S_a} \left[(\hat{n}\times\mathbf{E}(\mathbf{r}))\times\hat{n} + (\hat{n}\cdot\mathbf{E}(\mathbf{r}))\right](\frac{1}{R} + j\beta)\frac{e^{-j\beta R}}{R}\, dS'$$

$$= \int_{S_a} \mathbf{E}(\mathbf{r})(\frac{1}{R} + j\beta)\frac{e^{-j\beta R}}{R}\, dS'$$

This procedure for calculating the surface integrals around singular point is the same as that described in [37]. However, special attention should be paid to Eq.(C4) when a thin coating on a metallic object is concerned. In [37], it is assumed that **E** is continuous and finite on S_a, so that an average electric field can be taken out of the integral. But when the observed point is close the surface of a perfectly conducting body coated with thin magnetically lossy layer, the tangential component of electric field is not continuous across the magnetically lossy layer. Since the thickness of the layer is very thin, the contribution from the integral inside thin layer can be ignored and the significant contribution roots in the integral of **E** on the out surface of the coated layer over S_a . Therefore, (C4) is calculated as

$$\int_{S_a} \left[(\hat{n}\times\mathbf{E}(\mathbf{r}))\times\nabla'\Phi + (\hat{n}\cdot\mathbf{E}(\mathbf{r}))\nabla'\Phi\right]dS' \tag{C5}$$

$$= \mathbf{E}(\mathbf{r}|_{on\ the\ out-surface})\int_{S_a} (\frac{1}{R} + j\beta)\frac{e^{-j\beta R}}{R}\, dS'$$

$$= \mathbf{E}(\mathbf{r}|_{on\ the\ out-surface})\ \lim\ (\frac{1}{R} + j\beta)\frac{e^{-j\beta R}}{R}\, 2\pi R^2$$

$$= 2\pi\mathbf{E}(\mathbf{r}|_{on\ the\ out-surface})$$

Thus we see that when thegenral integral formulas is used to represent the fields for an object with a magnetically lossy coating, the electric field **E** resulted from the singular integral should be understood as the field on the out surface of a magnetically

lossy layer.

BIBLIOGRAPHY

BIBLIOGRAPHY

[1] T. K. Wu and L. L. Tsai. " Scattering from arbitrarily-shaped lossy dielectric bodies of revolution, " Radio Sci. vol. 12, pp. 709-718, Sept. 1977.

[2] P. W. Barber and C. Yeh, " Scattering of EM waves by arbitrarily shaped dielectric bodies," Appl. Opt., vol. 14, pp. 2864-2872, Dec. 1975

[3] M. A. Morgan and K. K. Mei, " Finite element computation of scattering by inhomogeneous penetrable bodies of revolution, " IEEE Trans. Antennas Propagat., vol. AP-27, pp. 202-214, Mar. 1979.

[4] D. E. Livesay and K-M Chen, " Electromagnetic fields induced inside arbitrarily shaped biological bodies, " IEEE Trans. Microwave Theory Tech., vol. MTT-22, pp. 1273-1280

[5] J. J. H. Wang, " numerical analysis of three-dimensional arbitrarily-shaped conducting scatterers by trilateral surface cell modelling," Radio Sci., vol. 13 , no. 6, pp. 947-952, Nov.-Dec. 1978.

[6] J. R. Mautz and R. F. Harrington, " Electromagnetic scattering from a homogeneous material body of revolution, " Arch. Elec. Ubertragung., vol. 33, pp. 71-80, Feb. 1979.

[7] R. F. Harrington, Field Computation by Moment Methods. New York: Macmillan, 1968.

[8] S. M. Rao, D. R. Wilton, and A. W. Glisson, " Electromagnetic scattering by surfaces of arbitrary shape, " IEEE Trans. Antennas Propagat., vol. AP-30, pp. 409-418, May. 1982.

[9] A. W. Glisson and D. R. Wilton, " Simple and efficient numerical methods for problems of electromagnetic radiation and scattering from surfaces, " IEEE Trans. Antennas Propagat., vol. AP-28, no. 5, pp. 593-603, Sept. 1980.

[10] S. M. Rao, " Electromagnetic scattering and radiation of arbitrary-shaped surfaces by triangular patch modeling, " PH.D. dissertation, Univ. Mississippi, University, MS, Aug. 1980.

[11] K. R. Umashankar and A. Taflove, " Analytical models for electromagnetic scattering, " Part-I, Final Rep., Contract F 19628-82-C-0140 to RADC/ESD, Hanscom Air Force Base, MA, June 1984.

[12] K. R. Umashankar and A. Taflove, " electromagnetic scattering by arbitrary shaped three-dimensional homogeneous lossy dielectric objects, " IEEE Trans. Antennas Propagat., vol. AP-34, no. 6, pp. 758-766, June. 1986.

[13] D. H. Schaubert, D. R. Wilton and A. W. Glisson, " A tetrahedral modeling for electromagnetic scattering by arbitrary shaped homogeneous dielectric bodies," IEEE Trans. Antennas Propagat., vol. AP-32, no. 1, pp. 77-85, Jan. 1984.

[14] O. C. Zienkiewicz, The Finite Element Method in Engineering Science. New York: McGraw-Hill,1971

[15] P. C. Hammer, O. P. Marlowe, and A. H. Stroud, " numerical integration over sinmplexes and cones, " Math. Tables Aids Comp., 10,

[16] K. D. Paulsen, D. R. Lynch, and J. W. Strohbehn, " Three-dimensional finite, bondary, and hybrid element solutions of the Maxwell equations for lossy dielectric media, " IEEE Trans. Microwave Theory Tech., vol. MTT-36, pp. 682-693, April. 1988

[17] A. Taflove, K. R. Umashankar, " Finite-difference time-domain (FT-TD) modeling of electromagnetic wave scattering and interaction problems, " IEEE Trans. Antennas Propagat., Newsletter, vol. 30, no. 2, pp. 5-20, April. 1988. IP [18] Ke-Li Wu, Gilles Y. Delisle, " Coupled finite element and boundary element methods in elecreomagnetic scattering problems, " 1988 IEEE AP-S International Sympsium.

[19] Dennis M. Sullivan, David T. Borup and OM P. Gandhi, " Use of the finite-differnce time-domain method in calculating EM absorption in human tissues, " IEEE Trans. Biomedical Engineering, Vol. BME-34, No. 2, pp148-157, Feb. 1987.

[20] Dennis M. Sullivan, OM P. Gandhi and Allen Taflove, " Use of the finite-differnce time-domain method for calculating EM absorption in man models, " IEEE Trans. Biomedical Engineering, Vol. BME-35, No. 3, pp179-185, Mar. 1987.

[21] A. Taflove and K.R. Umashankar, "Finite Difference Time-Domain (FD-TD) Modeling of Electromagnetic Wave Scattering and Interaction problems," IEEE Antennas and Propagat. Newsletter, Apr. 1988.

[22] K. S. Yee, " Numerical Solution of Initial Boundary Value Problems Involving Maxwell's Equations in Isotropic Media", IEEE Trans. on Antennas and Propagat., vol. AP-14, pp. 302-307, May 1966.

[23] A. Taflove and M. E. Brodwin, " Numerical Solution of Steady-State Electromagnetic Scattering Problrms Using the Time-Dependent Maxwell's Equations", IEEE Trans. on Microwave Theory and Techniques., vol. MTT-23, pp. 623-630, August. 1975.

[24] B. Enguist and A. Majda, " Absorbing Boundary Conditions for the Numerical Simulation of Waves" Mathematics of Computation, Vol. 31. no. 139, pp. 629-

651, July 1977

[25] G.D. Smith "Finite Diffrence Method,"

[26] A. Taflove and K.R. Umashankar, "The Finite Difference Time-Domain Method for Numerical Modeling of Electromagnetic Wave Interactions with Arbitrary Structures," Chapter 8 in "....", to be published.

[27] J. Fang and K. K. Mei, " A super absorbing boundary algorithm for solving electromagnetic problems by time domain finite difference method," 1988 IEEE AP-S International Symposium, Vol. II, pp. 472-475

[28] G. Mur, " Absorbing condition for the finite difference approximation of the time electromagnetic field equations, " IEEE Trans, Electromagn. Compat., Vol. EMC-23, pp377-382, Nov. 1981

[29] A. Taflove, K.R. Umashankar, B. Beker, and F. Harfoush, " Detailed FD-TD anlysis of electromagnetic fields penetrating narrow slots and lapped joints in thick conducting screens," IEEE Trans. on Antennas and Propagat., vol. AP-36, Feb. 1988

[30] A. Taflove and K.R. Umashankar, " Advanced numerical modeling of microwave penetration and coupling for complex structures," Final Report, Contract No. 6599805, Lawrence Livermore National Laboratory, Sep. 1987

[31] C. D. Talor, D. H. Lam and T. H. Shumpert, " Electromagnetic pulse scattering in time varying inhomogeneous media," IEEE Trans. on Antennas and Propagat., vol. AP-17, pp. 586-589, Sep. 1969

[32] D. E. Merewether, " Transient currents induced on a metallic body of revolution by an electromagnetic pulse media,"IEEE Trans. Electromagn. Compat., vol. EMC-13, pp. 41-44, May 1971.

[33] K. S. Kunz and K. M. Lee, " A three dimensional finite difference solution of the external response of an aircraft to a complex transient EM environment: Part 2 - The method and its implementation," IEEE Trans. Electromagn. Compat., vol. EMC-20, pp. 328-333, May 1978.

[34] K.R. Umashankar and A. Taflove, " A novel method to analyze electromagnetic scattering of complex objects," IEEE Trans. Electromagn. Compat., vol. EMC-24, pp. 397-405, Nov. 1982.